Analysis of the Effectiveness of Airborne Lidar Intensity for Predicting Organic Preservation Potential of Waterlogged Deposits

Project Manager
Keith Challis, HP Vista Centre, Birmingham Archaeology,
University of Birmingham, Edgbaston, Birmingham, B15 2TT
(0121 414 5563, k.challis@bham.ac.uk)

Report Text by

Dr Chris J Carey, HP VISTA Centre, Birmingham Archaeology,
University of Birmingham, Edgbaston, Birmingham, B15 2TT
(0121 414 7343, c.carey@bham.ac.uk)

Keith Challis, HP Vista Centre, Birmingham Archaeology,
University of Birmingham, Edgbaston, Birmingham, B15 2TT
(0121 414 5563, k.challis@bham.ac.uk)

Mark Kincey, HP VISTA Centre, Birmingham Archaeology,
University of Birmingham, Edgbaston, Birmingham, B15 2TT
(0121 414 7343, MEK894@bham.ac.uk)

Dr Andy J Howard, Institute of Archaeology and Antiquity,
University of Birmingham, Edgbaston, Birmingham B15 2TT
(0121 414 5497, a.j.howard@bham.ac.uk)

March 2008

PNUM 4782

Analysis of the Effectiveness of Airborne Lidar Intensity for Predicting Organic Preservation Potential of Waterlogged Deposits

Project Manager
Keith Challis, HP Vista Centre, Birmingham Archaeology,
University of Birmingham, Edgbaston, Birmingham, B15 2TT
(0121 414 5563, k.challis@bham.ac.uk)

Report Prepared by

Dr Chris J Carey, HP VISTA Centre, Birmingham Archaeology,
University of Birmingham, Edgbaston, Birmingham, B15 2TT
(0121 414 7343, c.carey@bham.ac.uk)

Keith Challis, HP Vista Centre, Birmingham Archaeology,
University of Birmingham, Edgbaston, Birmingham, B15 2TT
(0121 414 5563, k.challis@bham.ac.uk)

Mark Kincey, HP VISTA Centre, Birmingham Archaeology,
University of Birmingham, Edgbaston, Birmingham, B15 2TT
(0121 414 7343, MEK894@bham.ac.uk)

Dr Andy J Howard, Institute of Archaeology and Antiquity,
University of Birmingham, Edgbaston, Birmingham B15 2TT
(0121 414 5497, a.j.howard@bham.ac.uk)

March 2008

PNUM 4782

CONTENTS

FIGURES

Section 4

Section 5

TABLES

1 INTRODUCTION

1 INTRODUCTION

1.1 PREAMBLE

This document is the Stage 2 report for the English Heritage ALSF funded project *Analysis of the Effectiveness of Airborne Lidar Backscattered Laser Intensity for Predicting Organic Preservation Potential of Waterlogged Deposits* (PN4782).

Project work as originally envisaged comprised research focused on three themes:

1 Investigation of the principal of lidar intensity using ground based lidar survey as an analogue of airborne lidar.
2 Investigating airborne lidar intensity through the analysis of intensity measurements and ground based control information collected simultaneously with an Environment Agency (or similar) survey flight.
3 Investigation of archive lidar intensity data.

The project as originally conceived was modified due to the limitations of ground-based laser scanning, which meant that this technique did not provide an adequate analogue for airborne scanning, and the poor availability of intensity data from Environment Agency and others. A variation in the original project timing and scope to allow continuation of project work into a second year has been combined with a modified method and outcomes to allow completion of the objectives as originally set out (Challis *et al.* 2006). A full report on Stage 1 of the project is provided in Challis et al 2007. This document comprises a brief summary of the project background and aims (section 1), method statements (section 2), an account of the results of fieldwork and analysis of airborne lidar data (section 3), a discussion of the qualitative analysis of archive lidar intensity data (section 4), some discussion of the ability of lidar intensity to detect cultural archaeological remains (section 5) analysis and discussion of the impact of flight direction on airborne lidar intensity values (section 6) an overall discussion of results (section 7) and a concluding summary with a suggested protocol for the application of lidar data to geoarchaeological research (section 8). A list of references cited is provided in section 9.

1.2 AIRBORNE LASER SCANNING (LIDAR)

1.2.1 General Introduction

Airborne lidar has gradually assumed a place as part of the toolkit of remote sensing techniques available to archaeologists interested in the historic landscape. Published applications around the world include broad landscape studies (Barnes 2003; Bewley et al 2005; Bofinger et al 2006; Harmon et al 2006; Powlesland et al 2006), geoarchaeological mapping and prospection (Challis 2005; Challis 2006), investigation of the potential for lidar to detect upstanding archaeological remains beneath the vegetation canopy (Deveraux et al 2005; Doneus and Briese 2006; Risbol et al 2006; Sittler and Schellberg 2006), applications using lidar intensity images (Challis et al 2006; Carey et al 2006) and studies of the uses of lidar to contribute to the compilation and refinement of records of the historic environment (Holden et al 2002; Bewley 2003; Crutchley 2006; Challis et al in press).

1.2.2 The Lidar Principle

Airborne laser scanning uses the properties of coherent laser light, coupled with precise kinematic positioning provided by a differential global positioning system (DGPS) and inertial attitude determination provided by an inertial measurement unit (IMU), to produce horizontally and vertically accurate elevation measurements.

An aircraft mounted laser, most often a pulse laser working at rates in excess of 30 kHz, projects a coherent beam of light at the ground surface, the reflection of which is recorded by a sensitive receiver. Travel times for the pulse/reflection are used to calculate the distance from the laser to the reflecting object. To enable coverage of a broad area a swath beneath the moving aircraft is scanned by using rotating mirrors to direct the laser. The spatial resolution and scan swath width are determined by the frequency of the laser pulse and altitude of the aircraft at the time of survey. Typically the receiver is able to record multiple returns for a single pulse, allowing recording for example of a partial return from the top of a semi-opaque object such as a woodland canopy (usually referred to as a first-pulse (FP) return) and from the opaque ground beneath the canopy (a last-pulse (LP) return). Other information, such as the intensity (amplitude) of the backscattered laser pulse may also be recorded. Backscattered laser intensity measurements do not form a part of the standard data product supplied by EA. The lidar system used by EA, NERC and many UK-based commercial lidar providers (an Optech Airborne Laser Terrain Mapper) operates in the near infra-red (NIR: 1047nm) and so backscattered intensity is in-effect a record of the reflectance of earth surface materials at this wavelength.

The DGPS provide detailed three-dimensional information on the location of the laser unit, while the IMU provide information on the pitch, roll and yaw of the aircraft. A complete Lidar system comprises a scanning laser coupled with a DGPS and IMU linked through a computerised control, monitoring and recording unit. Post-survey processing of the simultaneously recorded laser, location and attitude data allows reconstruction of elevation values for the ground surface. Raw survey data in the form of a three dimensional point-cloud are projected to a local map datum, sorted, filtered and used to generate a regular grid of elevation values. A detailed technical discussion of Lidar may be found in Wehr and Lohr (1999) and Baltsavias (1999), details of the system used in the present study are contained in Optech 2003.

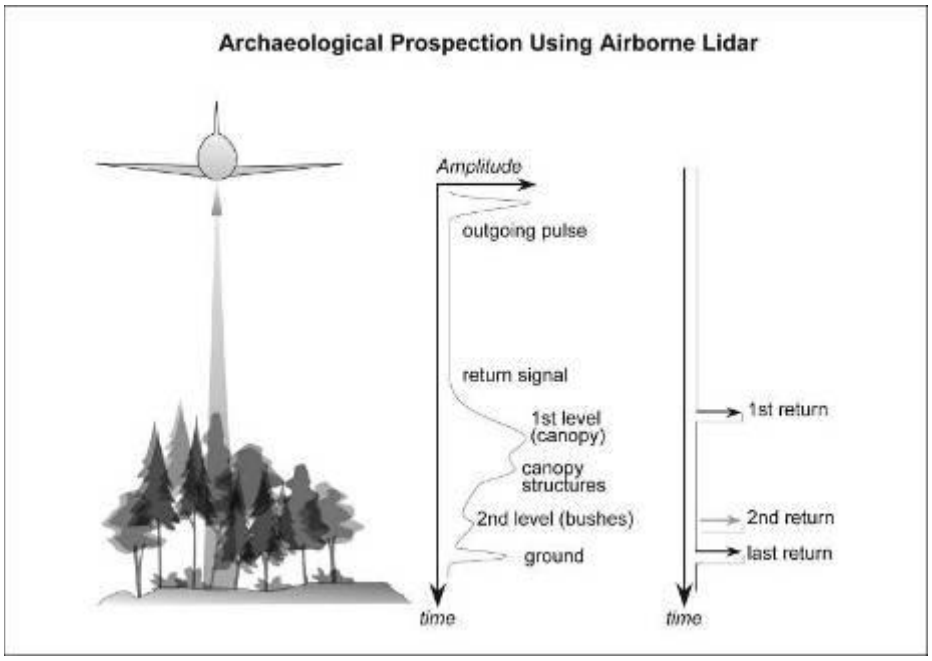

Fig. 1.1. The airborne lidar principle. Archaeological analysis makes use of both the elevation values and the intensity (amplitude) of each returned pulse.

1.2.3 Instrument Used

The lidar data used in the present study were supplied by Infoterra and were collected by a flight on 26th July 2007 flown using an Optech ALTM 2033 Lidar recording two returns (first and last). The Infoterra data was supplied as point cloud xyzi data in LAS format for first and last pulse returns processed to WGS84 datum. The point clouds were processed using Applied Imagery's Quick terrain modeller software to generate first and last pulse digital surface models at 1m spatial resolution, and 8-bit greyscale images derived from first and last pulse intensity values. The DSM and intensity images were further processed using Erdas Imagine 9 by reprojecting to British National Grid and converting ellipsoidal elevation values to orthographic values based on Ordnance Datum.

1.3 AIMS AND OBJECTIVES: INVESTIGATING LIDAR INTENSITY

The present stage of the project aimed to determine which soil and sediment properties affect airborne lidar intensity and the degree and significance of the relationships. Since it proved impossible to co-ordinate the research timetable of this project with the flying programme of a third party, as originally envisaged, a lidar flight was commissioned and undertaken by Infoterra Ltd to collect data in a broad study area selected for this project.

The aims of this section of research can be summarised as:

- To assess how effective lidar is at defining geomorphological and cultural archaeological features within the study areas.
- To compare lidar FP and LP intensity against a range of physical soil parameters.

  To quantify whether any direct linear relationships exist between physical soil parameters and lidar intensity.
- To investigated the impact of data collection parameters on lidar intensity.
- To assess differences in lidar FP and LP intensity values between adjacent swathes to determine if variance is introduced into the intensity data set during data capture.

The flight area was a *c*.50km^2 reach of the middle Trent Valley between Averham and Besthorpe focused on the South Muskham area of archaeological importance (Fig. 1.2). This area was chosen because of the density and quality of archaeological remains, much evidenced as cropmarks and the extent of high quality previous study of both cropmarks (*cf* Whimster 1989) and cultural material associated with these cropmarks (Garton 2002). The flight collected first pulse and last pulse ground elevation and intensity data at 1m spatial resolution. The flight was times for late July, when analysis of existing air-photographs suggests cropmark formation is at its peak.

Simultaneously with the survey flight, land cover, soil and sediment property data was collected at four test sites:

I. Area 3 (NGR: 481250, 359200): A pasture field with existing pasture mark visible at time of field survey.

II. Area 6 (NGR: 478560, 355030): A large palaeochannel within Holme Pierrepont Terrace, left as un-kept farmland.
III. Area 7 (NGR: 478760, 359800): An area of alluvial floodplain with a palaeochannel, left as un-kept farmland.
IV. Area 8 (NGR: 481810, 382970): A ploughed field bare earth site with minor palaeochannel bisecting Holme Pierrepont terrace.

In addition information on weather conditions prior to the flight was collected from all of the weather stations within the county of Nottingham and summary rainfall and soil moisture data were obtained from the Met Office and the Centre for Ecology and Hydrology. Using these data an attempt was made to gauge the impact of prevailing conditions on soil properties.

1.4 AIMS AND OBJECTIVES: INVESTIGATING OFF THE SHELF LIDAR DATA

As originally conceived the project aimed to investigate archive lidar data for selected river corridors of England and Wales held by Environment Agency. In the event, there proved to be no intensity data within the EA archive for areas of interest to the project team and work was restricted to examination of archive intensity data from Infoterra and Network Mapping. This section of the project progressed by more fully investigating intensity data from Infoterra for the Lockington study area, where a large archive of data is already held for the alluvial environment. This process was undertaken in a 'blind' manner, not allowing existing data from the site to hamper interpretation of the lidar intensity

The main aim of this theme was:

- To assess the potential of existing lidar intensity data to provide qualitative information on the character and preservation of palaeoenvironmental and cultural archaeological deposits.

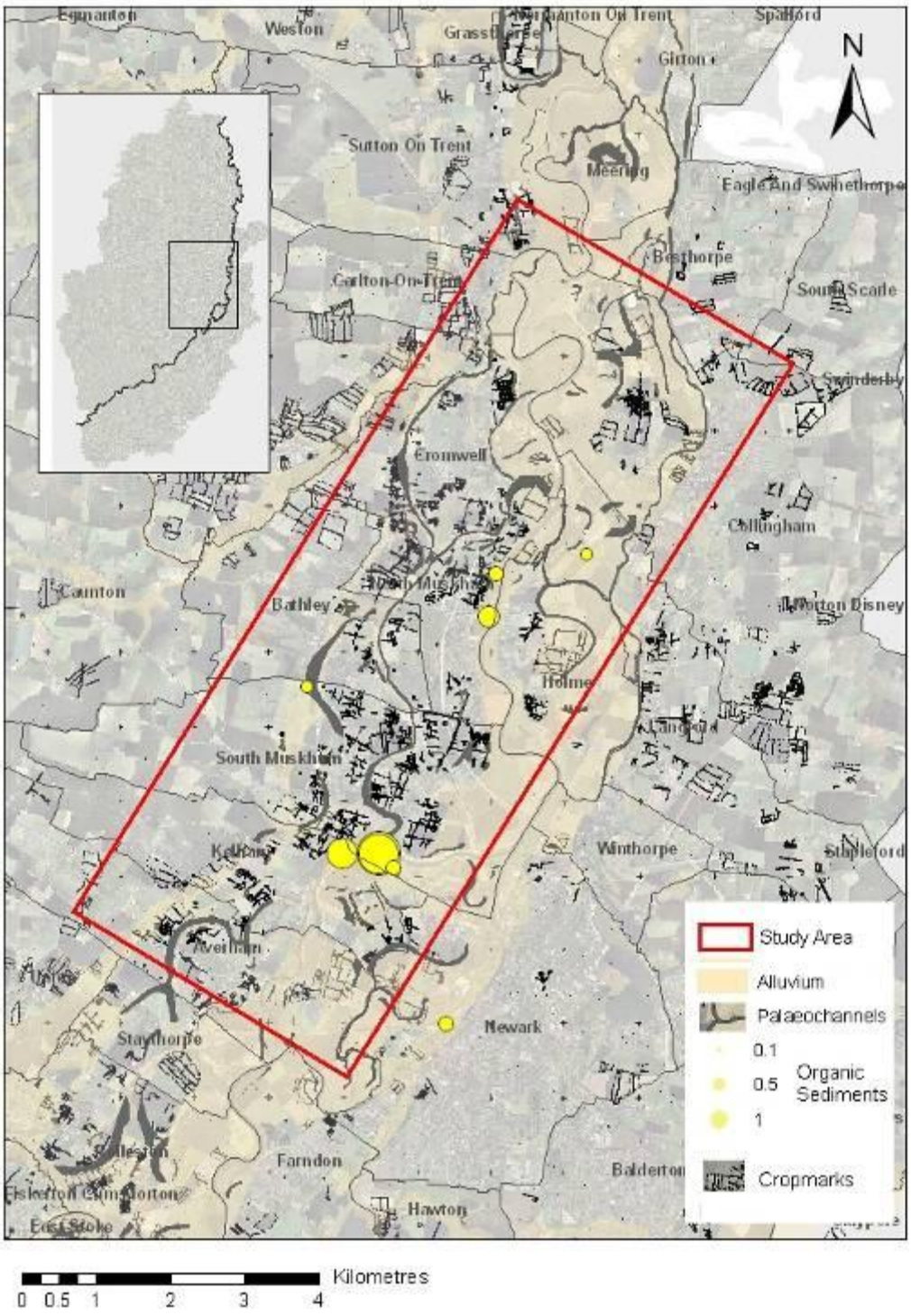

Fig 1.2: The Trent Valley north of Newark showing in red the extent of the airborne lidar survey. Shown also is the extent of the floodplain of the Trent, known palaeochannels and organic sediments within the floodplain and cropmarks mapped by the National Mapping Programme.

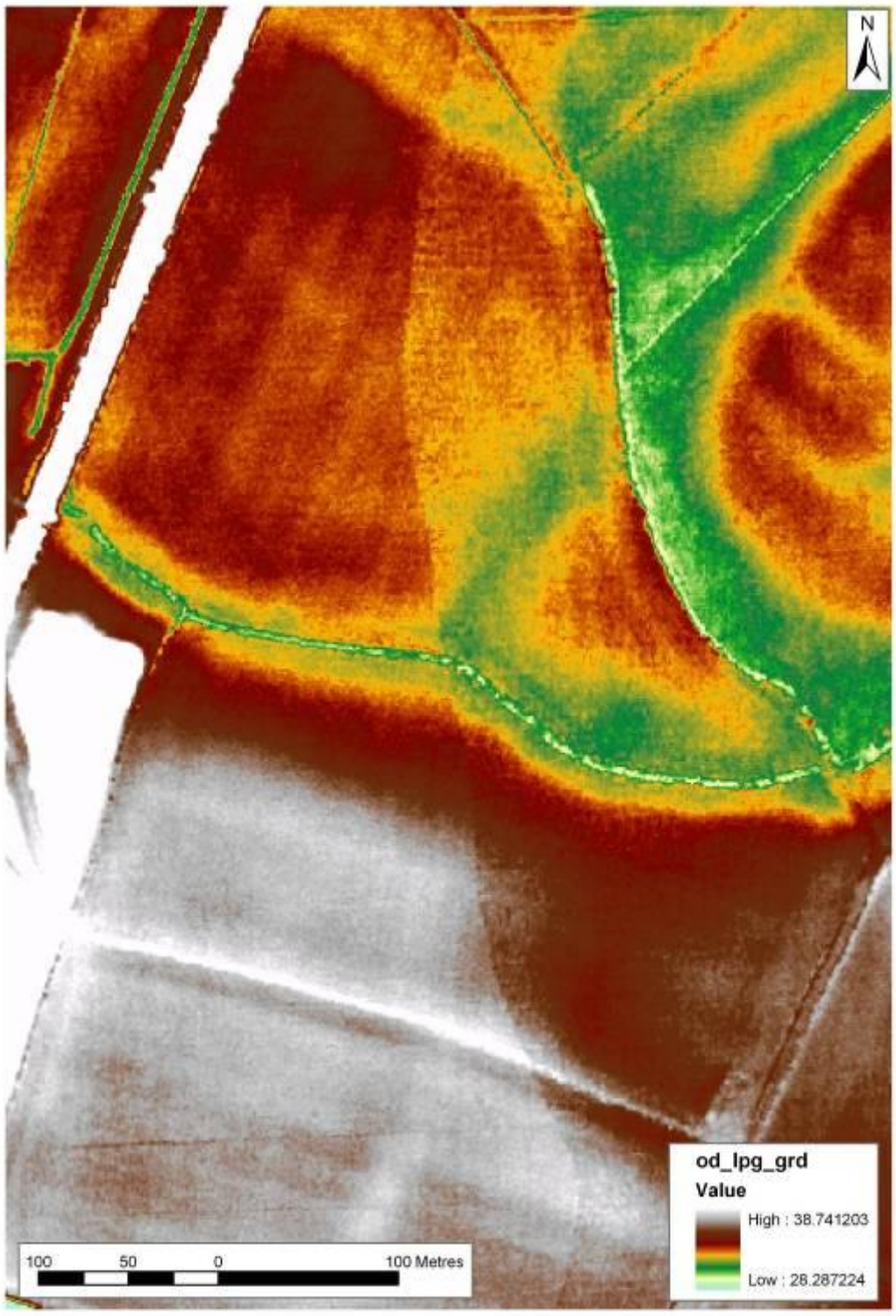

Fig 1.3: Part of the LP DSM model of topography from the Trent Soar confluence zone. There is an obvious join between flight swathes in the data set, running roughly north south.

2 METHOD STATEMENTS

2 METHODS STATEMENTS

2.1 SELECTION OF GROUND CONTROL SITES

In order to assess the ability of airborne lidar intensity data to characterise sediment moisture properties and identify areas indicative of a high potential for organic preservation, a lidar flight was undertaken. The flight covered Lower Trent Valley north of Newark in Trent, between Averham and Besthorpe (Fig. 2.1) and was undertaken in the last two weeks of July 2007, when cropmark formation was liable to be at its peak, allowing a direct comparison between intensity data and potential cropmark features. After initial field visits, eight possible ground control survey sites were selected that could allow measurements to be made of the physical sediment environment for direct comparison to the lidar intensity data. At the time of the flight four of these sites were accessible for fieldwork (Areas 3, 6, 7 and 8 described below), with a range of physical measurements made in each of the survey areas (Figs. 2.1, 2.2 and 2.3).

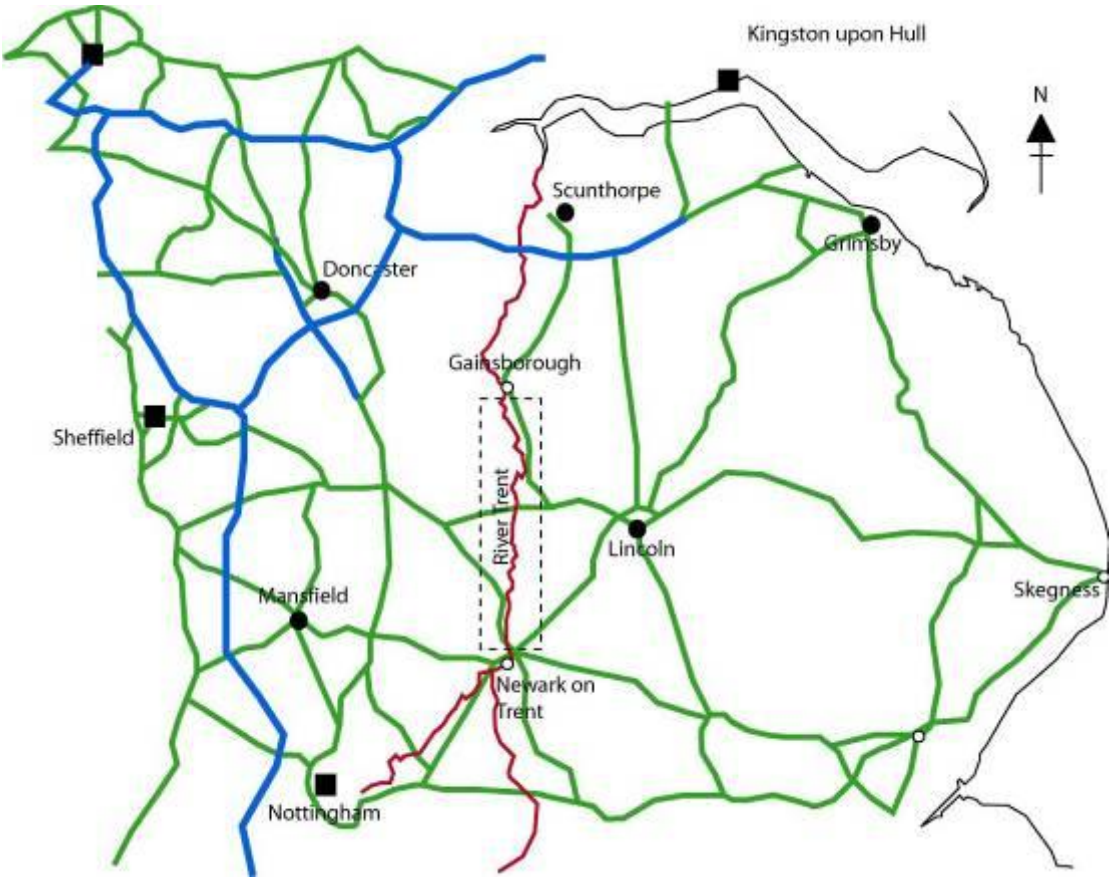

Fig 2.1: Schematic map of the study area of the Trent Valley, boxed area demarks the survey area for this project.

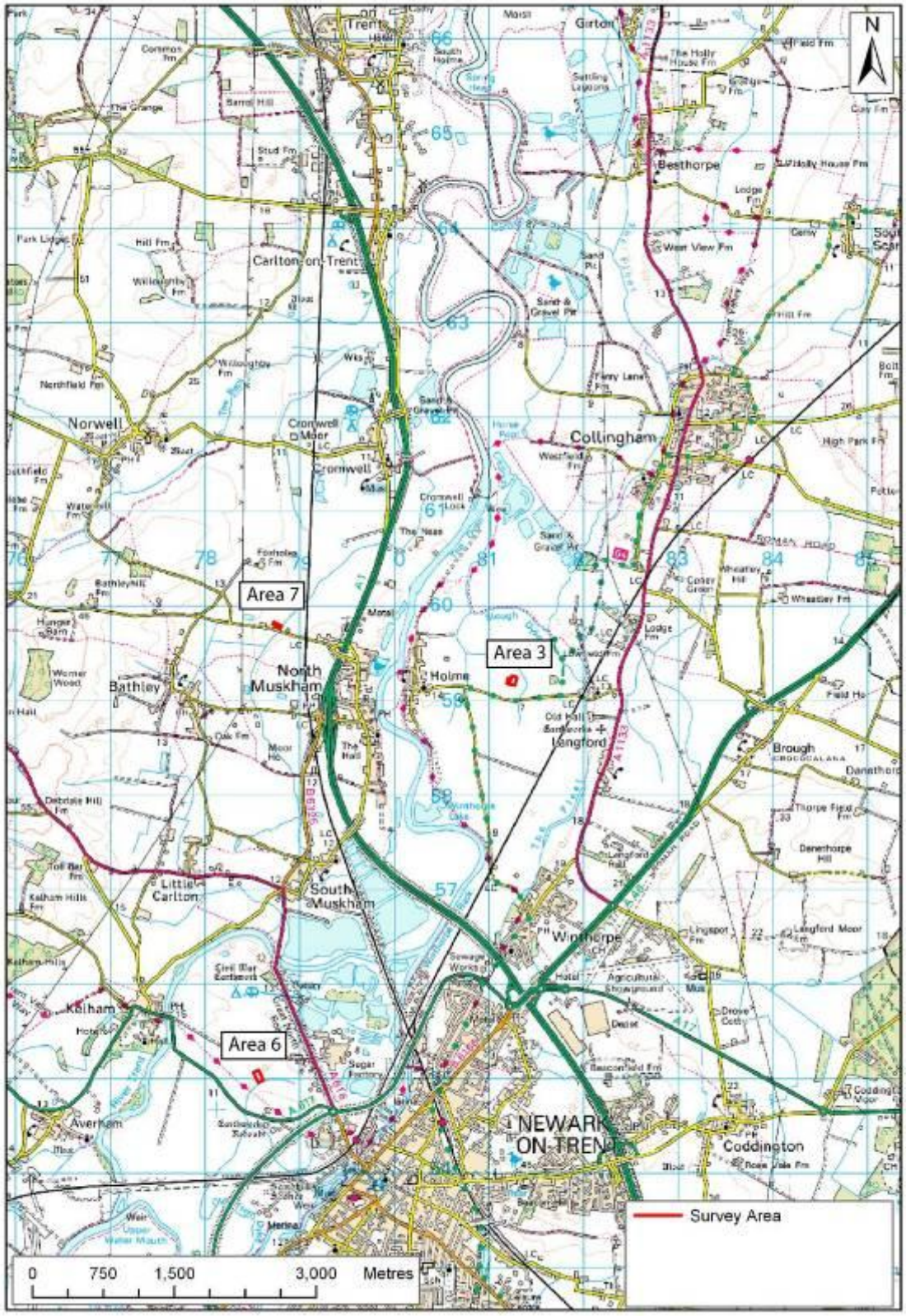

Fig 2.2: The location of the survey Areas 3, 6 and 7 within the Trent valley, north of Newark on Trent.

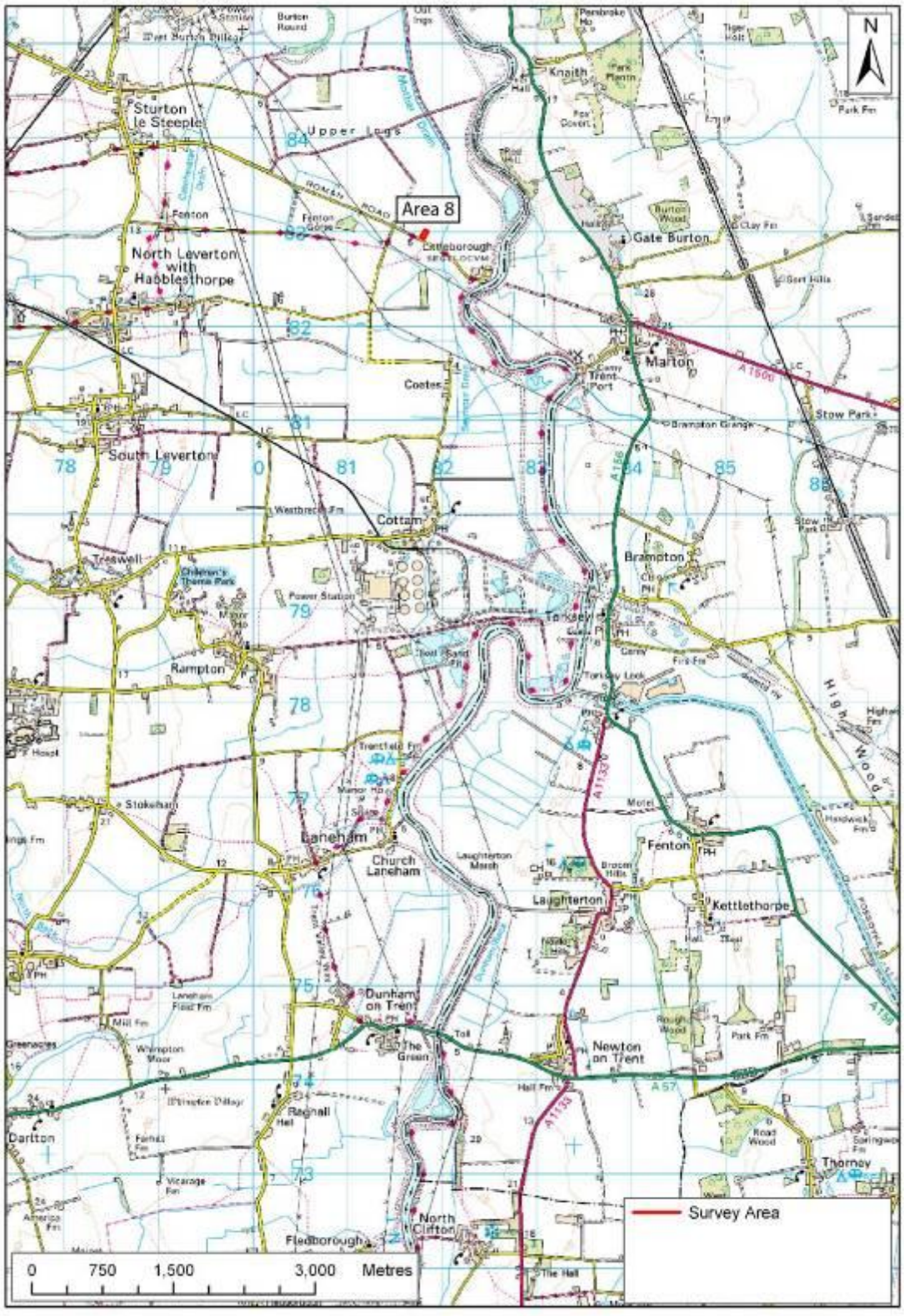

Fig 2.3: The location of survey Area 8, close to Sturton within the Trent valley.

2.1.1 Area 3

Area 3 is located Near Holme, north of Newark on Trent within the Trent valley (NGR: 481250, 359200, Fig. 2.4), on an area mapped as undifferentiated alluvium. The site was selected due to the presence of archaeological cropmark transcribed from aerial photography and recorded by the English Heritage National Mapping Programme. On field inspection a potential archaeological feature was visible within the study area as a pasture mark (Fig. 2.5), although this was in a different location to the original cropmark transcription. The survey of Area 3 investigated the ability of lidar intensity to detect the pasture mark through collection of field data over the pasture mark simultaneously with the lidar flight. Data capture at this site comprised earth resistance survey, soil moisture measurements and samples collected for soil organic analysis. Eight 30m x 30m grids were surveyed for earth resistance. Soil moisture and soil organic samples were taken on a grid measuring 62m by 90m, covering only six of the eight earth resistance grids. It was not possible to undertake a gouge core transect within area 3, due to the field having been recently replanted as improved pasture.

Fig 2.4: Part of the survey grid in Area 3, clearly showing the pasture mark coming from the middle left. Photograph looking north.

2.1.2 Area 6

Area 6 is located just to the north of Newark on Trent (Fig. 2.6), and comprises a palaeochannel adjacent to an area of terrace. The terrace is part of the Holme Pierrepont Terrace common in the middle Trent valley, having been formed in the Devensian, with the alluvium recorded as undifferentiated. The ground cover consisted of wild grasses, dock leaves and thistle, probably left as agricultural set aside ground (Fig. 2.7). This survey area tested whether lidar intensity could detect variations in sediment and vegetation composition between the palaeochannel and terrace geologies. Ground control data was collected to encompass the boundary between the palaeochannel and the area of Holme Pierrepont Terrace, which was visible in the field as a vegetation change and a topographic feature. Field data capture included a 120m long gouge core transect, sampling at 10m intervals. Six 30m by 30m grids were surveyed to capture earth resistance readings, soil moisture content readings and take soil organic samples.

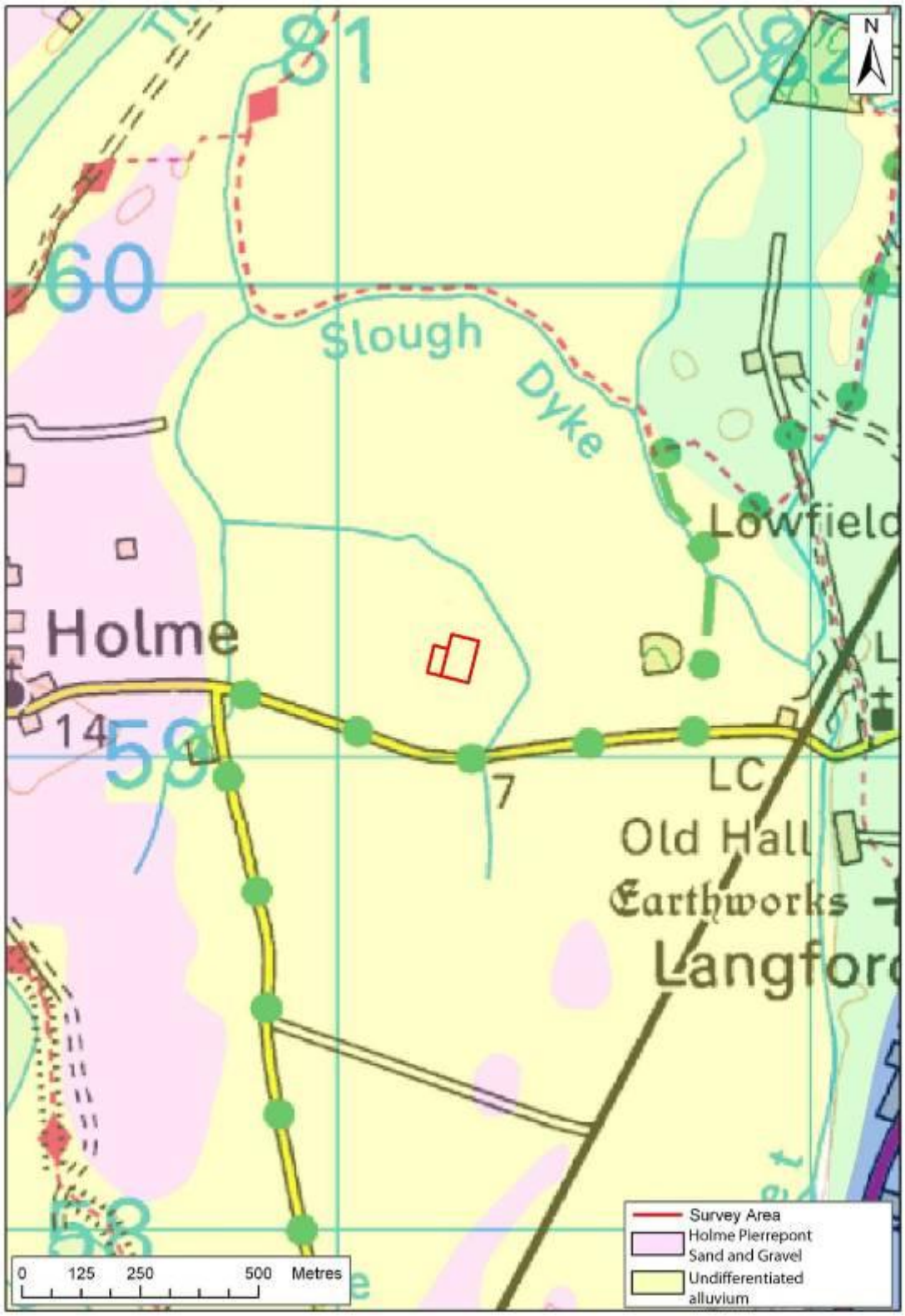

Fig 2.5: Location of Area 3 on BGS 1:50,000-drift geology map.

Fig 2.6: The location of Area 6, on 1:50,000 BGS drift geology map.

Fig. 2.7: Photograph of the palaeochannel in Area 6, with the higher terrace visible in the background as the raised topographic area. Photograph looking west.

2.1.3 Area 7

Area 7 was an area mapped as undifferentiated alluvium with a very small part of Holme Pierrepont Terrace included to the west of the survey area, and with clear changes in vegetation across the surface apparently related to changes in alluvial stratigraphy (Figs. 2.8 and 2.9). Survey in this area aimed to investigate the ability of lidar intensity to identify such changes in vegetation structure and hence underlying geology. The ground cover was set aside farmland and consisted of long grasses, thistle and dock. Ground control data was collected to investigate the changes in vegetation structure within a 32m by 92m area. Earth resistance and soil moisture content data were measured in the field, with soil samples removed for organic analysis. A 90m gouge core transect, sampling at 10m intervals was made across the survey area.

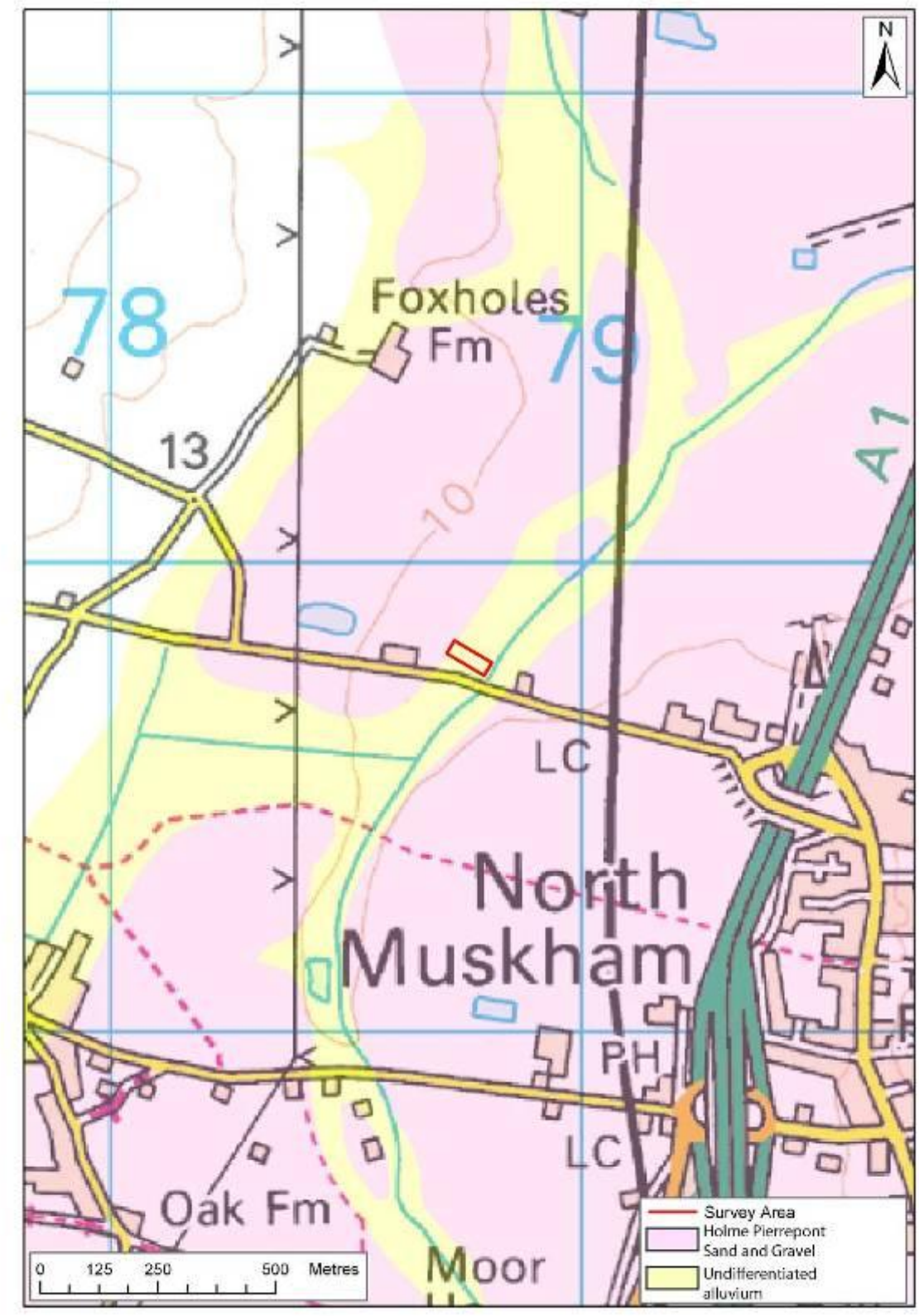

Fig. 2.8: The location of the survey Area 7, close to North Muskham, on 1:50,000 BGS drift geology map.

Fig. 2.9: Photograph of Area 7 showing a linear geomorphological feature dominated by the *Rumex spp.* growth. The photograph is looking east.

2.1.4 Area 8

Area 8 was located in the Lower Trent Valley at Littleborough, where airborne lidar data was collected for the EH ALSF FASTRAC project (PN 5366) as part of the same flight, and with the same parameters, as the present project (Fig. 2.10). Ground control data wqas collected for an area of Hole Pierrepont Terrace where a minor palaeochannel crossed the terrace and focused on the change between the minor palaeochannel and terrace (Fig. 2.11). The field was a recently harvested potato field, with bare soil and visible planting ridges for the potato crop. Here survey aimed to assess the ability of lidar intensity could detect changes in sediment composition affected by the minor palaeochannel and terrace units in bare soil conditions. Ground control data was collected over a 40m by 92m area, covering the palaeochannel and terrace edge. A 90m gouge core transect sampling at 10m intervals was also made. Earth resistance survey and soil moisture content levels were taken, and sediment samples recovered for soil organic analysis.

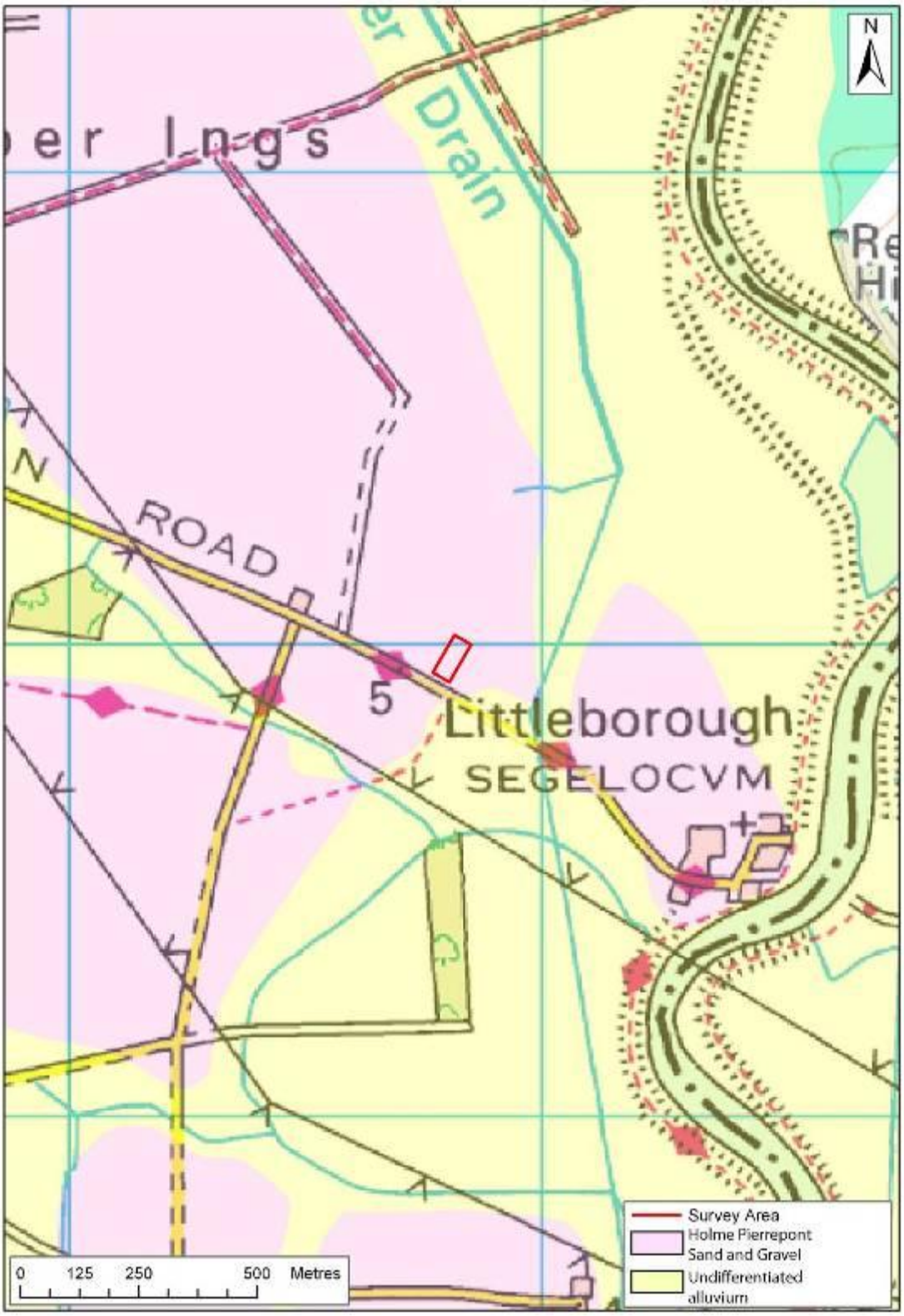

Fig 2.10: Area 8 location map, on 1:50,000 BGS drift geology map.

Fig 2.11: Area 8, showing the minor palaeochannel, demarked by the darker soil colouration, incised into a terrace deposit. The furrows from ploughing are clearly obvious. Photograph look northwest.

2.2 FIELD SAMPLING METHODS

2.2.1 General field methodology

Survey grids were set out using a LEICA RTK differential GPS system. Static observations were recorded over a single point for more than 6 hours at each site, allowing a Rinex correction of spatial location to high precision. All survey work was meticulously undertaken with the setting out and recording of sample locations using the GPS. Each site was photographed to provide a visual record of ground conditions.

2.2.2 Soil moisture content (%)

Soil moisture content data was collected as a proxy for potential sub-surface organic preservation. It was hypothesised that higher surface water contents reflect changes in sub-surface stratigraphy that have a higher capacity for the preservation of organic materials, for example in palaeochannels. A lateral 4m sample interval was selected to would allow relatively large surface areas to be covered, whilst still reflecting gross changes in sediment composition from geomorphological variation. Soil moisture data was measured in-situ using a Delta-T devices Theta Probe, which records aggregated volumetric soil moisture data for approximately the top 0.3m of the soil profile at each surveyed location. Field recorded soil moisture readings were directly compared to the lidar intensity results, to assess the correlation between the two variables. The soil moisture readings were manually entered into

the GIS-based centroid shapefiles for each study area and a raster grid created across the points using a tension spline interpolation function (Fig. 2.12).

2.2.3 Soil organic content (%)

Soil organic content was determined from soil samples collected from the same sample locations as the soil moisture content readings, thus allowing a direct comparison between the two variables. It was hypothesised that higher surface soil organic content reflects changes in sub-surface stratigraphy that have a higher capacity for the preservation of organic materials, such as in palaeochannels. A lateral 4m sample interval was selected that would allow relatively large surface areas to be covered, whilst still reflecting gross changes in sediment composition from geomorphological variation. The soil organic contents were directly compared to the lidar intensity results, to assess the correlation between the two variables.

A hand held t-bar screw auger was employed for sample retrieval, only sampling the top 5cm of soil. Sediment from each sample was transferred to a labelled sample bag and freeze dried. After freeze drying samples were sieved in a 2mm stainless steel sieve. Crucibles were dried overnight at $109^{O}C$ to remove any excess moisture. The crucibles were weighed (a) and then approximately 1g of the $\leq$2mm soil fraction was added to each crucible. The crucibles were again dried overnight at $109^{O}C$ to remove any moisture from the sediment. The crucibles and samples were weighed (b) and then placed in a muffle furnace at $450^{O}C$ for 4 hours. The crucibles and soil sample were then weighed again (c). The % organic mater of the soil was then calculated using the formula:

$$\% \text{ Organic matter} = \frac{(a - c)}{(a - b) * 100}$$

The soil organic content values were manually entered into the centroid shapefiles for each study area (see above) and a raster grid created across the points using a tension spline interpolation function (Fig. 2.13).

2.2.4 Earth resistance survey

Earth resistance data was collected as it allowed geomorphological changes to be seen via resistance readings, allowing clear definition sedimentary properties related to landform elements such as palaeochannels, terraces, etc. It also allowed large areas to be covered with a data resolution equivalent to that of the lidar data (a 1m data posting). As earth resistance is a shallow prospection tool, it allowed clarification and definition of any archaeological and geomorphological features to a depth of c. 75cm. Earth resistance data were collected using a Geoscan Research RM15 Resistance Meter and standard twin probe array. In all areas a grid size of 30m by 30m was used. Data was collected at a 1m sample interval, with a 0.5m probe separation, using 1m zig-zag traverses. Marked ropes were used to ensure accurate data collection. Data was downloaded into Geoplot (ver. 3.1) for processing, with further data manipulation in Surfer (ver. 8.0). From Surfer data was exported as XYZ ASCII files and placed into ArcGIS.

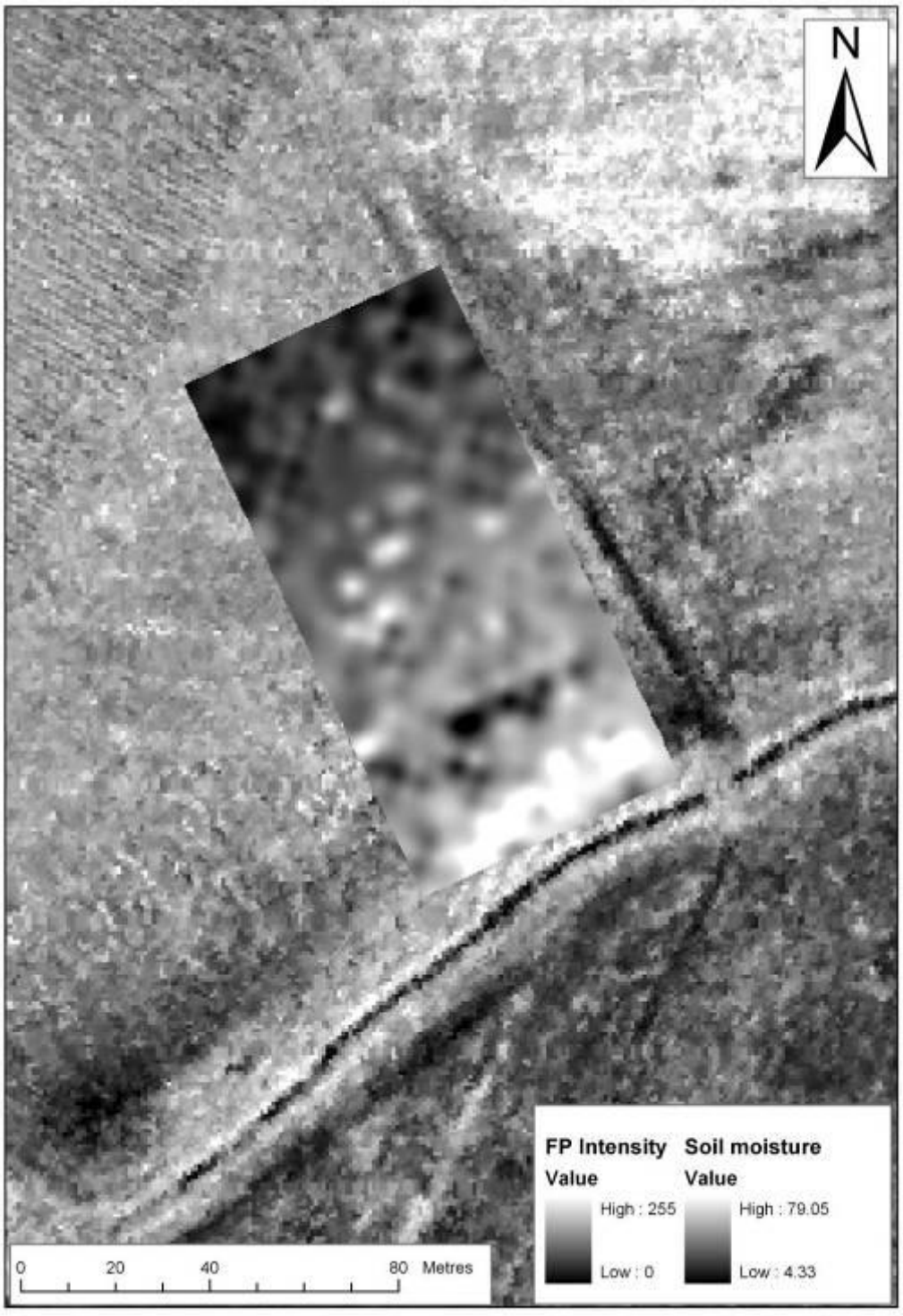

Fig. 2.12: An example soil moisture surface produced from the data in Area 6, superimposed on FP Intensity.

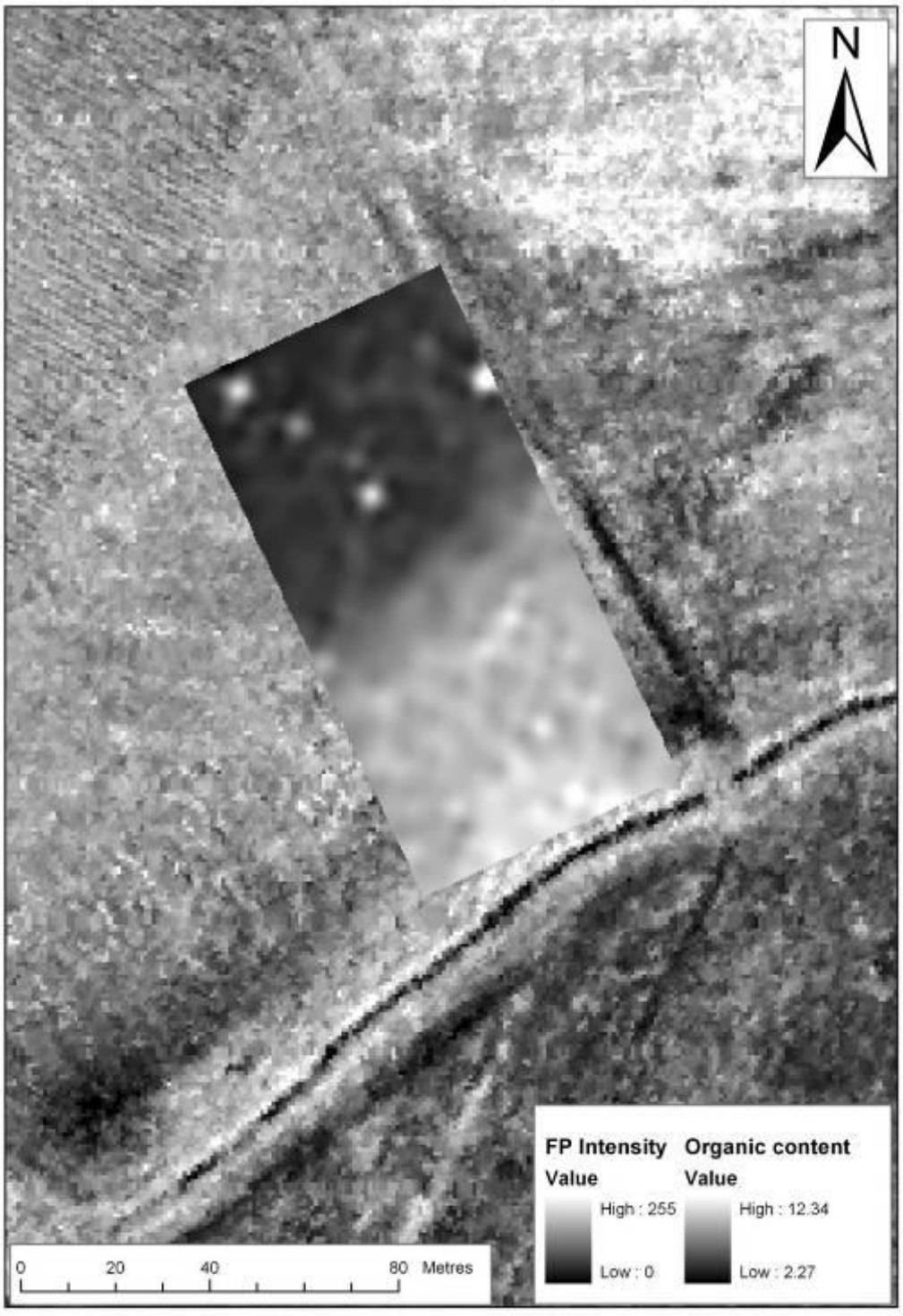

Fig 2.13: An example soil organic surface produced from the data in Area 6, superimposed on the FP intensity model.

2.2.5 Gouge core transect

Gouge core transects were undertaken on three of the four survey sites. The application of gouge sampling allowed variation in the sub-surface sediment architecture to be understood. This effectively ground truthed the preservation potential of different parts of the survey areas and the depth and complexity of the sedimentary sequences. The gouge core transects have allowed a visual comparison between variations in surface intensity and deeper sediment stratigraphies. Gouge core transects were undertaken using a 3cm diameter gouge core, coring at 10m intervals. Major changes in sediment composition were recorded, with stratigraphic transects produced from the results. Sediment logging occurred to the top of the sands and gravels.

2.3 AIRBORNE LIDAR PROCESSING

Lidar data was collected on 26th July 2007 using an Optech ALTM 2033 lidar recording two returns (first and last). Data was supplied by Infoterra as point cloud xyzi data in LAS format for first and last pulse returns processed to WGS84 datum. The point clouds were processed using Applied Imagery's Quick Terrain Modeller software to generate first and last pulse digital surface models at 1m spatial resolution, and 8-bit greyscale images derived from first and last pulse intensity values.

The DSM and intensity images were further processed using Erdas Imagine 9 by reprojecting to British National Grid and converting ellipsoidal elevation values to orthographic values based on Ordnance Datum.

The lidar DSM were imported into a geographical information system (GIS) developed using ESRI ArcGIS 9.2 to allow direct comparison with digital HER data and digitised, geocorrected aerial photography. Visual interpretation of the lidar data was based on the examination of shaded relief images generated within ArcGIS to identify anthropogenic features. Shading was calculated from four different azimuths, northwest (standard shading) north, northeast and east, since experimentation showed that some features were not evident if the DSM was shaded only from a single direction. Further analysis of the lidar DSM using carefully constrained colour ramps to differentially shade areas of relatively restricted variation in relief was used to assist in identifying geoarchaeological features.

2.3.1 GIS

GPS data was imported from fieldwork into ArcGIS to allowing the location of the survey areas. Shapefiles were created to define features such as edges of surface areas and also create 4m and 1m centroid files for the export of quantitative data. Data entered into the GIS included earth resistance, soil moisture content, soil organic content, Lidar FP and LP Intensity, Lidar DSM, 1:50,000 geological maps, 1:10,000 OS maps and 1:50,000 OS maps. The GIS allowed integration and qualitative visual inspection of data for each of the survey areas.

2.3.2 Statistical Analysis

Advanced statistical analysis was undertaken using data exported from ArcGIS as centroid files and processed in SPSS (ver. 15). Scattergraphs were produced to investigate linear relationships between variables. The strength of correlation was tested through computing Pearson Correlation Coefficients, with significant correlations flagged at 0.05 and 0.01 levels.

2.4 ANALYSIS OF DIRECTION OF FLIGHT

Lidar intensity values display a variety of responses to different sediment architectures. However, great variation in intensity response has been witnessed in single geomorphological units, indicating that variance has been introduced into the lidar data through factors not related to sediment architecture (Fig 2.14 and 2.15). Whilst some of this variance may be accountable by physical phenomena such as standing water, vegetation changes, etc, some is a product of data collection.

The largest potential source of variance in lidar data caused by instrumentation is the different directions of flight swathes undertaken during data capture. To test differences in response between flight data swathes the following methodology was employed. Areas of homogeneous land units were sought within the flight area that had a visually obvious join between adjacent flight swathes (Fig. 2.16). This was done through analysis of the FP intensity surface model within ArcGIS, rather than through field visits. A homogeneous land unit within this context was selected as a field with no visually obvious change in intensity other than that caused by different swathes. In total three study areas were selected within the lidar surface model (Fig. 2.16, Areas A, B and C).

Within ArcGIS rectangular polygons were created of identical size and orientation, each located within a different swathe. In order to undertake statistical analysis identically sized population were required from each polygon. However, the differences in data collection density between adjacent swathes meant that similarly sized polygons contained different population sizes.

To overcome this problem sample intensity values were extracted from the FP intensity surface model (Fig. 2.17). Sample polygons were created as a shapefile and with a 1m grid interval. Centroids were extracted from each grid cell within these polygons and assigned values from the FP intensity surface mode. This allowed the collections of point samples of similar size from adjacent flight swathes. The separate populations were then subject to means testing through the use of a One Way Analysis of Variance (ANOVA), allowing variance to be compared between and within populations.

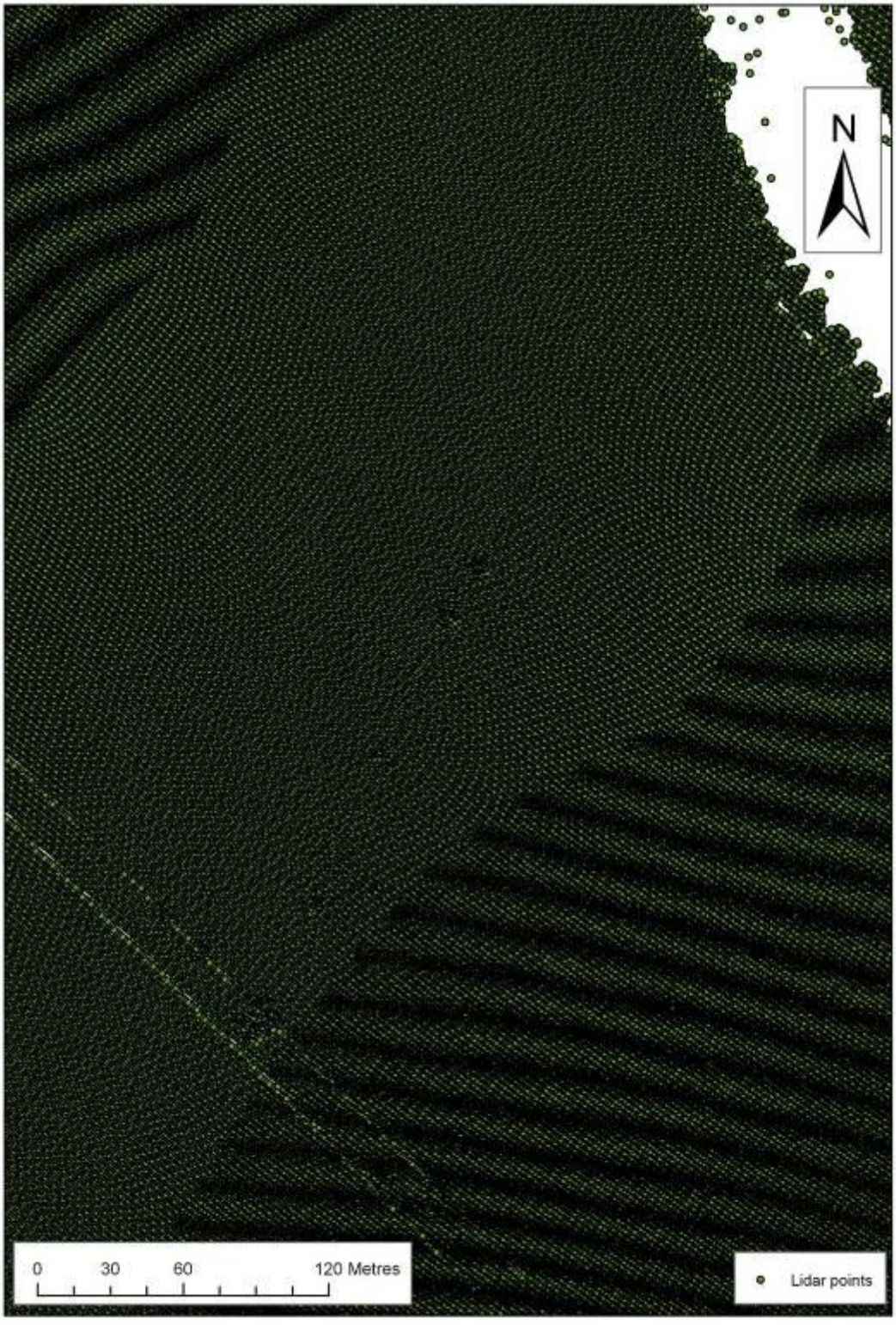

Fig. 2.14: The data collection points of adjacent swathes for the lidar intensity. There are clearly three different types of data collection in three different swathes within this small area.

Fig. 2.15: The same area as Fig. 2.14, with the FP intensity model displayed at 25% transparency, with underlying lidar point data.

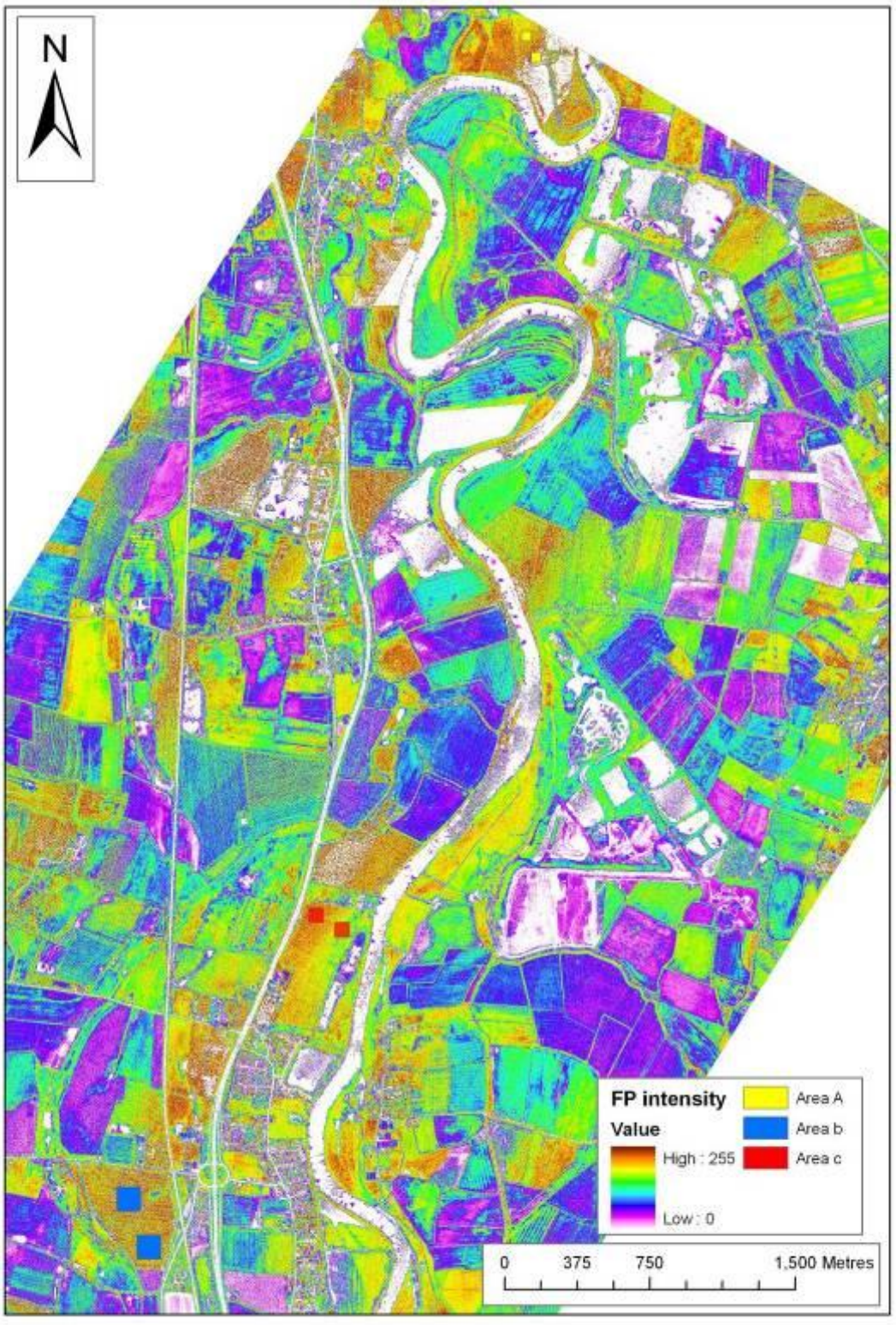

Fig 2.16: The three study areas for the analysis of flight direction, within the flight corridor.

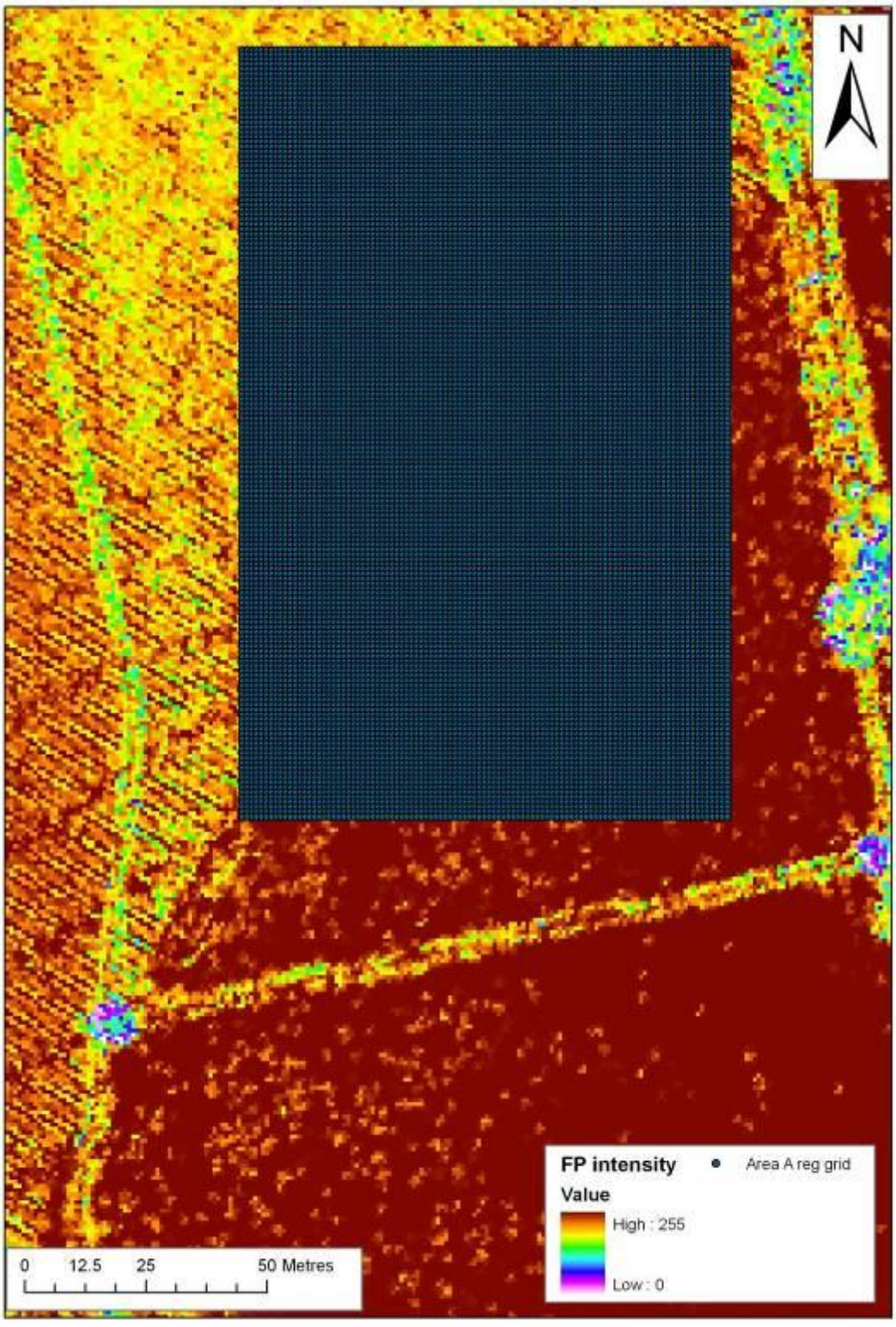

Fig 2.17: Homogenisation of different levels of data capture between adjacent flight swathes through extraction of XYZi values on a 1m posting from underlying FP intensity surface model.

2.5 IMPACT OF WEATHER AND GROUND CONDITIONS

The weather in July 2007 presented extreme conditions, with unprecedented May-July rainfall across much of the county and many catchments close to saturation in July (CEH 2008). The month, the wettest on record since 1888, saw extensive and protracted flooding in many areas. The extreme conditions rendered much of the month of July unsuitable for lidar data collection; when fine weather and clear skies finally prevailed, ground conditions were far from ideal for the formation of cropmarks, and near-saturated groundwater levels can be expected to have reduced the usual contrast in soil moisture levels between adjacent sediments with differing drainage characteristics.

2.5.1 Rainfall

The year preceding July 2007 had already seen high levels of rainfall, with Nottinghamshire receiving in excess of 130% of its usual rainfall over the previous twelve month period. Rainfall records from the Met Office show that in July 2007 both the average daily and the monthly total of rainfall in Nottinghamshire greatly exceeded the levels of preceding years and the county experienced between 120 and 200% of the average monthly rainfall for July (based on 1971-2000 figures; table 2.1). Across the country the accumulated May-July rainfall totals were exceptional (Fig. 2.18); in many places the equivalent of 6 months average rainfall fell in this period.

Year	Month	Monthly rainfall (cm)	Average daily rainfall (cm)
2004	May	1.954681	0.063054
	June	2.549331	0.084978
	July	3.22112	0.103907
2005	May	1.407317	0.045397
	June	1.993714	0.066457
	July	2.896811	0.093446
2006	May	3.23892	0.104481
	June	1.191547	0.039718
	July	1.736797	0.056026
2007	May	2.107639	0.067988
	June	6.775862	0.225862
	July	4.567755	0.147347

Tab 2.1: Rainfall for the months of May, June and July, from 2004, through to 2007. Field survey and lidar flight for this project occurred during July 2007. Source Met Office daily land surface data for Nottinghamshire. Used with permission.

2.5.2 Ground Water and Soil Moisture Levels

Soil moisture deficit levels in July 2007 were amongst the lowest on record, in many places 60-100mm below the 1961-90 end-of-July average (CEH 2008; Fig 2.18). Summer groundwater levels exceeded previous records and in many areas aquifers experienced substantial and unprecedented levels of summer recharge. In Nottinghamshire average soil moisture deficit (SMD) levels were in the 15-30mm range. Such levels are likely to have severely compromised cropmark formation, which usually occurs on when SMD is in excess of 40mm (Jones and Evans 1975, 7).

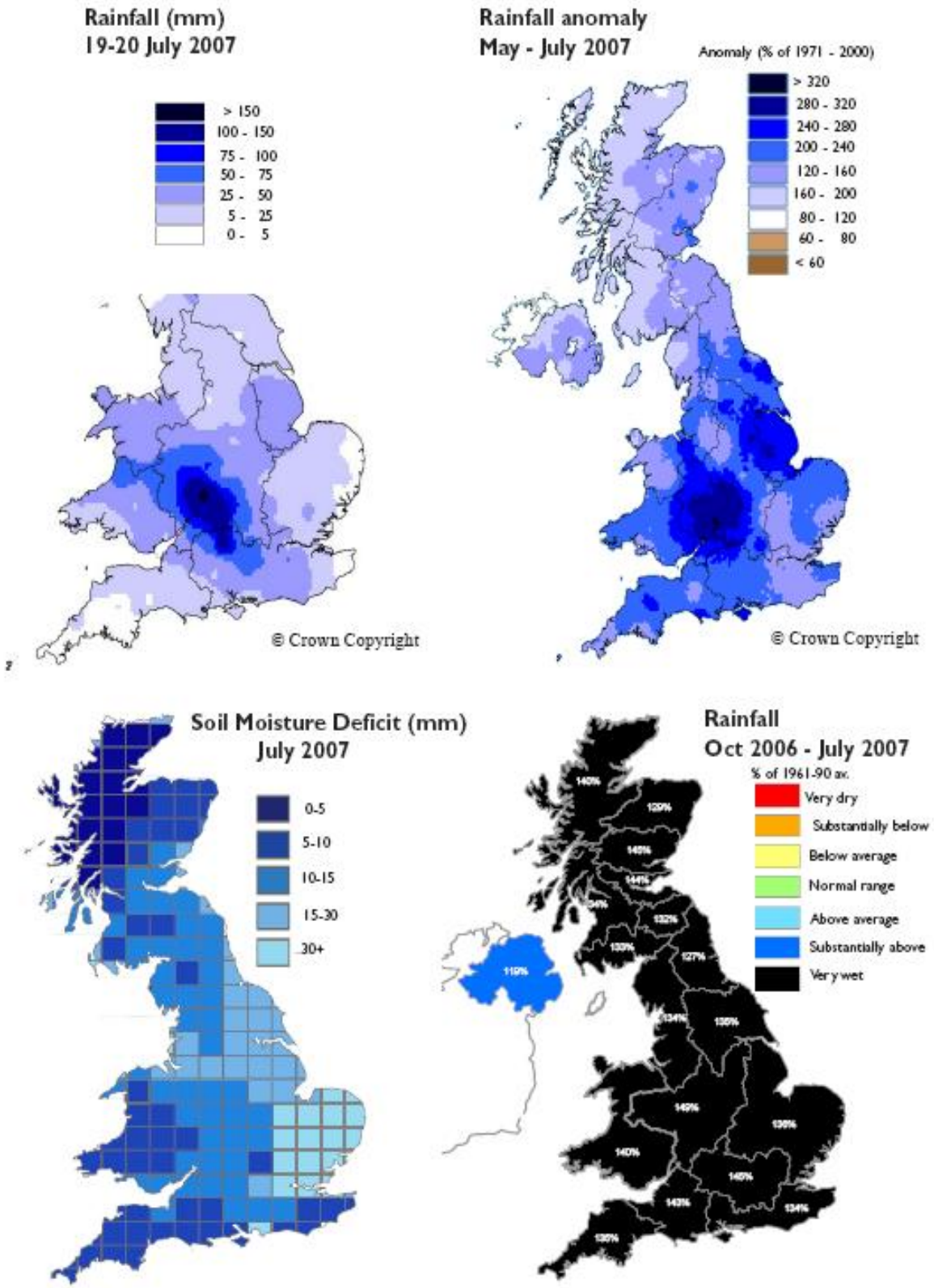

Fig 2.18. Summary rainfall and soil moisture maps for Great Britain for July 2007 (maps © CEH 2008).

3 RESULTS: INVESTIGATING AIRBORNE LIDAR INTENSITY

3 RESULTS INVESTIGATING AIR BORNE LIDAR INTENSITY

3.1 AREA 3

3.1.1 Area 3 geological background

Area 3 is located on an area mapped as undifferentiated floodplain alluvium (Fig. 3.1). The survey area was relatively flat, with little topographic variation. The survey grid in Area 3 had field survey undertaken in heavy rain and also bright sunny weather, with much standing water on the surface.

3.1.2 Area 3: Visual qualitative analysis

The analysis of the Area 3 data set begins with a qualitative visual examination of the data groups before a quantitative exploration.

Lidar

The study area location is shown on the lidar FP DSM (Fig. 3.2), FP intensity (Fig. 3.3) and LP intensity (Fig. 3.4). The DSM reveals little in the way of topographic variation within the study area. Both the FP and LP intensity images define a pasture mark (ie a variation in the colour and growth of the pasture covering the survey area indicating an underlying antropogenic archaeological feature) as a lighter band curving through the survey grid, towards the north of the survey area. Other lighter linear features are apparent within the survey grid, and this is a result of trampling at the grid edge during data capture.

Earth Resistance

The earth resistance survey clearly defines a ditch running through the survey area, correlating with the pasture mark (Fig. 3.5). Whilst the topography from the DSM shows little variation, the earth resistance data clearly shows much greater subtly in sediment composition across the survey area. Areas of higher resistance to the northeast and southwest of the survey indicate terrace deposits, and a lower resistance linear feature trending northwest to southwest potentially indicates a palaeochannel.

The details of the earth resistance data is not matched by that seen in the FP and LP intensity data sets (Figs. 3.6 and 3.7). The low resistance ditch feature evident as a pasture mark, whilst clearly visible in the earth resistance data, is only just visible in the intensity data sets. Further to this, the areas of higher resistance terrace deposits and lower resistance potential palaeochannel are not visually evident in the intensity data sets.

Soil Organic Content and Soil Mositure

The surface model produced from the soil organic data shows lower soil organic content to the north of the study area. However, overall the soil organic data shows little correlation to either the DSM (Fig. 3.8), FP intensity (Fig. 3.9) and LP intensity (Fig. 3.10) data sets. The strongest visual correlation comes between the features identified in the earth resistance survey and the soil organic data, with the areas of terrace having lower soil organic content and the potential palaeochannel having slightly elevated organic content. The surface produced from the soil moisture data produces a curious distribution, with no real structure evident in the data. There is little correlation between the soil moisture values and the DSM (Fig. 3.11), FP intensity (Fig. 3.12) and LP intensity (Fig.3.13).

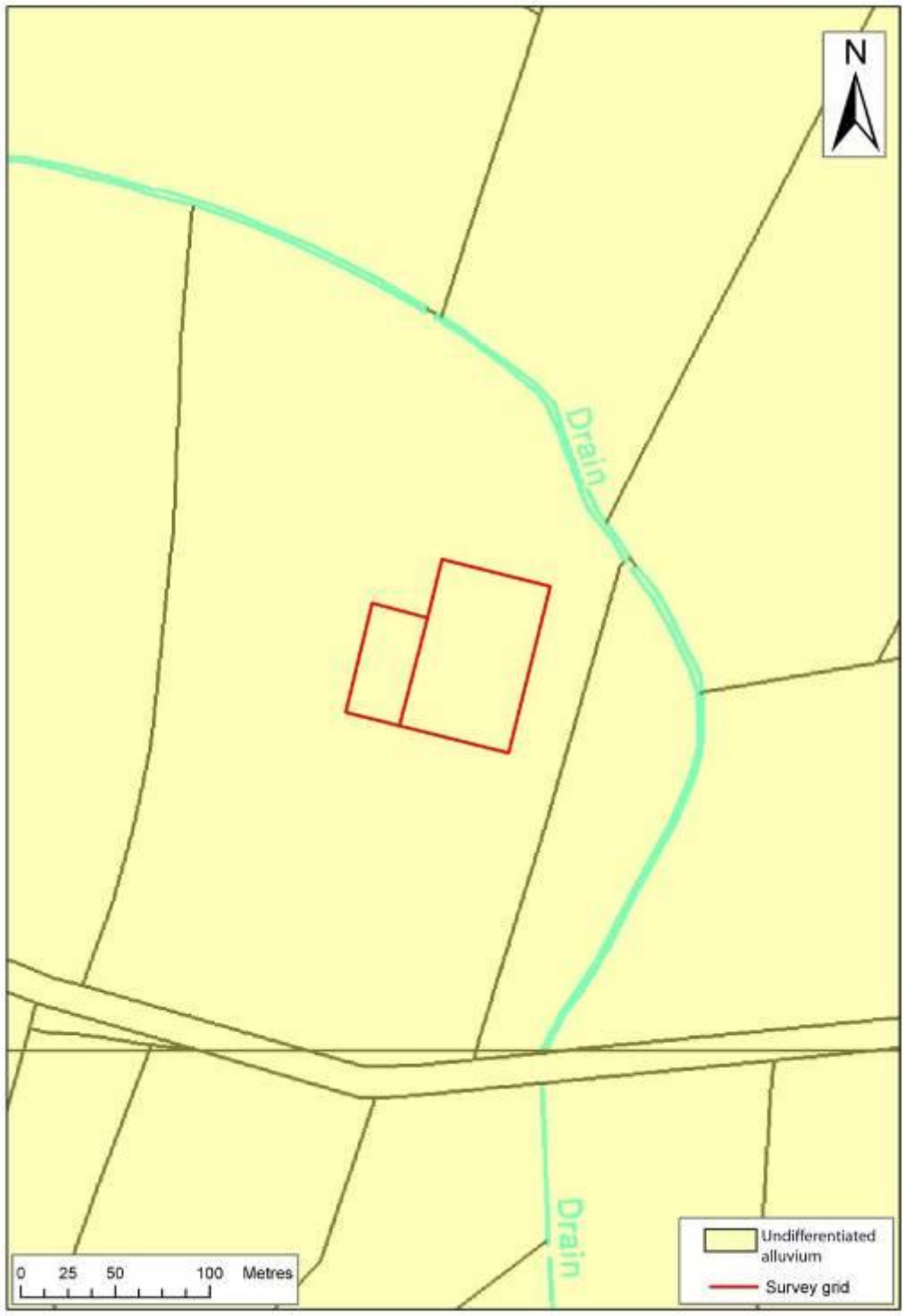

Fig. 3.1: The survey grid of Area 3 shown against the 1:50,000 BGS map. As can be seen Area 3 is located on a segment of undifferentiated alluvium.

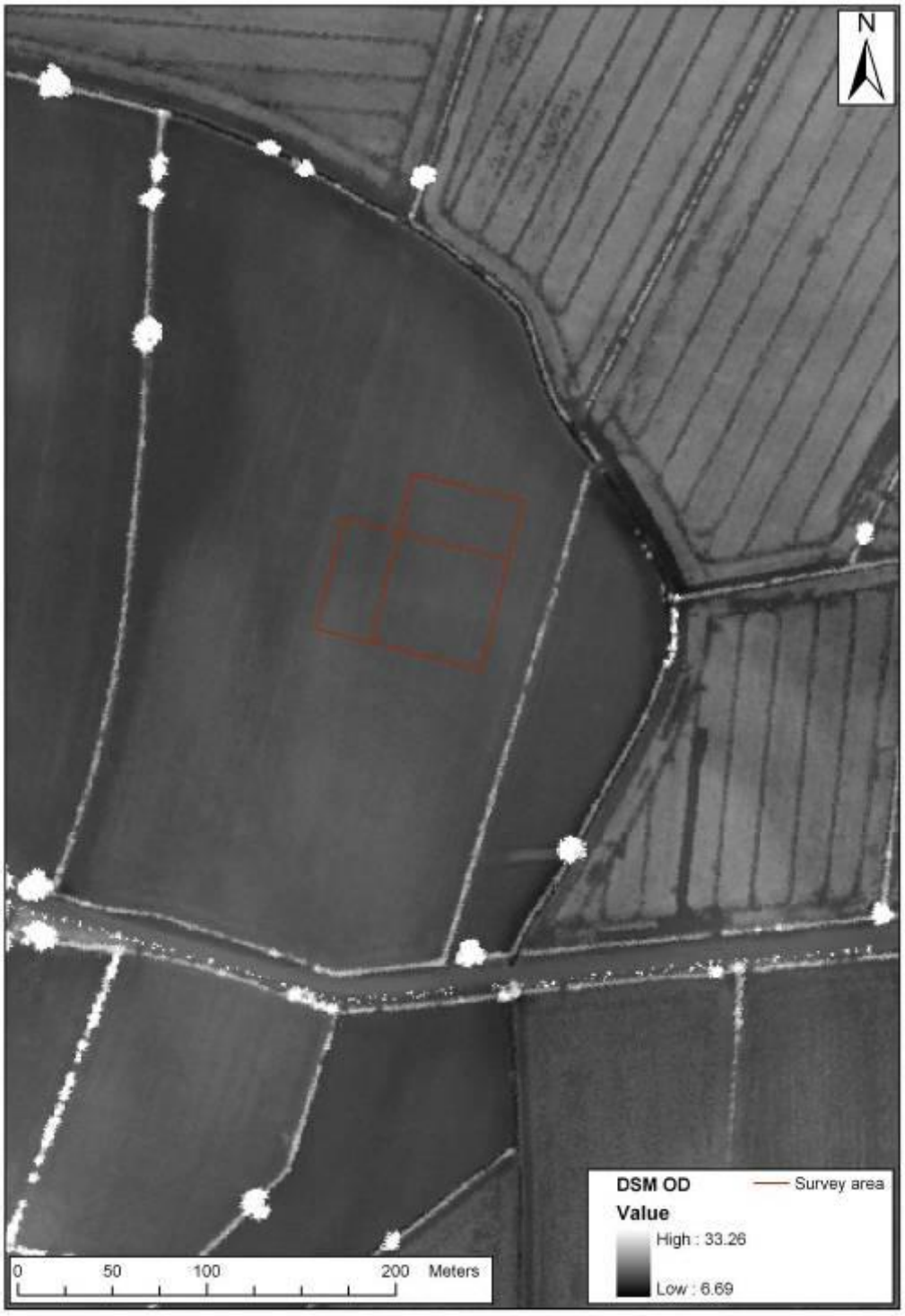

Fig 3.2: The survey area shown on topography (FP DSM).

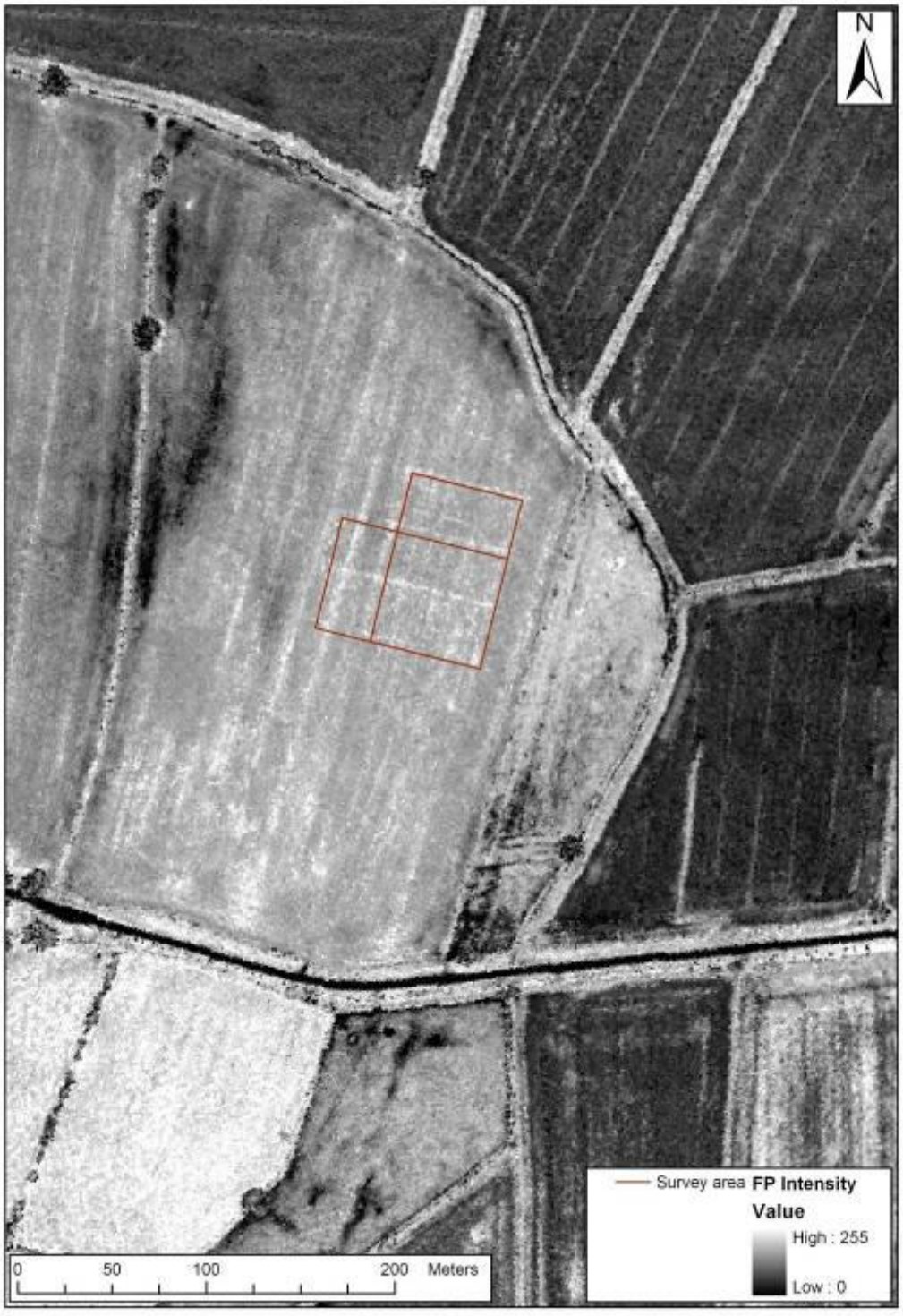

Fig 3.3: The survey area shown on FP intensity.

Fig 3.4: The survey area shown on LP intensity.

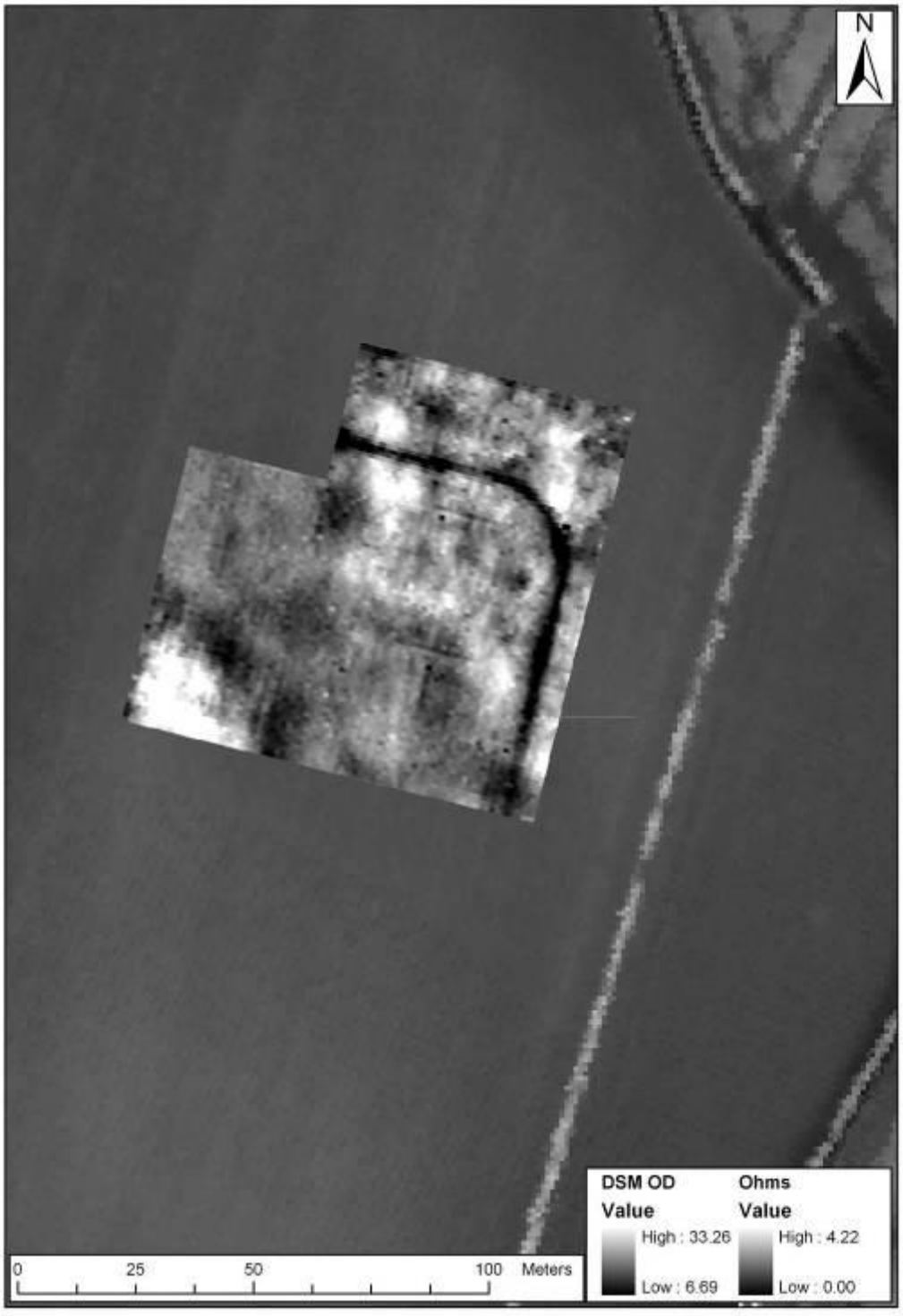

Fig 3.5: Earth resistance Ohms on DSM OD.

Fig 3.6: Earth resistance Ohms on FP intensity.

Fig 3.7: Earth resistance Ohms superimposed on LP intensity.

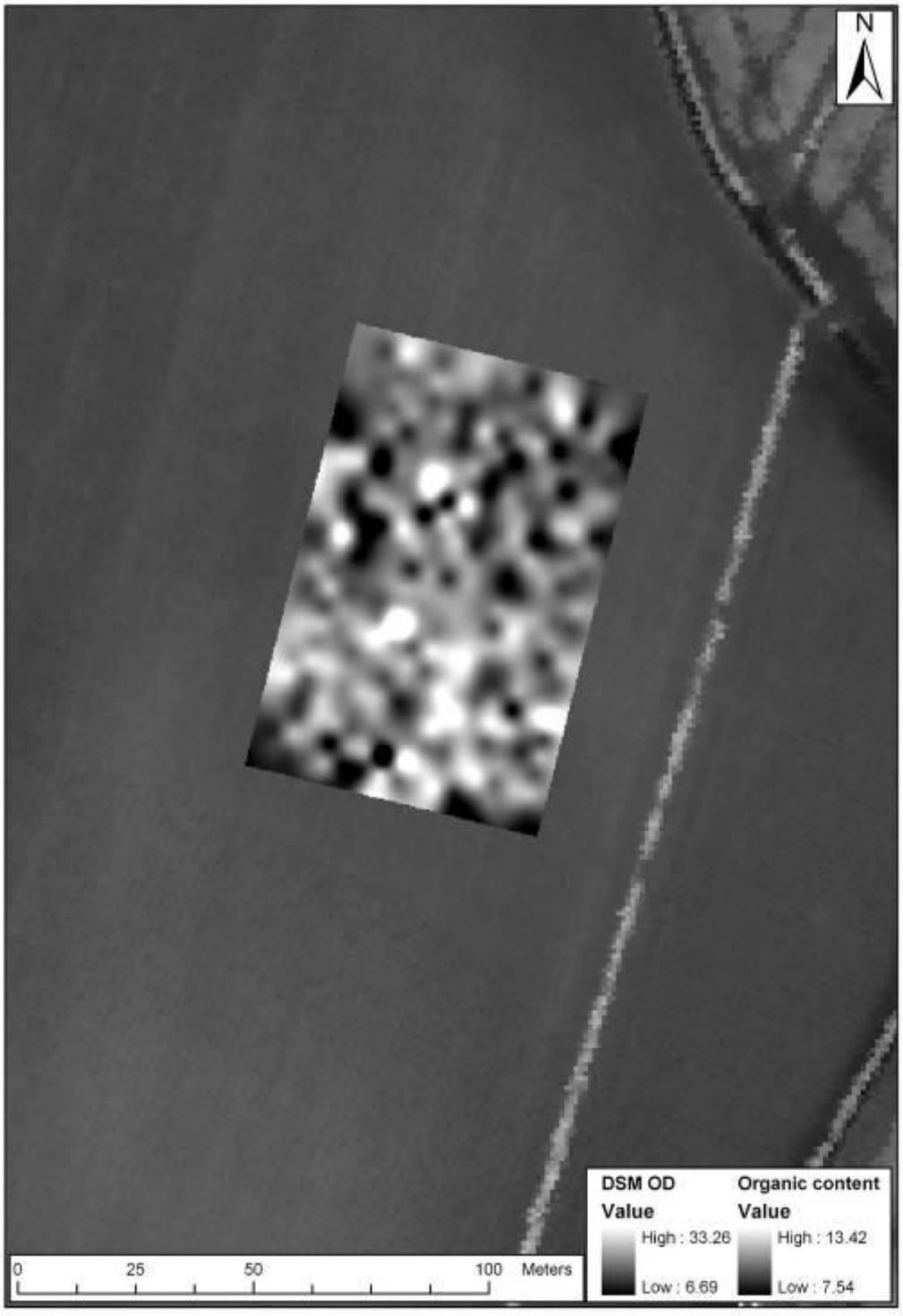

Fig 3.8: Organic content superimposed on DSM OD.

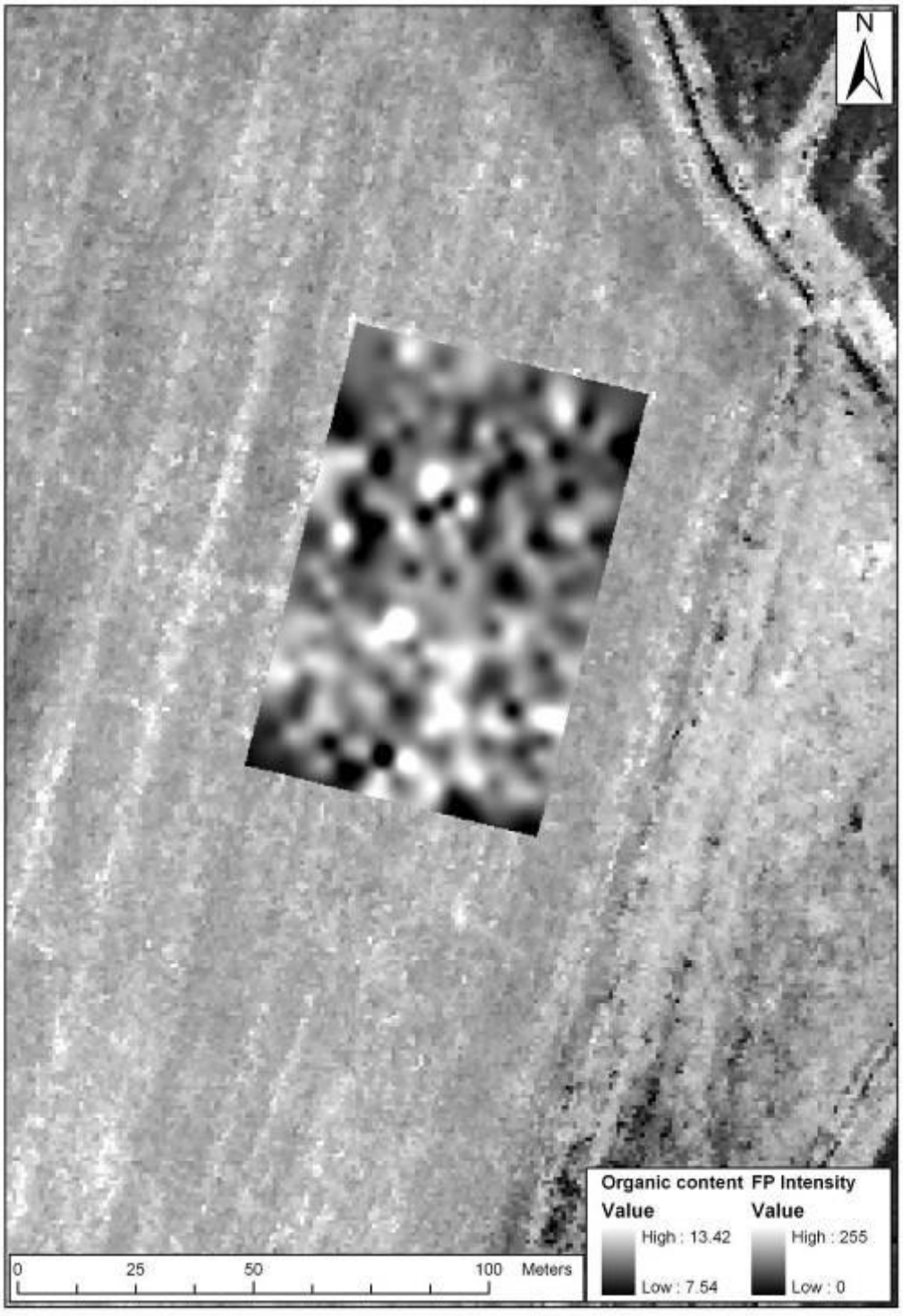

Fig 3.9: Organic content superimposed on FP intensity.

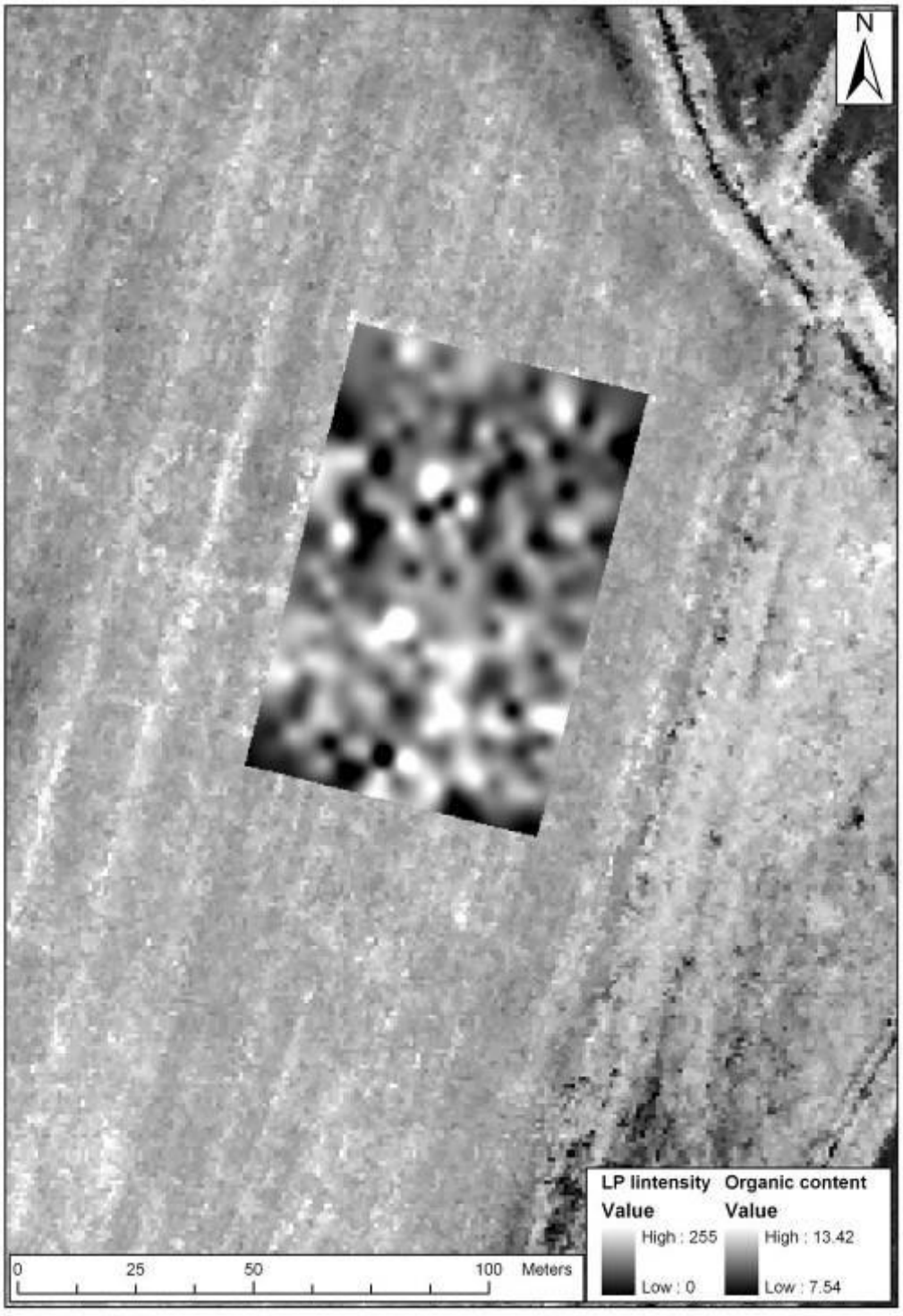

Fig 3.10: Organic content superimposed on LP intensity.

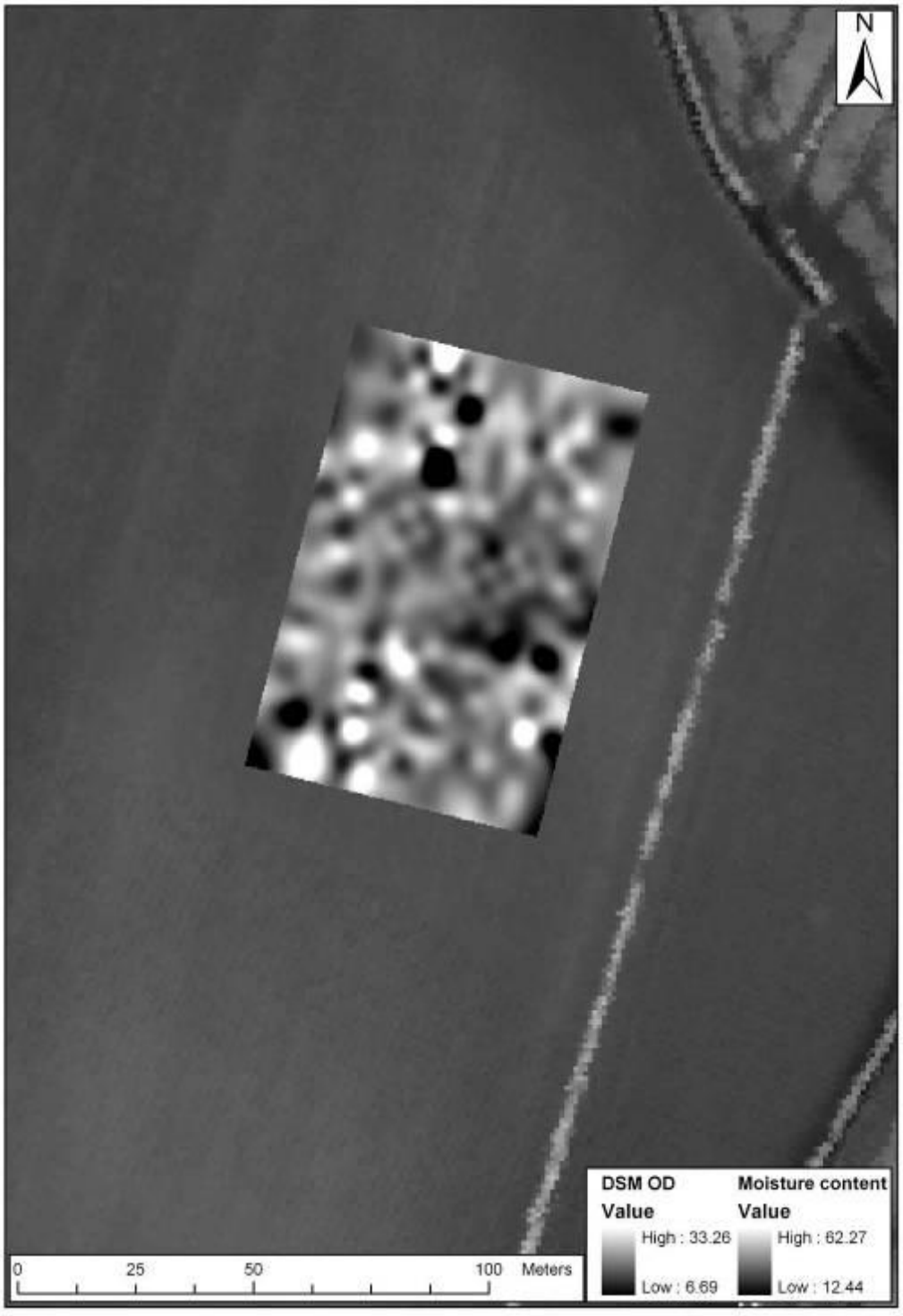

Fig 3.11: Soil moisture content superimposed on DSM OD.

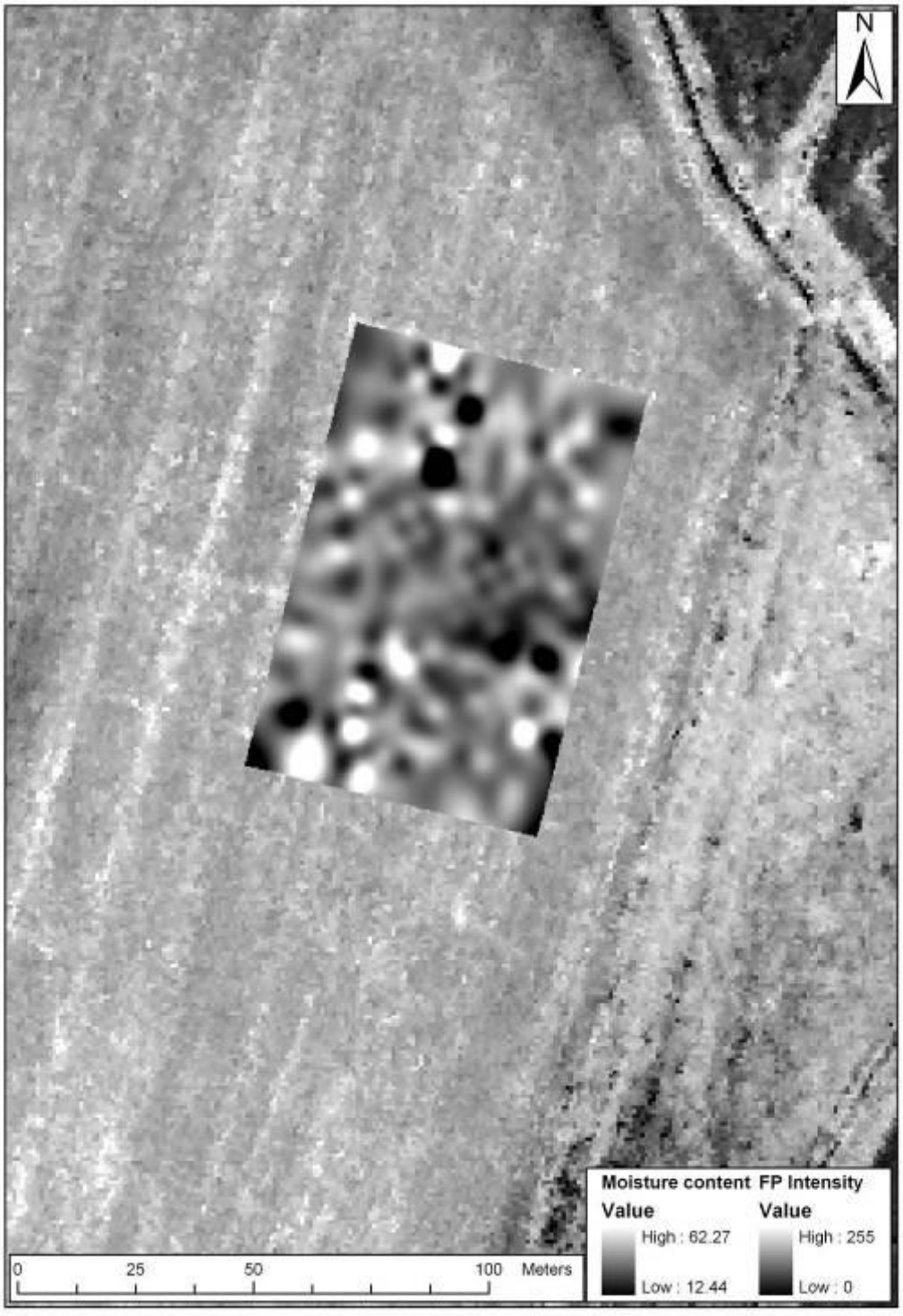

Fig 3.12: Soil moisture content superimposed on FP intensity.

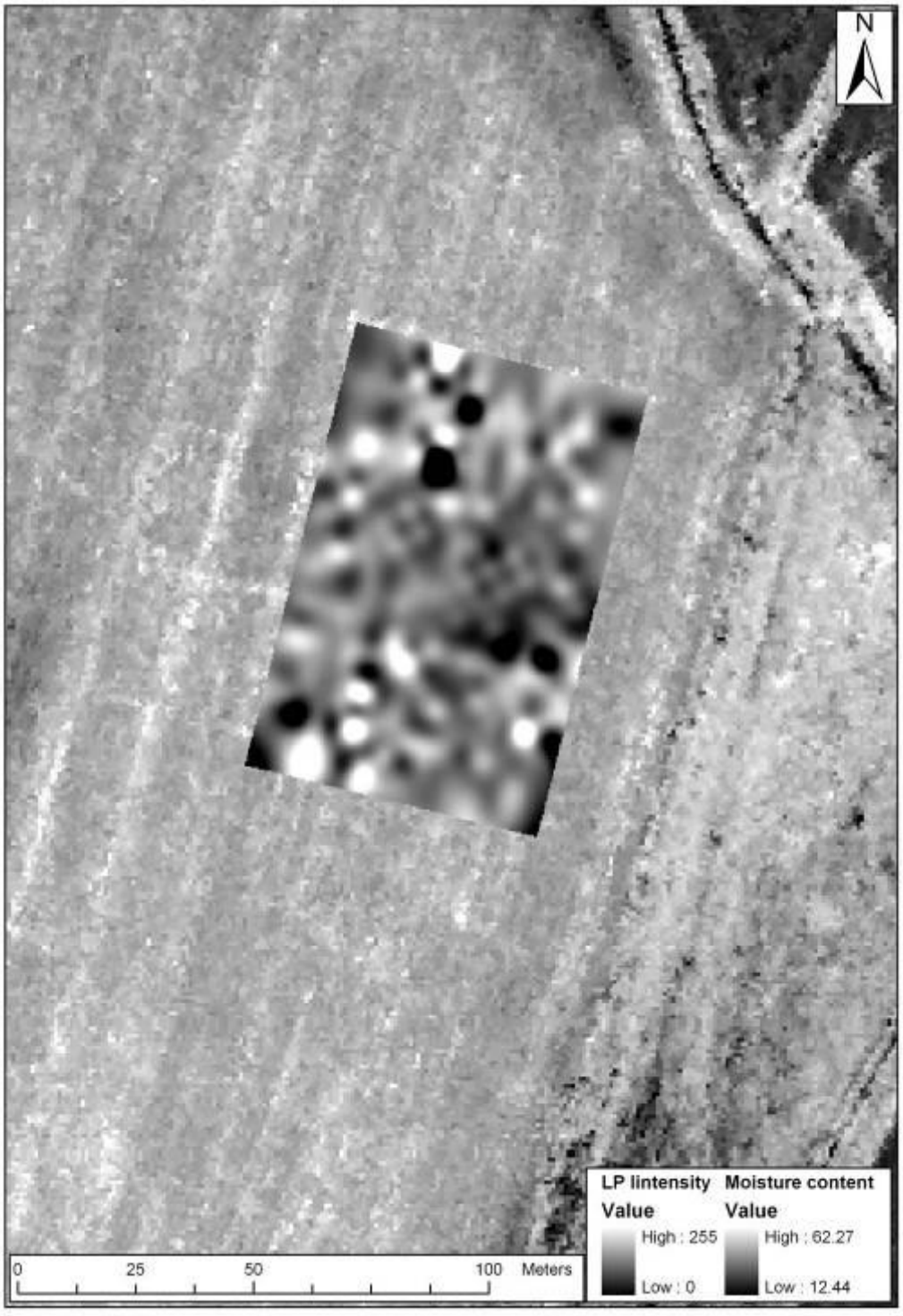

Fig 3.13: Soil moisture content superimposed on LP intensity.

3.1.3 Area 3: 4m data set analysis

The relationship of the lidar DSM, FP and LP intensity data, and physical soil properties is poorly defined. However, it is possible that this is a product of variation in sample interval between the soil moisture and soil organic data (4m interval) and the lidar data (1m interval). The quantitative statistical analysis used a standard 4m data posting, comparing equal population sizes between all data sets.

The relationship between Ohms (earth resistance survey) and the topographic data values (DSM) shows the variation seen in the earth resistance survey is not a product of topography, with a very weak linear positive relationship (Fig. 3.14; linear R square 0.009). The earth resistance Ohms values show little linear correlation to FP and LP intensity (both weak linear negative relationships), indicating that the intensity values in this survey area do not reveal the subtly in subsurface variation seen by shallow prospection (Figs. 3.15 and 3.16; FP linear R square 0.017, LP linear R square 0.029).

The soil organic data displays a very weak linear positive relationship to topography defined by the DSM (Fig. 3.17; linear R square 0.018). Soil organic content also displays a weak linear positive relationship to FP intensity (Fig. 3.18; linear R square 0.000545) and also to LP intensity (Fig. 3.19; linear R square 0.005). Likewise, the soil moisture data shows a very weak negative linear relationship to topography (Fig. 3.20; linear R square 0.000327). Soil moisture and FP intensity have a very weak negative linear relationship (Fig. 3.21; linear R square 0.000136), as do soil moisture and LP intensity (Fig. 3.22; linear R square 0.000829).

Whilst the lidar data shows no linear relationship to the individual soil variables, the intensity data does display a weak linear relationship to topography. Both the FP and LP intensity when plotted against the DSM reveal weak positive linear relationships (Fig. 3.23; FP linear R square 0.086 and Fig. 3.24; linear R square 0.079). This indicates that in survey Area 3 variations in intensity values are not caused by topographic variation, although the reasons for variation in intensity values is also not explained by the soil parameters measured. The individual soil parameters also show weak linear inter-variable relationships. Earth resistance Ohms and soil organic content display a weak linear negative relationship (Fig. 3.25; linear R square 0.033) and Ohms and soil moisture content also displays a weak negative linear relationship (Fig. 3.26; linear R square 0.007). Soil moisture content and soil organic content have a weak negative linear relationship (Fig. 3.27; linear R square 0.009).

A table of the Pearson Correlation Coefficients describes the strength of the correlation between variables, although as clearly evidenced by the scattergraphs none of these relationships are linear (Tab. 3.1). The earth resistance Ohms reveals a positive relationship with the soil organic content at the 0.05 level, with FP intensity at the 0.05 level and LP intensity at the 0.01 level. Topography defined through the LP DSM reveals a significant correlation with FP and LP intensity at the 0.01 level and soil organic content at the 0.05 level. However, as these correlations are not linear these must be mathematically complex relationships and are not able to be used in a robust, predictive manner. The soil moisture data shows no correlation to any of the variables.

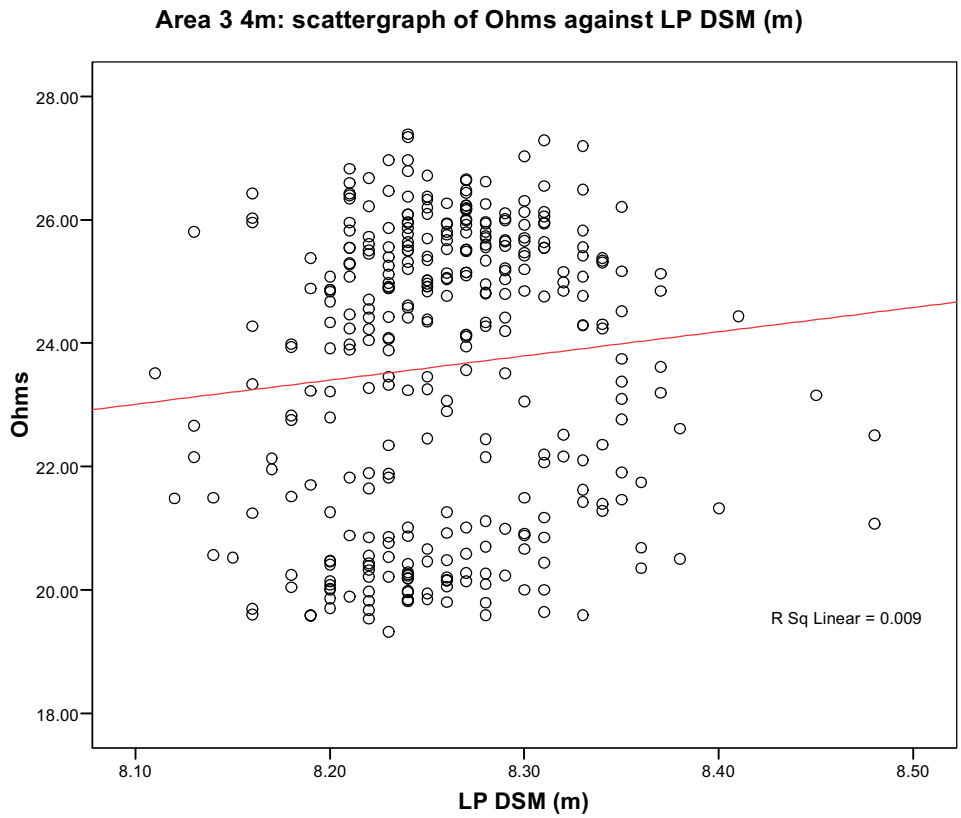

Fig 3.14: Ohms against LP DSM.

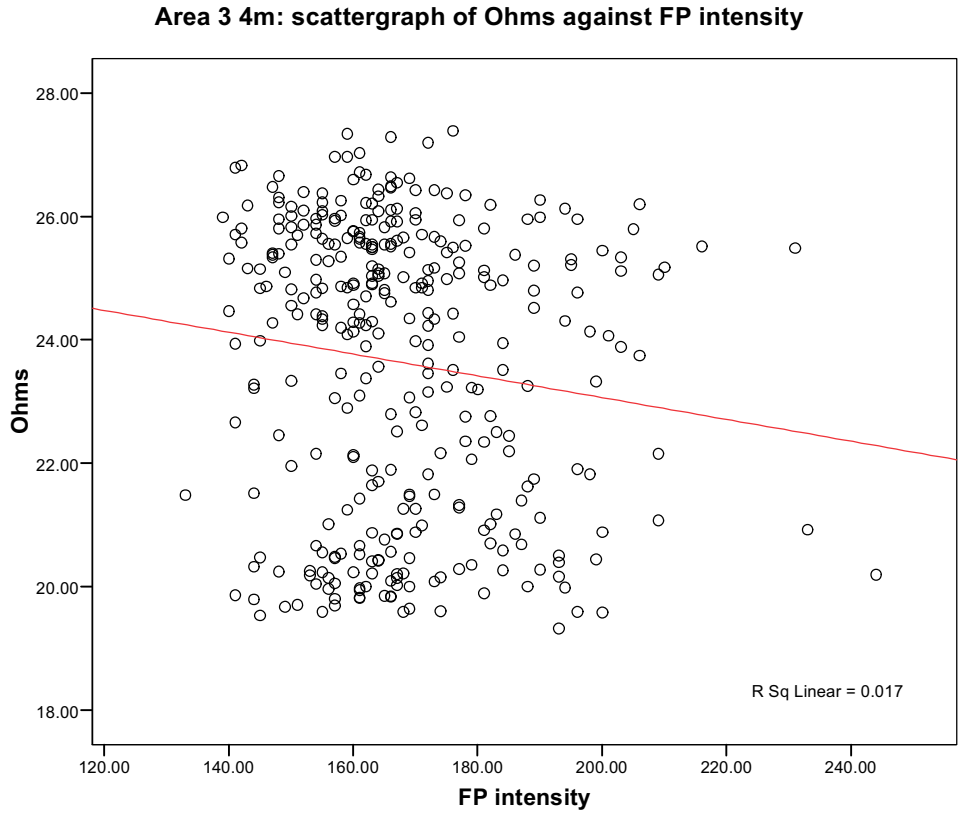

Fig 3.15: Ohms against FP intensity.

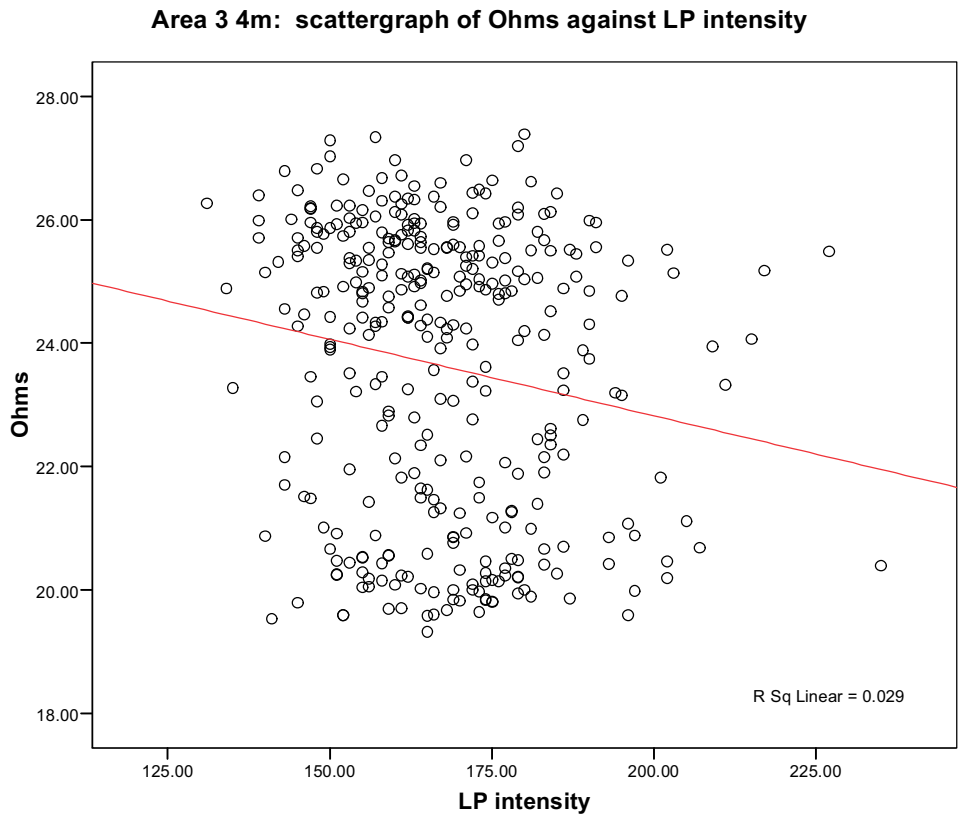

Fig 3.16: Ohms against LP intensity.

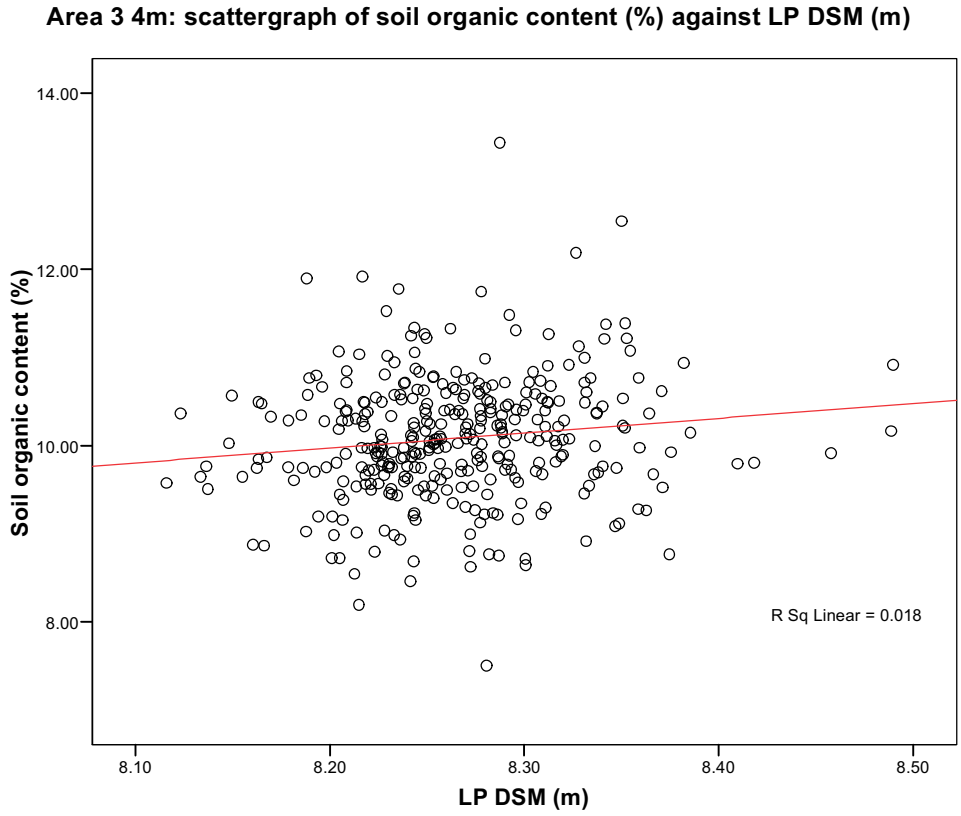

Fig 3.17: Soil organic content against LP DSM.

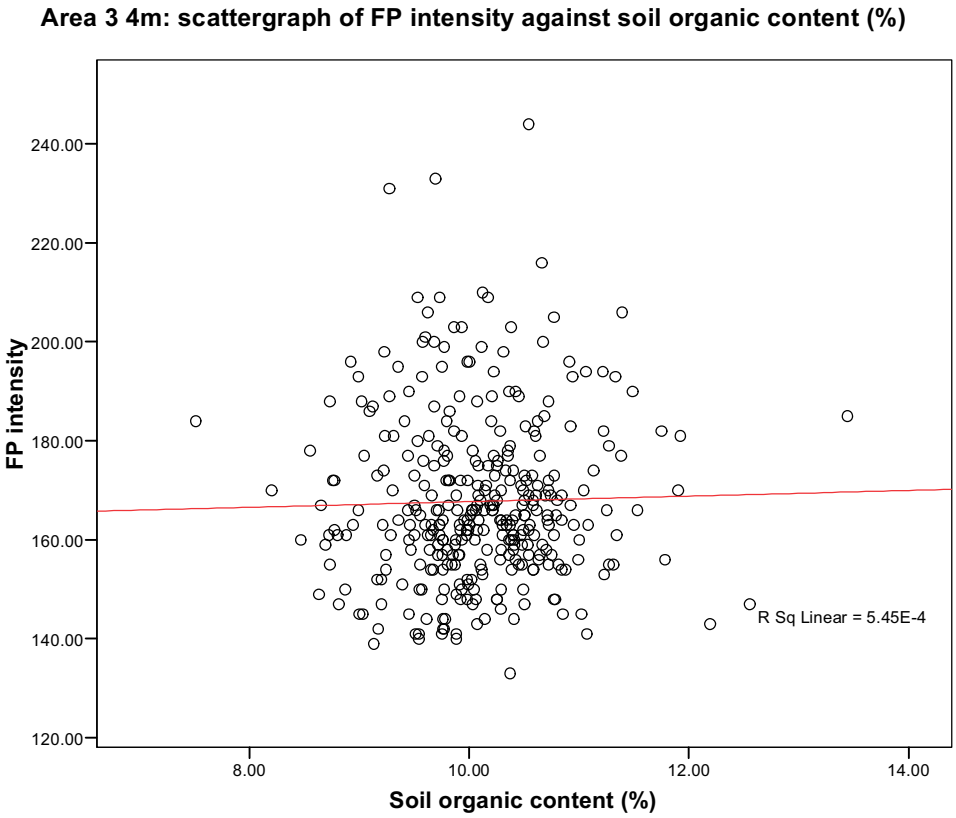

Fig 3.18: FP intensity against soil organic content.

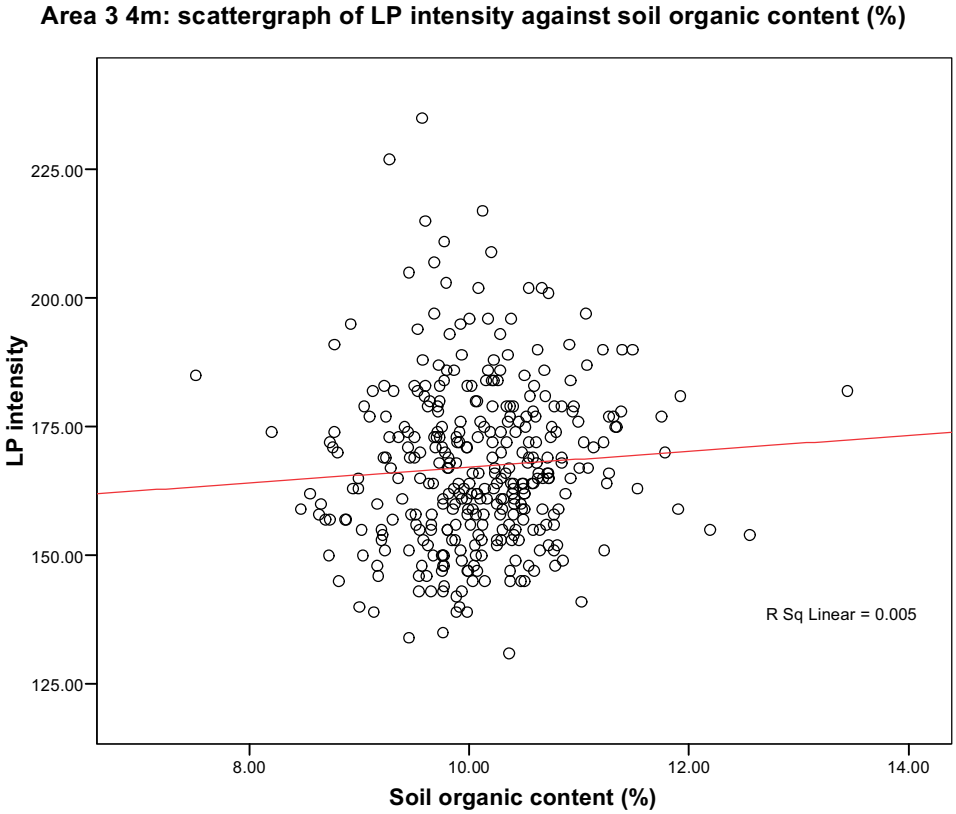

Fig 3.19: LP intensity against soil organic content.

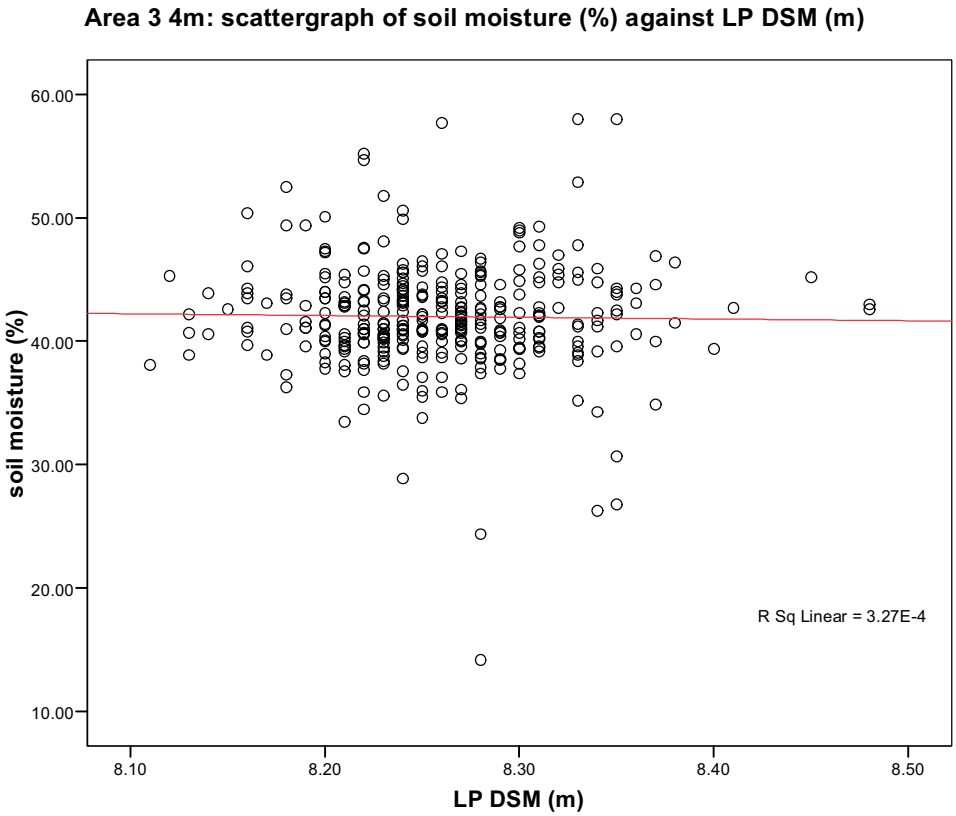

Fig 3.20: Soil moisture against LP DSM.

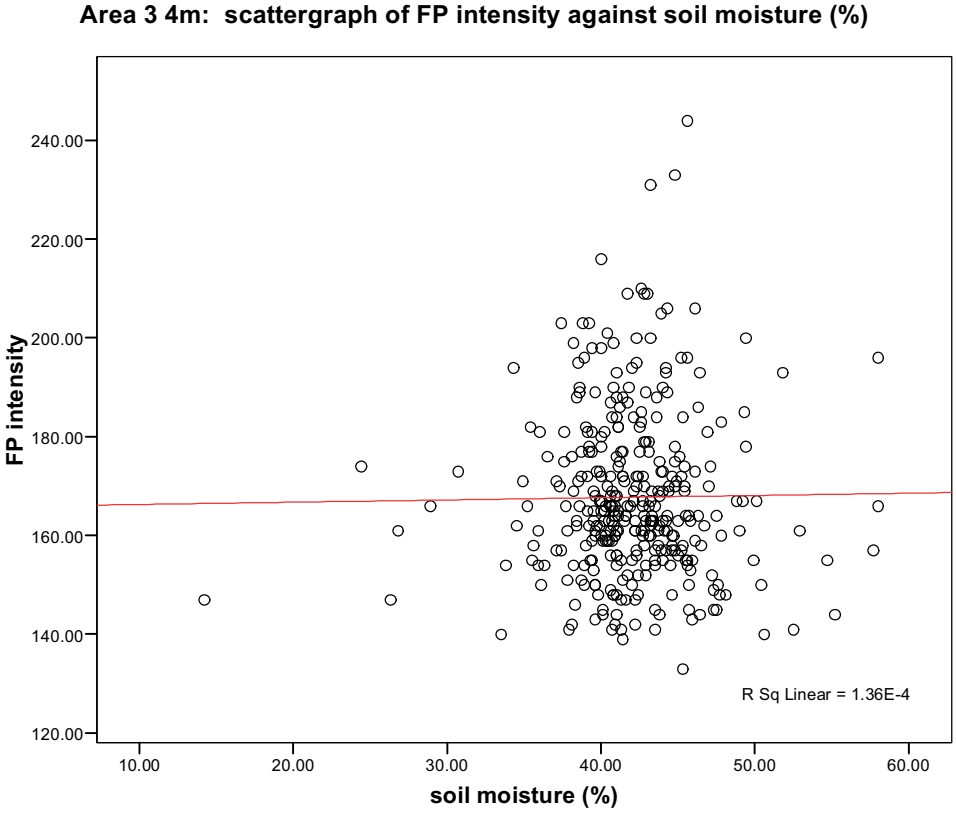

Fig 3.21: FP intensity against soil moisture.

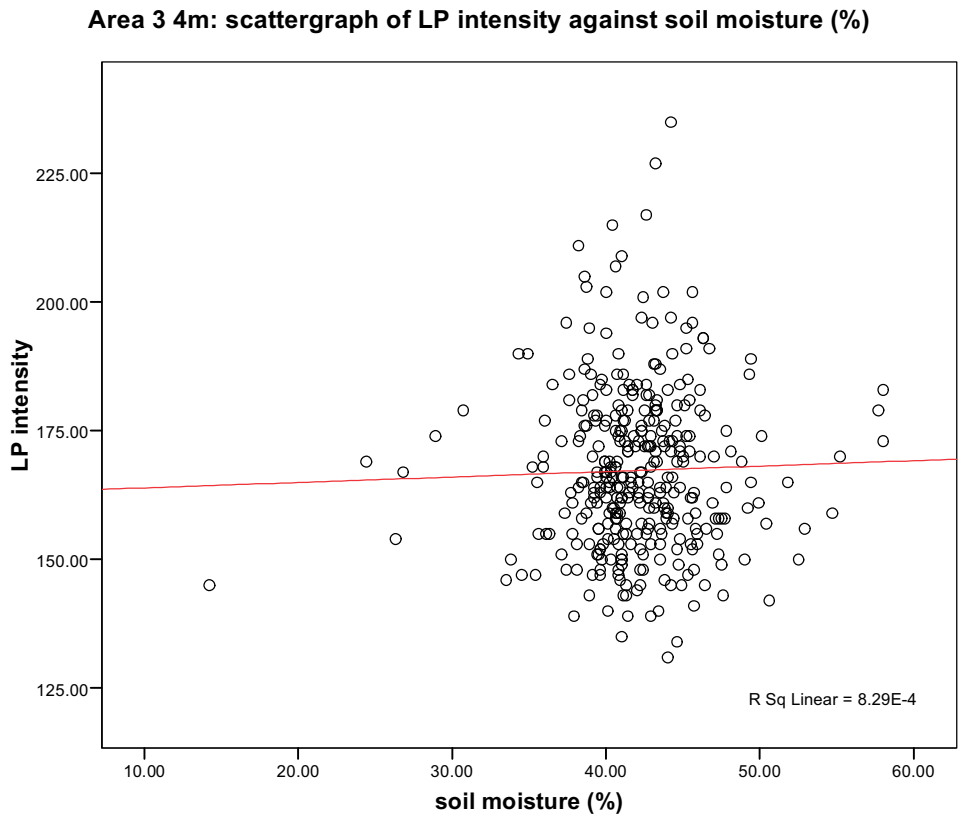

Fig 3.22: LP intensity against soil moisture (%).

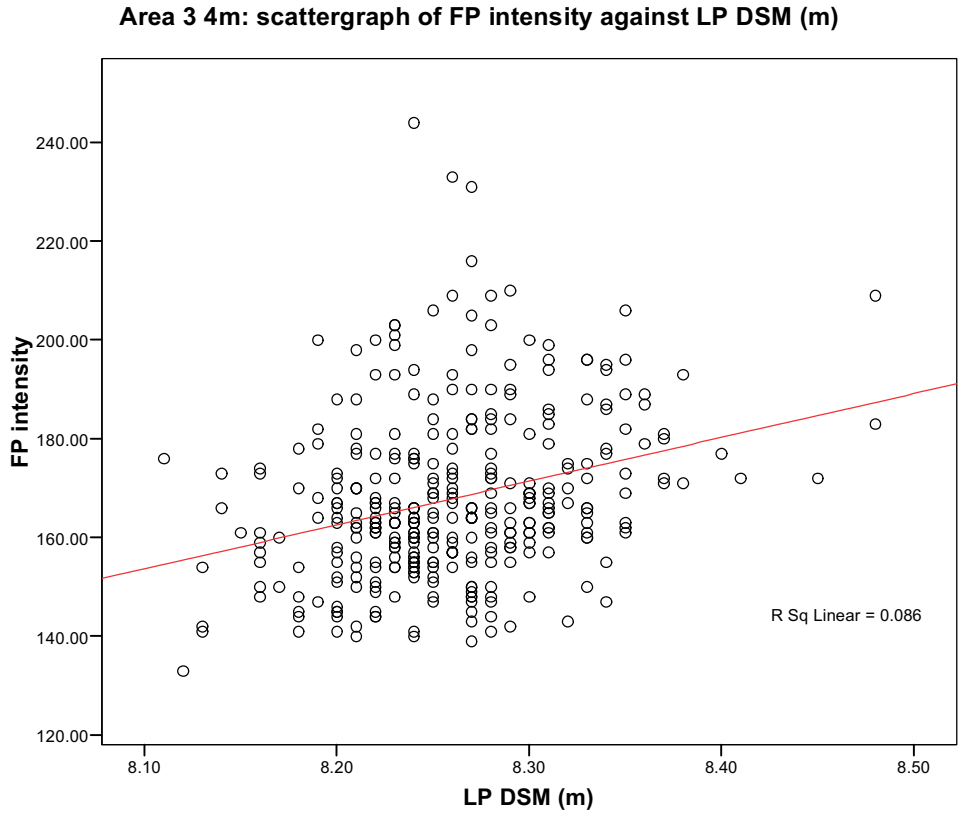

Fig 3.23: FP intensity against LP DSM.

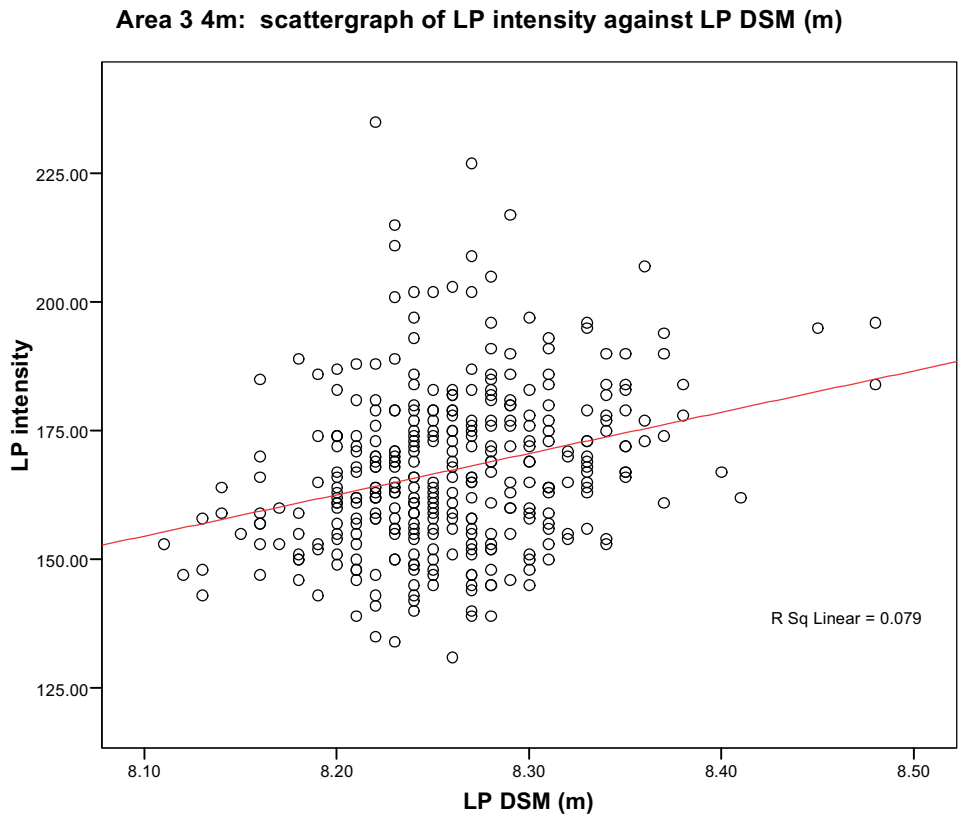

Fig 3.24: LP intensity against LP DSM.

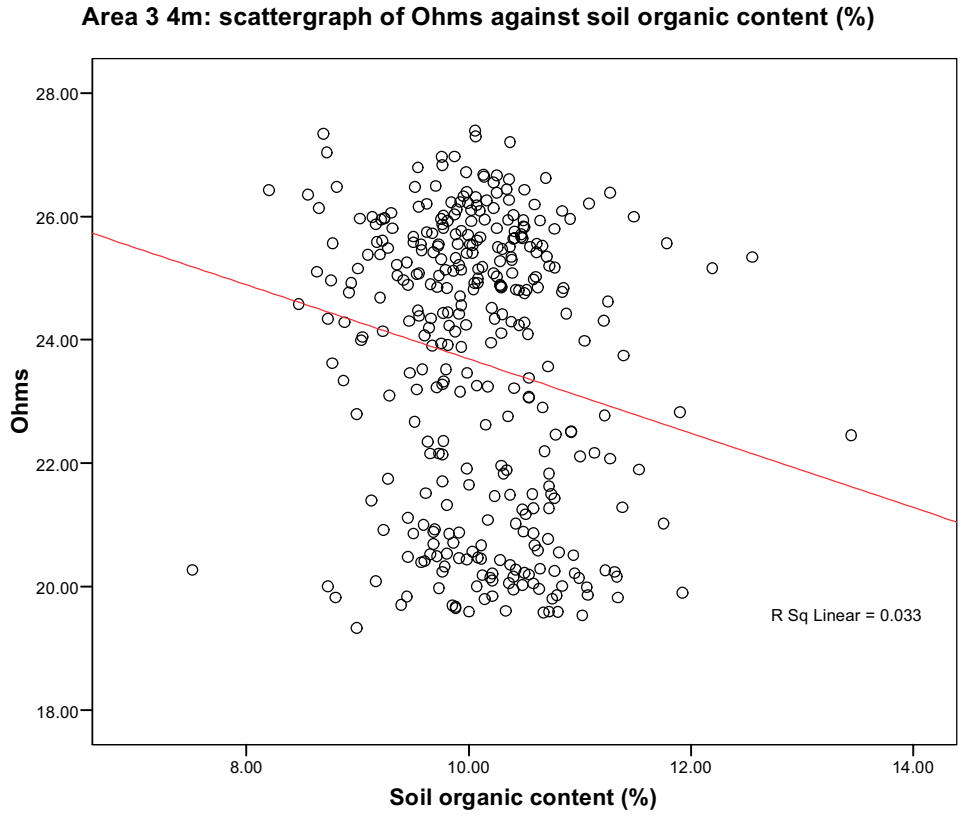

Fig 3.25: Ohms against soil organic content.

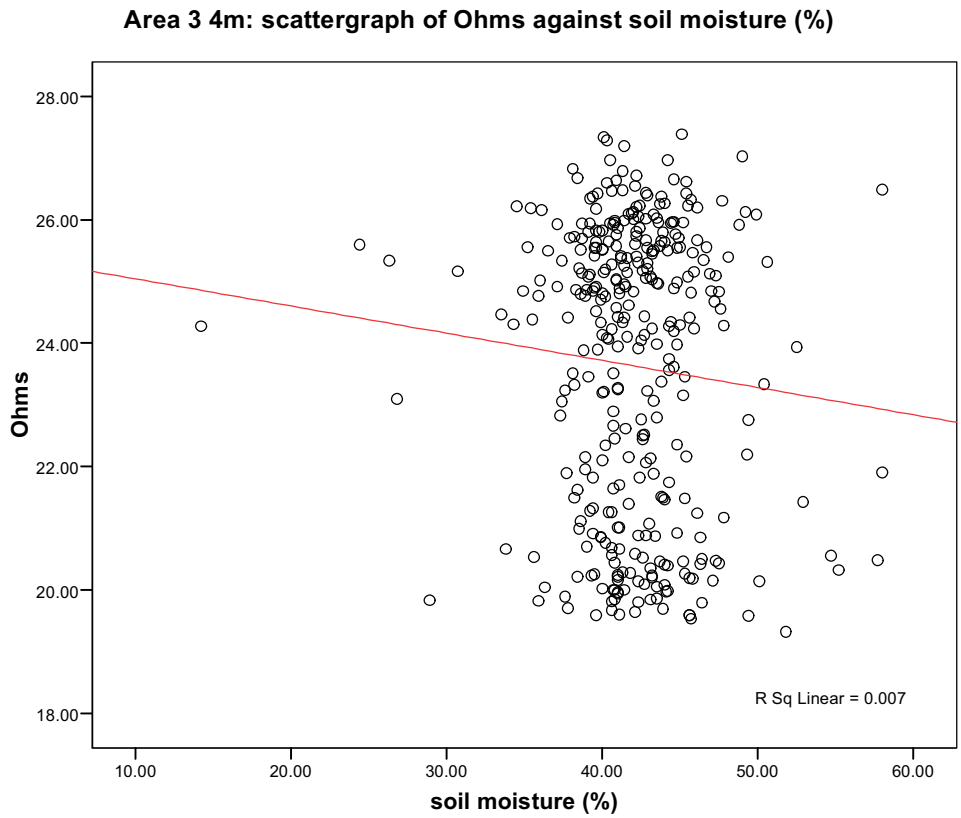

Fig 3.26: Ohms against soil moisture.

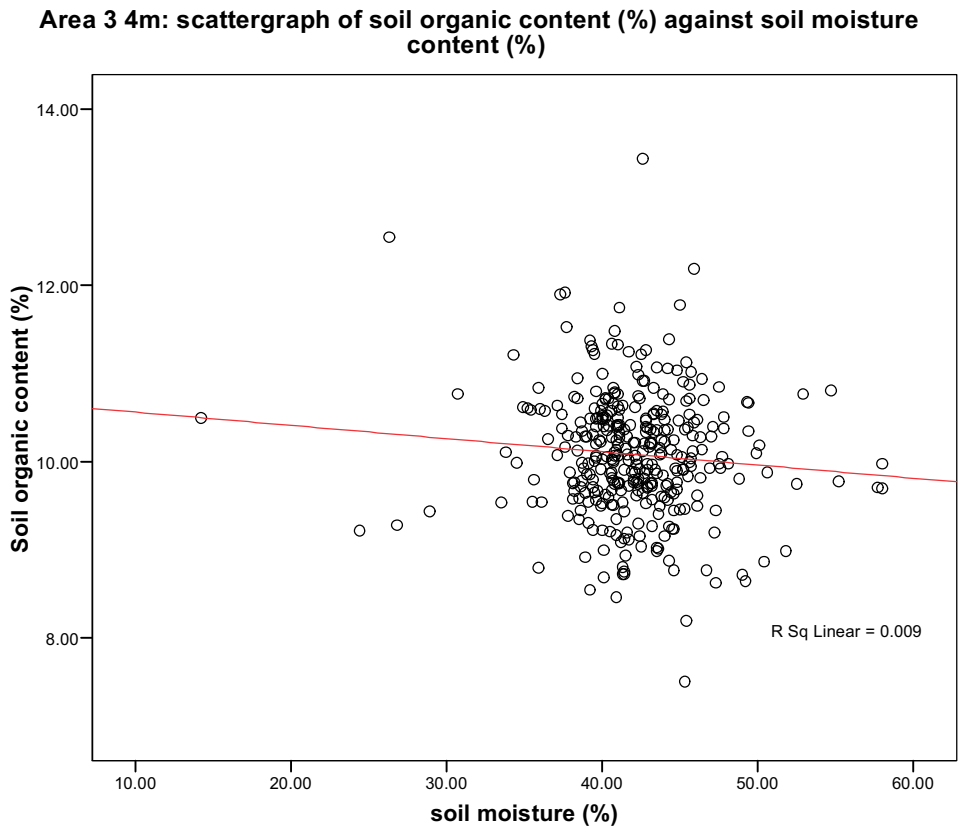

Fig 3.27: Soil organic content against soil moisture content.

Correlations

		soil moisture (%)	Ohms	LP DSM (m)	FP intensity	LP intensity	Soil organic content (%)
soil moisture (%)	Pearson Correlation	1	-.082	-.020	.012	.029	-.093
	Sig. (2-tailed)		.128	.712	.829	.594	.085
	N	345	345	345	345	345	345
Ohms	Pearson Correlation	-.082	1	.088	-.129*	-.170**	-.181**
	Sig. (2-tailed)	.128		.102	.017	.002	.001
	N	345	345	345	345	345	345
LP DSM (m)	Pearson Correlation	-.020	.088	1	.290**	.282**	.134*
	Sig. (2-tailed)	.712	.102		.000	.000	.013
	N	345	345	345	345	345	345
FP intensity	Pearson Correlation	.012	-.129*	.290**	1	.626**	.023
	Sig. (2-tailed)	.829	.017	.000		.000	.666
	N	345	345	345	345	345	345
LP intensity	Pearson Correlation	.029	-.170**	.282**	.626**	1	.068
	Sig. (2-tailed)	.594	.002	.000	.000		.211
	N	345	345	345	345	345	345
Soil organic content (%)	Pearson Correlation	-.093	-.181**	.134*	.023	.068	1
	Sig. (2-tailed)	.085	.001	.013	.666	.211	
	N	345	345	345	345	345	345

*. Correlation is significant at the 0.05 level (2-tailed).

**. Correlation is significant at the 0.01 level (2-tailed).

Tab 3.1: Pearson Correlation Coefficients of the relationships between variables in Area 3.

3.1.4 Area 3: 1m data set analysis

The analysis of the Area 3 1m data set allowed the comparison of variables collected on the same spatial resolution, namely the lidar topography and intensity data sets, and the earth resistance data. The analysis of the Area 3 1m data set shows the same trends as analysis of the smaller sub-set of Area 3 at 4m. The visual analysis of the surfaces produced from the earth resistance survey and to a lesser degree the intensity data sets, highlighted the parch mark of a ditched enclosure. However, the earth resistance data did show a number of additional features not visible in the intensity data.

The soil resistance data (Ohms) has a very weak linear relationship with FP intensity (Fig. 3.28; linear R square 0.002). This very weak negative relationship is somewhat surprising considering that both of these variables identified the ditch in their surfaces. Likewise, LP intensity and soil resistance (Ohms) have a weak negative linear relationship (Fig. 3.29; linear R square 0.001). The earth resistance data shows a stronger linear positive relationship with the LP DSM (Fig. 3.30; linear R square 0.226), highlighting the influence of geomorphology on sediment architecture. Both the FP intensity and the LP intensity show weak linear positive relationships with the LP DSM (Fig. 3.31; FP linear R square 0.081 and Fig. 3.32; LP linear R square 0.076). This indicates that intensity variation is largely independent of topography within this study area.

However, the table of computed Pearson Correlation Coefficients (Tab. 3.2) displays strong inter-variable correlation between FP intensity, LP intensity, Ohms and LP DSM. All these correlations are significant at the 0.01 level. Whilst these relationships are not linear, and currently cannot be used in a predictive manner, there are clearly strong inter-variable correlations. More research is required to understand the mathematical form of these non-linear relationships between variables.

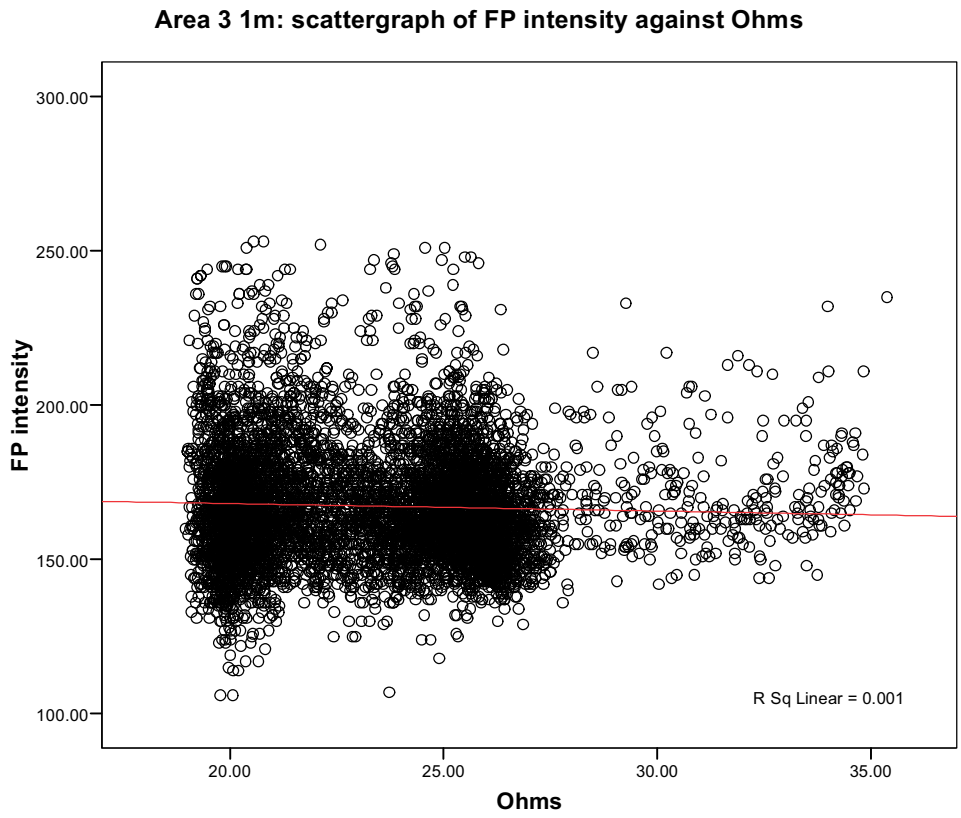

Fig 3.28: FP intensity against Ohms.

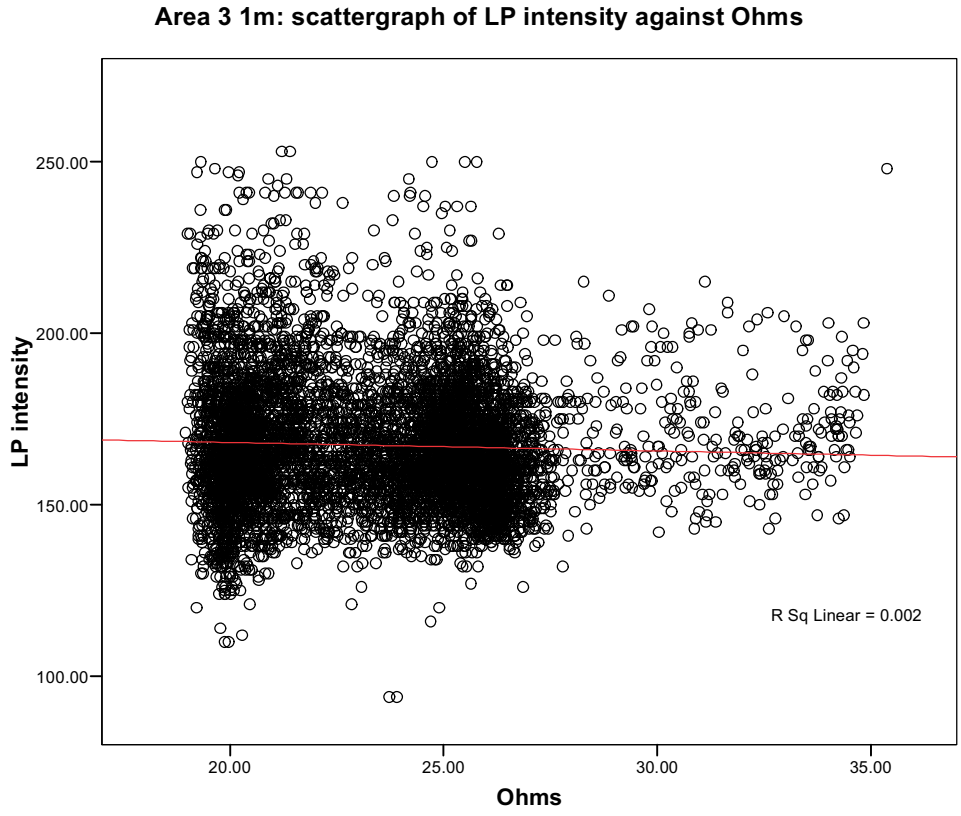

Fig 3.29: LP intensity against Ohms.

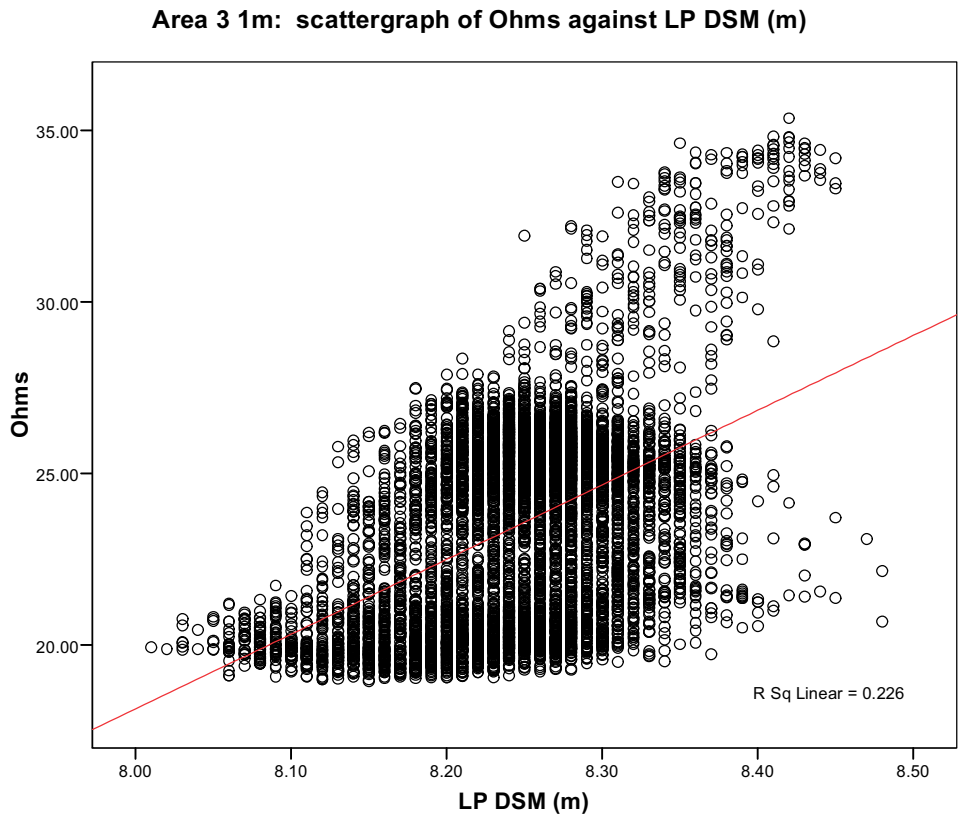

Fig 3.30: Ohms against LP DSM.

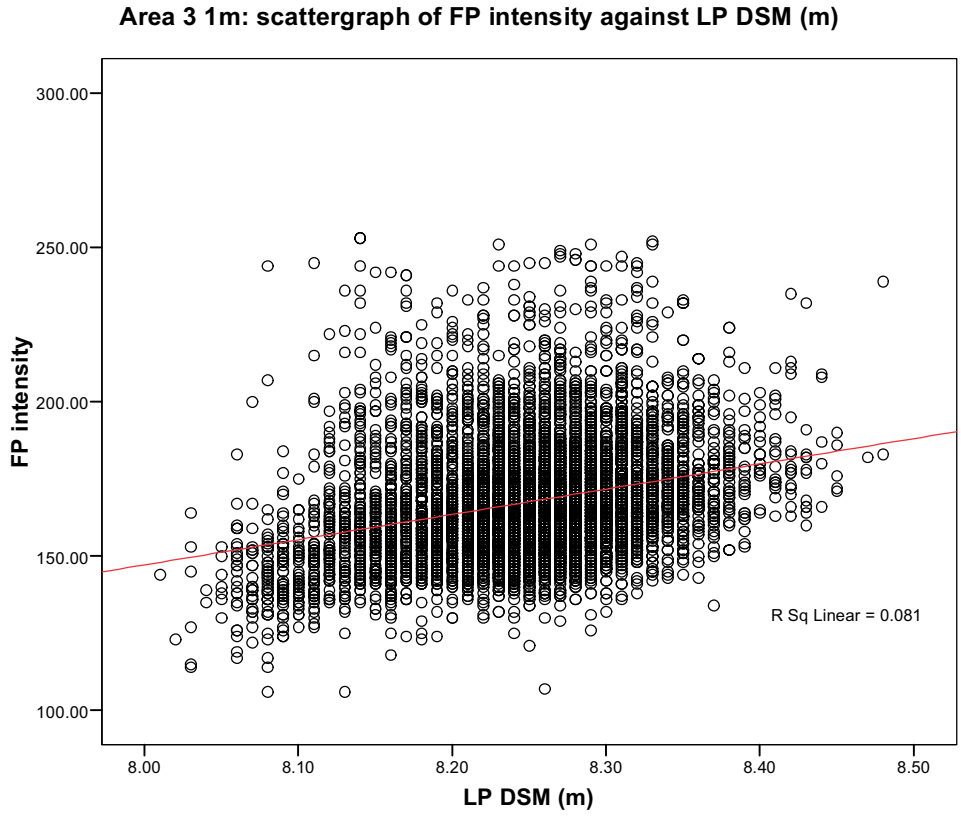

Fig 3.31: FP intensity against LP DSM.

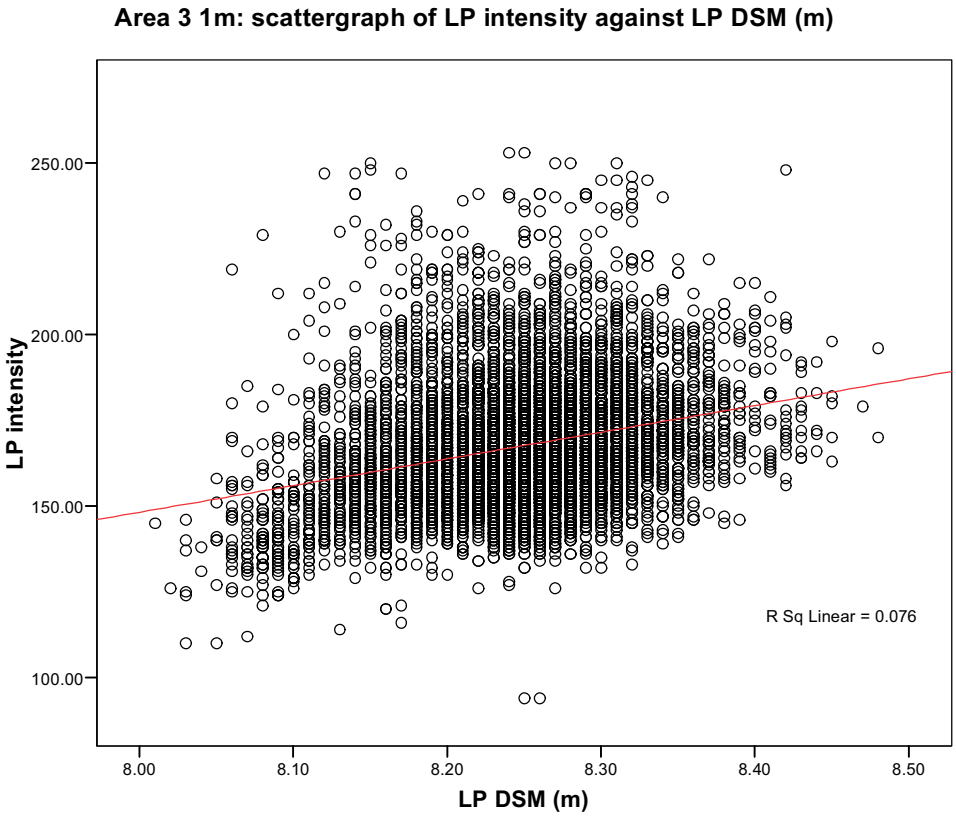

Fig 3.32: LP intensity against LP DSM.

Correlations

		Ohms	LP DSM (m)	FP intensity	LP intensity
Ohms	Pearson Correlation	1	.475**	-.039**	-.040**
	Sig. (2-tailed)		.000	.001	.001
	N	7320	7320	7320	7320
LP DSM (m)	Pearson Correlation	.475**	1	.285**	.276**
	Sig. (2-tailed)	.000		.000	.000
	N	7320	7320	7320	7320
FP intensity	Pearson Correlation	-.039**	.285**	1	.683**
	Sig. (2-tailed)	.001	.000		.000
	N	7320	7320	7320	7320
LP intensity	Pearson Correlation	-.040**	.276**	.683**	1
	Sig. (2-tailed)	.001	.000	.000	
	N	7320	7320	7320	7320

**. Correlation is significant at the 0.01 level (2-tailed).

Tab 3.2: Table of Pearson Correlation Coefficients from the 1m data set analysis. There are highly significant correlations between variables, although these relationships are non-linear.

3.1.5 Area 3 summary of main results

The analysis of the Area 3 data sets produced clear results. Within this study area there is some visual correlation between FP and LP intensity and an archaeological pasture mark. The pasture mark is not evident as a topographic feature; the archaeological feature causing the pasture mark is much more clearly defined by earth resistance survey. Although there is some visual correlation between lidar FP and LP intensity, and earth resistance survey, this mathematical relationship is non-linear in form. However, the analysis of the 1m data set shows this to be a statistically valid correlation. Unfortunately, for the purposes of remote sensing of archaeological remains using lidar intensity, as this relationship is currently non linear it cannot be used in a predictive or robust manner. Indeed, the strongest linear relationship was between lidar topography LP DSM and earth resistance Ohms. The lidar data sets did not display a visual correlation to the soil organic and soil moisture surfaces. The graphical analysis of these data sets shows there to be non-linear relationships between soil moisture, soil organic content and the lidar data sets. The table of computed correlation coefficients did show that soil organic content did display a significant correlation to lidar topography (LP DSM). These results suggest that topographic variation may be a more robust predictive indicator of organic preservation and waterlogged deposits than lidar intensity data.

The results from the visual analysis of the surface models is summarised as:

- Part of a pasture mark in the field survey area is visible in lidar intensity data indicating potential for the identification of anthropogenic archaeology from crop and pasture marks.
- The earth resistance data provided much greater clarity on the geomorphology and archaeology of the survey area than the lidar DSM, FP and LP intensity data sets.

The results from the quantitative analysis of the Area 3 4m data set are summarised as:

- The lidar data sets of FP intensity, LP intensity and LP DSM do not show a visual or linear relationship to soil organic content.
- The lidar data sets of FP intensity, LP intensity or LP DSM do not show a visual or linear relationship to soil moisture content.
- The lidar data sets of FP intensity, LP intensity or LP DSM do not show a visual or linear relationship to earth resistance Ohms.
- There was not a visual or linear relationship between soil moisture content and soil organic content.
- Correlations do exist between the lidar data sets and the earth resistance data sets. However, these relationships are mathematically non-linear and therefore cannot be used in a predictive capacity within the study area.

The results from the 1m data set analysis are summarised as:

- The relationship between earth resistance Ohms and lidar intensity and topography is non-linear.
- Earth resistance Ohms shows a statistically significant (0.01 level) correlation to FP intensity, LP intensity and LP DSM.
- The lidar data sets of LP DSM, LP intensity and FP show non-linear relationships.

- The lidar data sets of LP DSM, LP intensity and FP display strong inter-variable correlation.

3.2 AREA 6

3.2.1 Area 6 geological background

Survey Area 6 was located to investigate the difference between an area of Holme Pierrepont Sand and Gravel Terrace and a palaeochannel, mapped as undifferentiated alluvium (Fig. 3.33). The palaeochannel and terrace were visible as topographically distinct features in the field. The survey of Area 6 was undertaken in inclement weather with light showers. There was much standing water visible on the surface of the palaeochannel during field survey.

3.2.2 Area 6: Visual qualitative analysis

The analysis of Area 6 begins with a qualitative visual assessment of the data sets followed by a quantitative exploration of the Area 6 4m and 1m data sets. Ground data collection in Area 6 covered part of a large palaeochannel graduating onto a terrace deposit. The palaeochannel and the terrace are clearly visible on the DSM topographic model (Fig. 3.34), with the palaeochannel to the south of the survey grid and the higher terrace deposit visible to the north of the survey grid. The FP intensity data also reveals a change between the south of the study area and the north of the study area (Fig. 3.35). This pattern is repeated in the LP intensity data (Fig. 3.36). Thus the lidar topography and intensity data all show a visual difference between the palaeochannel and terrace.

The earth resistance survey data (Ohms) shows this differentiation between the palaeochannel and the terrace (Fig. 3.37). Lower resistance values are recorded within the palaeochannel, indicating increased soil moisture, whilst much higher resistance values are recorded on the terrace deposit, indicating shallower deposits and lower soil moisture levels. Whilst the visual correlation is strongest between the earth resistance data and LP DSM data, the lidar FP and LP intensity data also display visual correlation with the earth resistance data (Figs. 3.38 and 3.39).

The soil organic content data has a strong visual correlation to the topography (LP DSM; Fig. 3.40). Lower soil organic contents are recorded on the terrace deposits, whilst much higher soil organic contents are recorded within the palaeochannel. Likewise, the soil organic data visually correlates with the lidar FP and LP data (Figs. 3.41 and 3.42). The soil moisture content also highlights the difference between the palaeochannel and the terrace. Elevated soil moisture contents are recorded in the palaeochannel, with much lower moisture contents on the terrace. This is again in good agreement with lidar topography (LP DSM; Fig. 3.43), FP intensity (Fig. 3.44) and LP intensity (Fig. 3.45) data.

In contrast to the relatively small anthropogenic archaeological features of Area 3, Area 6 was surveyed to cover much larger geomorphological features. As a consequence of the marked changes between geomorphological units, the lidar data effectively visually defines variations in landform surface. The earth resistance data visually displays a good correlation with the lidar data. The differentiation between the terrace and the palaeochannel are evident through changes in soil moisture content and soil organic content.

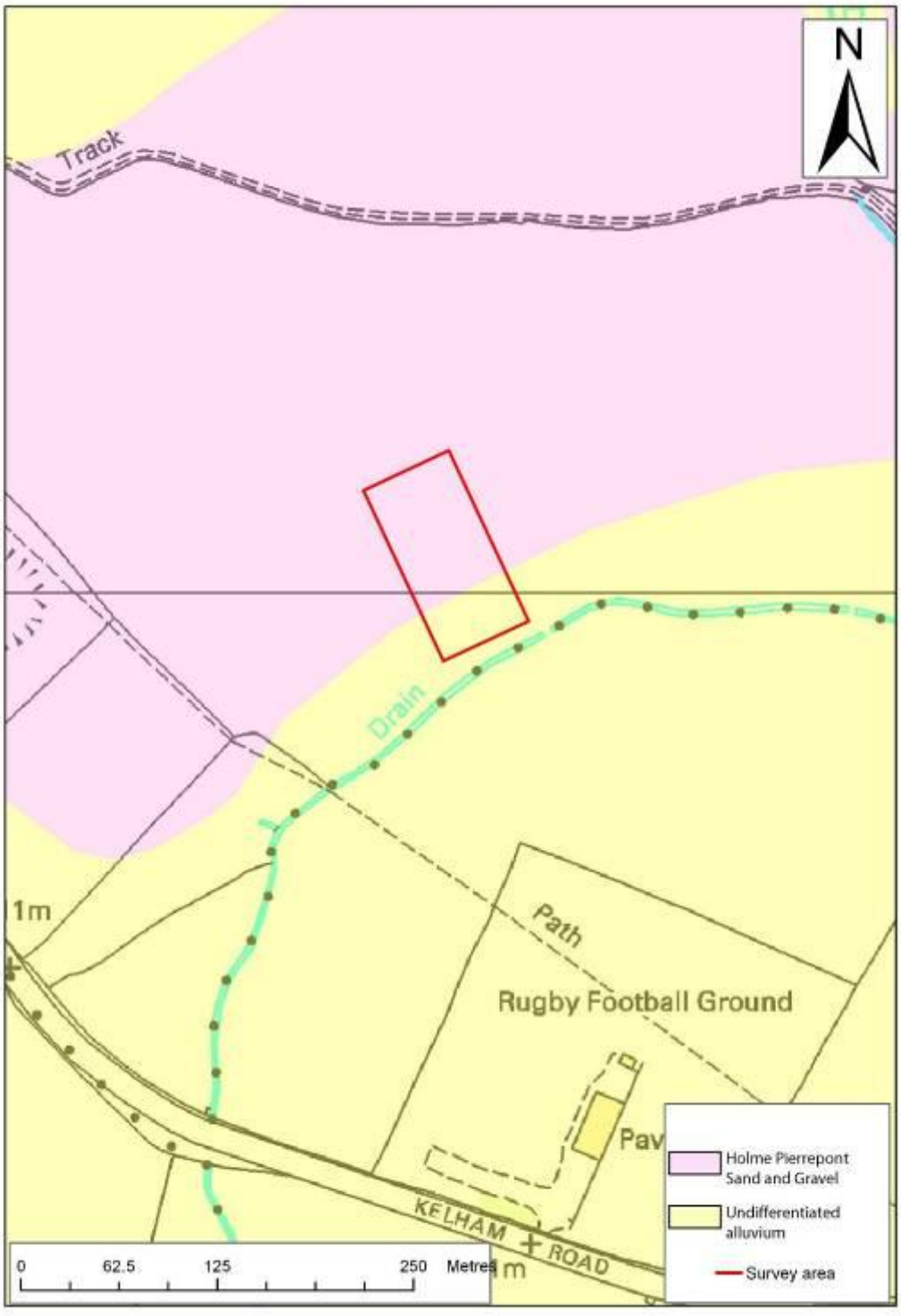

Fig. 3.33: Geological units over the Area 6 survey grid, BGS 1:50, 000 data. The survey grid covered part of the Holme Pierrepont Terrace, and part of a palaeochannel represented by undifferentiated alluvium.

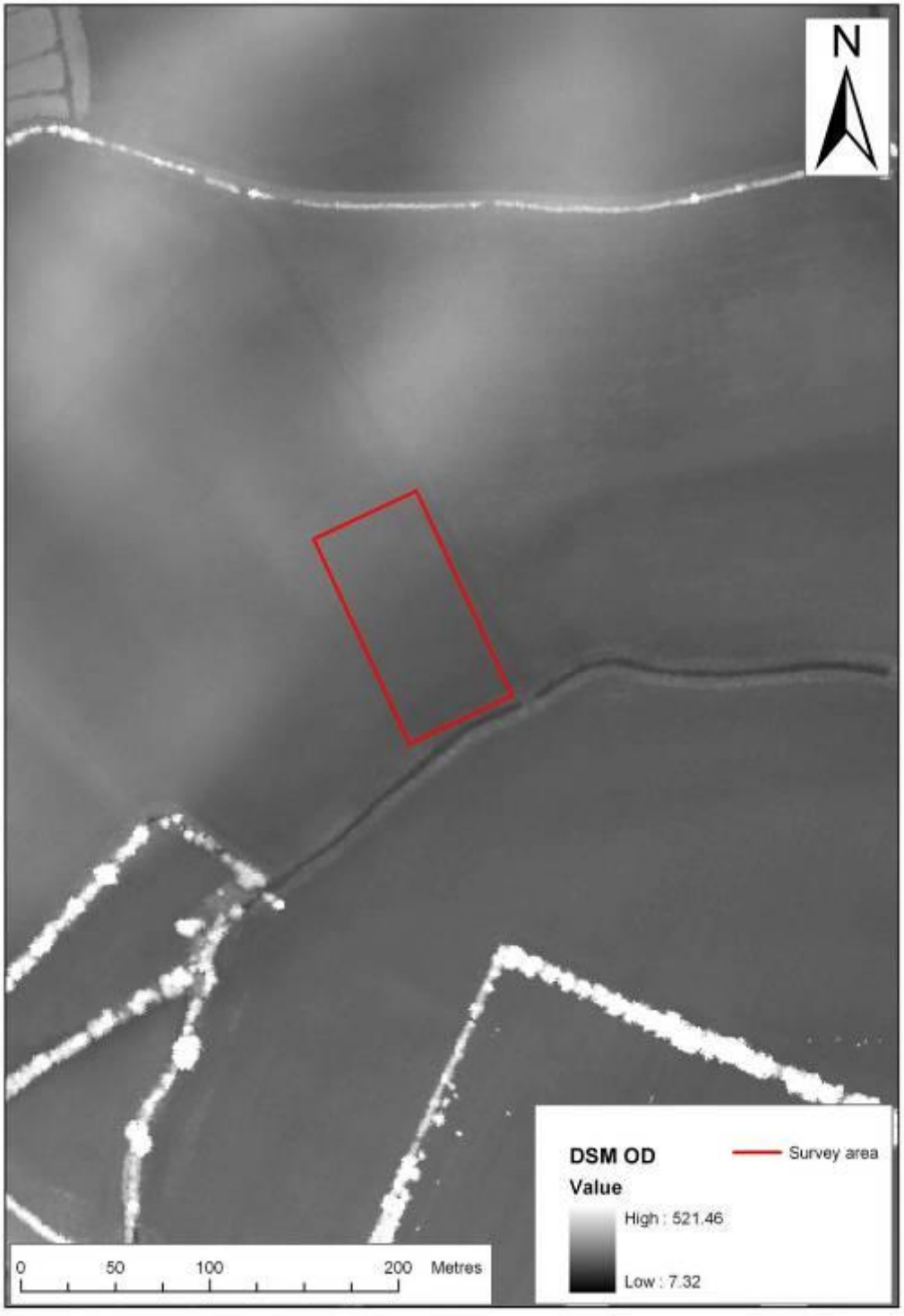

Fig 3.34: The survey area shown on topography (DSM OD).

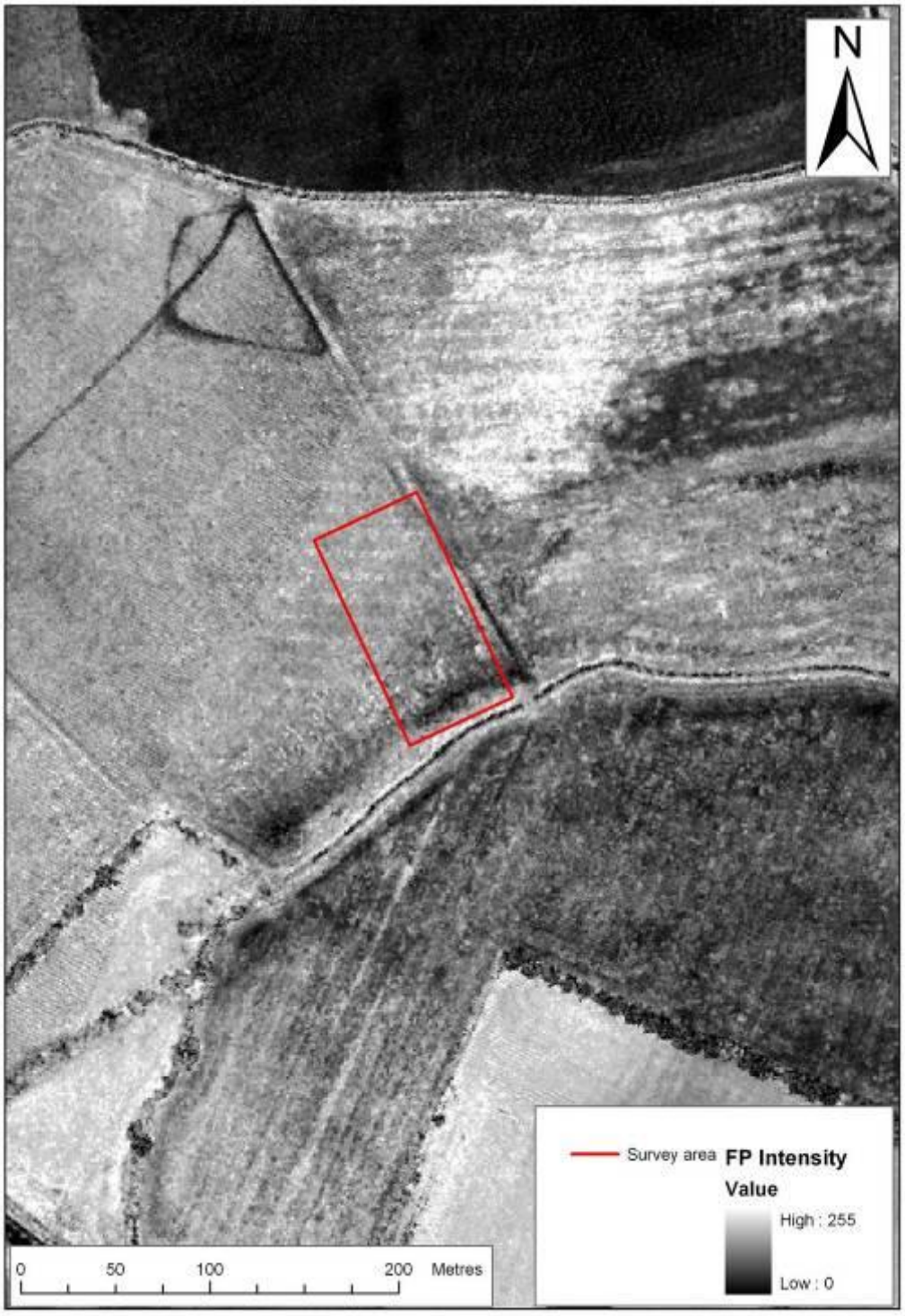

Fig 3.35: The survey area shown on FP intensity.

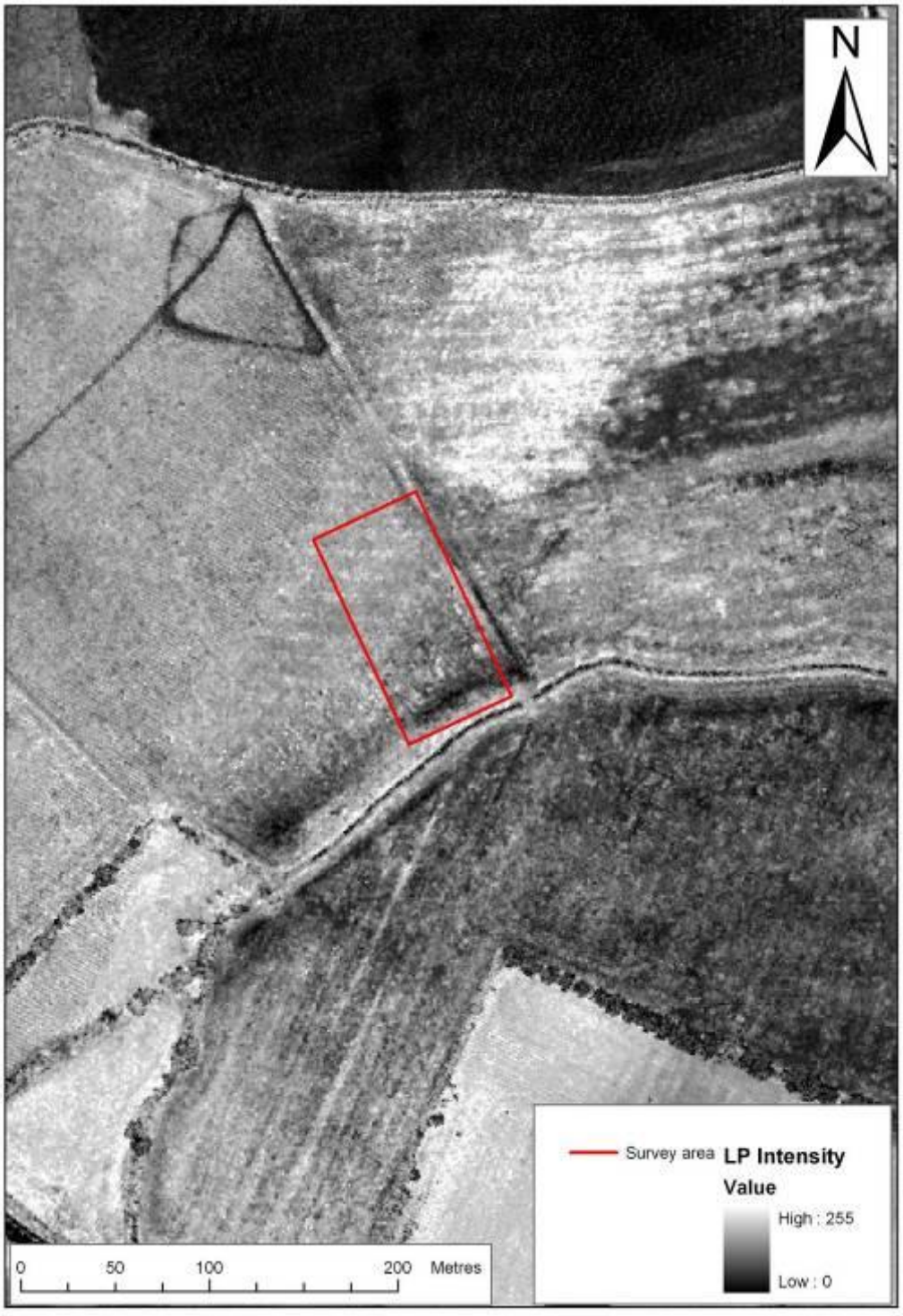

Fig 3.36: The survey area shown on LP intensity.

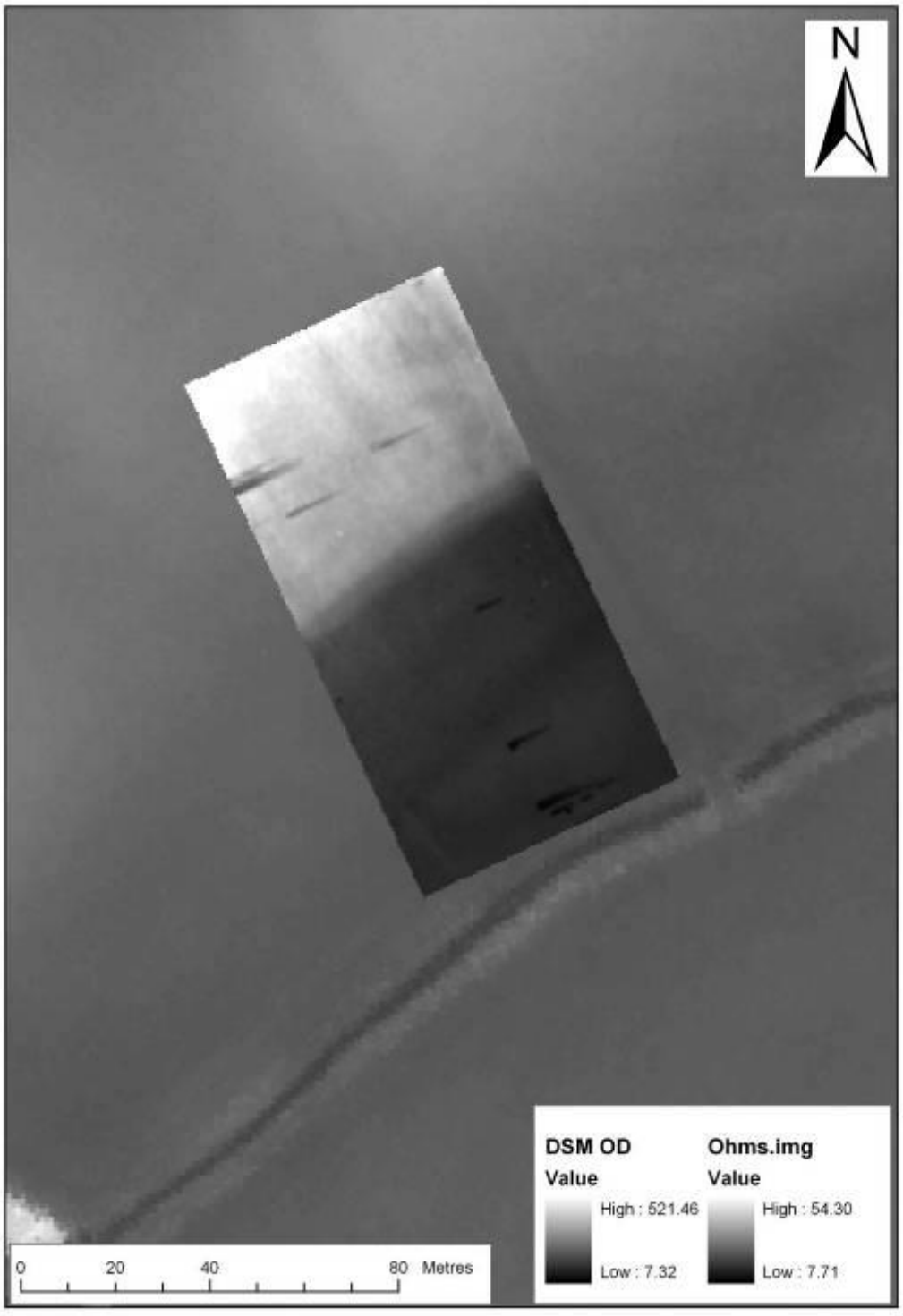

Fig 3.37: Earth resistance Ohms on DSM OD.

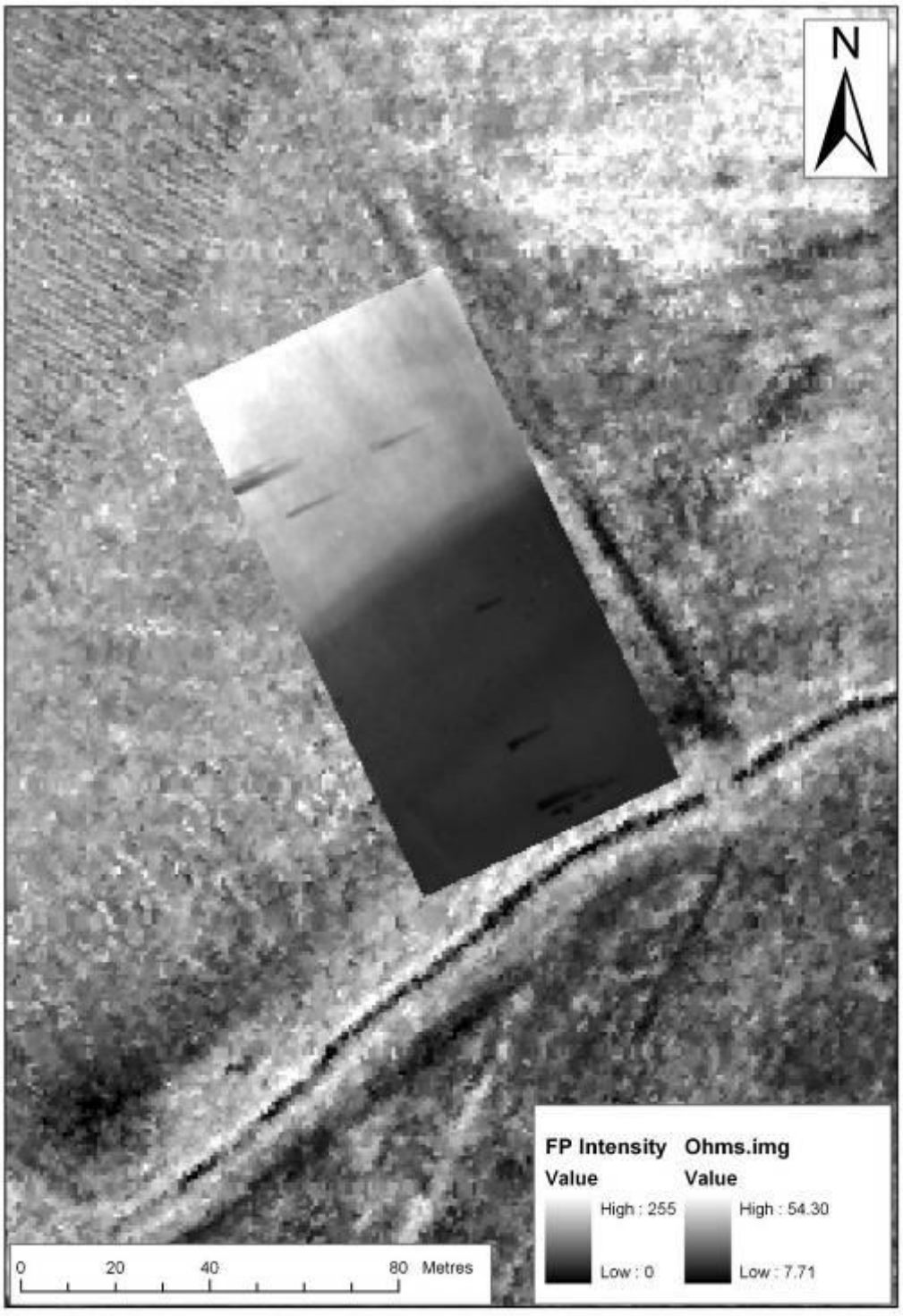

Fig 3.28: Earth resistance Ohms on FP intensity.

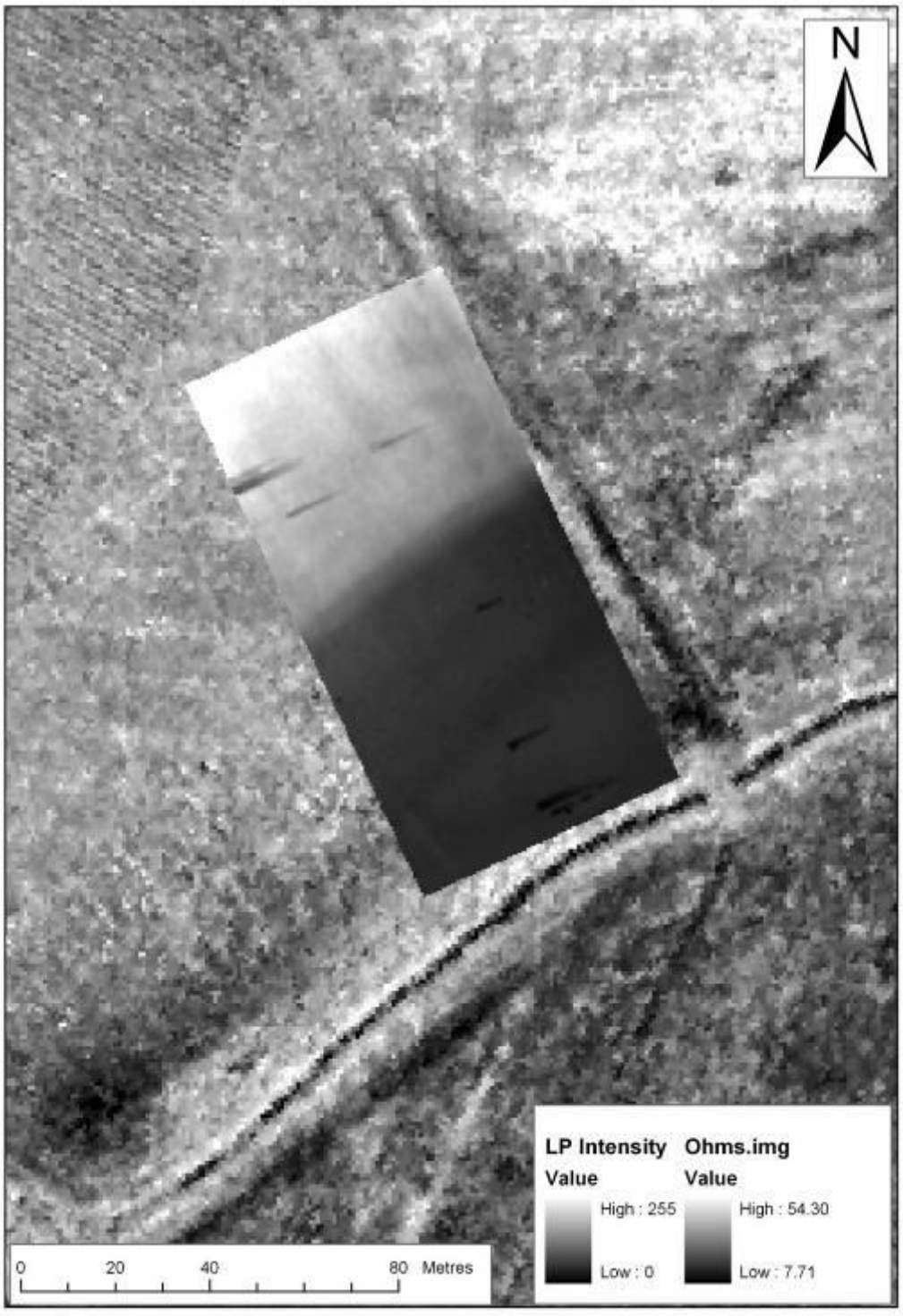

Fig 3.29: Earth resistance Ohms superimposed on LP intensity.

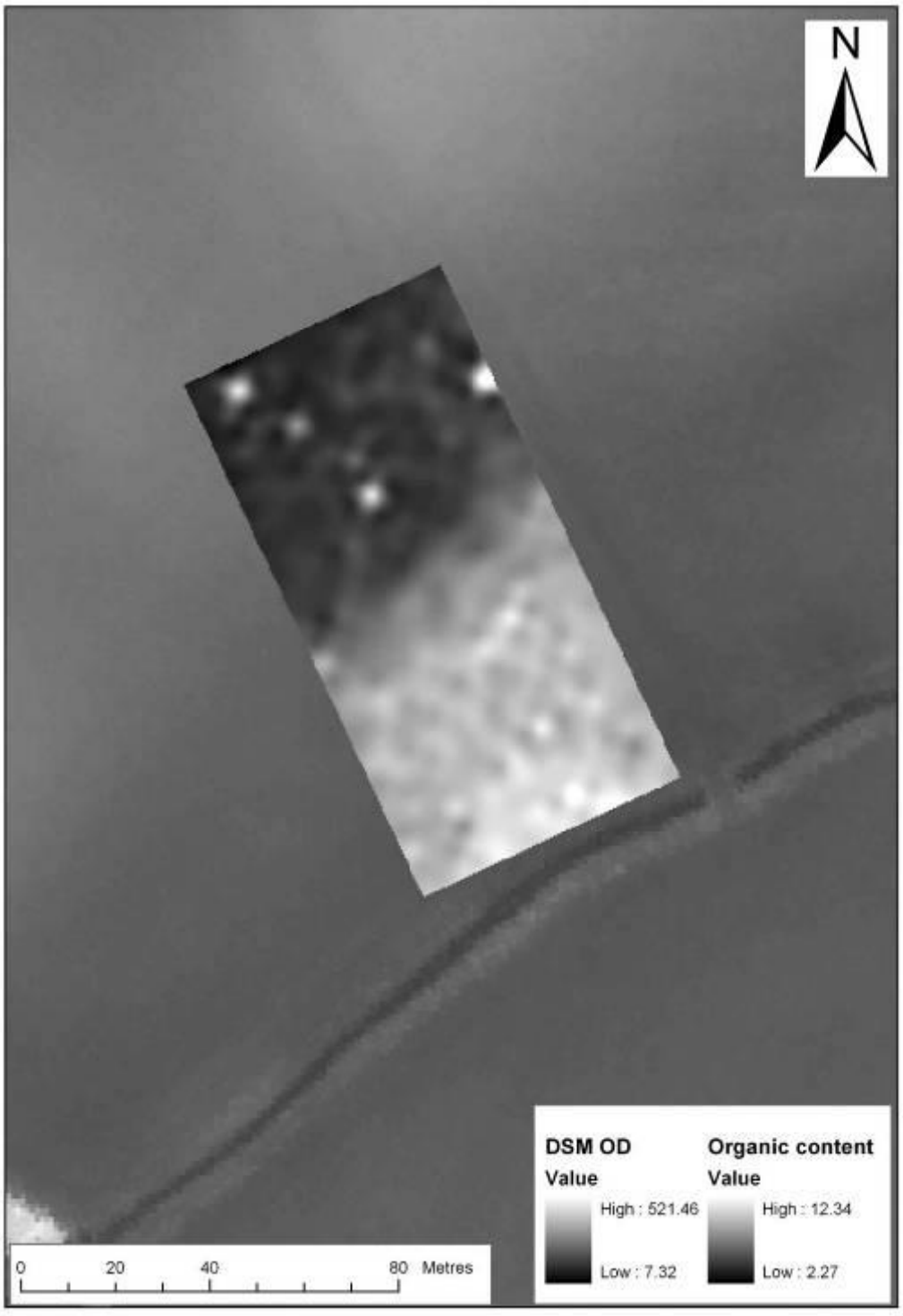

Fig 3.30: Organic content superimposed on DSM OD.

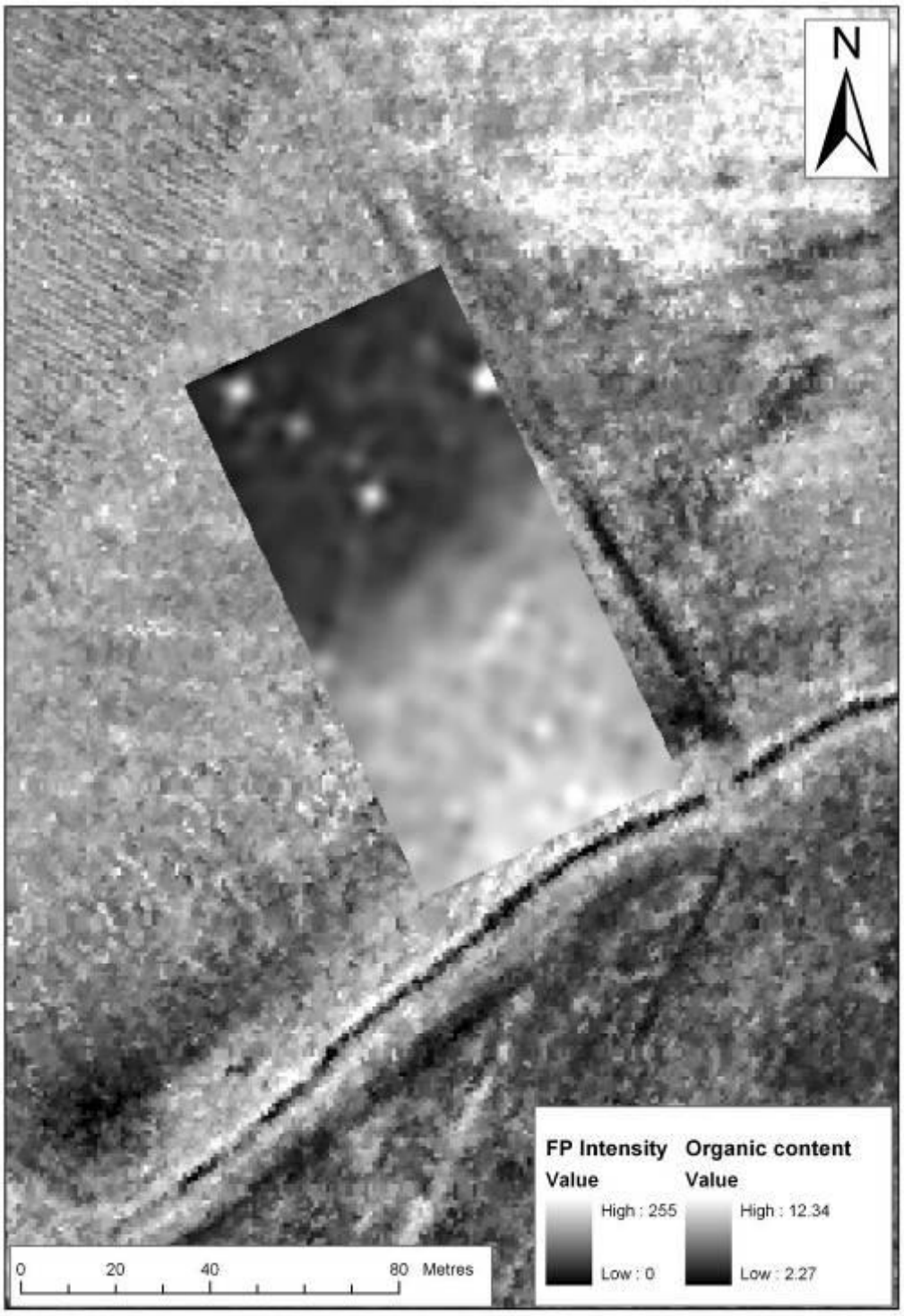

Fig 3.31: Organic content superimposed on FP intensity.

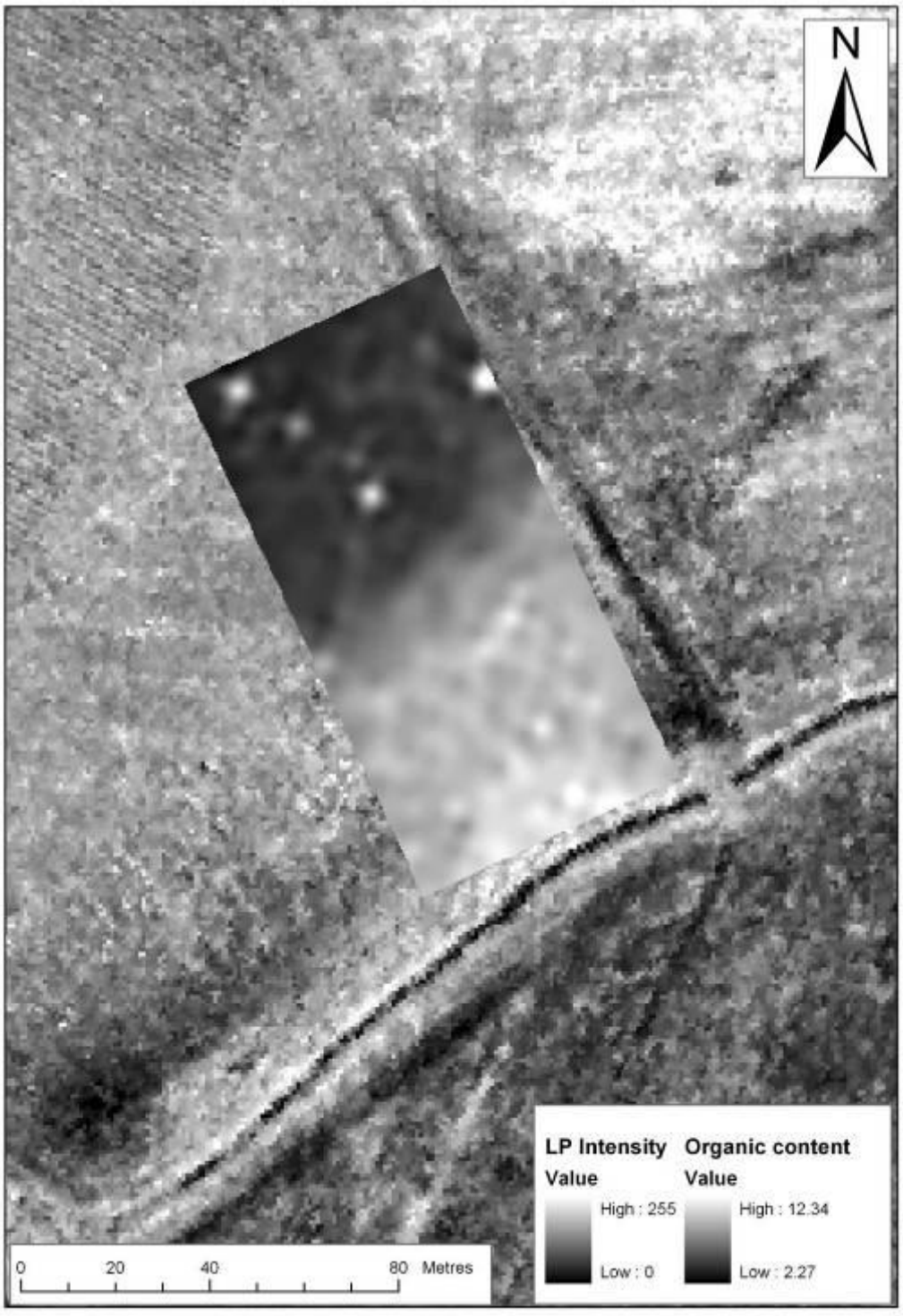

Fig 3.32: Organic content superimposed on LP intensity.

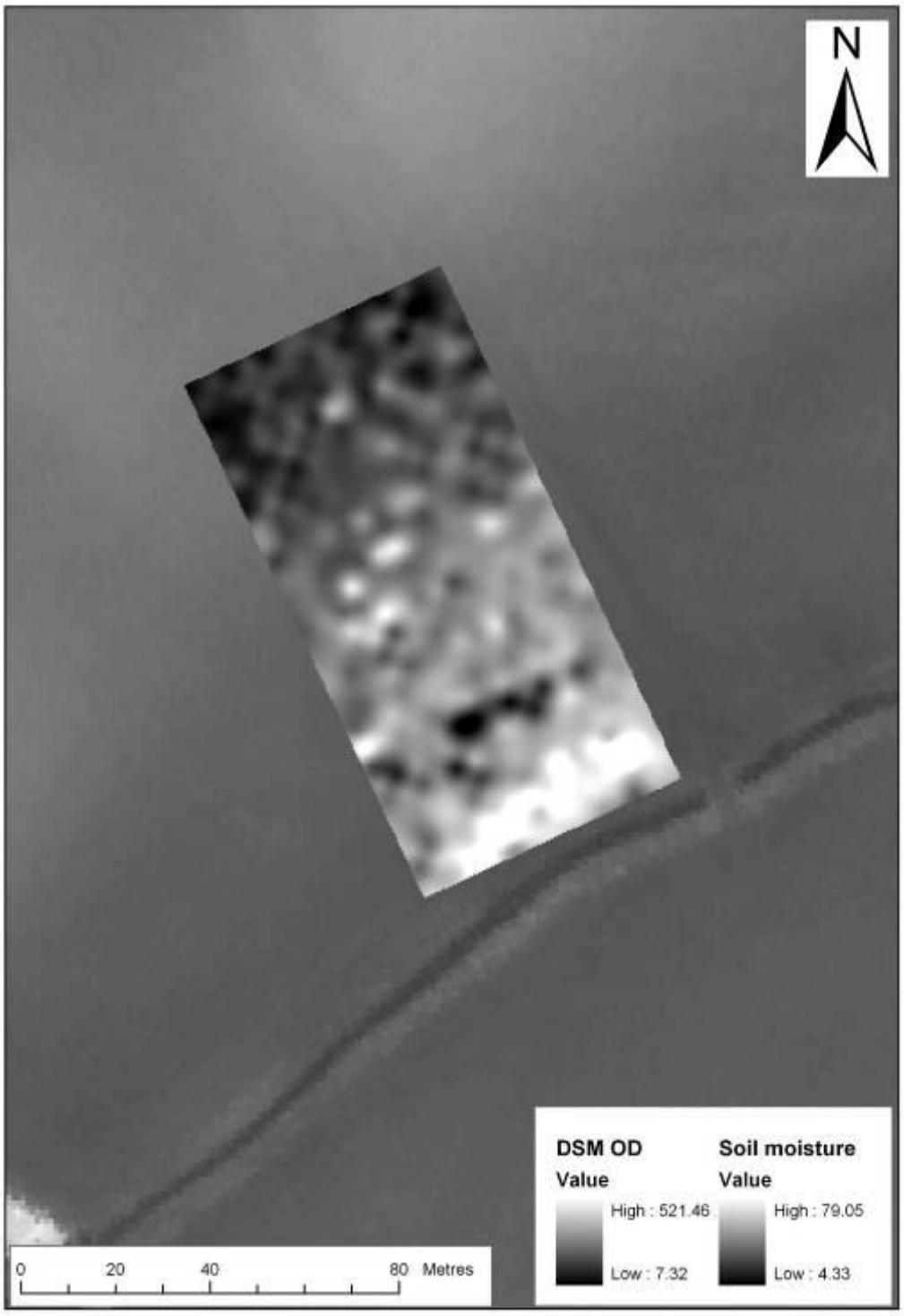

Fig 3.33: Soil moisture content superimposed on DSM OD.

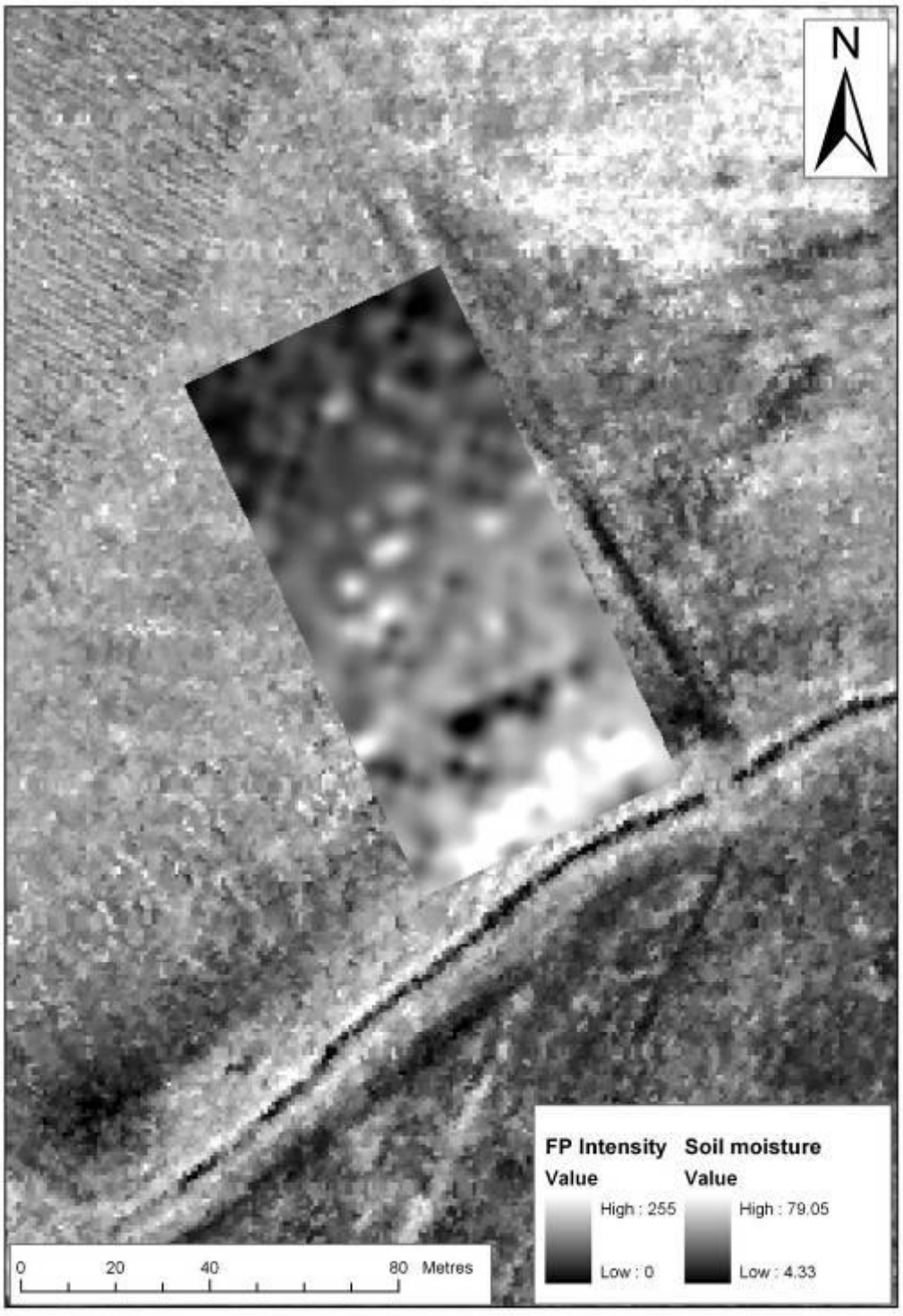

Fig 3.34: Soil moisture content superimposed on FP intensity.

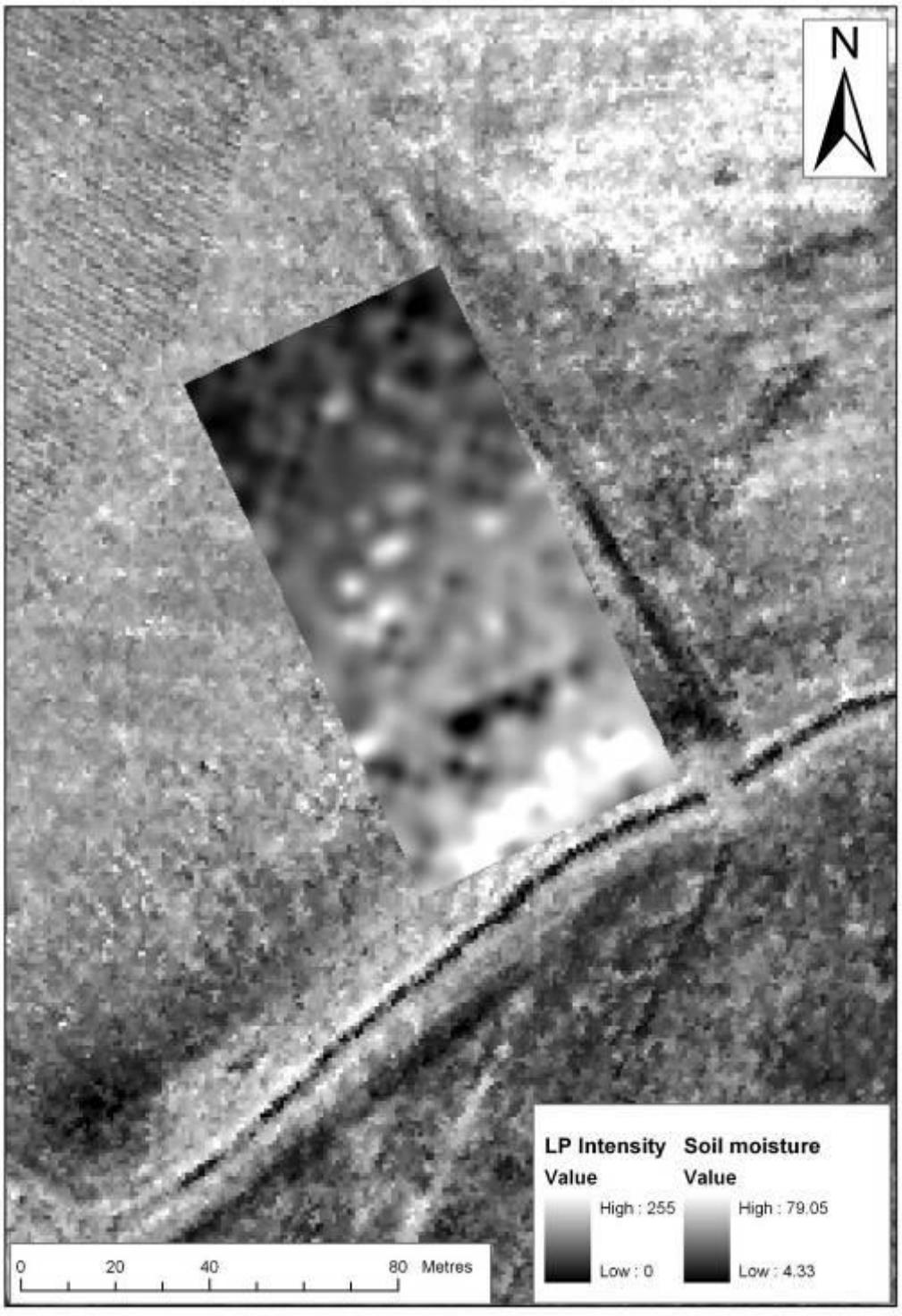

Fig 3.35: Soil moisture content superimposed on LP intensity.

3.2.3 Area 6: 4m data set analysis

The visual assessment of the Area 6 data set suggests a high level of inter-variable correlation between variables, due to the different variables each identifying the geomorphological change between the terrace and the palaeochannel. The scattergraph of Ohms against LP DSM highlights the importance of geomorphology in Area 6, with a strong linear positive relationship between the variables (Fig. 3.36; linear R square 0.91). The graph visibly displays how the earth resistance survey is highlighting the main trends of the palaeochannel and the terrace within the survey area. The relationship of the FP intensity and the LP intensity with Ohms are again positive, but relatively weak when compared to the topographic data (Figs. 3.37 and 3.38; linear R square values of 0.24 and 0.23 respectively). This suggests that the intensity data has a large degree of variance introduced by factors other than the gross changes in geomorphology.

Soil organic content displays a strong negative linear relationship to topography, defined by the lidar DSM (Fig. 3.39; linear R square 0.79). As topography increases the organic content of the soil decreases, highlighting the difference between the topographically lower palaeochannel and higher terrace. Much weaker relationships are observed between the lidar intensity data and soil organic content, with both graphs displaying moderate negative linear relationships (Fig. 3.40 and 3.41; linear R square values of 0.35 and 0.32 respectively).

The soil moisture contents show the same trend as the soil organic content data, although the relative strength of the relationships is weaker (Fig. 3.42). Soil moisture has a negative linear relationship with topography, with a linear R square value of 0.57, lower than the corresponding value for topography and soil organic content (linear R square 0.79). Again, like the soil organic data, the soil moisture data shows weaker relationships with the lidar FP and LP intensity data, both moderate negative linear relationships (Fig. 3.43; FP linear R square 0.345 and Fig. 3.44; linear R square 0.324).

The inter-relationships of the lidar data are also interesting. Both FP and LP intensity show moderate linear positive relationships to the LP DSM, with R square values of 0.33 and 0.35 respectively (Figs. 3.45 and 3.46). Ohms displays a strong negative relationship to soil organic content (Fig. 3.47; linear R square 0.72). The relationship of Ohms to the soil organic content again highlights how both these variables are a product of the geomorphology and the marked difference between the palaeochannel and terrace deposits. Ohms displays a moderate negative linear relationship to the soil moisture values (Fig. 3.48; linear R square 0.46). Lastly, the relationship of soil moisture and soil organic content displays a moderate linear positive relationship (Fig. 3.49; linear R square 0.43).

The computed table of correlation coefficients highlights the degree of inter-variable correlation visible in the Area 6 4m data graphical analysis (Tab. 3.3). All of the variables show highly significant correlations between each other, all at the 0.01 level. However, the graphical analysis clearly shows that not all of these relationships are linear. Whilst all these variables are highly correlated, this does not mean that lidar intensity can be used in a predictive sense to identify waterlogged and organic rich deposits, since some of the relationships are non-linear in form.

The linear graphical analysis of the variables showed that soil moisture and soil organic contents were most strongly related to topography, this being a function of the geomorphological variation within the study area. A very strong graphical linear relationship was also witnessed between topography and earth resistance data. The corresponding

relationships of Ohms, soil organic content and soil moisture content were graphically visibly weaker when compared to the lidar intensity FP and LP data sets. These data suggest that for use in a predictive capacity, topography would be a better indicator of waterlogged and organic rich deposits than either FP or LP intensity.

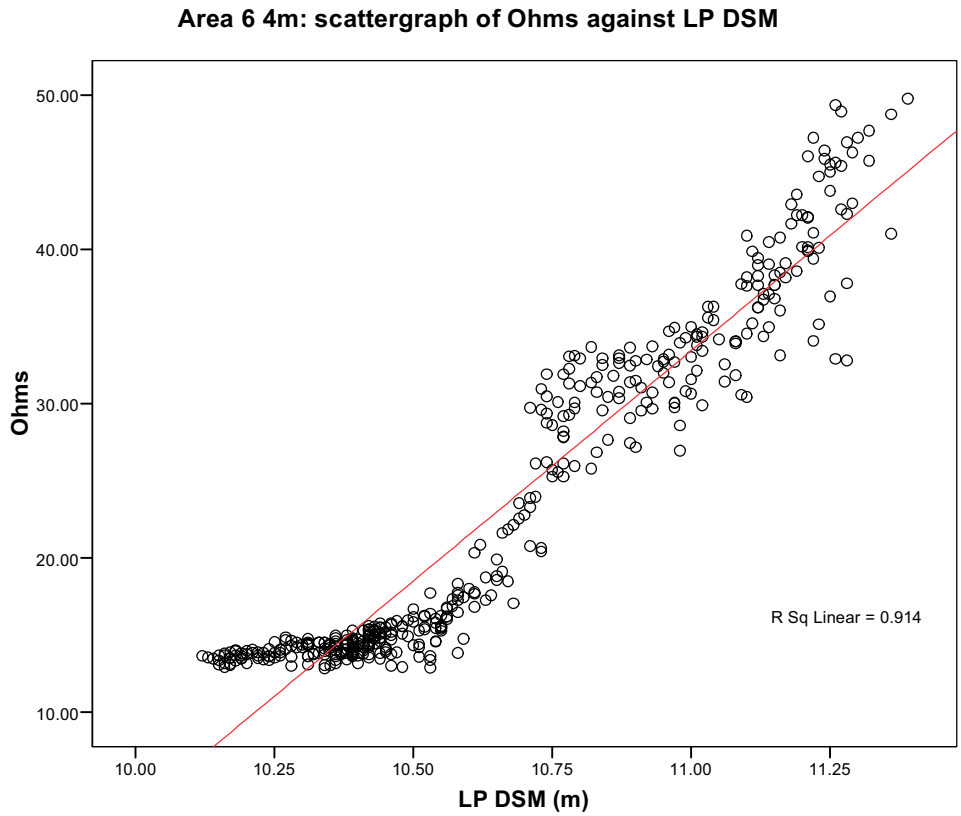

Fig 3.36: Ohms against LP DSM.

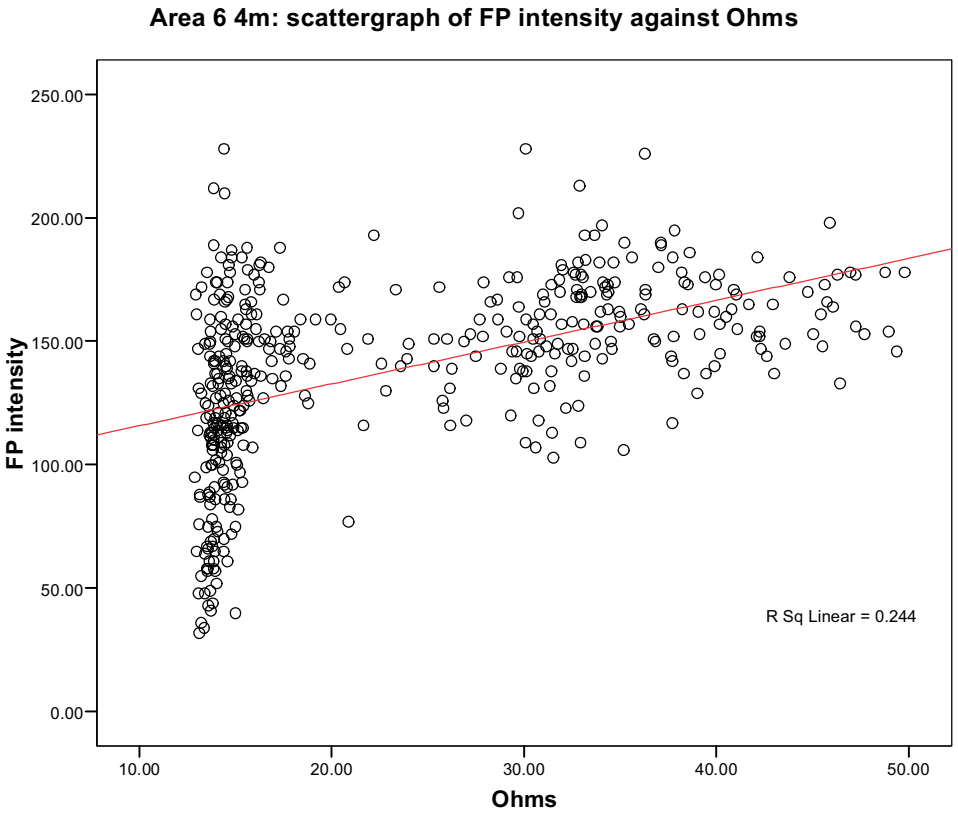

Fig 3.37: Ohms against FP intensity.

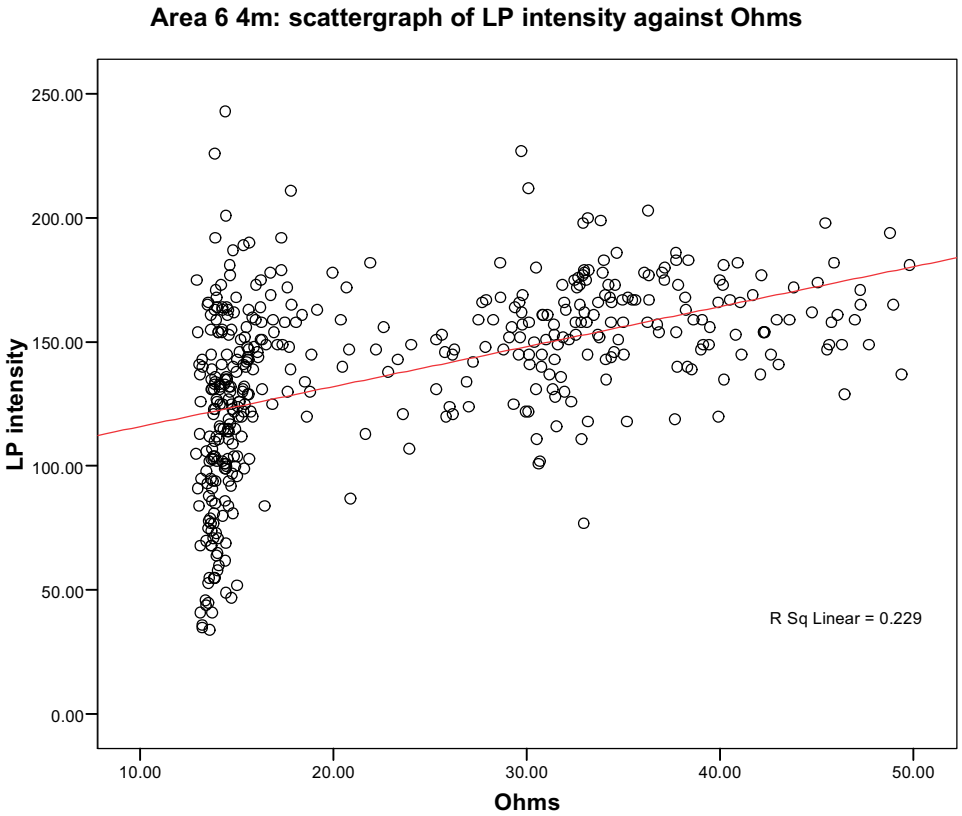

Fig 3.38: Ohms against LP intensity.

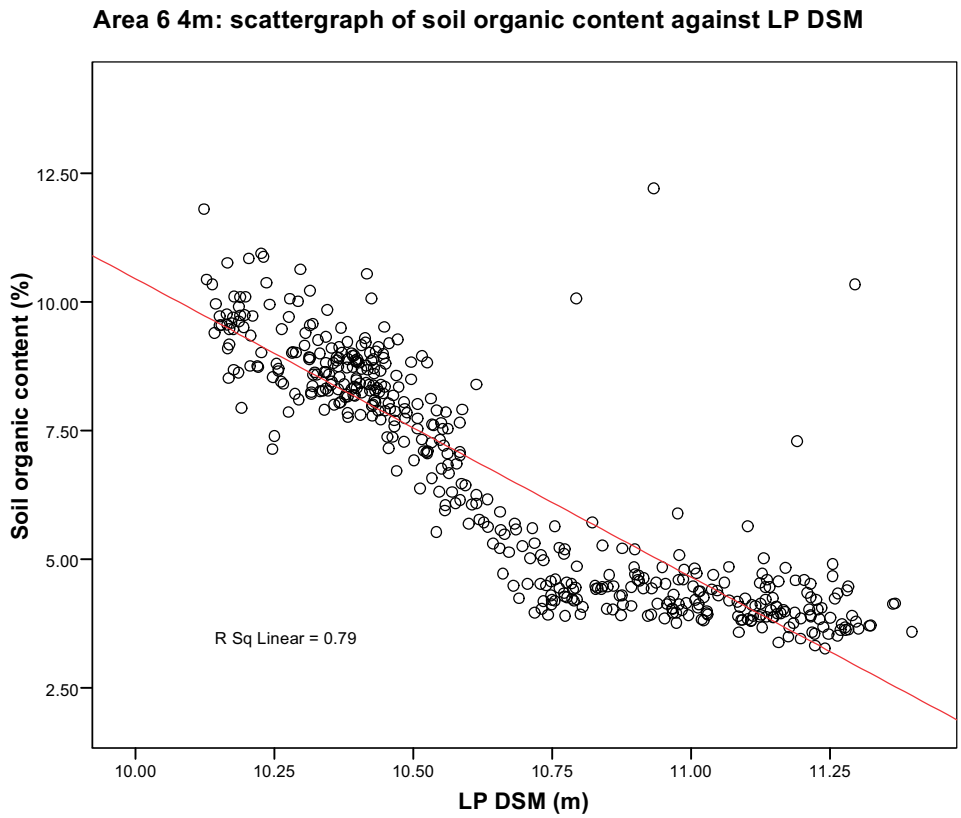

Fig 3.39: Soil organic content against LP DSM.

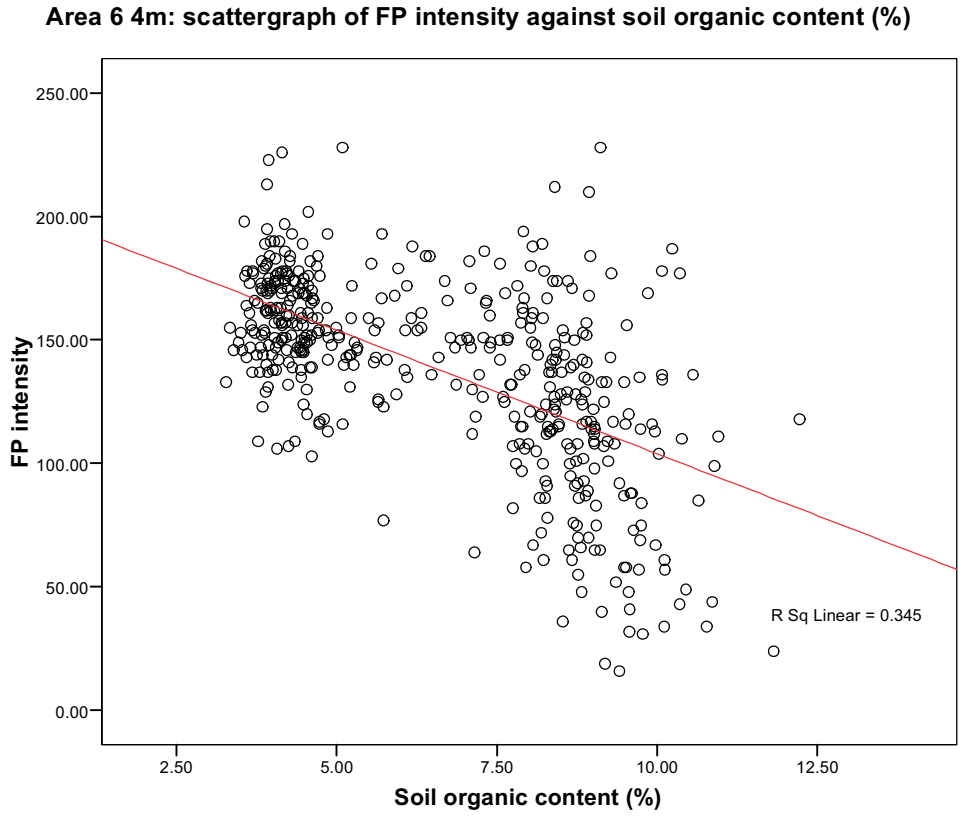

Fig 3.40: FP intensity against soil organic content.

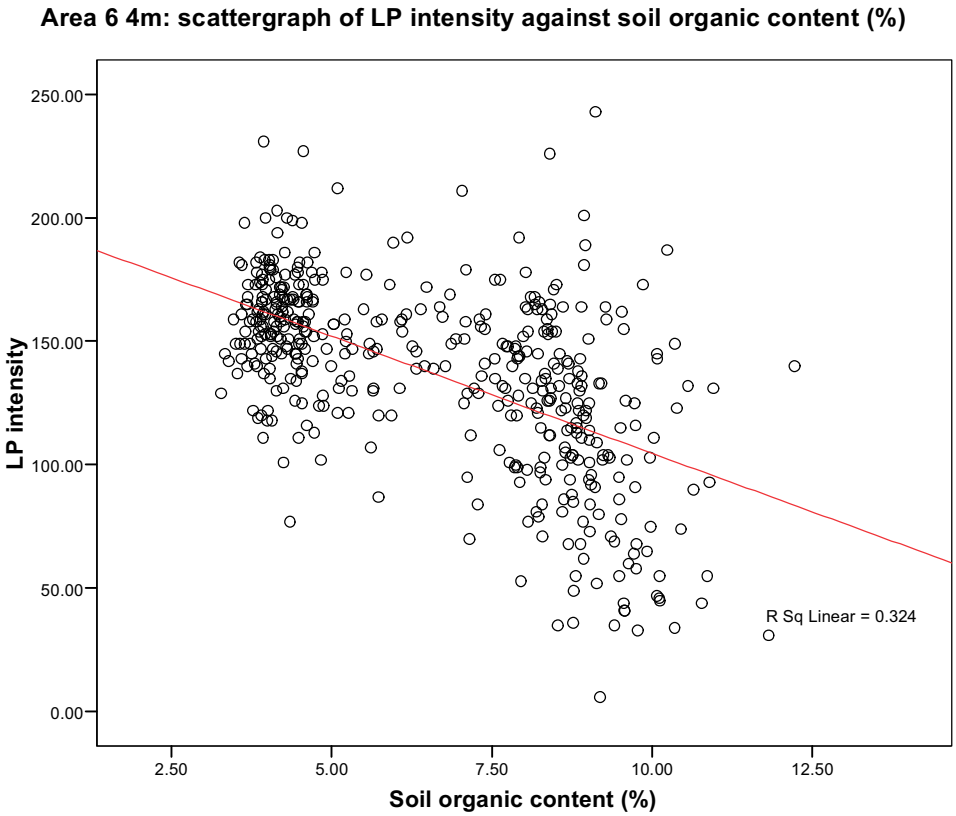

Fig 3.41: LP intensity against soil organic content.

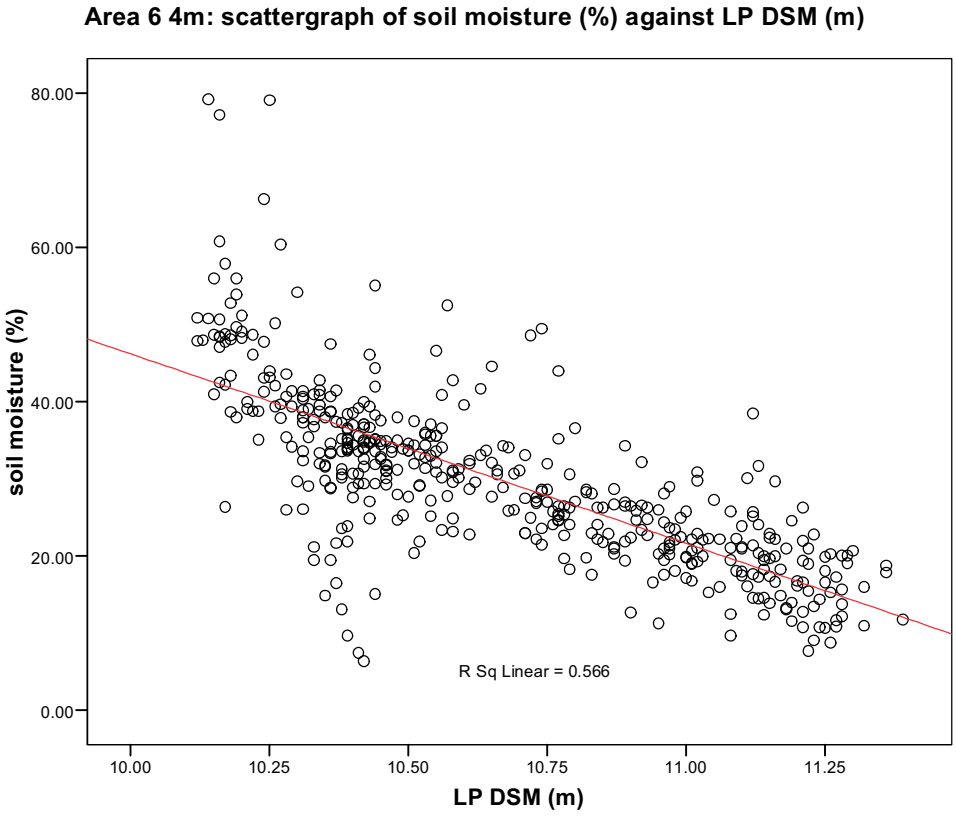

Fig 3.42: Soil moisture against LP DSM.

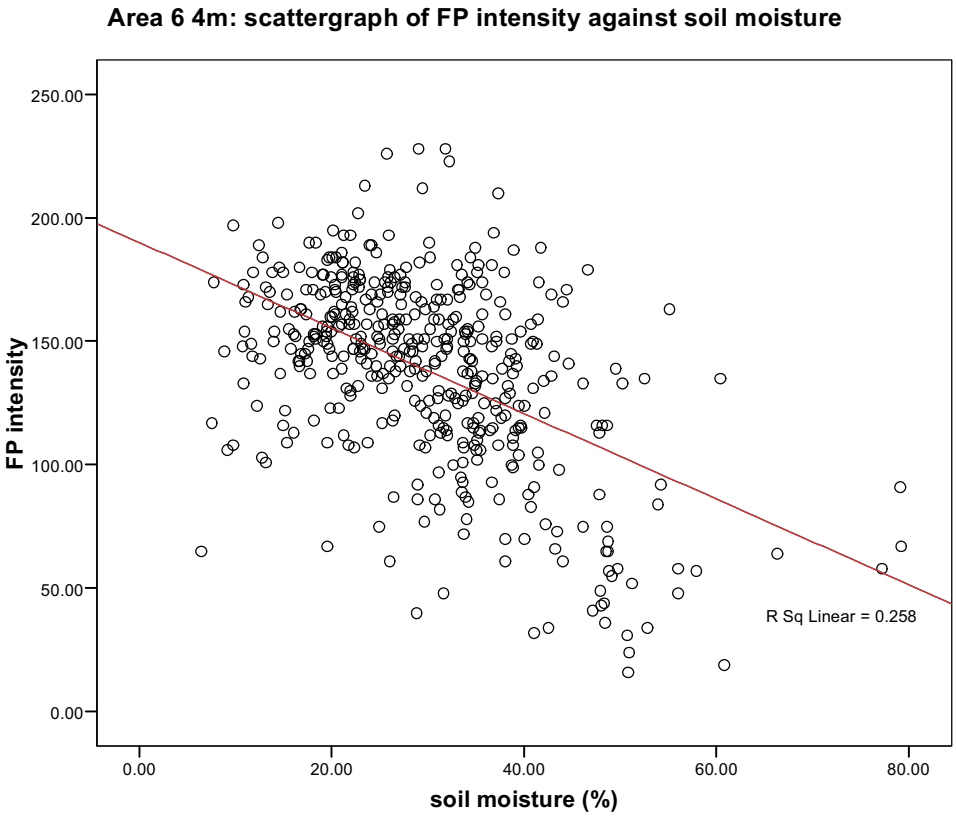

Fig 3.43: FP intensity against soil moisture.

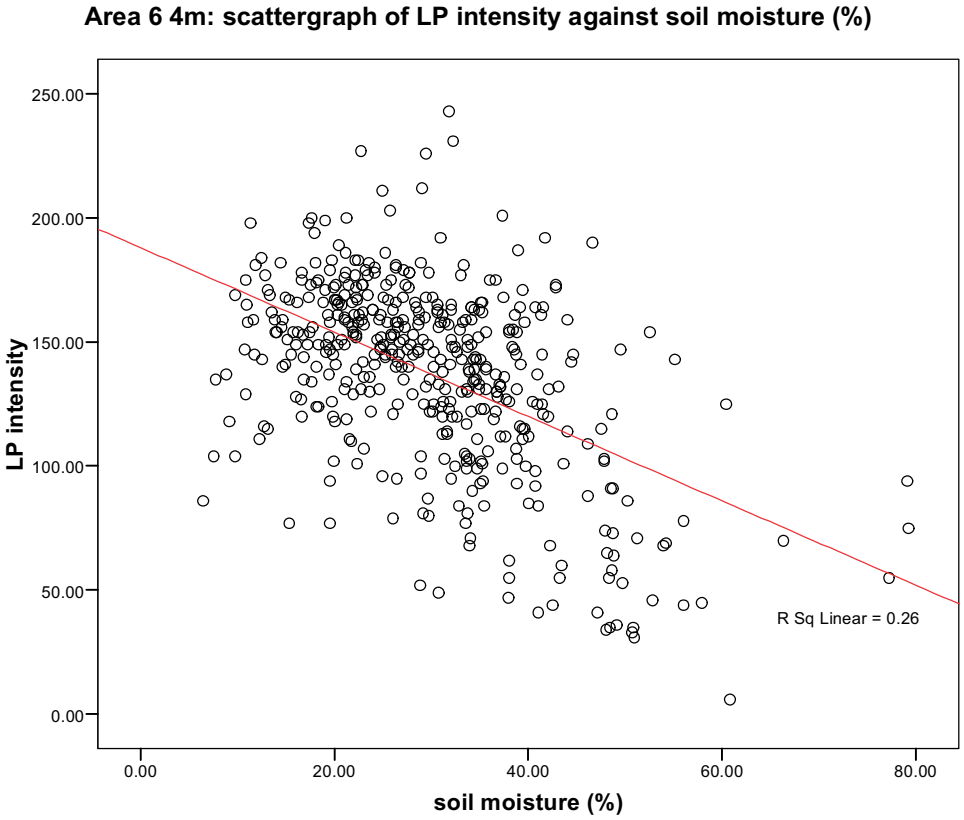

Fig 3.44: LP intensity against soil moisture (%).

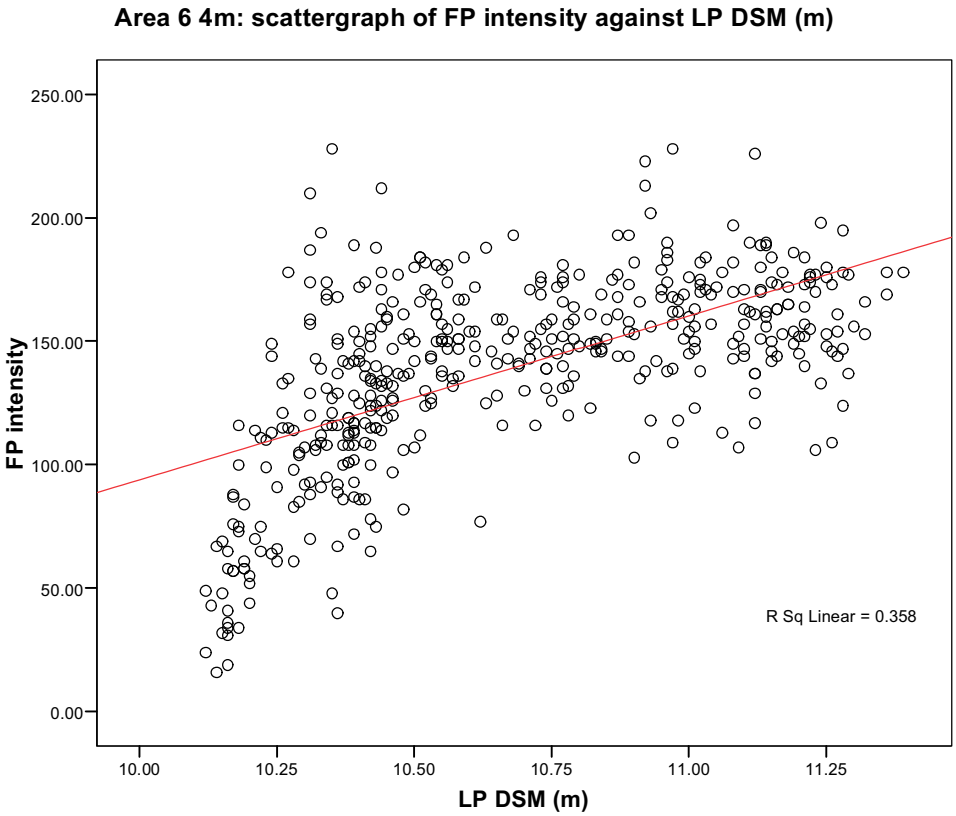

Fig 3.45: FP intensity against LP DSM.

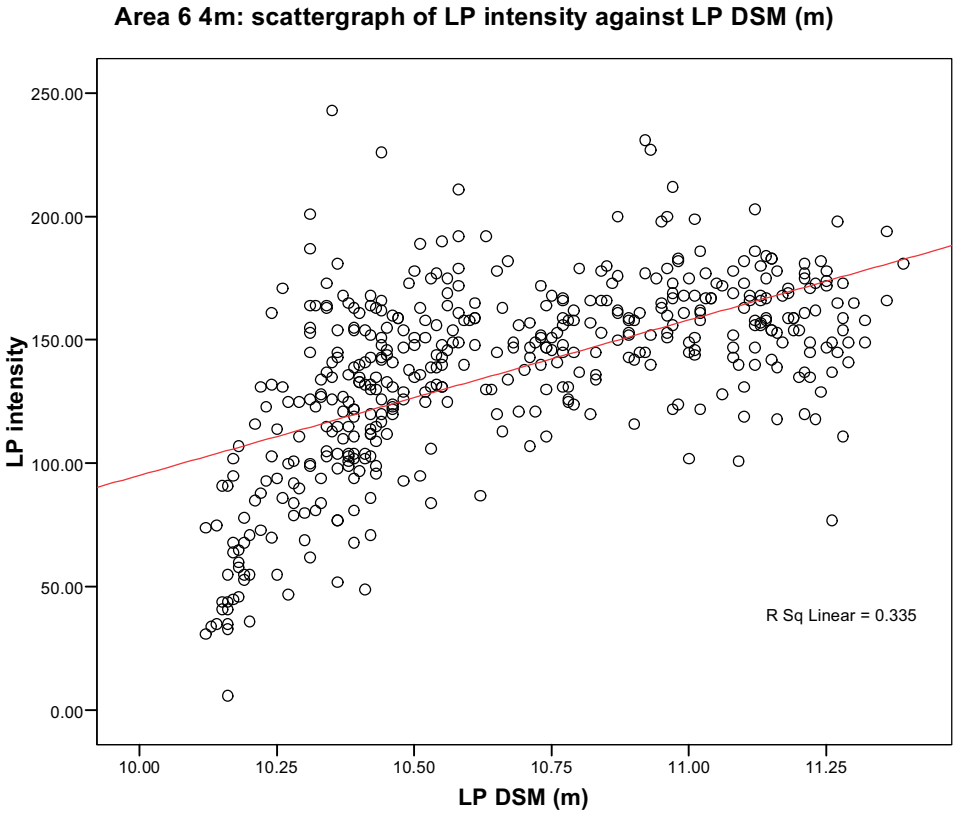

Fig 3.46: LP intensity against LP DSM.

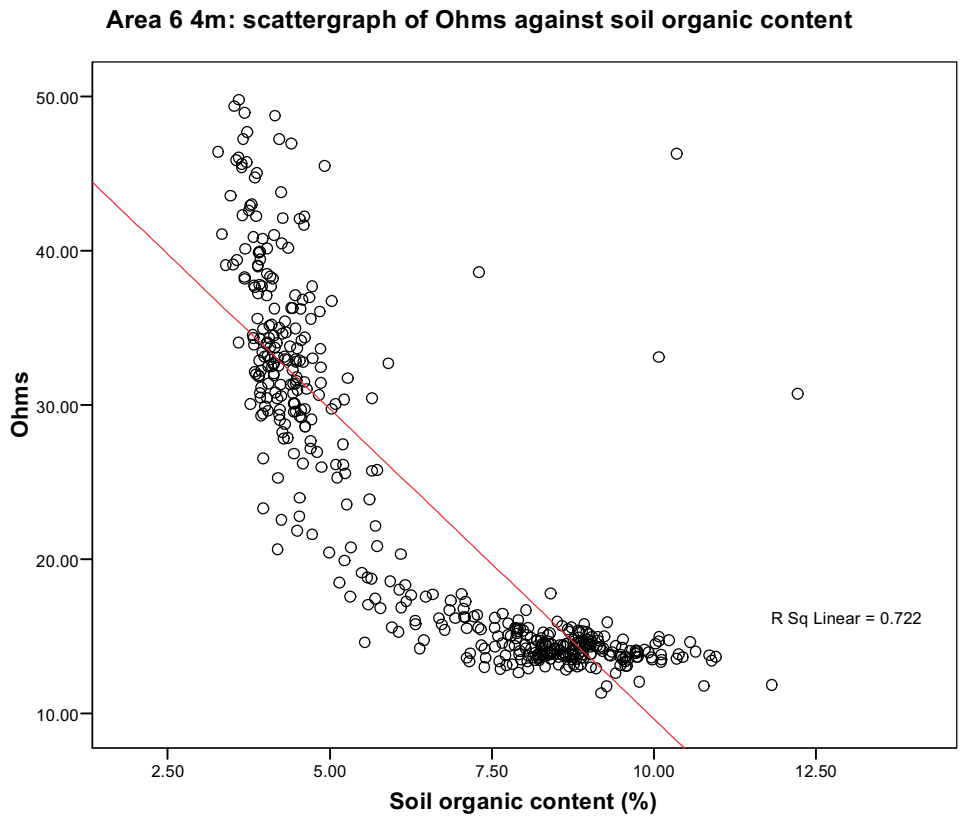

Fig 3.47: Ohms against soil organic content.

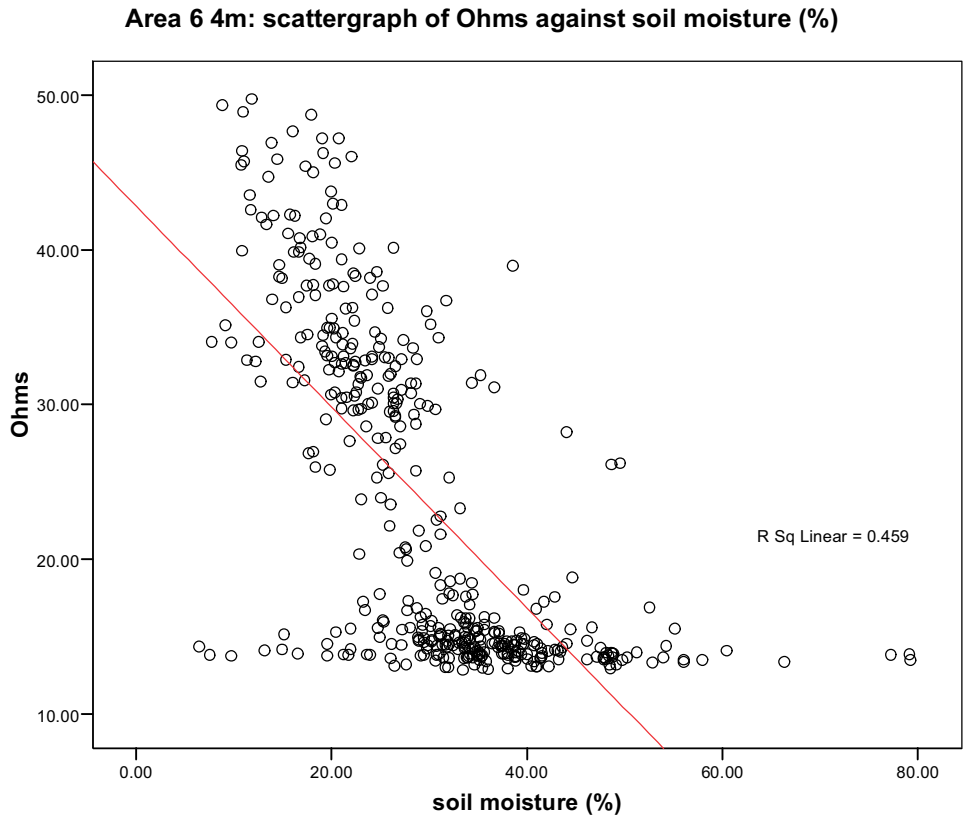

Fig 3.48: Ohms against soil moisture.

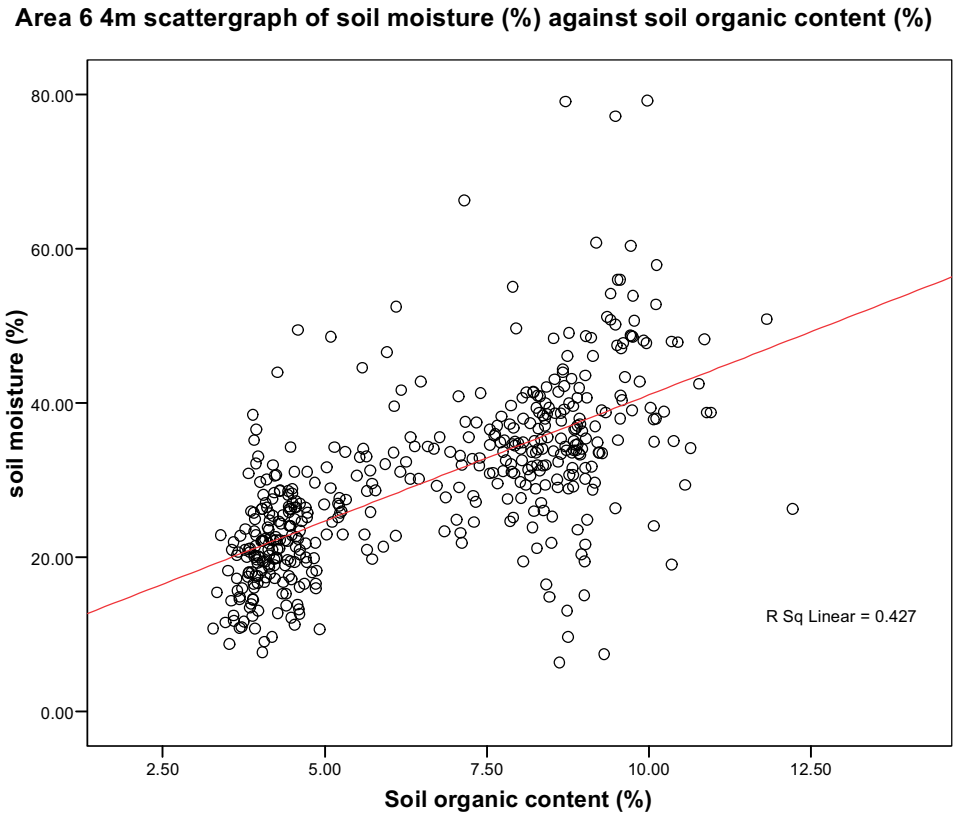

Fig 3.49: Soil organic content against soil moisture content.

Correlations

		soil moisture (%)	Ohms	LP DSM (m)	FP intensity	LP intensity	Soil organic content (%)
soil moisture (%)	Pearson Correlation	1	-.687**	-.752**	-.508**	-.510**	.653**
	Sig. (2-tailed)		.000	.000	.000	.000	.000
	N	450	450	450	450	450	450
Ohms	Pearson Correlation	-.687**	1	.954**	.504**	.490**	-.850**
	Sig. (2-tailed)	.000		.000	.000	.000	.000
	N	450	450	450	450	450	450
LP DSM (m)	Pearson Correlation	-.752**	.954**	1	.598**	.578**	-.889**
	Sig. (2-tailed)	.000	.000		.000	.000	.000
	N	450	450	450	450	450	450
FP intensity	Pearson Correlation	-.508**	.504**	.598**	1	.868**	-.587**
	Sig. (2-tailed)	.000	.000	.000		.000	.000
	N	450	450	450	450	450	450
LP intensity	Pearson Correlation	-.510**	.490**	.578**	.868**	1	-.569**
	Sig. (2-tailed)	.000	.000	.000	.000		.000
	N	450	450	450	450	450	450
Soil organic content (%)	Pearson Correlation	.653**	-.850**	-.889**	-.587**	-.569**	1
	Sig. (2-tailed)	.000	.000	.000	.000	.000	
	N	450	450	450	450	450	450

**. Correlation is significant at the 0.01 level (2-tailed).

Tab 3.3: Pearson Correlation Coefficients of the relationships between variables in area 6 4m data set.

3.2.4 Area 6: 1m data set analysis

The Area 6 1m data analysis used the earth resistance Ohms, LP DSM, FP intensity and LP intensity variables, all with a 1m data posting. Ohms displays a weaker linear relationship to topography within the Area 6 1m data set compared to the Area 6 4m data set analysis, with a moderate negative linear relationship (Fig. 3.50; linear R square 0.51). Conversely, the FP intensity data set displays a stronger relationship with Ohms in the Area 6 1m data set analysis, with a negative linear relationship (Fig. 3.51; linear R square 0.61). Ohms has a weaker negative linear relationship with LP intensity (Fig. 3.52; linear R square 0.275). Within this survey area, with a distinct set aside vegetation structure, the results indicate that FP intensity is a more reliable indicator of geomorphology than the LP intensity, suggesting that changes in vegetation structure, most evident in FP data which comprises returns from the top of the vegetation cover, are reflecting changes in geomorphology.

The FP intensity displays a very strong relationship to the LP DSM (Fig. 3.53, linear R square 0.914). This again suggests that changes in vegetation structure are representing larger changes in topography, here a product of geomorphology. However, in contrast the LP intensity return has a much weaker linear positive relationship with LP DSM (Fig. 3.54: linear R square 0.238). This difference in the relationship of the FP and LP intensity to LP DSM indicates that vegetation is a better indicator of changes in geomorphology via the FP intensity return, rather than changes in ground surface structure and character as defined by the LP intensity return. The table of computed correlation coefficients demonstrates strong inter-variable relationships between all of the variables at the 0.01 level (Tab. 3.4).

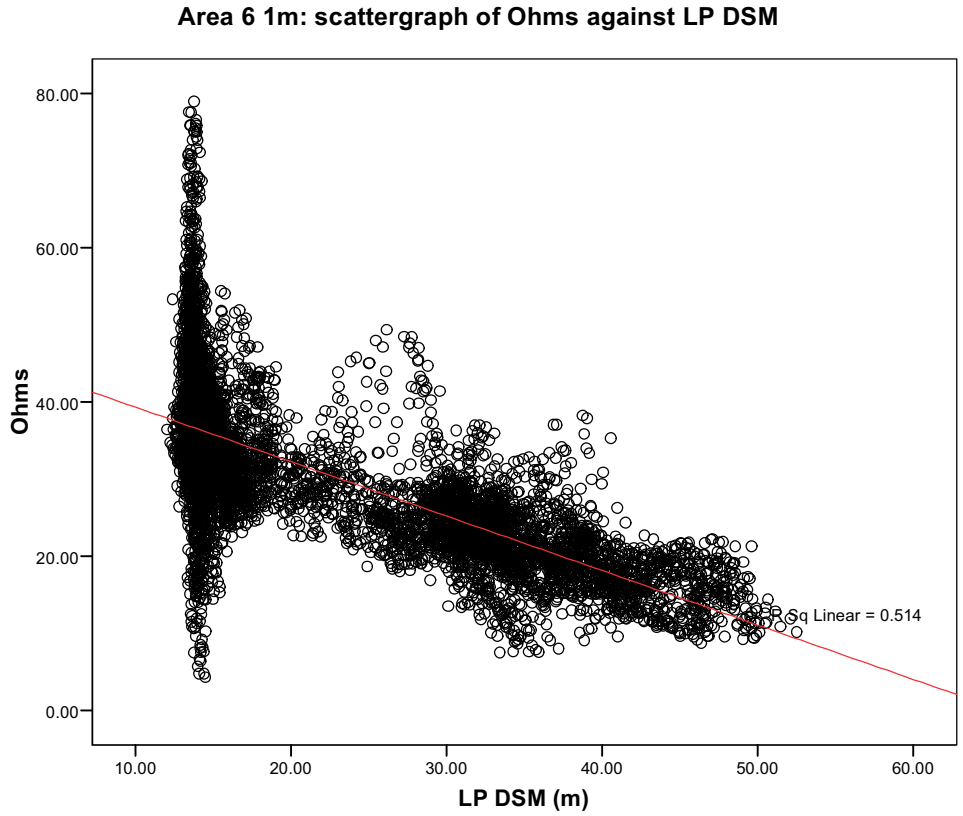

Fig 3.50: Ohms against LP DSM.

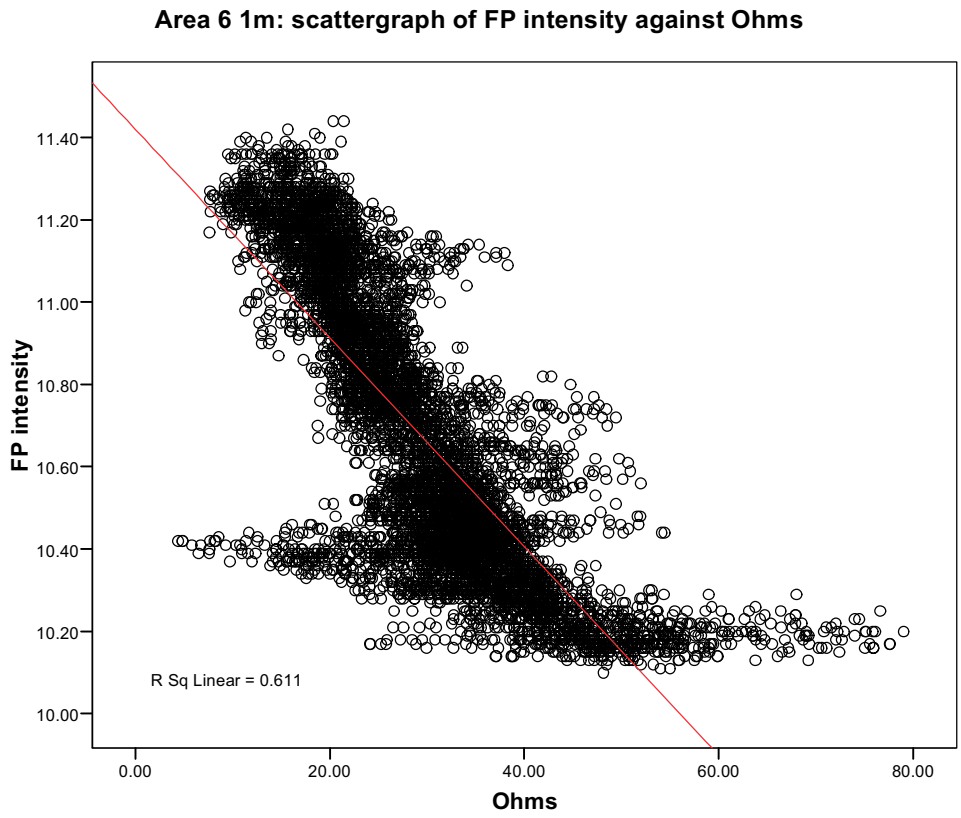

Fig 3.51: FP intensity against Ohms.

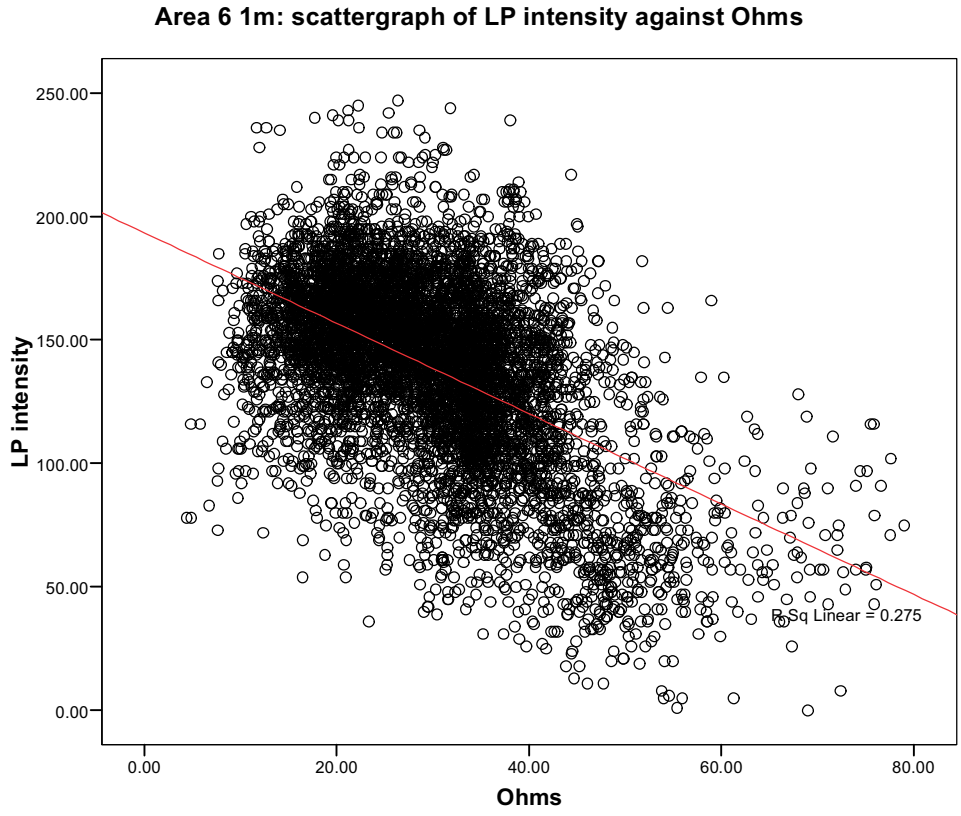

Fig 3.52: LP intensity against Ohms.

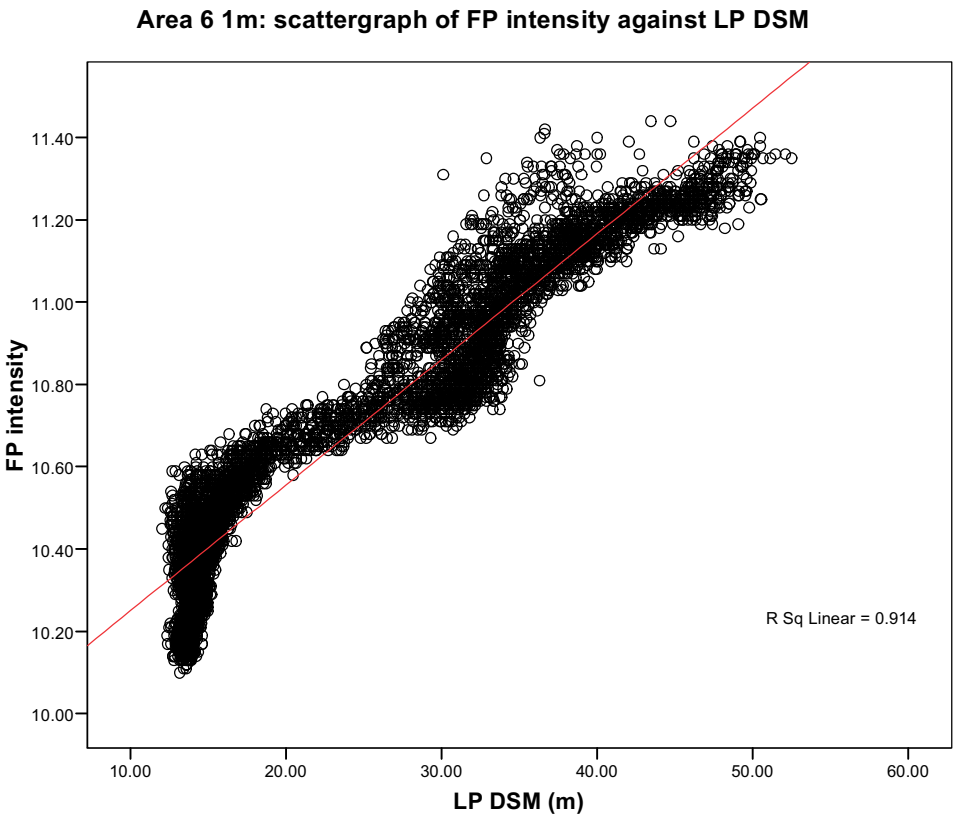

Fig 3.53: FP intensity against LP DSM.

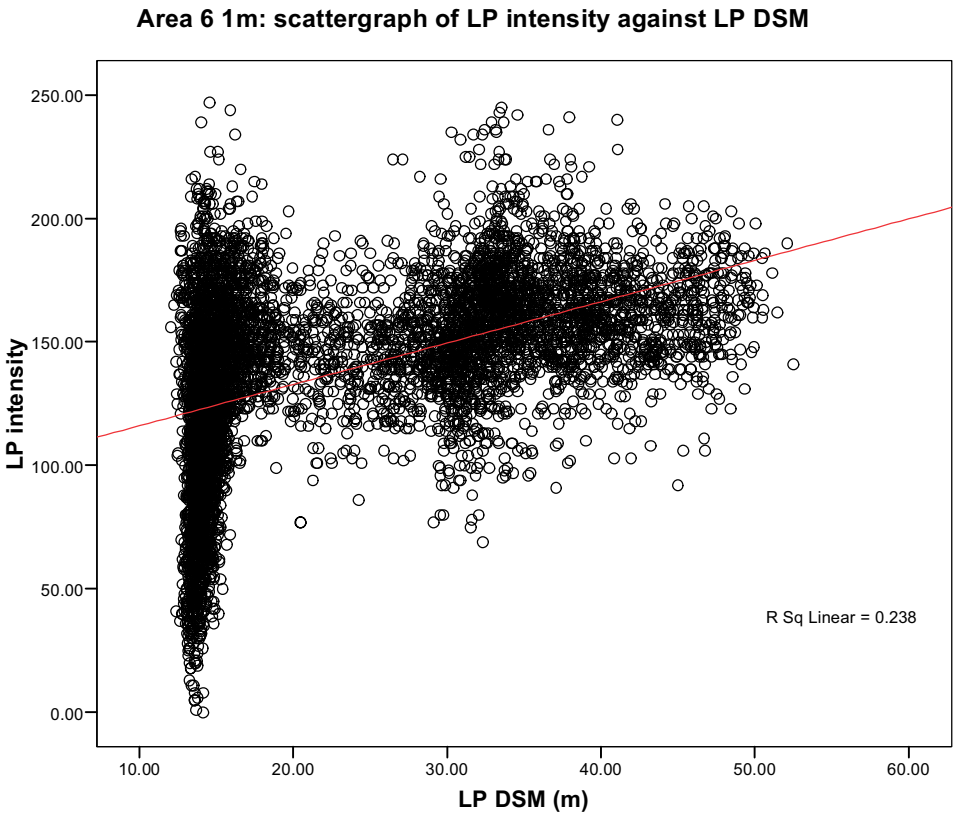

Fig 3.54: LP intensity against LP DSM.

Correlations

		Ohms	LP DSM (m)	FP intensity	LP intensity
Ohms	Pearson Correlation	1	-.717**	-.781**	-.524**
	Sig. (2-tailed)		.000	.000	.000
	N	6960	6960	6960	6960
LP DSM (m)	Pearson Correlation	-.717**	1	.956**	.488**
	Sig. (2-tailed)	.000		.000	.000
	N	6960	6960	6960	6960
FP intensity	Pearson Correlation	-.781**	.956**	1	.571**
	Sig. (2-tailed)	.000	.000		.000
	N	6960	6960	6960	6960
LP intensity	Pearson Correlation	-.524**	.488**	.571**	1
	Sig. (2-tailed)	.000	.000	.000	
	N	6960	6960	6960	6960

**. Correlation is significant at the 0.01 level (2-tailed).

Tab 3.4: Table of Pearson Correlation Coefficients from the 1m data set analysis.

3.2.5 Area 6 relationship of surface intensity to sub-surface sediment stratigraphy

A gouge core transect (Fig. 3.55) was used to record the changes in sediment stratigraphy from the palaeochannel to the terrace. The gouge core transect reveals the palaeochannel to have relatively deep deposits, (c. 2.5m), with a complex internal stratigraphy (Fig. 3.56). The upper stratigraphy of the palaeochannel is dominated by a stiff brown silty clay (Unit A), an orange brown stiff clay (Unit B) and an orange brown grey stiff clay (Unit C) on the south of the palaeochannel. To the north of the palaeochannel the upper stratigraphy is dominated by a brown grey sandy clay (Unit F) and a grey clay (Unit Q). The lower stratigraphy of the palaeochannel is complicated, revealing a number of different sediment units, showing changes between clay and sand dominated units (Units D, E, G, I, J, K, L, M, N, O, P, Q, S and T).

The alluvial stratigraphy of the terrace is notably different to that of the channel, with much shallower deposits located on top of the terrace gravels. The sediment stratigraphy is simpler, with only five sediment units. An orange brown grey stiff clay (Unit B), an orange brown grey stiff clay (Unit C) and a grey sandy clay (Unit H) are witnessed at the palaeochannel margin at the edge of the terrace. Moving north the above gravel terrace alluvium consists of an orange grey clayey medium sand (Unit R), located beneath the units A and B.

The FP and LP intensity values are shown plotted against the changes in sediment stratigraphy (Fig. 3.57). These results across a single transect show that intensity returns have a marked contrast between the palaeochannel and terrace deposits, which visually correlates with the changes in sediment stratigraphy. However, whilst the terrace deposits show generally higher intensity values, the palaeochannel shows variation in the intensity response. Both the FP and LP intensity data have extremely high and low values across the palaeochannel. It might be argued that the large spike in the FP and LP intensity data sets over the palaeochannel coincides with the change in complex stratigraphy within the palaeochannel, above the units (F, P, L, K, H, M and N). This change in sub-surface sediment architecture may be reflected in the surface sediments, such as through standing water, depicted by the spike FP and LP intensity data sets. However, the palaeochannel does show generally high soil organic contents compared to the terrace and as such a more even

response across the palaeochannel compared to the terrace would be required if FP and LP intensity were to be used a robust predictive manner for the identification of organic rich deposits.

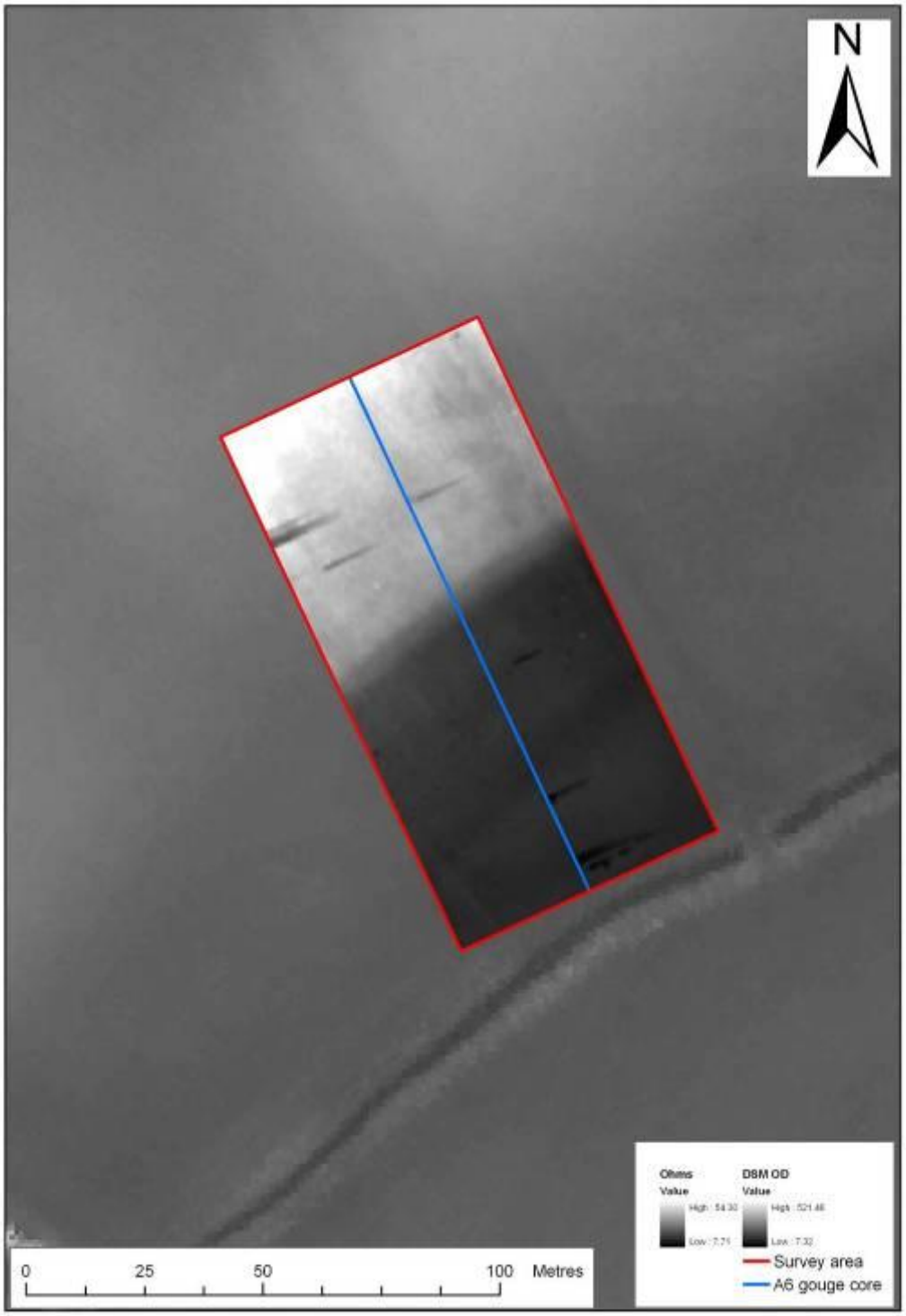

Fig 3.55: The location of the Area 6 gouge core transect.

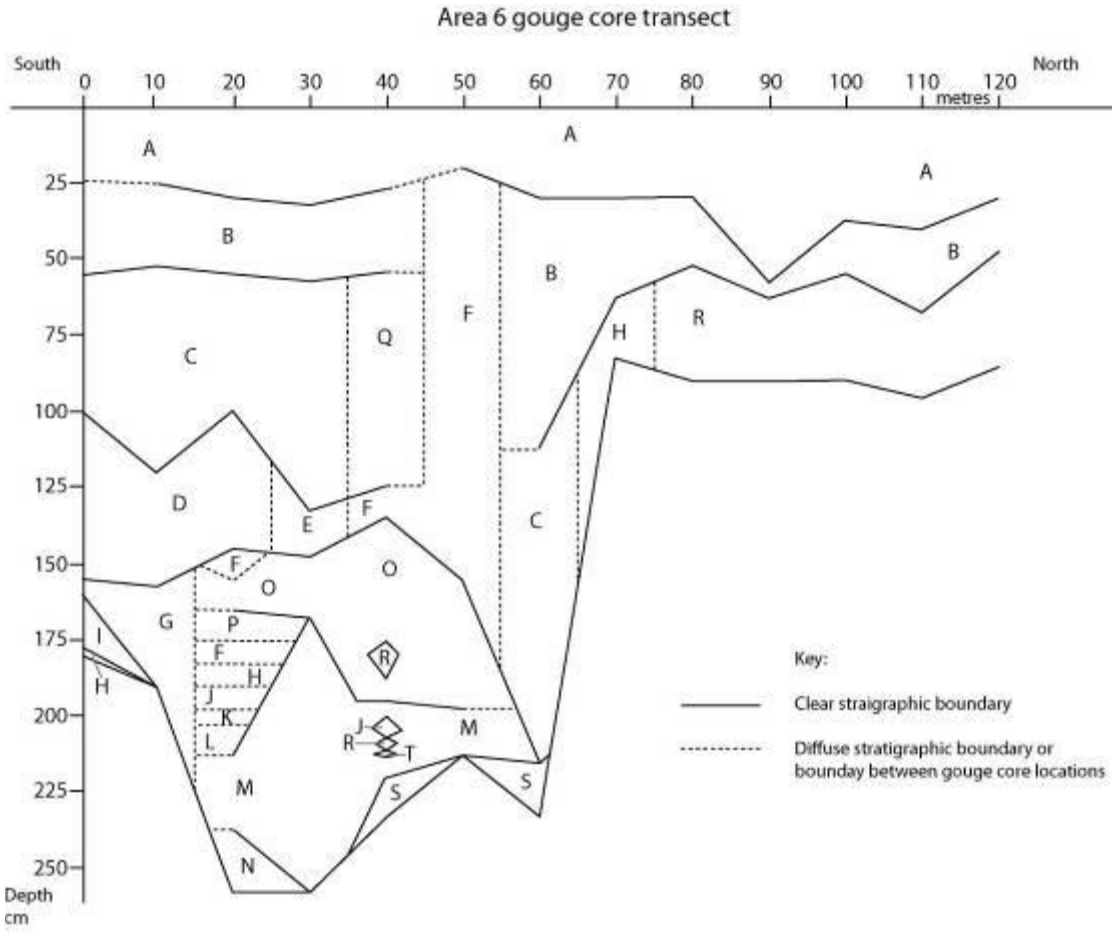

A = stiff grey brown silty clay, trace of sand and charcoal
B = orange grey brown stiff clay, trace of sand, Fe and Mn mottling with charocal
C = orange grey brown stiff clay, heaving Mn and Fe mottling
D = brown grey clay, trace of sand, Fe and Mn mottling
E = grey brown clayey sand, Fe mottling and charocal
F = brown grey sandy clay
G = grey olive brown clay, trace of sand Fe mottling
H = grey sandy clay, Fe mottling
I = light grey clayey coarse sand, interbedded with orange med sand containing organic humic staining
J = orange grey coarse/medium sand
K = banded grey sandy clay
L = dark grey sandy clay
M = dark grey clay, trace of sand
N = sand (not recovered)
O = grey clay, trace of sand, Fe mottling
P = grey brown med coarse sand
Q = grey clay, trace of sand, Fe and Mn mottling
R = orange grey clayey sand medium
S = dark grey sand, trace of sand
T = dark grey clayey sand

Fig 3.56: The Area 6 gouge core transect. The palaeochannel has a deeper more complex above gravel alluvial stratigraphy compared to the terrace.

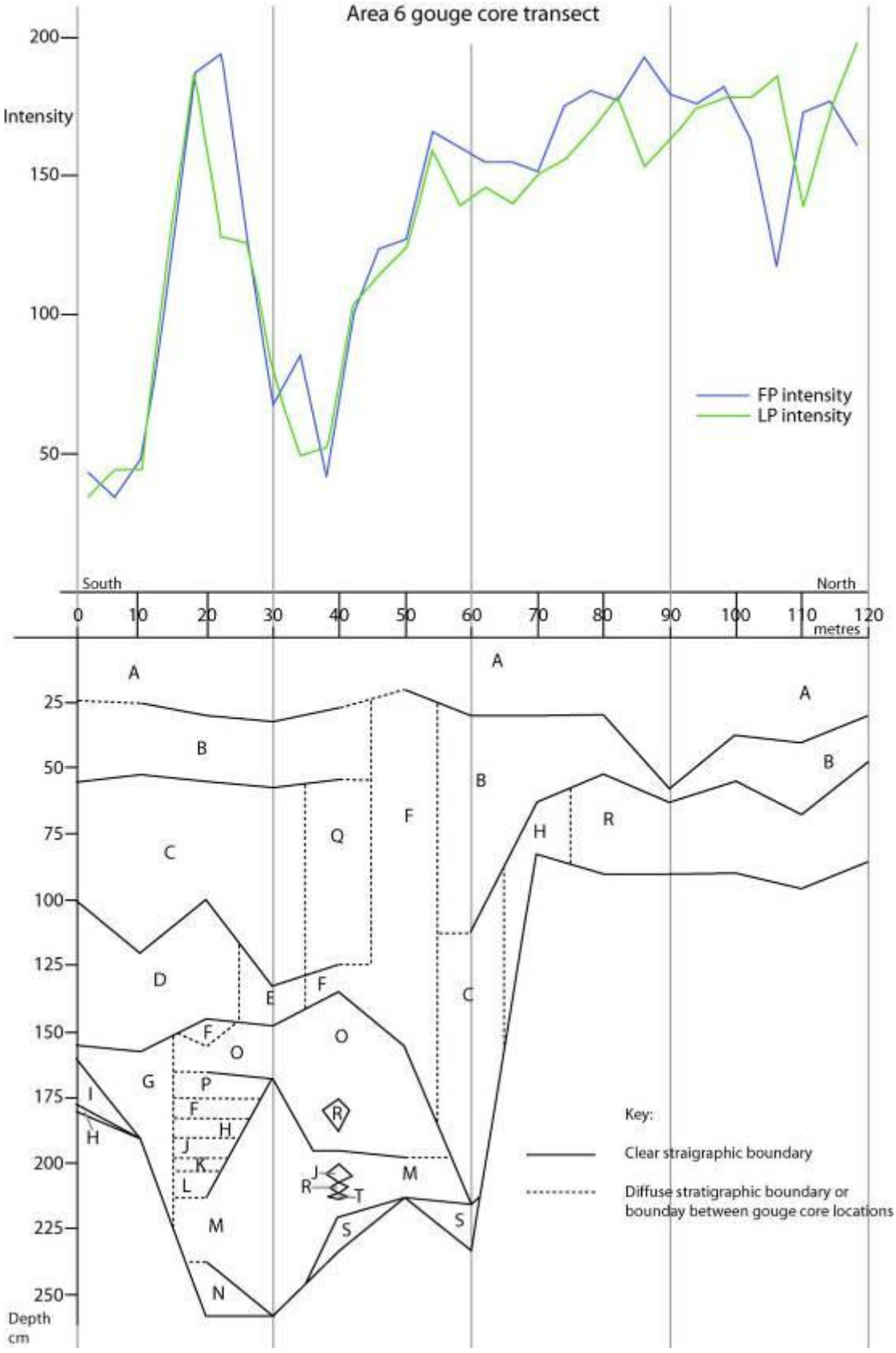

Fig 3.57: The FP and LP intensity values shown against the above gravel alluvial stratigraphy, Area 6. Changes in intensity response are visible between the palaeochannel and the terrace. However, marked variation in intensity response is seen over the palaeochannel, indicating that both FP and LP intensity cannot be used is a robust predictive manner for the identification of organic rich deposits.

3.2.6 Area 6 summary of main results

The analysis of the lidar data for Area 6 has produced some interesting, at times contradictory, results. However, several broad themes have emerged from this survey.

The Area 6 visual qualitative analysis revealed:

- The terrace and palaeochannel geomorphological units were definable in the LP DSM, FP intensity and LP intensity data.
- The palaeochannel displayed higher soil organic content and soil moisture content compared to the terrace
- The palaeochannel had lower earth resistance values (Ohms) compared to the terrace.

The Area 6 4m data set analysis revealed:

- Ohms displayed a strong negative linear relationship to LP DSM.
- Ohms displayed a weaker negative linear relationship with both FP and LP intensity.
- Soil organic content displayed a strong negative linear relationship to LP DSM.
- Soil organic content displayed a weaker negative linear relationship with both FP and LP intensity.
- Soil moisture content displayed a moderate negative linear relationship to LP DSM.
- Soil moisture content displayed a weaker negative linear relationship with both FP and LP intensity.
- These results indicate that topography defined by the LP DSM is the best indicator of variation in geomorphology and organic preservation (within Area 6).

The Area 6 1m data set analysis revealed:

- Ohms displayed a moderate linear negative relationship to LP DSM.
- Ohms had a stronger negative linear to relationship to FP intensity, but a weak negative linear relationship to LP intensity.
- FP intensity had a very strong linear positive correlation with LP DSM.
- LP intensity had a moderate positive linear relationship with LP DSM.
- The differences between the relationship of FP intensity and LP intensity to LP DSM, suggests that changes in vegetation structure are a better indicator of geomorphology that intensity reflection from the ground surface, within Area 6.

The Area 6 relationship of surface intensity to sub-surface sediment stratigraphy revealed:

- The palaeochannel had a deeper, more complex alluvial stratigraphy than the terrace.
- Both FP and LP intensity showed a change between the terrace and palaeochannel units
- This change in FP and LP intensity between units was not consistent.
- Both FP and LP intensity revealed extremely high and low values over the palaeochannel, potentially a product of standing surface water causing data spikes.

3.3 AREA 7

3.3.1 Area 7 geological background

Area 7 is located almost entirely on a section of undifferentiated alluvium, which bisects part of the Holme Pierrepont Terrace (Fig. 3.58). At the northwest edge, the survey area covers part of the Holme Pierrepont Terrace. The geomorphology is indicative of a Holocene palaeochannel that has partially eroded into an area of older Devensian terrace. The vegetation structure within the area suggess linear features within the undifferentiated alluvium, such as palaeochannels and potential scroll bars. The survey in Area 7 was undertaken in bright and sunny conditions, but with much standing water on the surface.

3.3.2 Area 7: Visual qualitative analysis

The analysis of Area 7 data begins with a visual qualitative analysis. The topography defined by the lidar DSM clearly differentiates between the Holme Pierrepont Terrace and the unit of lower undifferentiated alluvium (Fig. 3.59). Whilst there is some level of topographic variation within the undifferentiated alluvium of Area 7, it is not possible to define any further discrete structure from the DSM. The FP intensity does not define the difference between the Holme Pierrepont Terrace and topographically lower undifferentiated alluvium (Fig. 3.60). However, the FP intensity does clearly display variation within the survey Area 7, trending in the same direction as the vegetation differences recorded during field survey. The LP intensity data produces a very similar results to the FP intensity, and again variation is observed within the ground survey grid (Fig. 3.61).

The earth resistance data brings greater clarity to the Area 7 ground survey grid. Plotted against the DSM topography (Fig. 3.62), the earth resistance data shows a relatively high resistance feature at the extreme northwest edge of the grid, representing the transition from lower alluvium to higher terrace. A low resistance feature is evident in the data trending northwest to southeast and is interpreted as a palaeochannel. The east of the survey grid displays intermediate resistance values, interpreted as Holocene alluvium adjacent to the palaeochannel. The earth resistance data is in good agreement with the lidar DSM, with both techniques identifying the change between Holocene alluvium and Home Pierrepont Terrace. However, the earth resistance data also defines the form of a palaeochannel within the survey grid, a feature not apparent on the lidar DSM.

The earth resistance data when shown against the FP data both display similar data trends, although these trends do not correlate exactly (Fig. 3.63). For example, the palaeochannel defined by earth resistance data is visible as a change in the FP intensity data, although the location of the two features do not match exactly. To the southeast of the survey grid there is subtle change in earth resistance data on the area of the undifferentiated alluvium and this visually correlates with changes in FP intensity. The LP intensity data is extremely similar to the FP intensity data, with the same broad visual correlation between intensity and earth resistance Ohms (Fig. 3.64).

The soil organic content data produce surprising results. The soil organic content data is shown against the DSM, and the location of the palaeochannel is clearly defined as an area of low soil organic content, compared to the area of floodplain adjacent to the palaeochannel to the southeast of the survey grid (Fig. 3.65). The area of low soil organic content broadly correlates with changes in FP and LP intensity (Figs. 3.66 and 3.67), although the relationship between the intensity data sets and the soil organic contents is not exact.

In contrast, the soil moisture data reveals the palaeochannel as an area of high soil moisture content (Fig. 3.68), with lower soil moisture values on the floodplain to the east of the survey grid. The variation seen in both FP and LP intensity again broadly correlates with the changes in soil moisture values, but this visual correlation is not exact (Figs. 3.69 and 3.70). In summary, the visual analysis of the Area 7 data sets has revealed a low resistance feature with relatively high soil moisture content and relatively low organic content, interpreted as a palaeochannel. To the east of this within the survey grid there is an area of higher resistance values, higher soil organic values and higher soil moisture values. The FP and LP intensity data sets show greater variation in the data across the survey grid than the topographic DSM. This probably reflects changes in vegetation structure, which were noted on site during data capture.

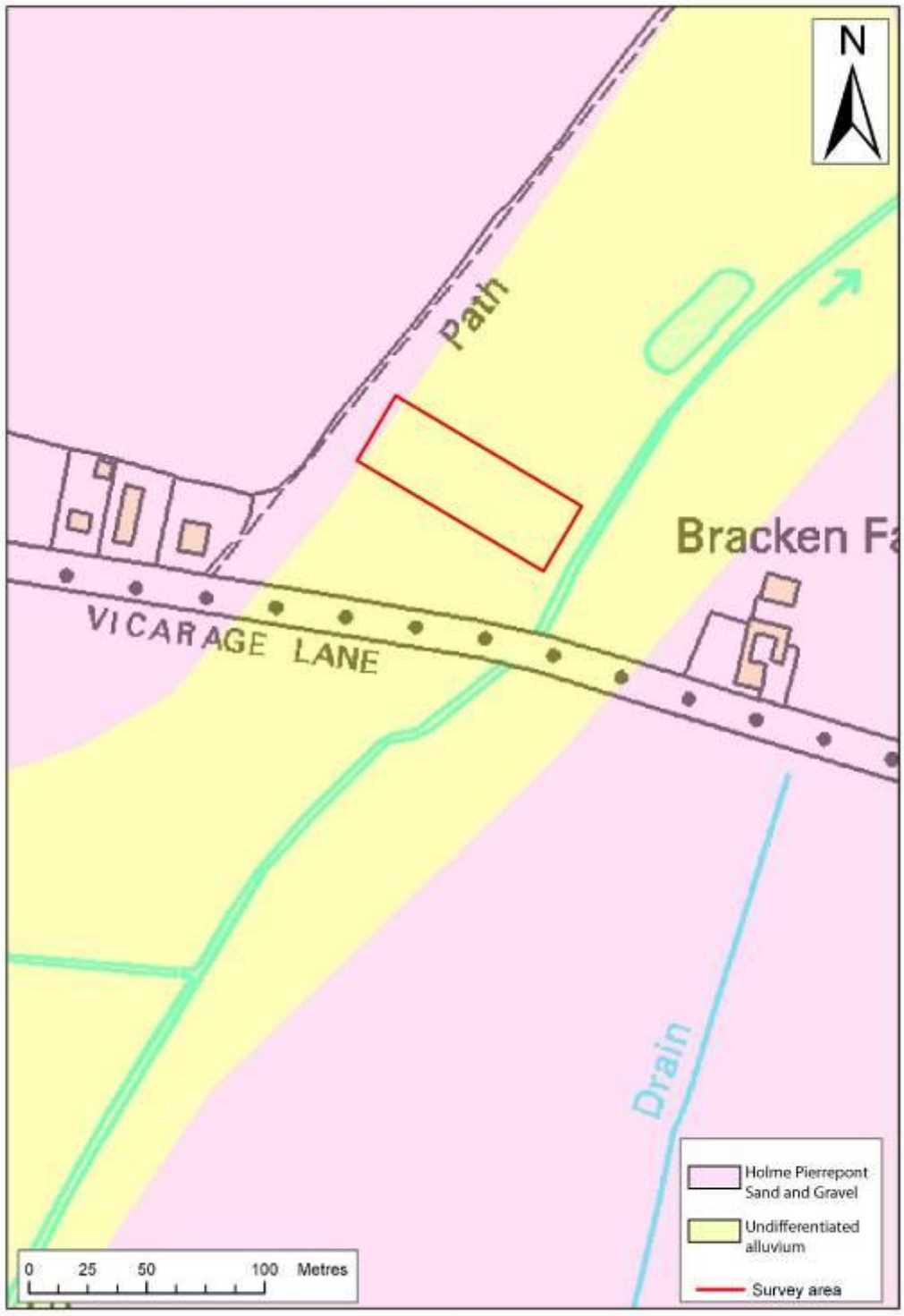

Fig 3.58: The 1:50, 000 BGS geological mapping around Area 7.

Fig 3.59: The survey area shown on topography (DSM OD).

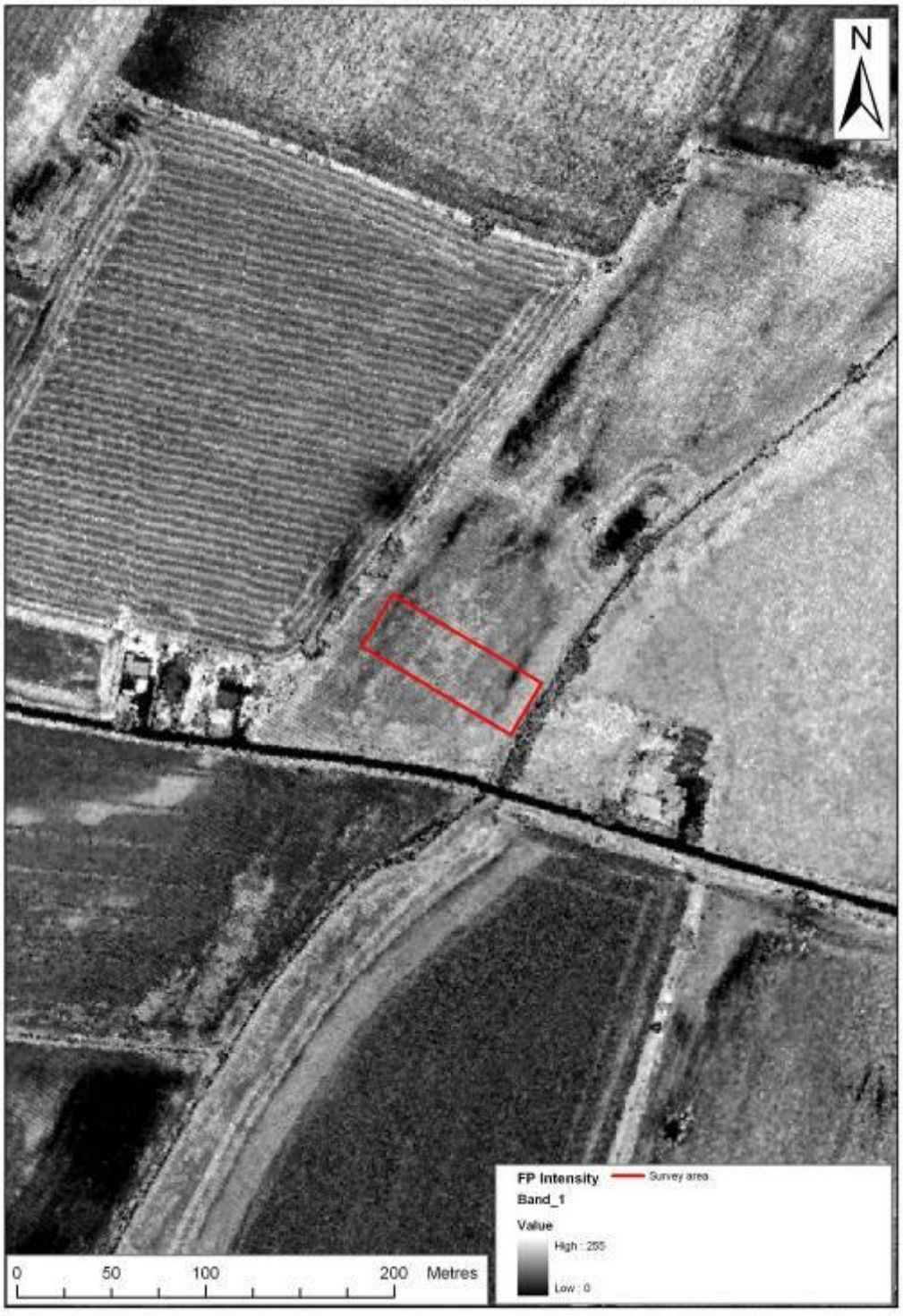

Fig 3.60: The survey area shown on FP intensity.

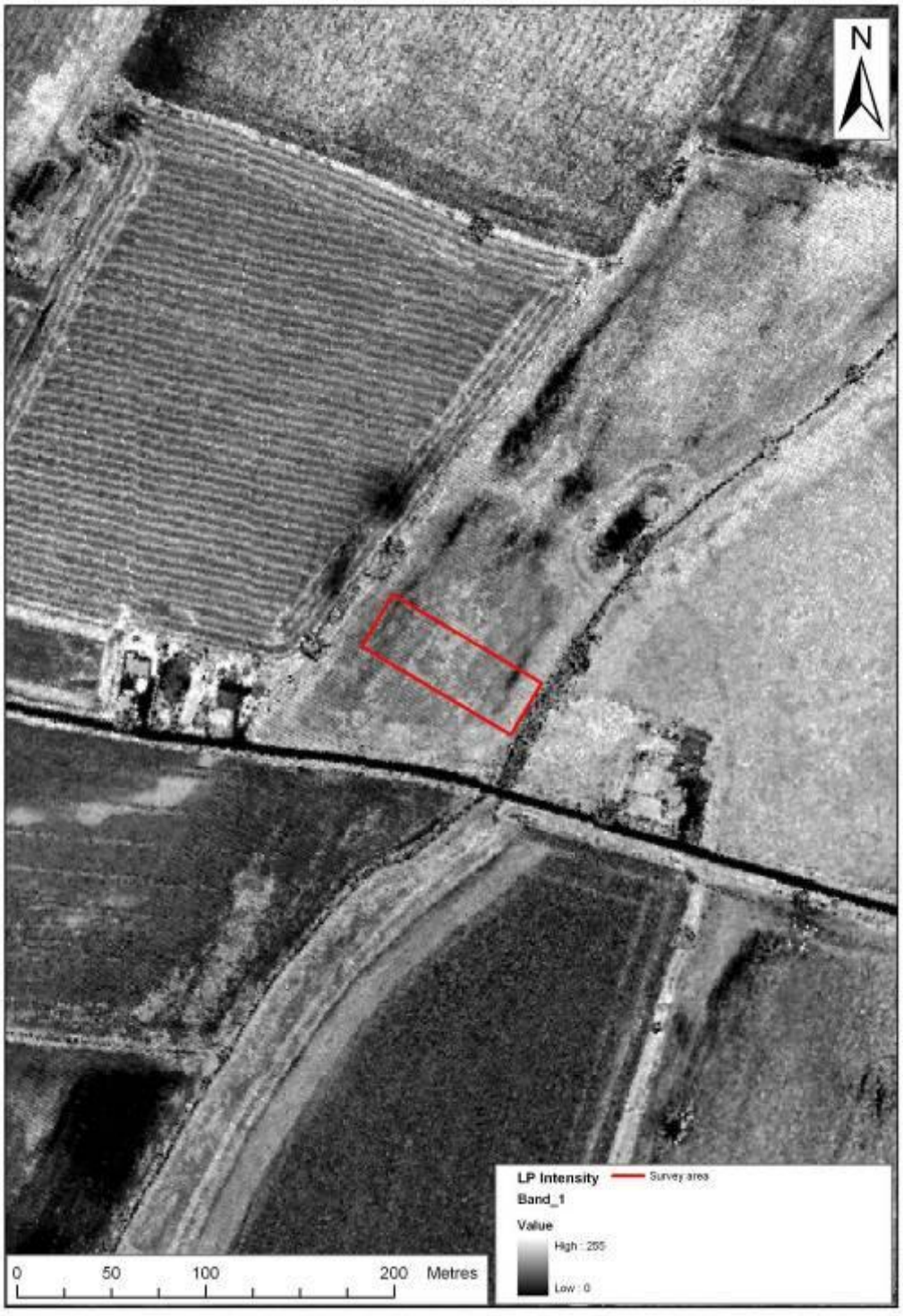

Fig 3.61: The survey area shown on LP intensity.

Fig 3.62: Earth resistance Ohms on DSM OD.

Fig 3.63: Earth resistance Ohms on FP intensity.

Fig 3.64: Earth resistance Ohms superimposed on LP intensity.

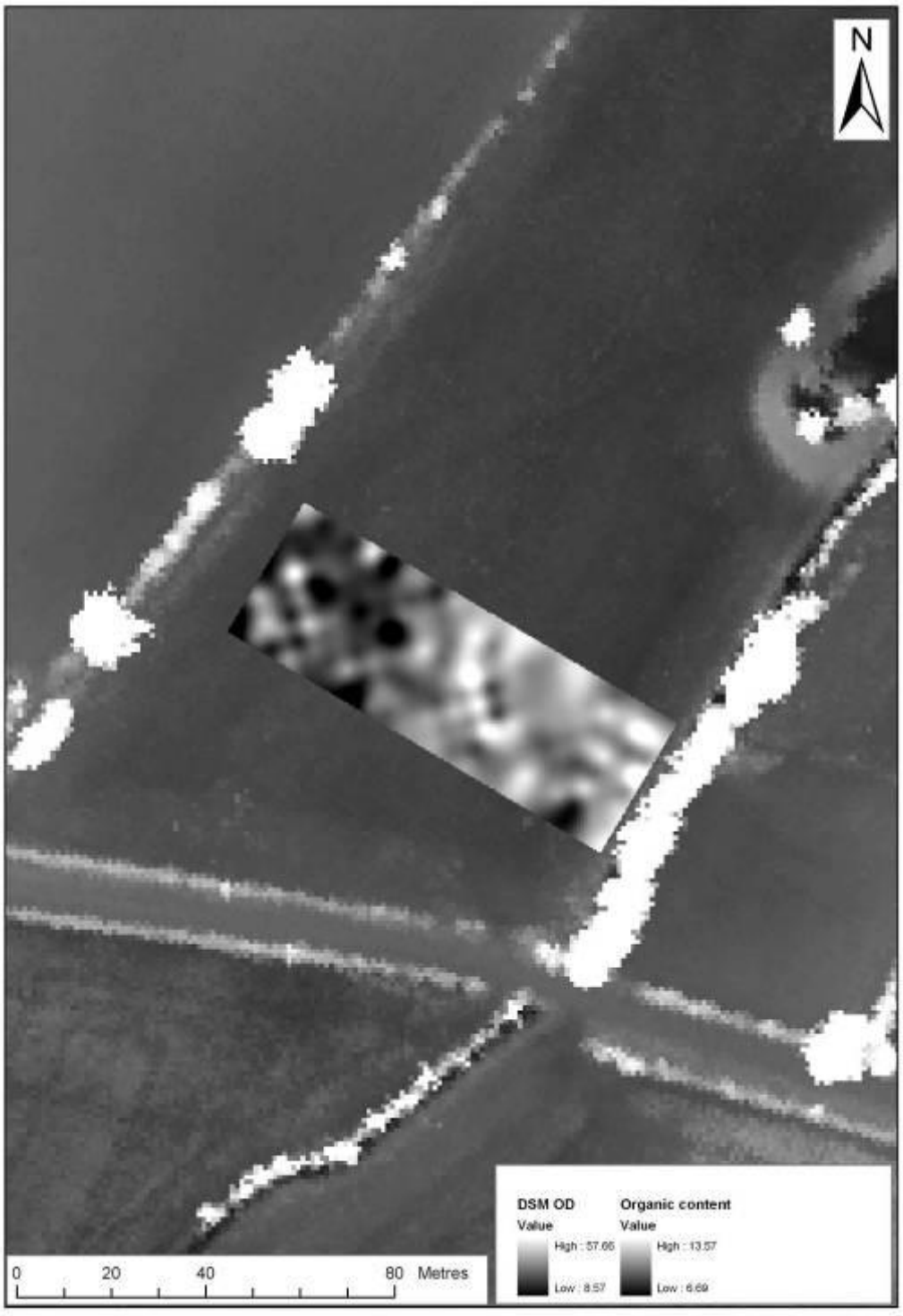

Fig 3.65: Organic content superimposed on DSM OD.

Fig 3.66: Organic content superimposed on FP intensity.

Fig 3.67: Organic content superimposed on LP intensity.

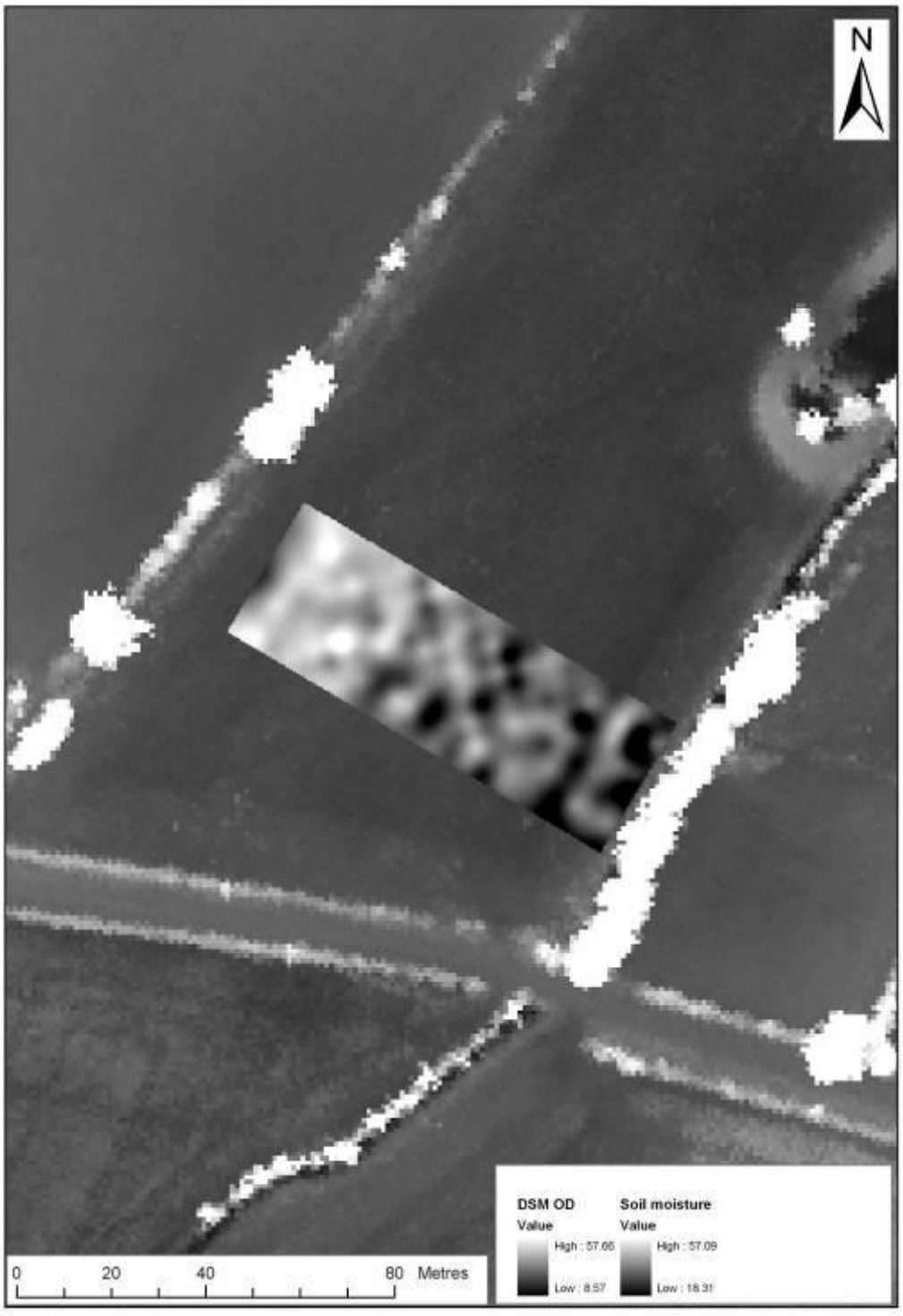

Fig 3.68: Soil moisture content superimposed on DSM OD.

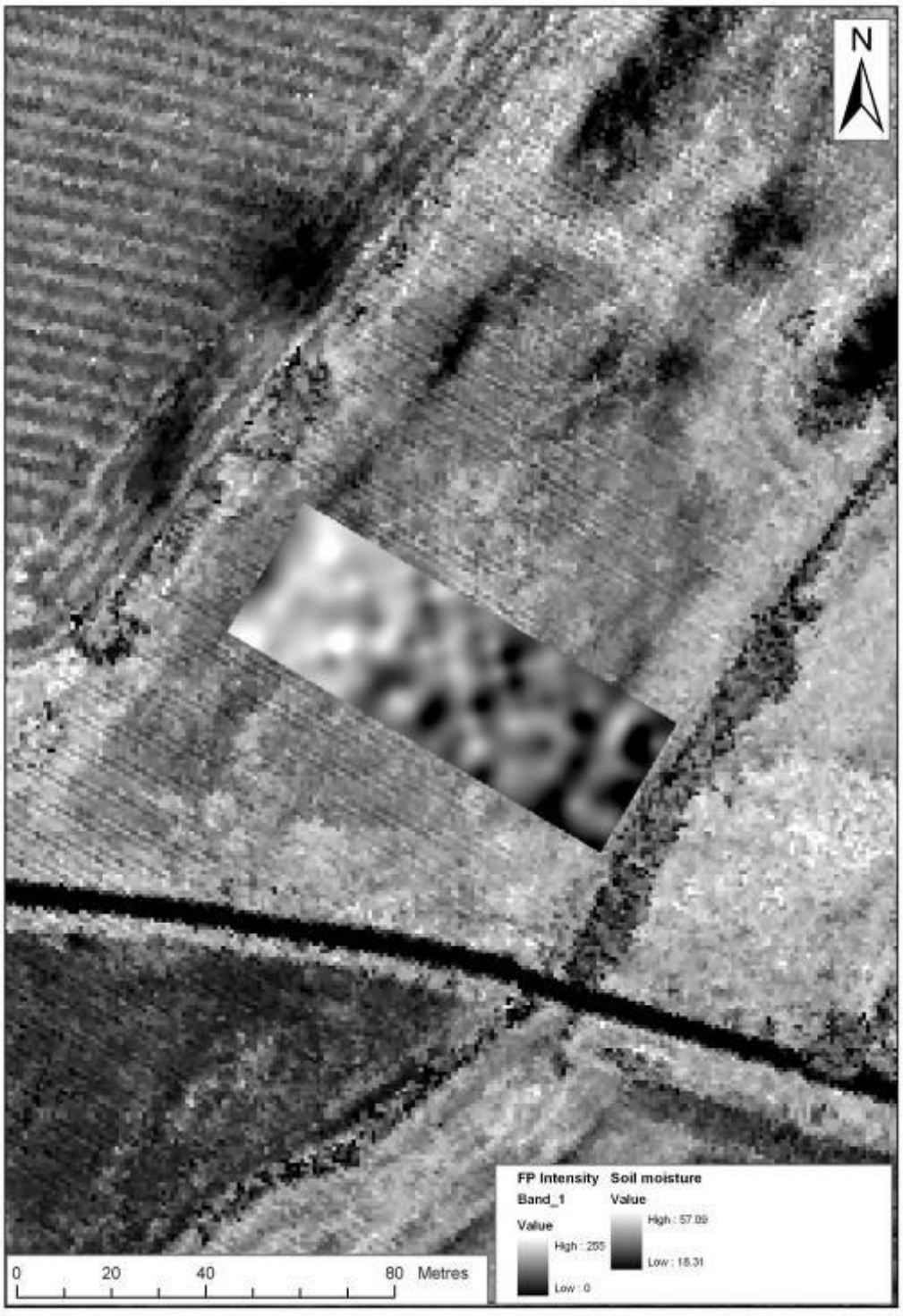

Fig 3.69: Soil moisture content superimposed on FP intensity.

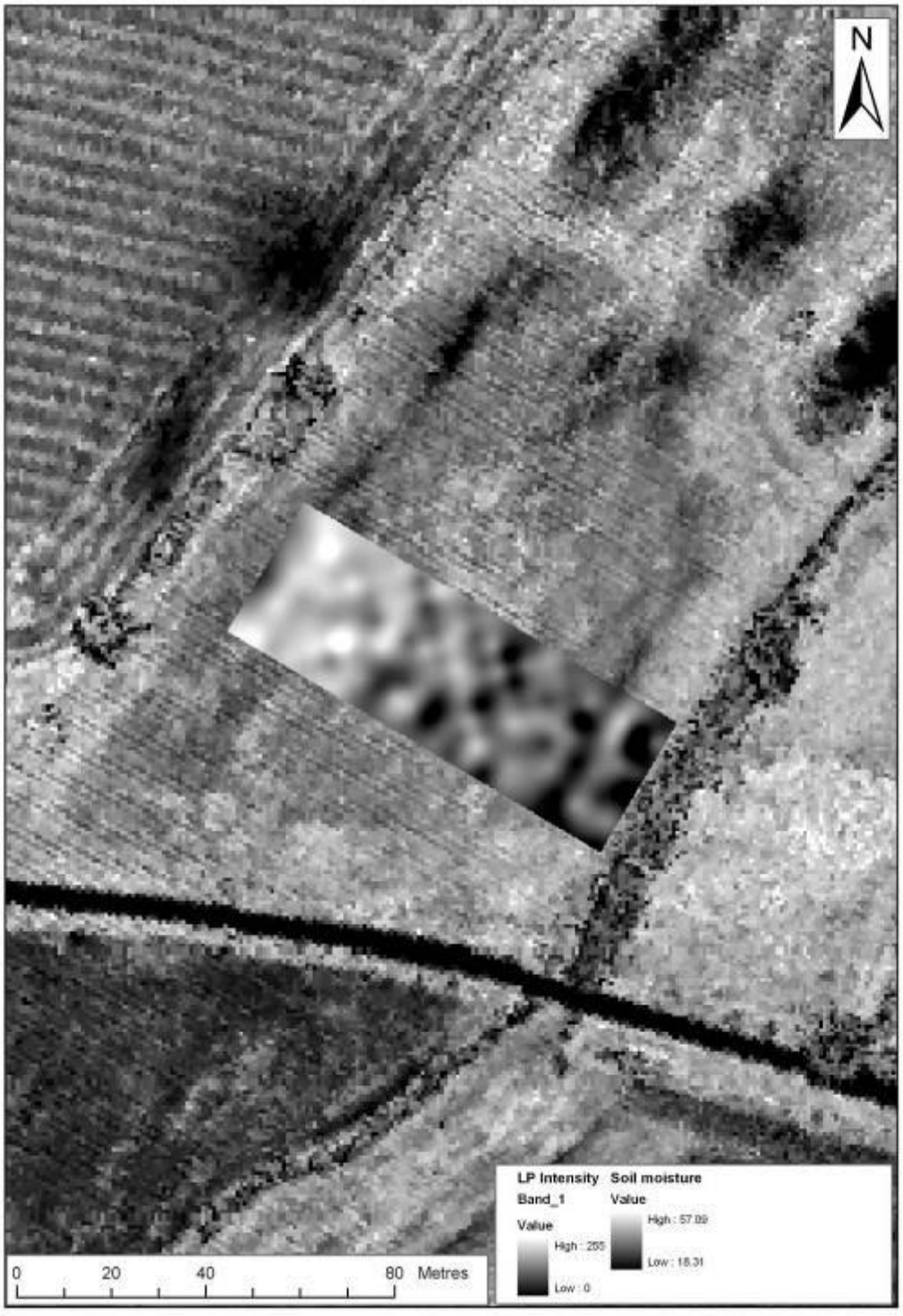

Fig 3.70: Soil moisture content superimposed on LP intensity.

3.3.3 Area 7: 4m data set analysis

Analysis of the Area 7 4m data shows a weak negative linear relationship between Ohms and LP DSM (Fig. 3.71; R square 0.055). This is in agreement with the visual analysis of the two variables, where changes in topography were less marked, but the earth resistance data revealed a feature interpreted as a palaeochannel. The relationship of Ohms to FP intensity reveals a weak positive linear relationship (Fig. 3.72; R square 0.022), as does Ohms to LP intensity (Fig. 3.73; R square 0.045). This relationship of Ohms to the FP and LP intensity data demonstrate that the features identified by the earth resistance survey do not have a mathematically linear relationship to the anomalies revealed by intensity.

Soil organic content and topography have a weak, negative linear relationship (Fig. 3.74; R square 0.06). FP intensity reveals a weak positive relationship with soil organic content (Fig. 3.75; R square 0.085), as does LP intensity (Fig. 3.76; R square 0.045). Soil moisture shows a weak positive linear relationship to topography (Fig. 3.77; R square 0.045) and weak negative linear relationships to FP intensity (Fig. 3.78; R square 0.17) and LP intensity (Fig. 3.79; R square 0.15). From this analysis, the soil variables defined by soil moisture content, soil organic content and earth resistance Ohms, can be seen to have only weak linear relationships to the lidar topography, FP intensity and LP intensity. This demonstrates that lidar data in this survey area is of limited value in defining areas of high preservation potential.

There are weak linear positive relationships between the lidar data variables, again instructive that the changes in topography and the changes in intensity are not identifying the same features (Fig. 3.80; R square 0.03 and Fig. 3.81; R square 0.011). The soil survey variables also show weak linear graphical relationships, with Ohms and soil organic content having a weak positive linear relationship (Fig. 3.82; R square 0.062). Ohms and soil moisture have a weak negative linear relationship (Fig. 3.83; R square 0.147). The distribution of soil organic content was unexpected; with higher soil organic content visible outside the palaeochannel and this is reflected in a weak positive negative linear relationship with soil moisture (Fig. 3.84; R square 0.13).

As observed within other data sets within this project the table of correlation coefficients for the Area 7 4m data set reveals extremely significant relationships between variables (Tab. 3.5). All of the variables show significant correlations to each other at the 0.01 level, except for FP intensity and Ohms and FP intensity and LP DSM, which have significant correlations at the 0.05 level. Only the LP intensity and LP DSM variables show no significant correlation. However, although the data set does display correlation between variables, graphical analysis has shown this correlation to be non-linear, and the form of the correlation is therefore unknown. Thus unless these relationships can be made linear through advanced data manipulation, these linear relationships cannot be used for regression and prediction in a robust manner.

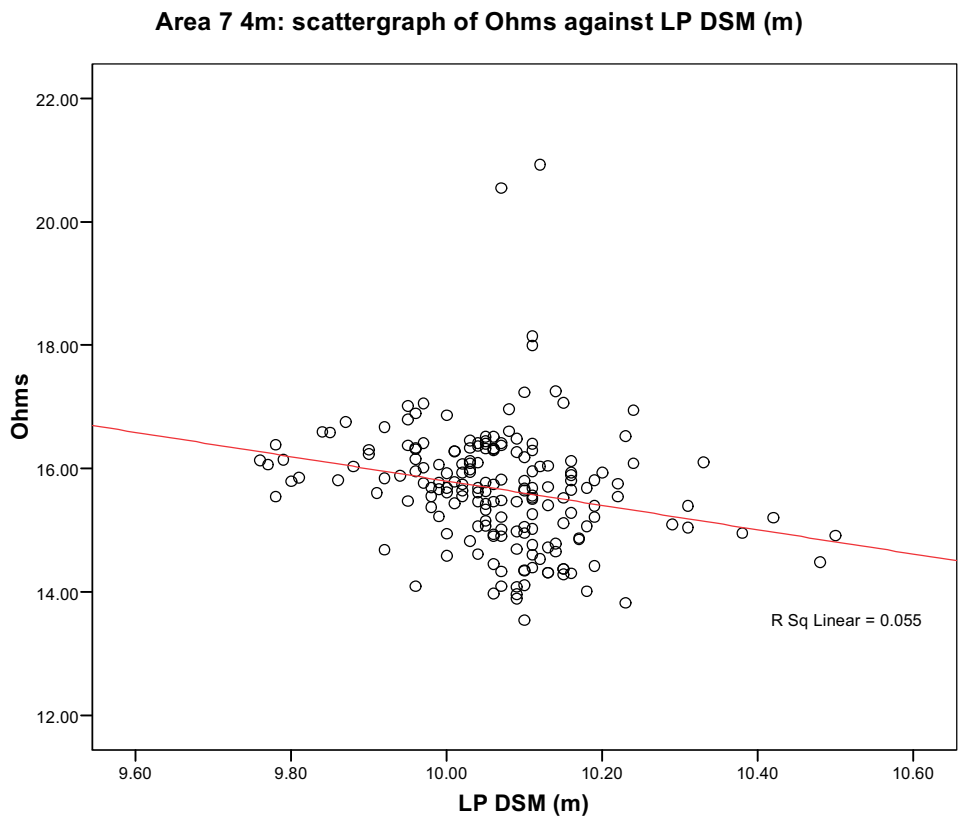

Fig 3.71: Ohms against LP DSM.

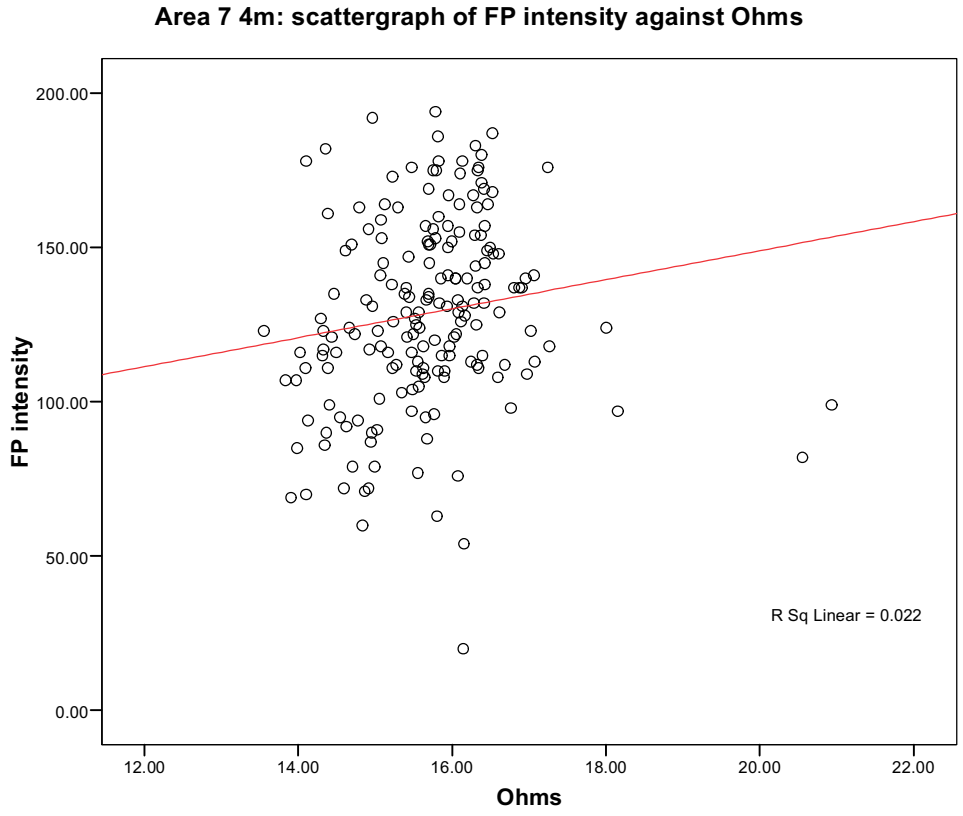

Fig 3.72: Ohms against FP intensity.

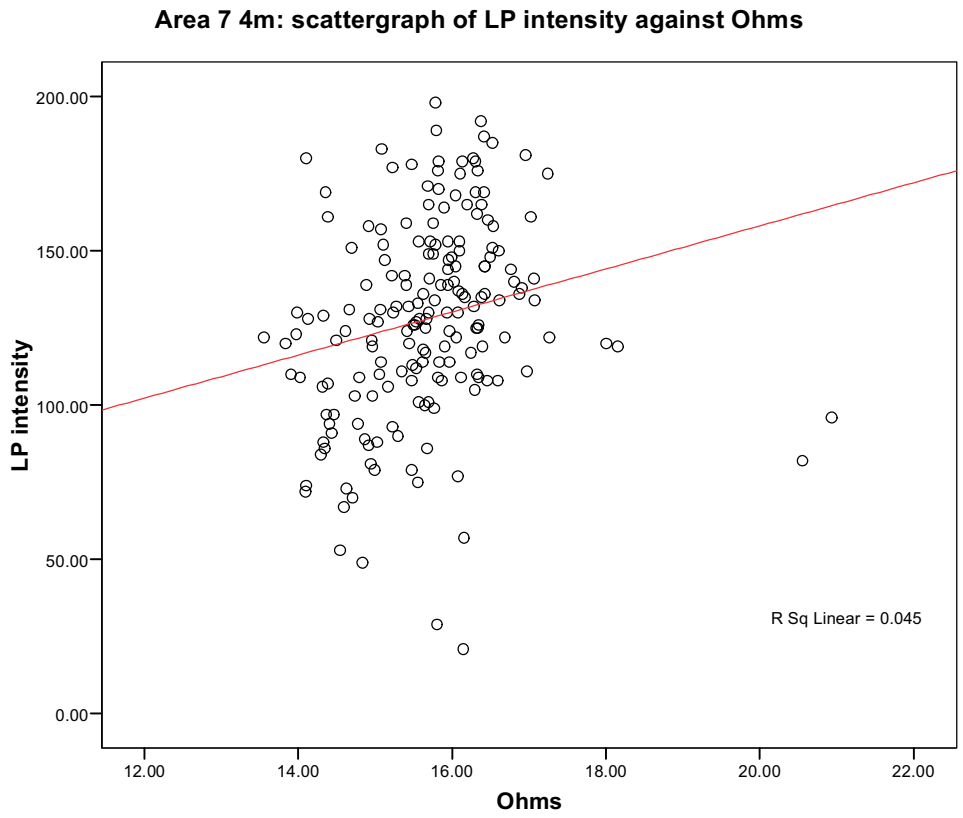

Fig 3.73: Ohms against LP intensity.

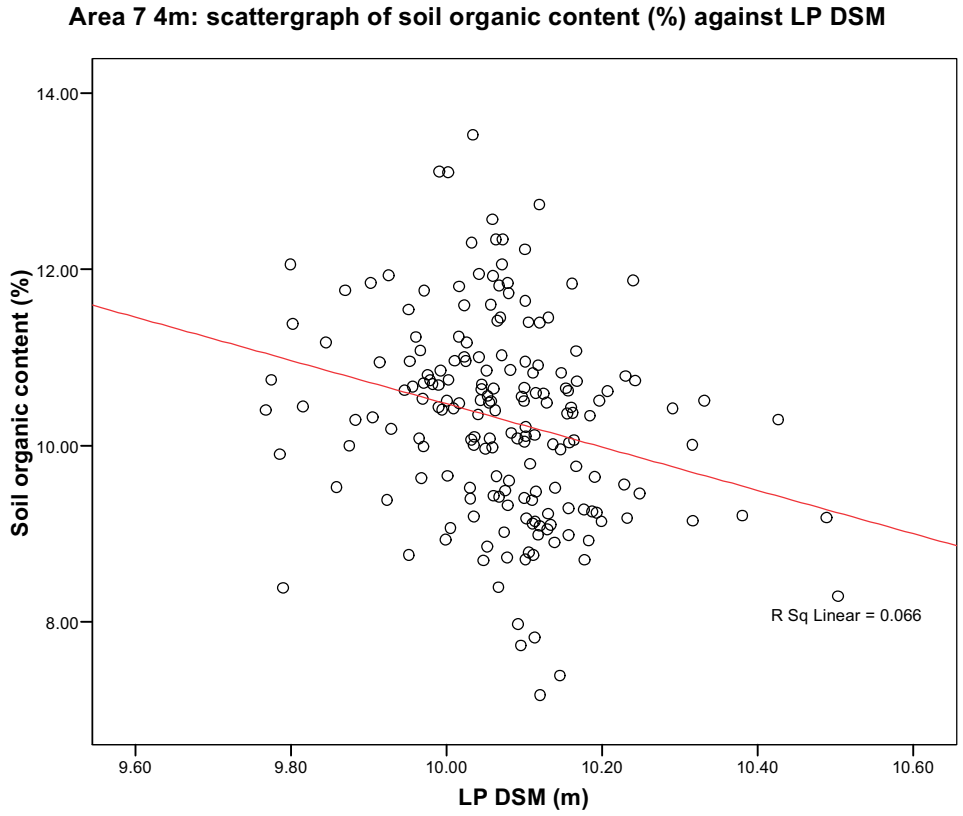

Fig 3.74: Soil organic content against LP DSM.

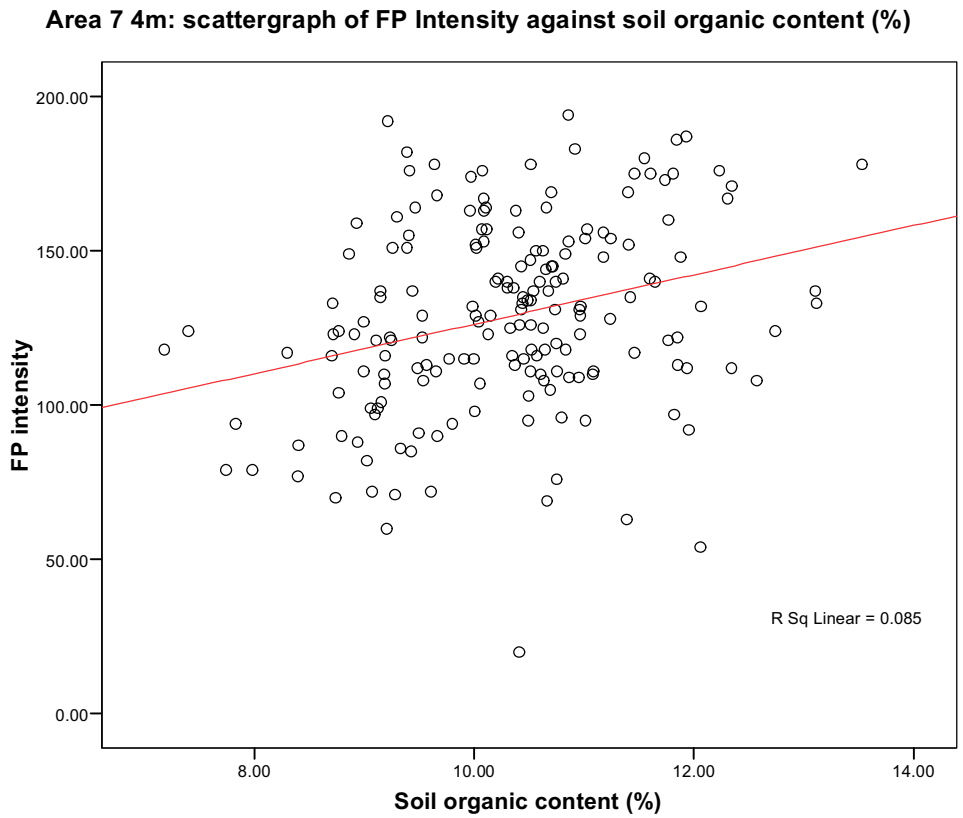

Fig 3.75: FP intensity against soil organic content.

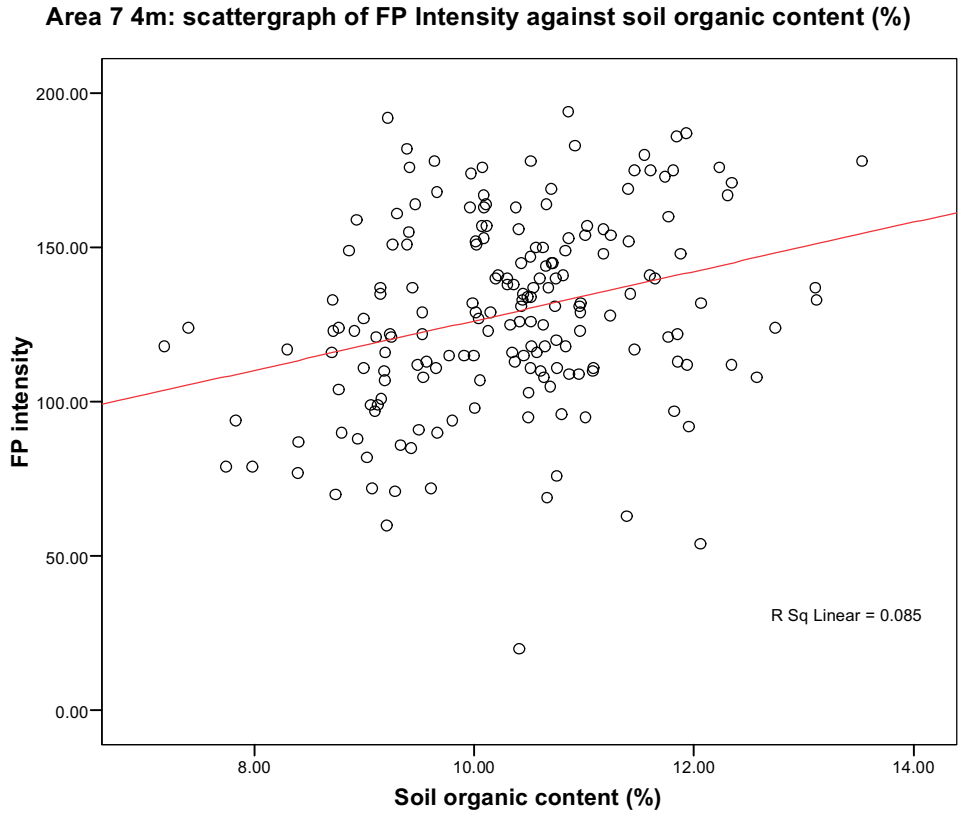

Fig 3.76: LP intensity against soil organic content.

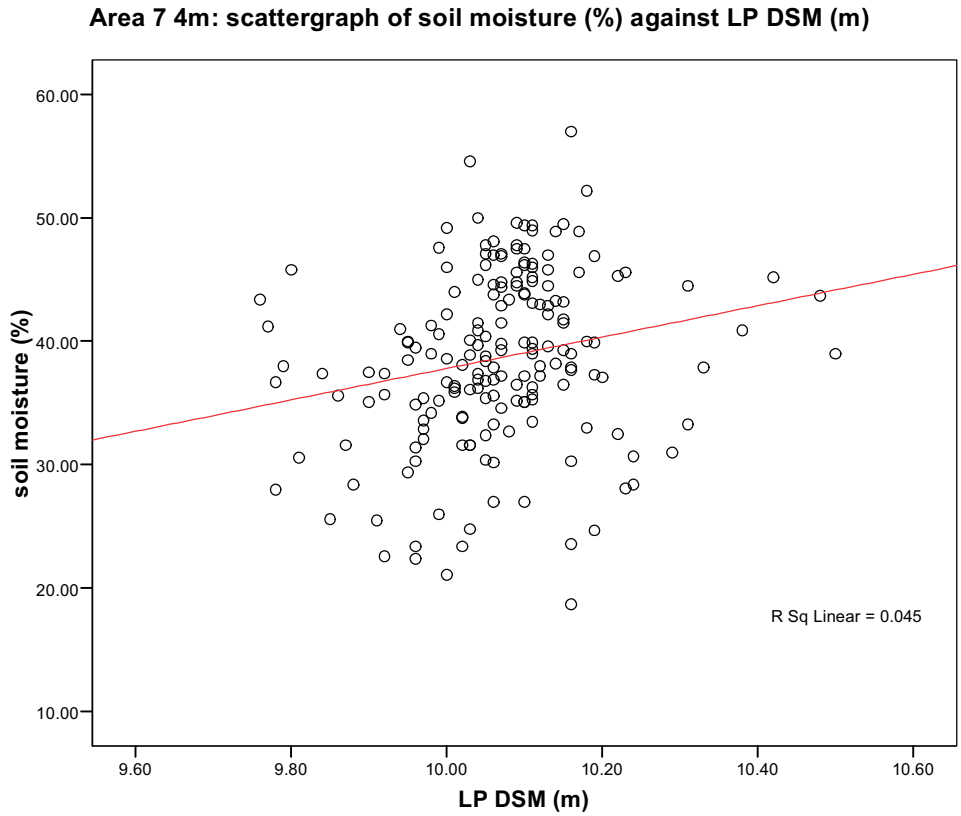

Fig 3.77: Soil moisture against LP DSM.

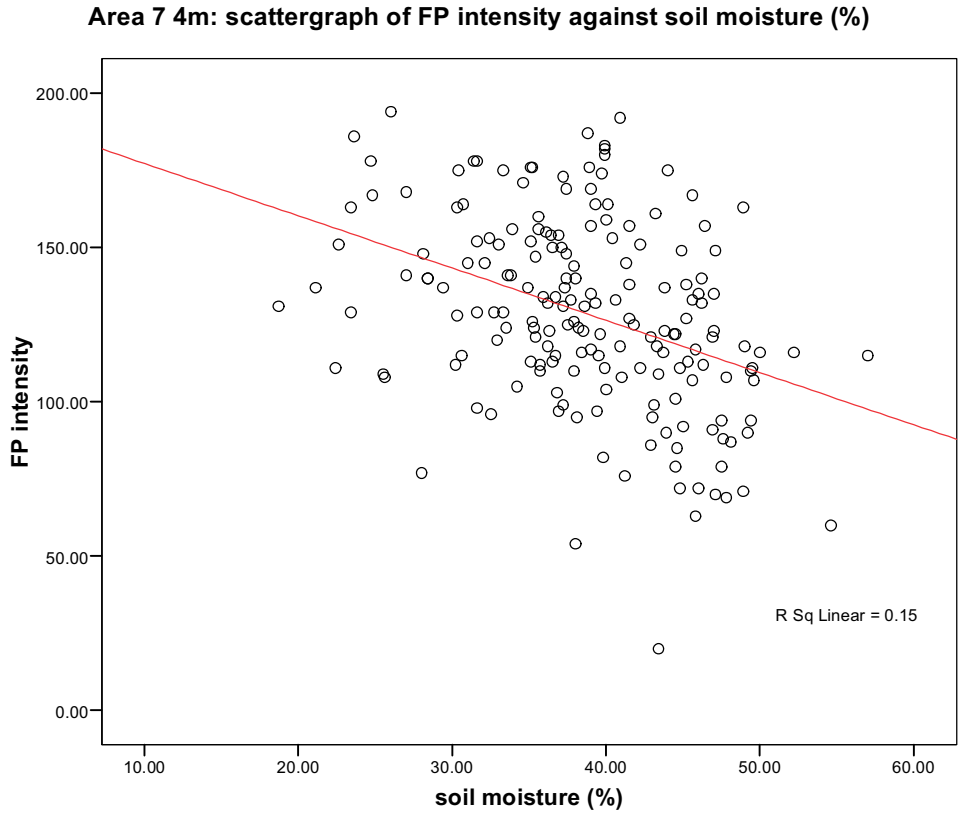

Fig 3.78: FP intensity against soil moisture.

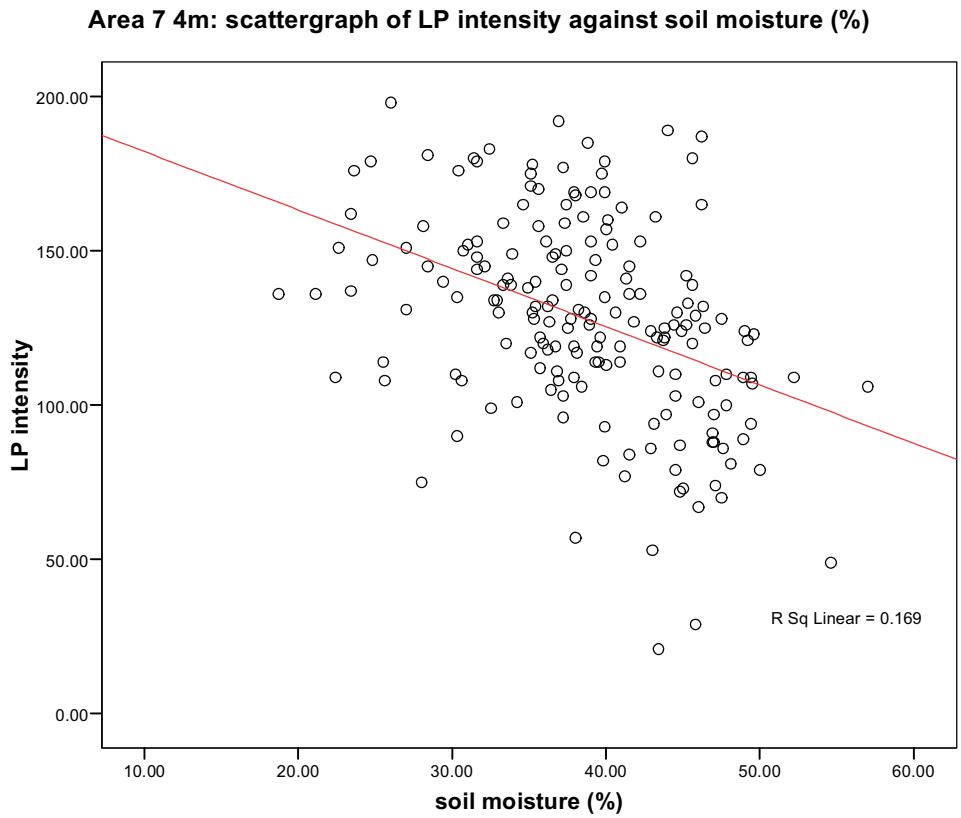

Fig 3.79: LP intensity against soil moisture (%).

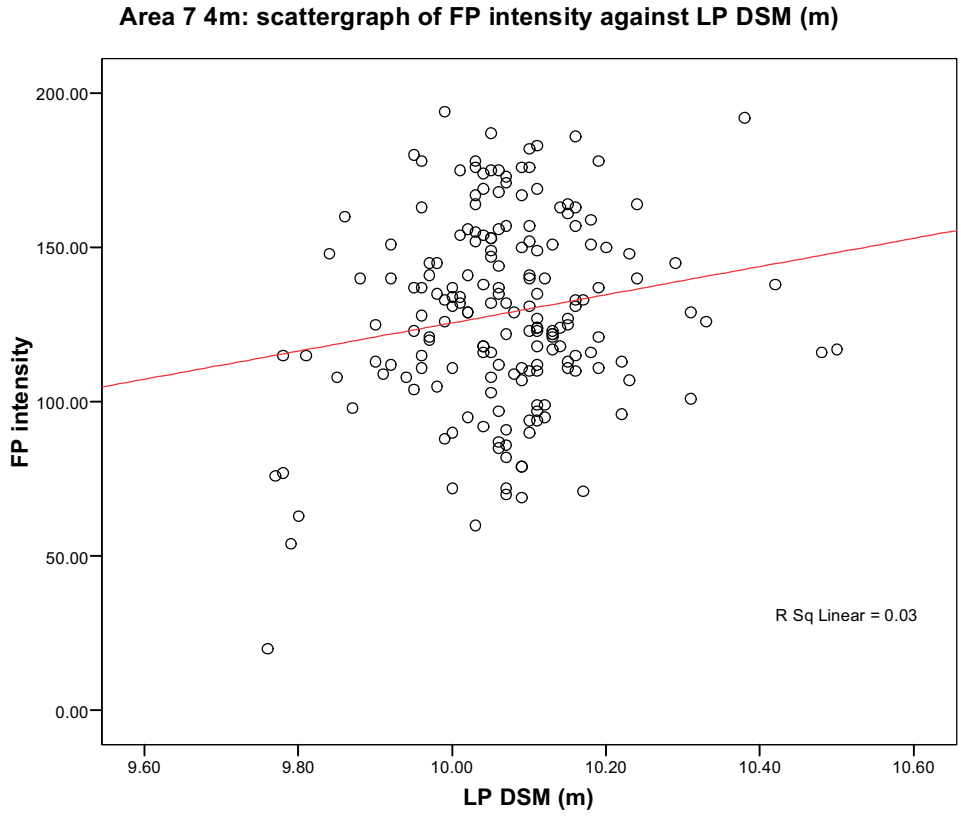

Fig 3.80: FP intensity against LP DSM.

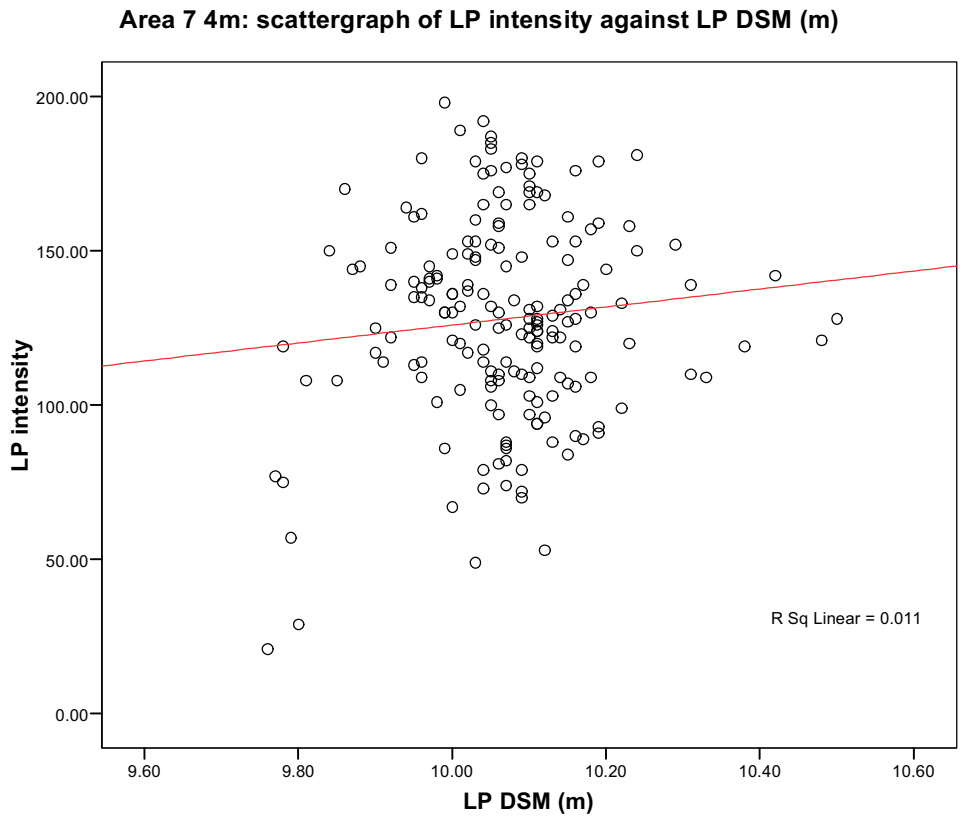

Fig 3.81: LP intensity against LP DSM.

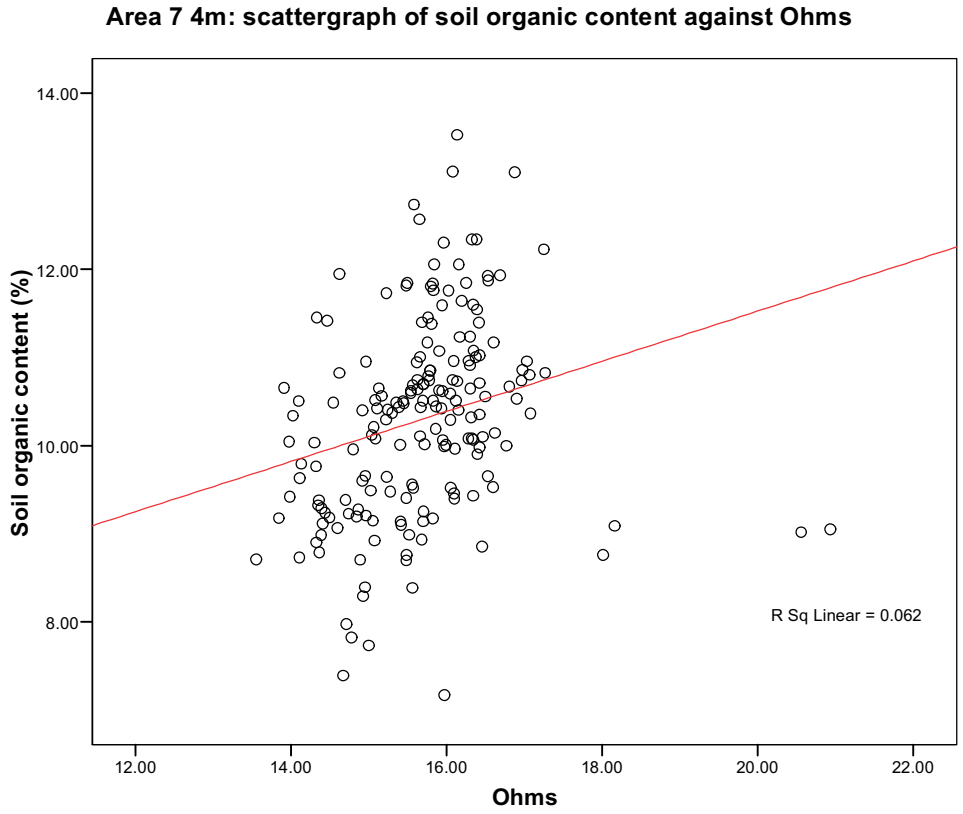

Fig 3.82: Ohms against soil organic content.

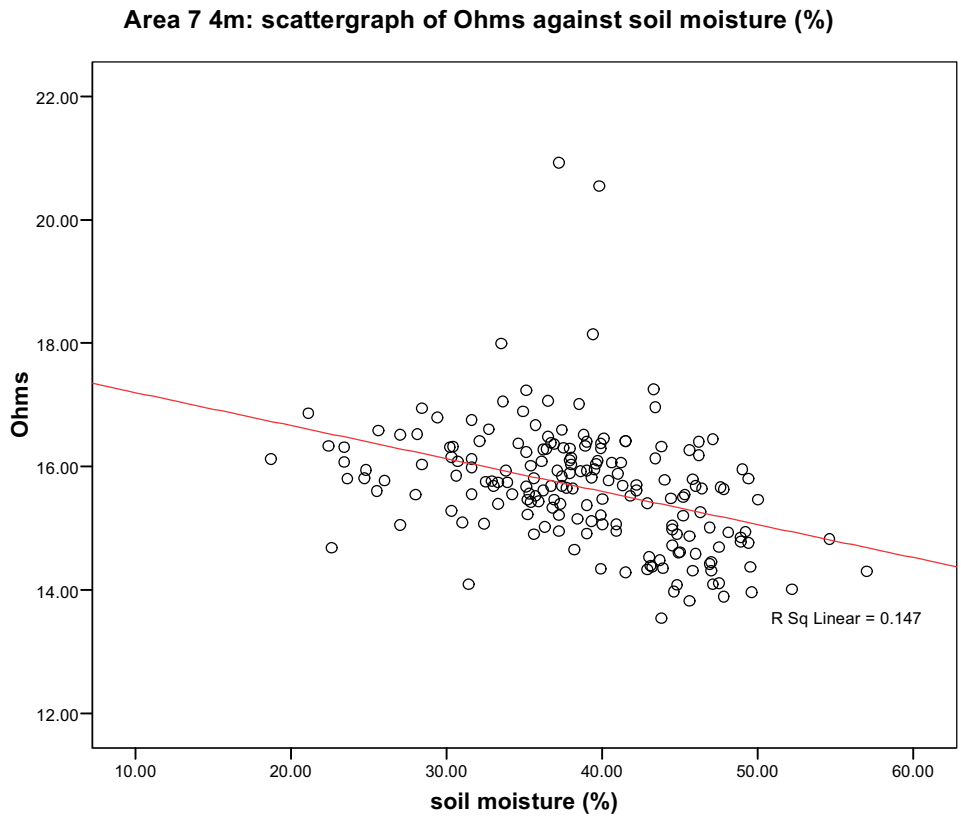

Fig 3.83: Ohms against soil moisture.

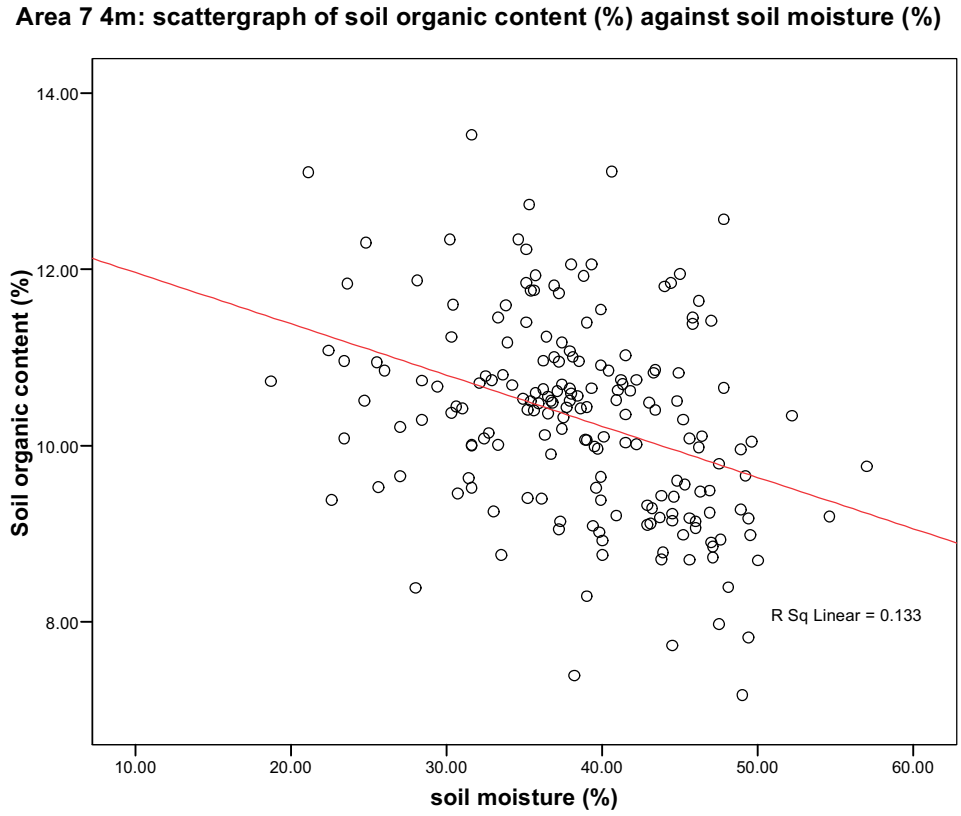

Fig 3.84: Soil organic content against soil moisture content.

Correlations

		soil moisture (%)	Ohms	LP DSM (m)	FP intensity	LP intensity	Soil organic content (%)
soil moisture (%)	Pearson Correlation	1	-.383**	.213**	-.387**	-.411**	-.365**
	Sig. (2-tailed)		.000	.004	.000	.000	.000
	N	184	184	184	184	184	184
Ohms	Pearson Correlation	-.383**	1	-.237**	.150*	.212**	.249**
	Sig. (2-tailed)	.000		.001	.043	.004	.001
	N	184	184	184	184	184	184
LP DSM (m)	Pearson Correlation	.213**	-.237**	1	.170*	.104	-.257**
	Sig. (2-tailed)	.004	.001		.021	.160	.000
	N	184	184	184	184	184	184
FP intensity	Pearson Correlation	-.387**	.150*	.170*	1	.804**	.291**
	Sig. (2-tailed)	.000	.043	.021		.000	.000
	N	184	184	184	184	184	184
LP intensity	Pearson Correlation	-.411**	.212**	.104	.804**	1	.293**
	Sig. (2-tailed)	.000	.004	.160	.000		.000
	N	184	184	184	184	184	184
Soil organic content (%)	Pearson Correlation	-.365**	.249**	-.257**	.291**	.293**	1
	Sig. (2-tailed)	.000	.001	.000	.000	.000	
	N	184	184	184	184	184	184

**. Correlation is significant at the 0.01 level (2-tailed).

*. Correlation is significant at the 0.05 level (2-tailed).

Tab 3.5: Pearson Correlation Coefficients of the relationships between variables in Area 7 4m data set.

3.3.4 Area 7: 1m data set analysis

The analysis of the Area 7 1m data set only uses the variables of topography, FP intensity, LP intensity and Ohms, as each of these variables has a 1m data posting. Ohms has a weak negative linear relationship to LP DSM (Fig. 3.85; R square 0.05). Ohms have a weak positive relationship to FP intensity (Fig. 3.86; R square 0.07) and a weak positive relationship to LP intensity (Fig. 3.87; R square 0.064). Within the lidar data there are only weak linear relationships demonstrated, with FP intensity and LP DSM having a very weak positive relationship (Fig. 3.88; R square 0.01) and LP intensity and LP DSM (Fig. 3.89; R square 0.01). The table of correlation coefficients of the 1m data set shows all of the variables are significantly correlated at the 0.01 level (Tab. 3.6). However, as these correlations are non-linear in form, they cannot be used in a predictive manner.

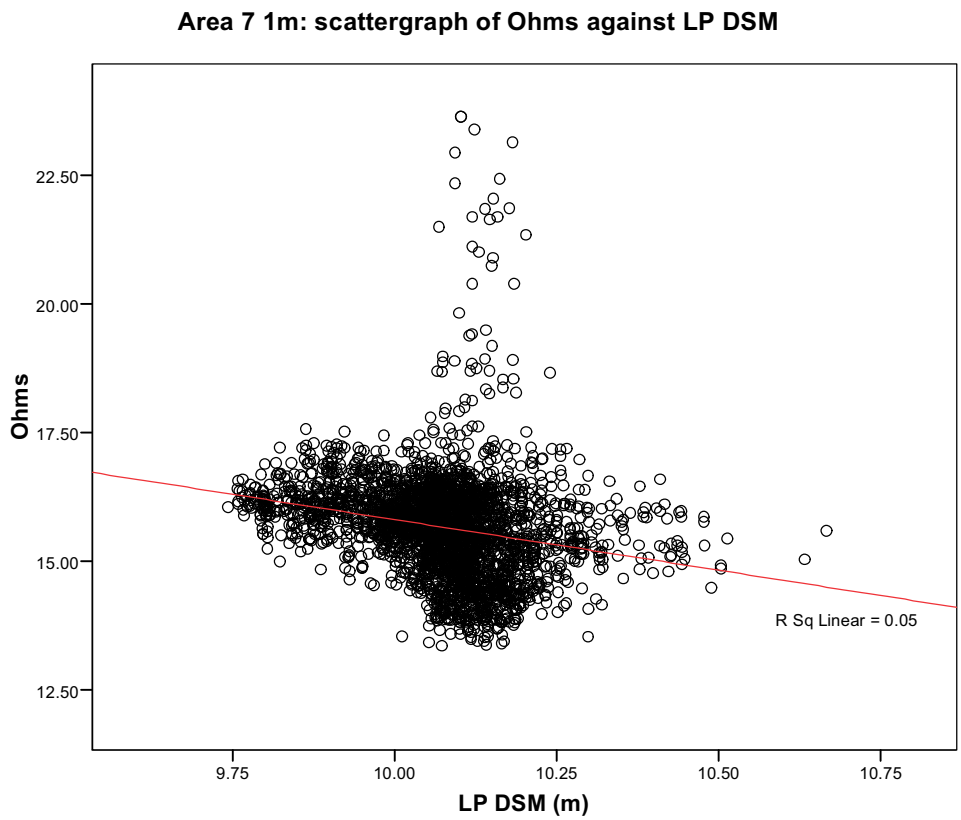

Fig 3.85: Ohms against LP DSM.

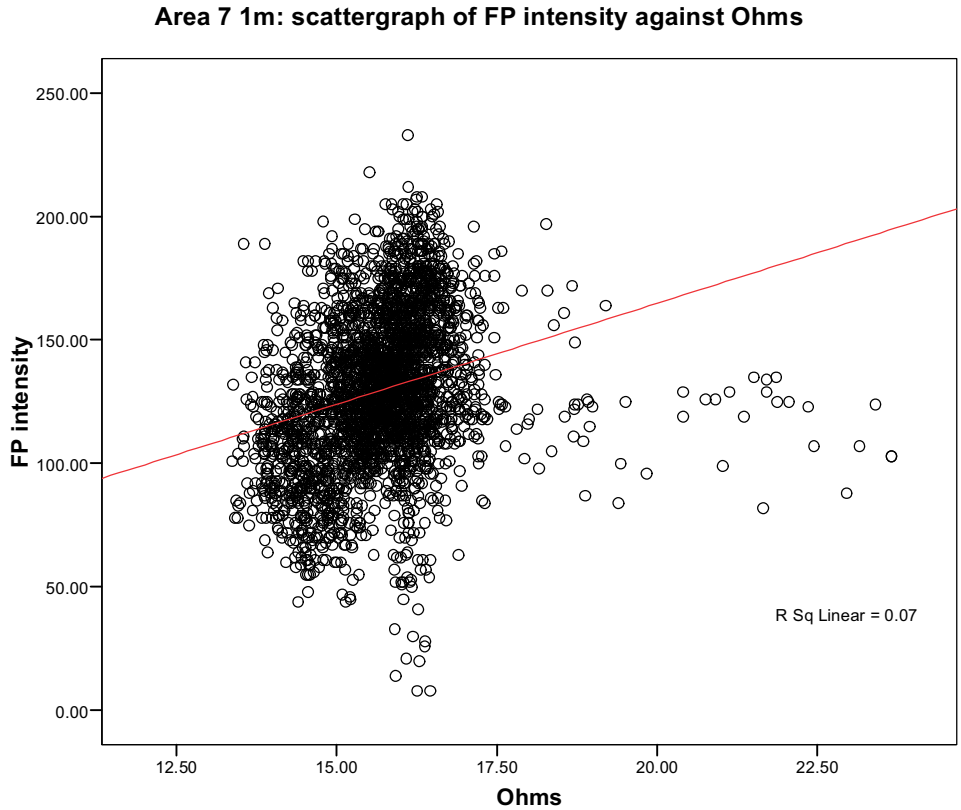

Fig 3.86: FP intensity against Ohms.

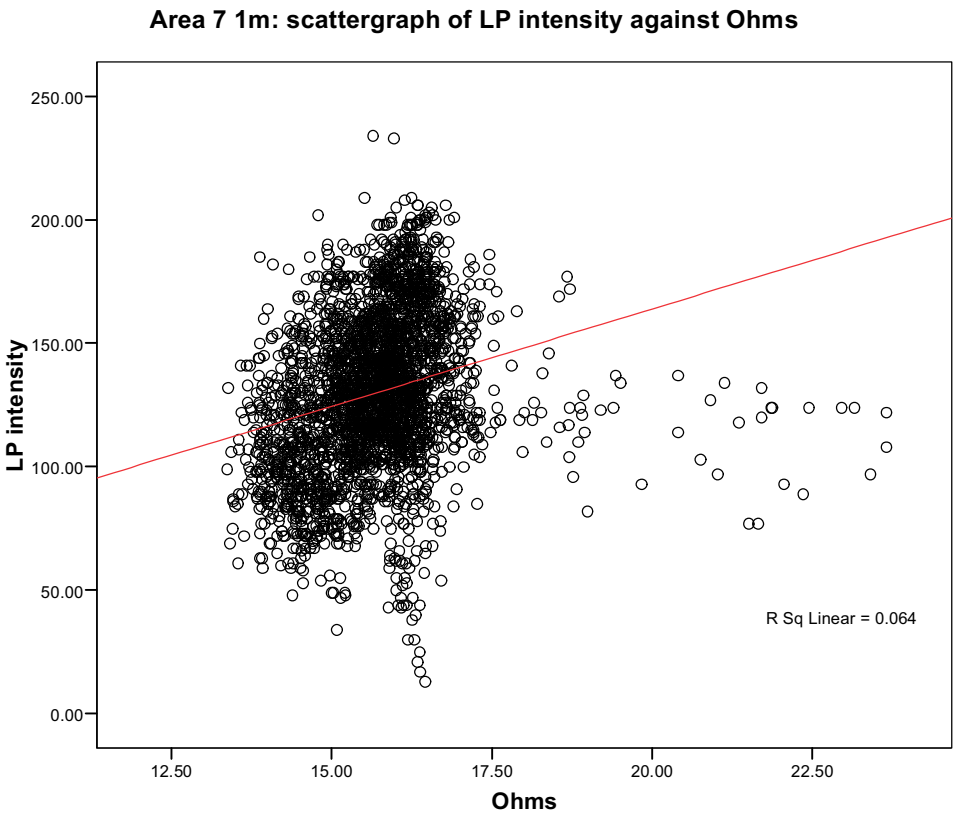

Fig 3.87: LP intensity against Ohms.

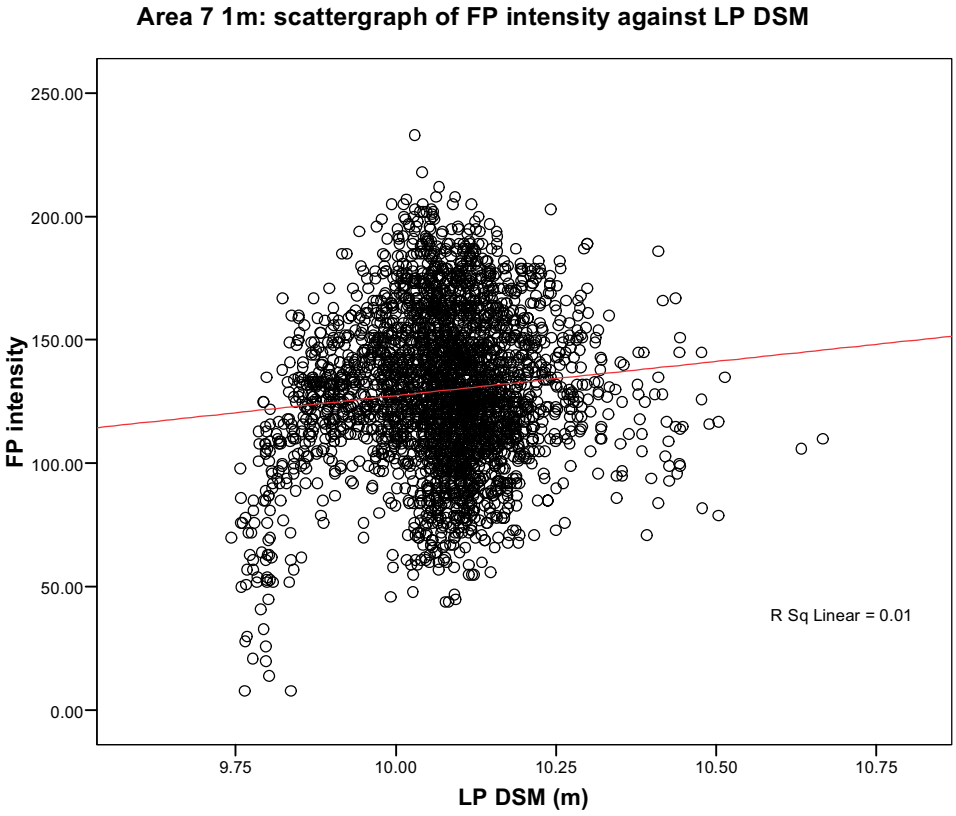

Fig 3.88: FP intensity against LP DSM.

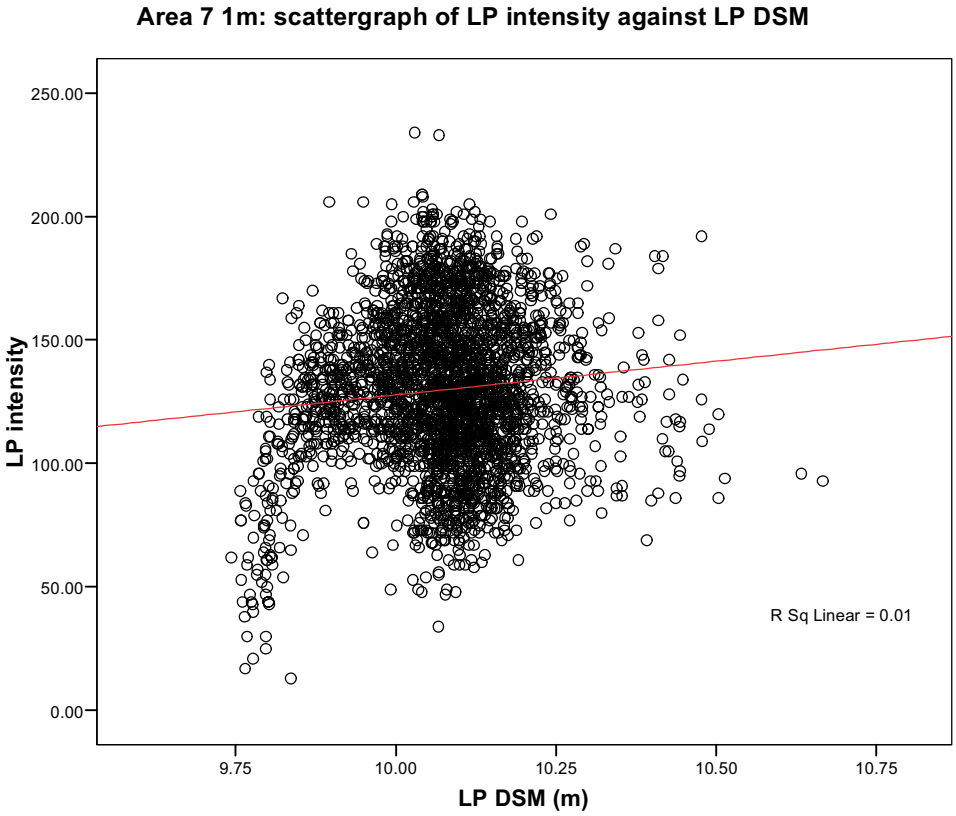

Fig 3.89: LP intensity against LP DSM.

Correlations

		Ohms	LP DSM (m)	FP intensity	LP intensity
Ohms	Pearson Correlation	1	-.224**	.264**	.252**
	Sig. (2-tailed)		.000	.000	.000
	N	2944	2944	2944	2944
LP DSM (m)	Pearson Correlation	-.224**	1	.102**	.099**
	Sig. (2-tailed)	.000		.000	.000
	N	2944	2944	2944	2944
FP intensity	Pearson Correlation	.264**	.102**	1	.780**
	Sig. (2-tailed)	.000	.000		.000
	N	2944	2944	2944	2944
LP intensity	Pearson Correlation	.252**	.099**	.780**	1
	Sig. (2-tailed)	.000	.000	.000	
	N	2944	2944	2944	2944

**. Correlation is significant at the 0.01 level (2-tailed).

Tab 3.6: Area 7 1m data set correlations. Again extremely significant correlations are seen between variables, but the form of these correlations is non-linear.

3.3.5 Area 7 relationship of surface intensity to subsurface sediment stratigraphy

A gouge core transect for Area 7 was made from northwest to southeast through the centre of the survey grid (Fig. 3.90). The transect recorded an alluvial stratigraphy that was fairly homogeneous across the transect to a depth of c. 50 – 55cm, with a grey clay, trace of silt and sand (Unit A) underlain by a light grey clay, trace of silt and sand, Fe mottling (Unit A1) (Fig. 3.91). This has importance in understanding the comparison of the lidar data sets to the earth resistance data sets. The earth resistance survey used a twin probe array with a 0.5m probe separation, giving an effective penetration depth of c.75cm (Gaffney and Gater 2003). This effectively is mapping the lower more heterogeneous sediment units that clearly change between the floodplain and the palaeochannel. In contrast, the lidar data sets are only measuring surface changes and the gross sediment architecture can be seen to be broadly homogeneous in the upper stratigraphy. This could potentially explain the marked contrast between the earth resistance data and the lidar data sets.

The palaeochannel is defined as an area of deeper above gravel alluvium, with a relatively complex alluvial stratigraphy. There are a series of differing basal sand units (Units L, D, E, G I and J). Within the palaeochannel there is also unit B, a dark grey brown olive peaty clay. This extends onto the adjacent floodplain, where it is interbedded with unit A1. The transect clearly records the difference between the palaeochannel and shallower floodplain stratigraphies.

The graph of FP and LP intensity against the transect stratigraphy is ambiguous (Fig. 3.92). Some relatively low values are recorded in both the FP and LP intensity responses over the palaeochannel, especially in the last pulse. In contrast, the adjacent floodplain is visible as data of generally higher response in the FP and LP intensity. However, the data is spiky and both FP and LP intensity reveal high data spikes in the palaeochannel and low data spikes on the floodplain. In summary, there is little predictive visual correlation between the FP and LP intensity graphs and the sediment stratigraphy, due to noise in the intensity data. This noise could be caused by a number of factors, particularly standing water and vegetation changes.

Fig 3.90: Location of the Area 7 gouge core transect.

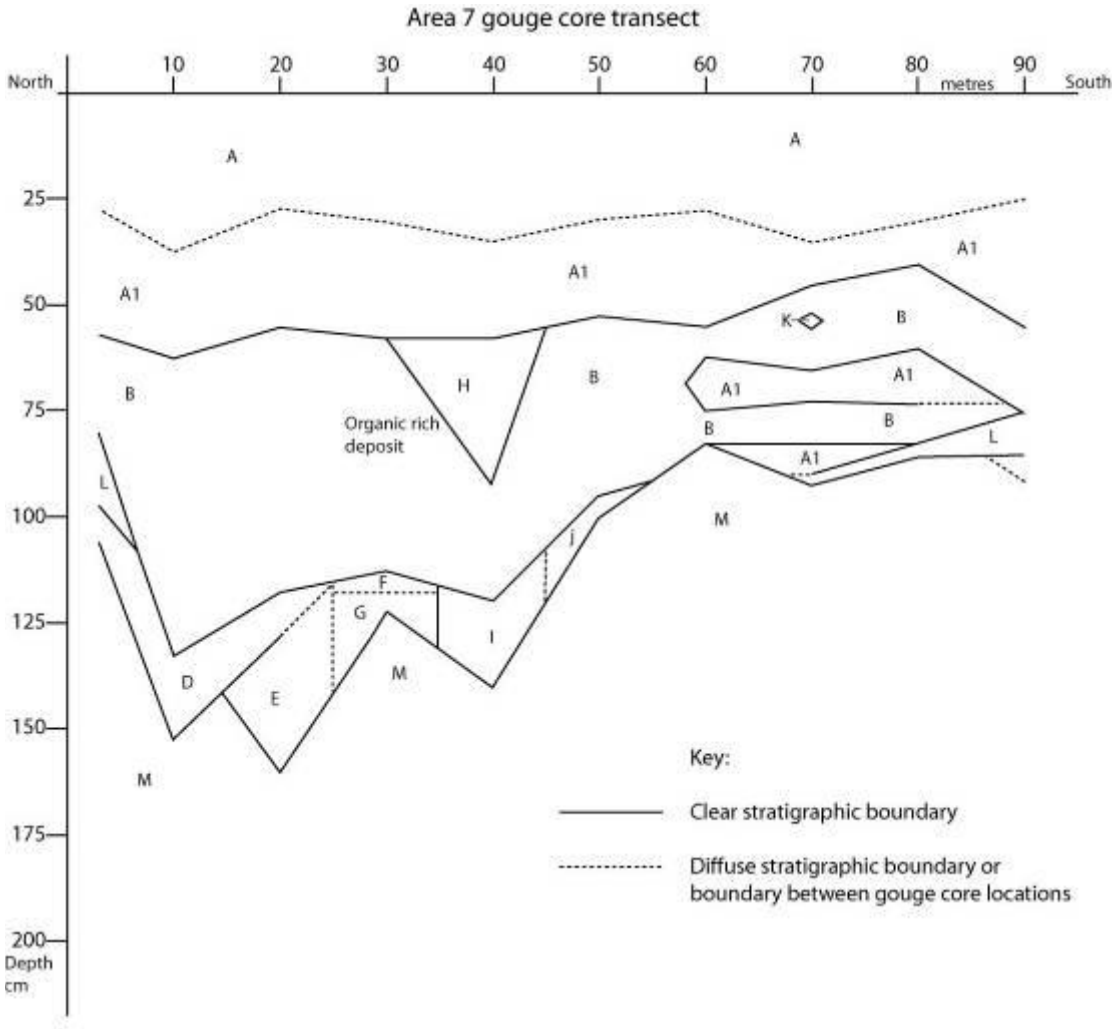

A = grey clay, trace of silt and sand
A1 = light grey clay, trace of silt and sand, Fe mottling
B = dark grey olive brown peaty clay, trace of sand and organic rich
C = light grey clay, trace of sand, Fe mottling, visible organic remains
D = light grey coarse to medium clayey sand, some limited organic remains
E = dark grey sandy clay, orgnaic rich
F = light grey stiff clay, trace of sand
G = olive grey sandy, clayey peat, with small clasts
H = band of clast supported grey clay, Fe mottling, possible made ground
I = grey sandy clay, organic clay
J = grey brown coarse sand, with small clasts <2cm
K = olive brown peaty clay, Fe mottling
L = grey coarse sand
M = gravel

Fig 3.91: The Area 7 gouge core transect showing the sediment stratigraphy. Between 0 - 55m a palaeochannel is evident, with a deeper above gravel alluvial stratigraphy, whilst the above gravel alluvium on the floodplain between 55 – 90m is shallower.

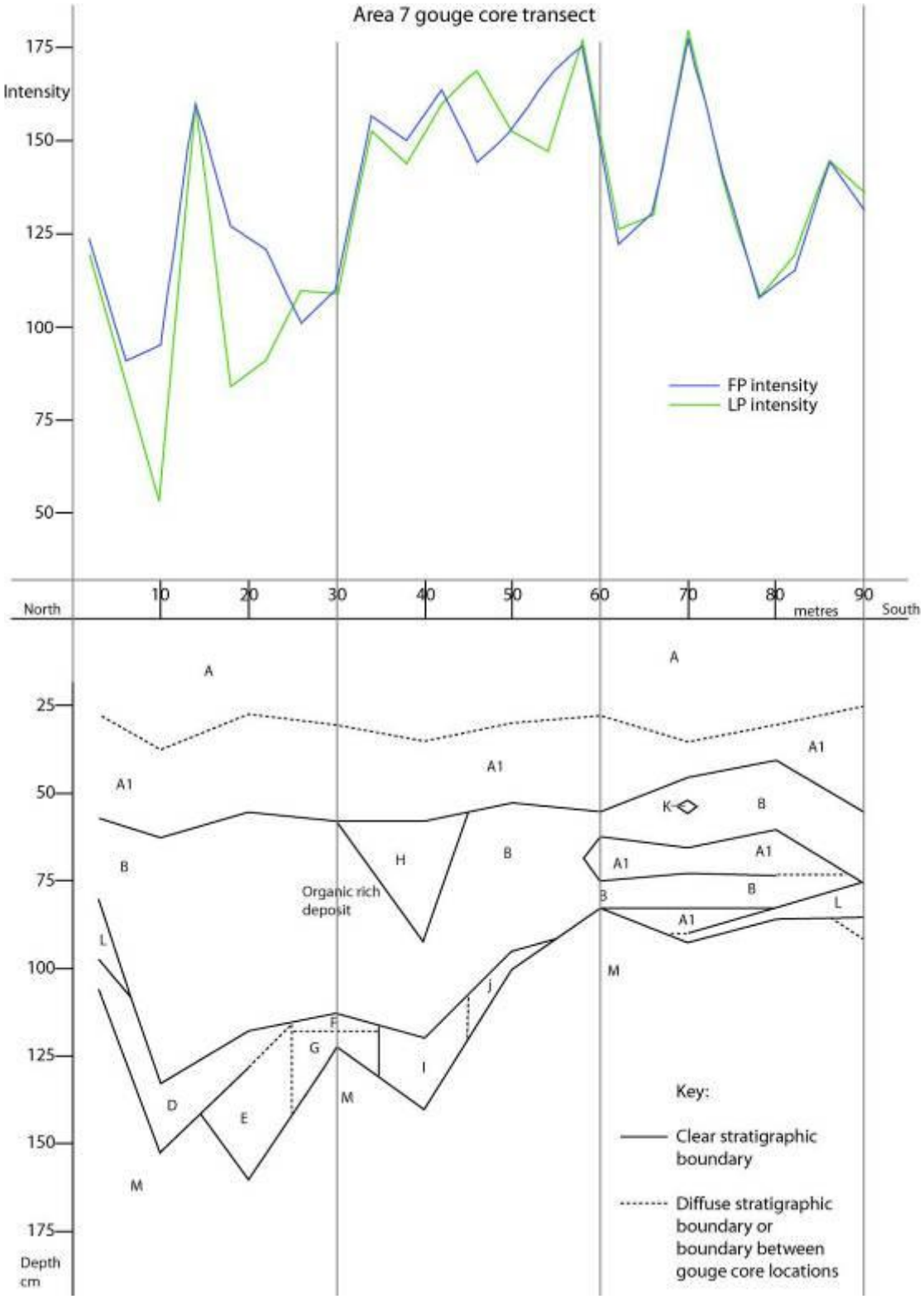

Fig 3.92: Area & gouge core transect shown against FP and LP intensity response. There is ambiguity between the stratigraphy and the intensity values.

3.3.6 Area 7 summary of main results

The analysis of the Area 7 data has revealed weak visual relationships between soil variables such as organic content and the lidar data. Although significant correlations were seen in the quantification of the data variables, these correlations were non-linear in form, and cannot be used in a predictive manner.

The results from the visual analysis of the Area 7 data are summarised as:

- The LP DSM identified the change between the Holme Pierrepont Terrace and the lower undifferentiated floodplain alluvium.
- The FP and LP intensity data sets did not identify the change between the Holme Pierrepont Terrace and the lower undifferentiated floodplain alluvium.
- On the undifferentiated floodplain alluvium, both the FP and LP data sets revealed variation not visible in the LP DSM.
- The earth resistance data identified the presence of a palaeochannel on the area of undifferentiated alluvium.
- The palaeochannel was not clearly defined as a discrete feature in the lidar LP DSM, FP intensity and LP intensity data.
- The palaeochannel was evident in the soil organic content data as an area of low organic content.
- The palaeochannel was evident in the soil moisture content data as an area of higher soil moisture content.

The results from the analysis of the Area 7 4m data set are summarised as:

- The earth resistance data revealed weak linear relationships to the lidar LP DSM, FP intensity and LP intensity variables.
- The soil organic content data revealed weak linear relationships to the lidar LP DSM, FP intensity and LP intensity variables.
- The soil moisture content data revealed weak linear relationships to the lidar LP DSM, FP intensity and LP intensity variables.
- Soil moisture content and soil organic content revealed a relatively weak negative relationship, with increasing soil moisture content showing lower soil organic contents.
- Significant correlations were observed within the Area 7 4m data set, many significant at the 0.01 level.
- However, the graphical analysis proved these correlations between lidar data and the soil variables to be non-linear in form and therefore not currently usable within a robust predictive model.

The results from the Area 7 1m data set analysis are summarised as:

- Weak linear relationships were visible between earth resistance Ohms and the lidar data sets.
- The lidar data set of LP DSM showed weak linear relationships to FP intensity and LP intensity.
- All of the variables in the Area 7 1m data analysis showed significant correlations to each other at the 0.01 level.
- However, the graphical analysis proved the correlations to be non-linear in form and therefore not currently usable within a robust predictive model.

Overall, the results from the Area 7 survey were disappointing. The palaeochannel was identifiable through both the FP and LP surface models. However, both FP and LP intensity displayed weak linear relationships to soil moisture and soil organic content. The visual relationship of FP and LP intensity to sub-surface stratigraphy was also ambiguous. The survey area showed little topographical variation, except for the change to the Holme Pierrepont Terrace at its northwestern edge. As a result, lidar was of limited use in identifying areas of high potential for preservation using either topography or intensity. Again the earth resistance survey, although time consuming, was the best tool for the identification of geomorphological features.

3.4 AREA 8

3.4.1 Area 8 geological background

Area 8 is located near Sturton-le-Steeple in the Lower Trent Valley and is situated on a segment of Holme Pierrepont Terrace (Fig. 3.93). The geomorphology of the study area indicated a relatively minor palaeochannel traversing the survey area towards to the south of the survey grid. During lidar data collection and field data capture, the survey area was ploughed bare soil. This was ideal for assessing lidar intensity variation against sediment structure only, with no variance being introduced into the data set through vegetation reflectance. The survey in Area 8 was undertaken during bright and sunny conditions, with a small amount of standing water visible over the minor palaeochannel.

3.4.2 Area 8: Visual qualitative analysis

The analysis of Area 8 begins with a visual qualitative assessment data. The LP DSM data clearly shows the terrace to the north of the survey area, with the minor palaeochannel traversing NE-SW in the southern half of the survey grid (Fig. 3.94). The topographic change of the terrace and the minor palaeochannel was marked in the field, as were the ploughing furrows. The plough furrows are not easily evident on the lidar topographic data, but the differentiation between the palaeochannel and terrace is recognisable.

The FP intensity data shows the differentiation between the terrace and the minor palaeochannel with great clarity (Fig. 3.95). The north to south plough furrows are also visible on the FP intensity data. However, within this survey grid and surrounding area, larger geomorphological trends are difficult to discern from the intensity data, due to a flight swathe boundary occurring just to the north of the survey area, providing a stark contrast between adjacent flight lines. The LP intensity data shows a very similar pattern to the FP intensity data, with the terrace, palaeochannel and plough furrows evident (Fig. 3.96). The lack of surface vegetation within the survey grid means that both FP and LP intensity returns reflect the surface sediments and therefore should produce similar results.

The earth resistance survey shows good detail of the geomorphology within the survey grid. When superimposed on the LP DSM lidar data, the earth resistance data clearly defines the plough furrows to the north of the survey grid, trending north - south (Fig. 3.97). The furrows are evident as features of lower resistance, with the ridges are evident as features of higher resistance. To the south of the ground survey area the minor palaeochannel is definable as an area of lower resistance, which has better definition than in the LP DSM alone. The very south of the survey grid shows an area of intermediate resistance, higher than the palaeochannel, but overall lower than the plough furrows to the north of the survey grid.

The earth resistance surface model when shown against the FP intensity data produces an impressive visual correlation between data sets (Fig. 3.98). The plough furrows defined in Ohms correlate with linear features identifiable on the FP intensity data. Both Ohms and intensity define the palaeochannel, and the segment of terrace to the south of the survey grid. Likewise, the visual correlation between Ohms and LP intensity is impressive, with both data sets again defining the plough furrows, the minor palaeochannel and the segment of terrace to the south of the survey grid (Fig. 3.99).

Fig 3.93: The 1:50, 000 BGS geological mapping around Area 8.

The soil organic data shows an ambiguous distribution (Fig. 3.100), with an overall low soil organic content. The soil organic data when superimposed on LP DSM shows elevated organic contents within the palaeochannel compared to the northern part of the survey grid. However, the palaeochannel is not clearly defined, potentially due to the coarse sampling interval and overall relatively low soil organic content. The soil organic data when superimposed on the FP intensity shows the minor palaeochannel more clearly defined by FP intensity, and a corresponding change in higher soil organic values within the minor palaeochannel (Fig. 3.101). The LP intensity data shows an almost identical pattern to the FP intensity and hence soil organic data (Fig. 3.102).

The soil moisture data shows a clearer picture than the soil organic data. Soil moisture shown against LP DSM defines the area of terrace to the north of the survey grid, the minor palaeochannel and the area of terrace to the south of the survey grid (Fig. 3.103). However, the highest soil moisture values peak to the southern edge of the palaeochannel. This is visible more clearly when the soil moisture data is shown against FP and LP intensity data (Figs. 3.104 and 3.105).

In summary, Area 8 has surveyed a segment of Holme Pierrepont Terrace bisected by a minor palaeochannel. The lidar DSM, FP intensity and LP intensity have all defined the change between the palaeochannel and the terrace. The earth resistance data produced the clearest definition of this geomorphological change and recorded additional features such as plough furrows. Both the soil moisture and soil organic data indicated different sediment properties between the terrace and minor palaeochannel. This visual assessment indicates that there is significant inter-variable correlation within this data set, which will be explored in the Area 8 4m statistical analysis.

Fig 3.94: The survey area shown on topography (DSM OD).

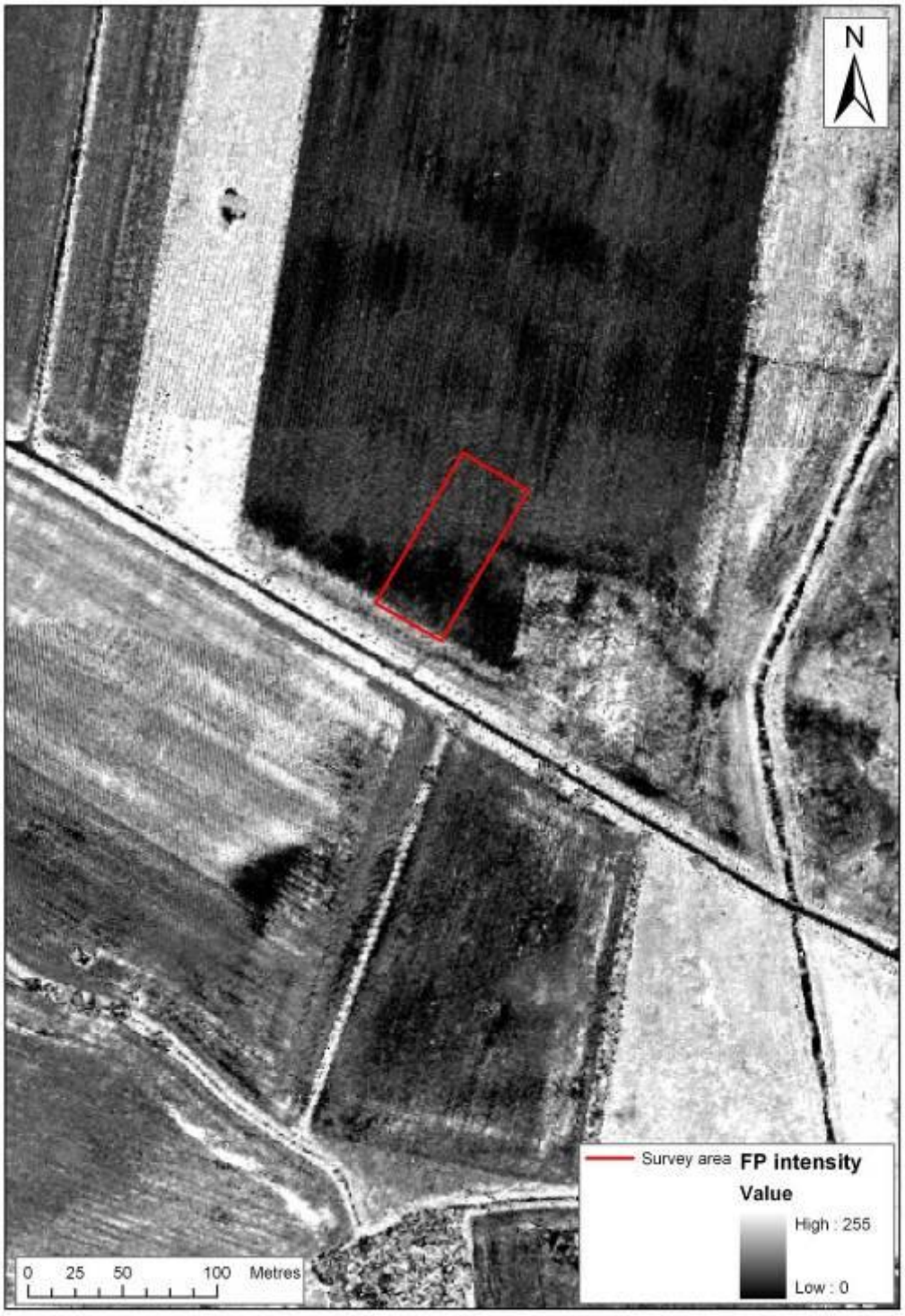

Fig 3.95: The survey area shown on FP intensity.

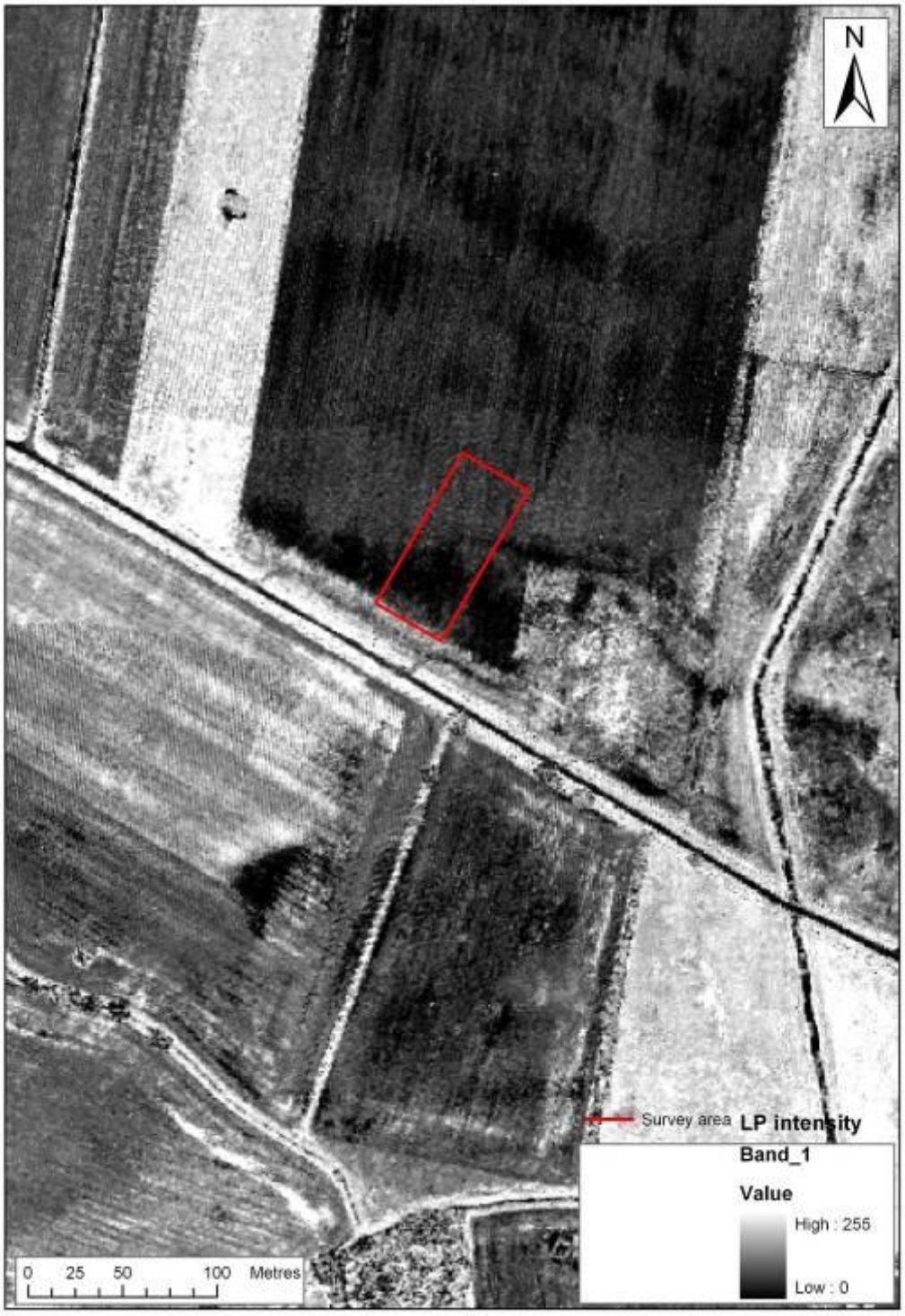

Fig 3.96: The survey area shown on LP intensity.

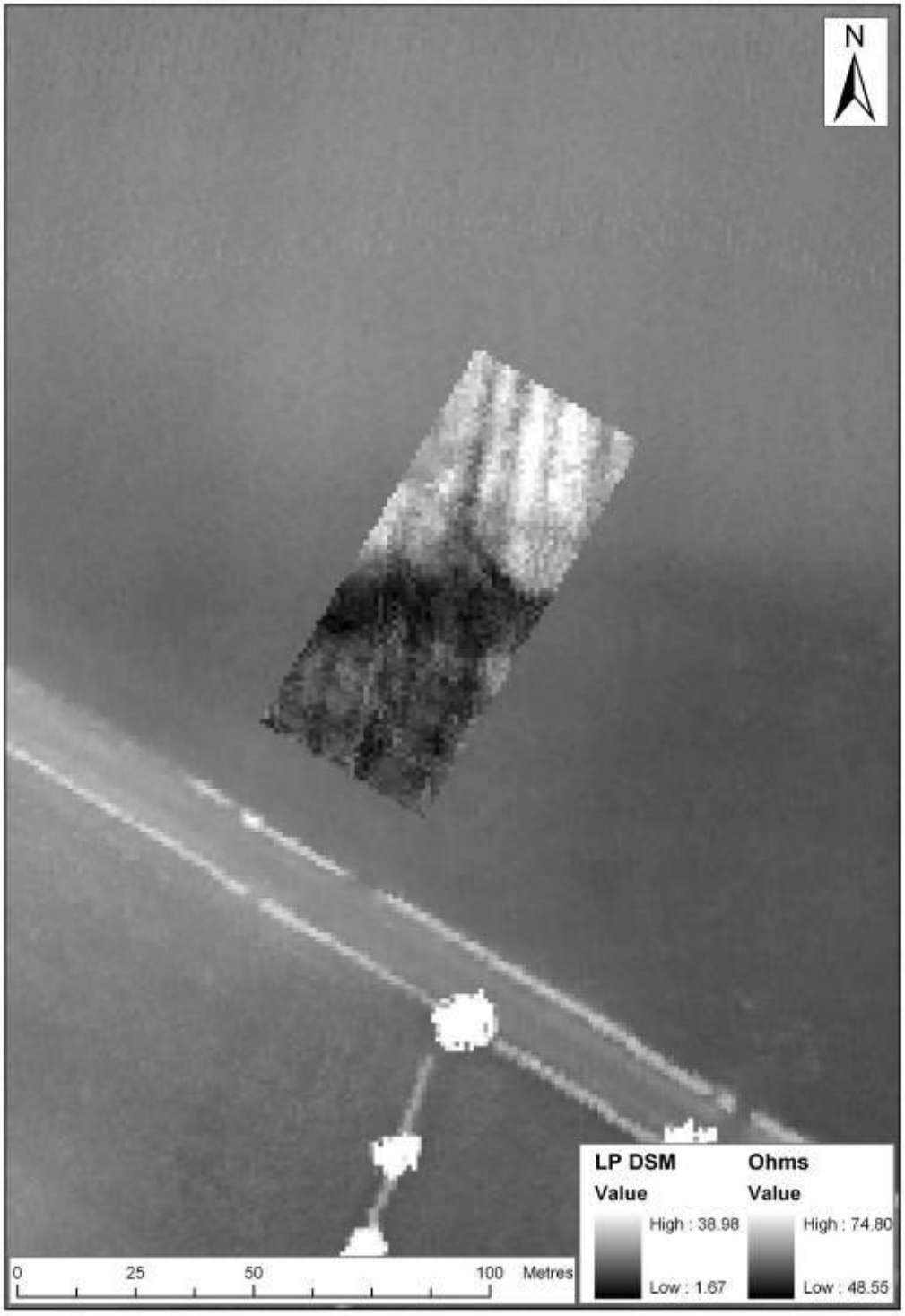

Fig 3.97: Earth resistance Ohms on DSM OD.

Fig 3.98: Earth resistance Ohms on FP intensity.

Fig 3.99: Earth resistance Ohms superimposed on LP intensity.

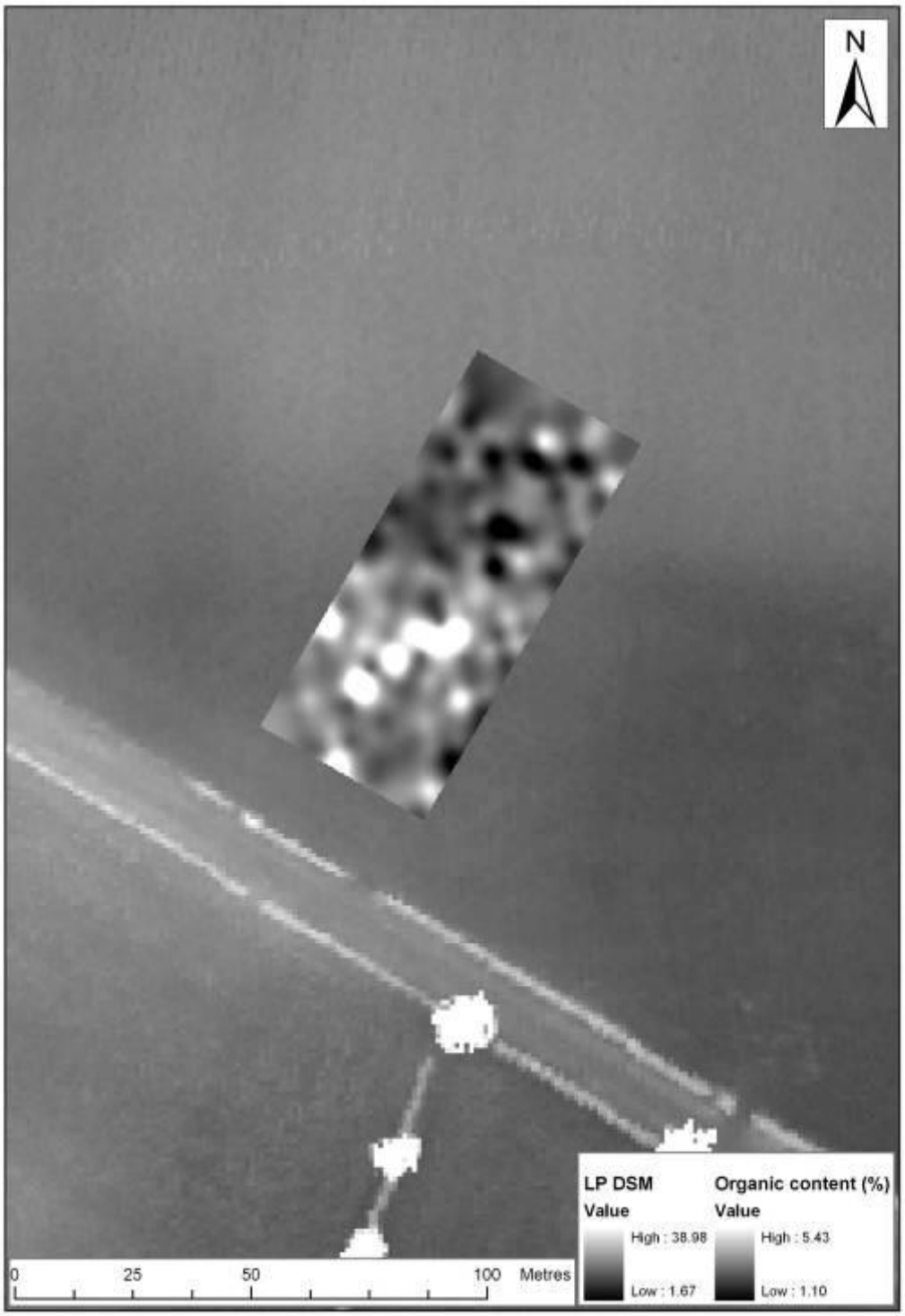

Fig 3.100: Organic content superimposed on DSM OD.

Fig 3.101: Organic content superimposed on FP intensity.

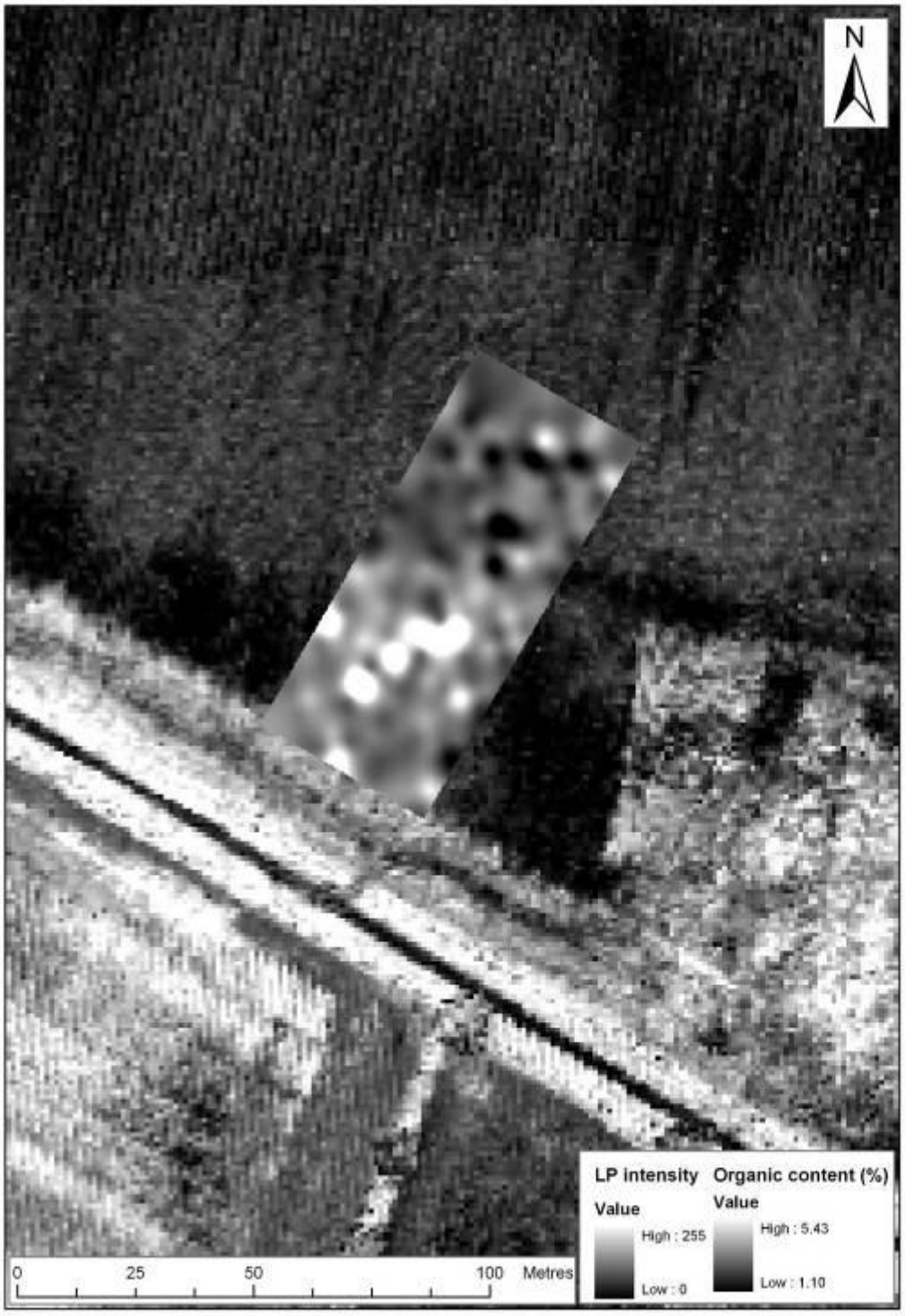

Fig 3.102: Organic content superimposed on LP intensity.

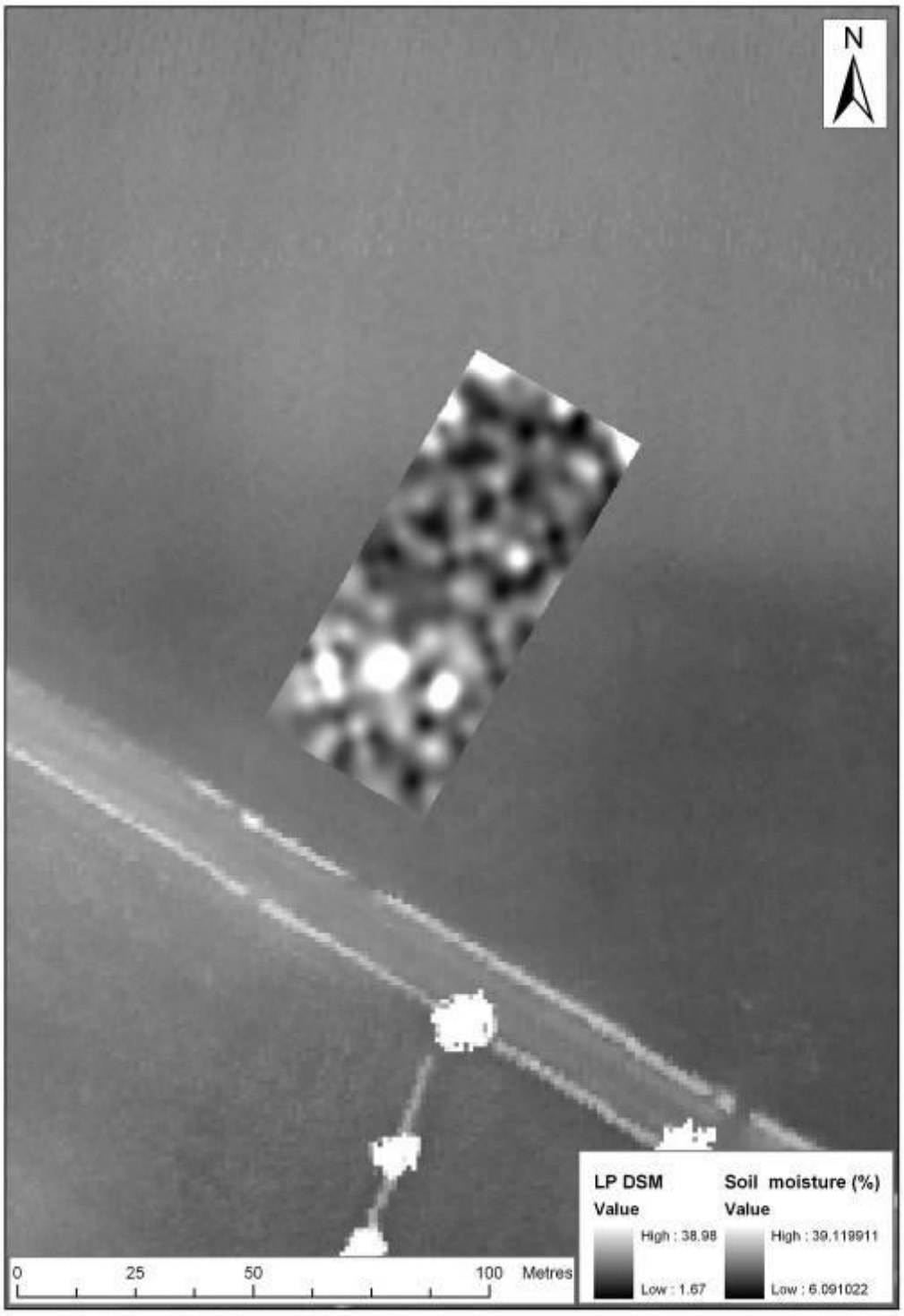

Fig 3.103: Soil moisture content superimposed on DSM OD.

Fig 3.104: Soil moisture content superimposed on FP intensity.

Fig 3.105: Soil moisture content superimposed on LP intensity.

3.4.3 Area 8: 4m data set analysis

The Area 8 4m data set is composed of the variables of LP DSM, FP intensity, LP intensity, soil moisture content, soil organic content and Ohms sampled at a 4m resolution across the ground survey grid. Ohms displays a strong positive relationship with topography defined by the LP DSM (Fig. 3.106; linear R square 0.726). This is indicative that geomorphology is the dominant factor in causing changes in sediment architecture, reflected through the earth resistance survey as changes in Ohms. Contrastingly, FP intensity displays a weak positive linear relationship with Ohms (Fig. 3.107; linear R square 0.147). LP intensity displays a slightly stronger relationship to Ohms than FP intensity, although it is still a relatively weak linear positive relationship (Fig. 3.108; linear R square 0.254). The earth resistance survey produced the clearest definition of geomorphology with the survey area and has a strong relationship with topography, but weak relationships with FP and LP intensity. This strongly suggests that FP and LP intensity do not define changes of sediment architecture and hence geomorphology within the survey grid.

Soil organic content has a weak negative linear relationship with topography defined through the LP DSM (Fig. 3.109; linear R square 0.134). A weaker negative linear relationship is observed between soil organic content and FP intensity (Fig. 3.110; linear R square 0.077). There is also a weak negative linear relationship between LP intensity and soil organic content, although this is slightly stronger than the corresponding linear relationship for FP intensity (Fig. 3.111; linear R square 0.135). Soil moisture content shows a very weak linear negative relationship with topography defined through the DSM (Fig. 3.112; linear R square 0.033). Soil moisture content also displays weak negative linear relationships with FP intensity (Fig. 3.113; linear R square 0.03) and LP intensity (Fig. 3.114; linear R square 0.065).

From the analysis of the sediment properties and lidar data, it is evident that topography and Ohms relate most closely to the changes in geomorphology within the ground survey grid. Soil organic content and soil moisture content displays a weak linear relationships to topography and also intensity, indicating that FP intensity, LP intensity, soil moisture content and soil organic content are not defining the geomorphological change within the survey grid.

The inter-variable relationships are interesting. FP intensity against LP DSM shows a weak linear positive relationship (Fig. 3.115; linear R square 0.194). LP intensity shows a stronger linear positive relationship to LP DSM (Fig. 3.116; linear R square 0.362). Soil organic content shows a weak negative linear relationship to Ohms (Fig. 3.117; linear R square 0.113). Soil moisture content shows a very weak linear negative relationship to Ohms (Fig. 3.118; linear R square 0.046). Lastly, soil organic content shows a weak positive linear relationship to soil moisture content (Fig. 3.119; linear R square 0.037).

Therefore, within Area 8 the lidar data shows little linear relationship between topography and intensity. Likewise, the soil properties of Ohms, soil organic content and soil moisture content, show weak linear relationships to each other. If it is accepted that topography and Ohms produce the best definitions of geomorphology within the survey grid, then soil moisture content, soil organic data, FP and LP intensity, all weakly define this geomorphological change.

The table of inter-variable correlations within the Area 8 4m data set reveals statistically significant correlations between all of the variables at the 0.01 level (Tab. 3.7). Such high levels of inter-variable correlations have been seen in other survey area data, such as Area 6

4m and Area 7 4m. However, the graphical analysis of these relationships shows these relationships to be non-linear in form. Therefore, it is not possible to make robust predictions using a linear regression model, about sediment properties based on either FP or LP intensity.

The Area 8 4m data analysis clearly shows that FP and LP intensity have weak linear relationships to changes in geomorphology within the ground survey grid. Again the best tools for identifying changes in geomorphology are earth resistance survey and topography. However, it should also be emphasised that within this data set topography and Ohms still displayed weak linear relationships to soil organic and soil moisture contents, indicating that neither soil moisture or soil organic contents were reliably identifying changes in geomorphology between the terrace and the palaeochannel.

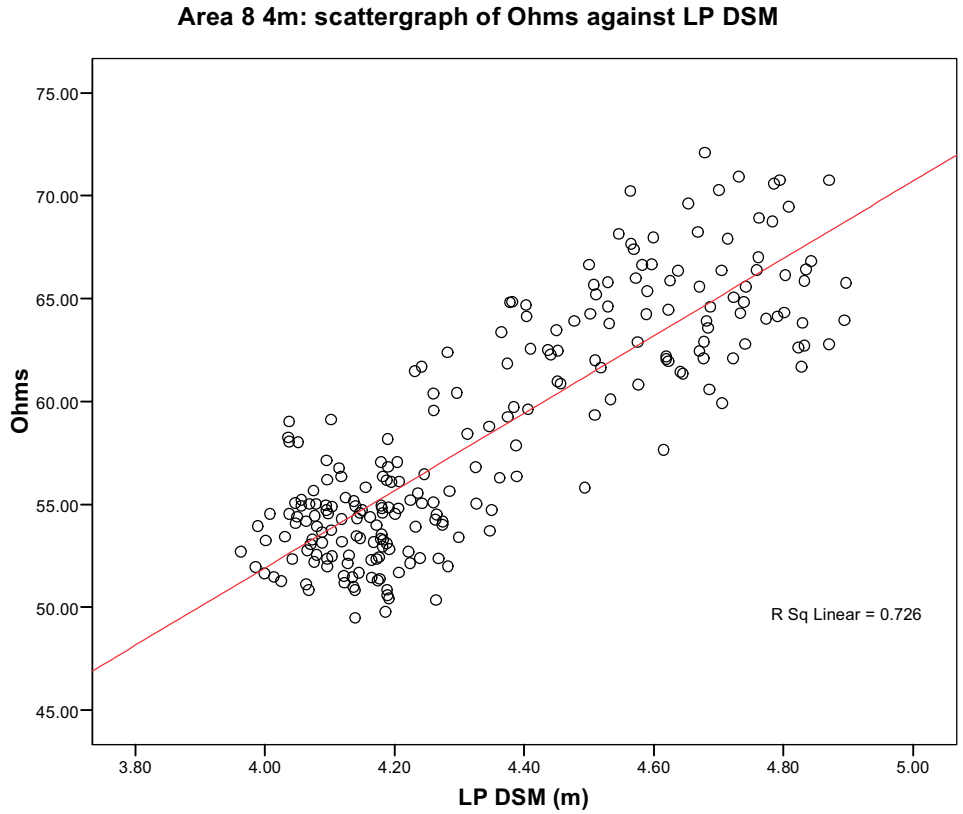

Fig 3.106: Ohms against LP DSM.

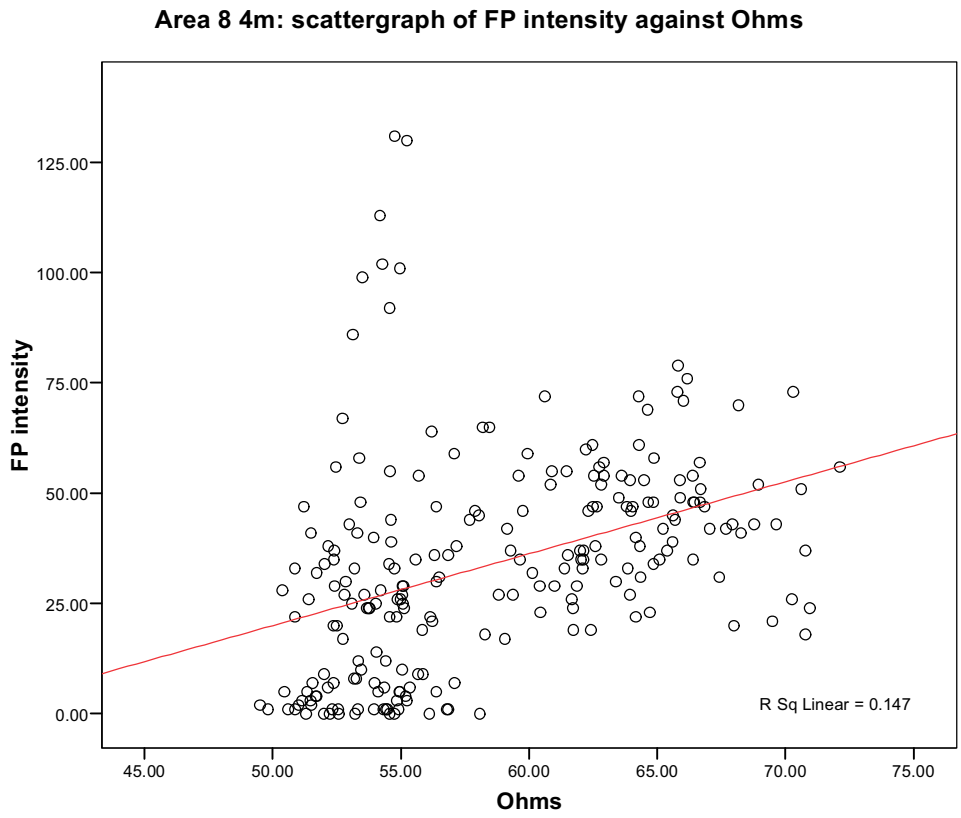

Fig 3.107: Ohms against FP intensity.

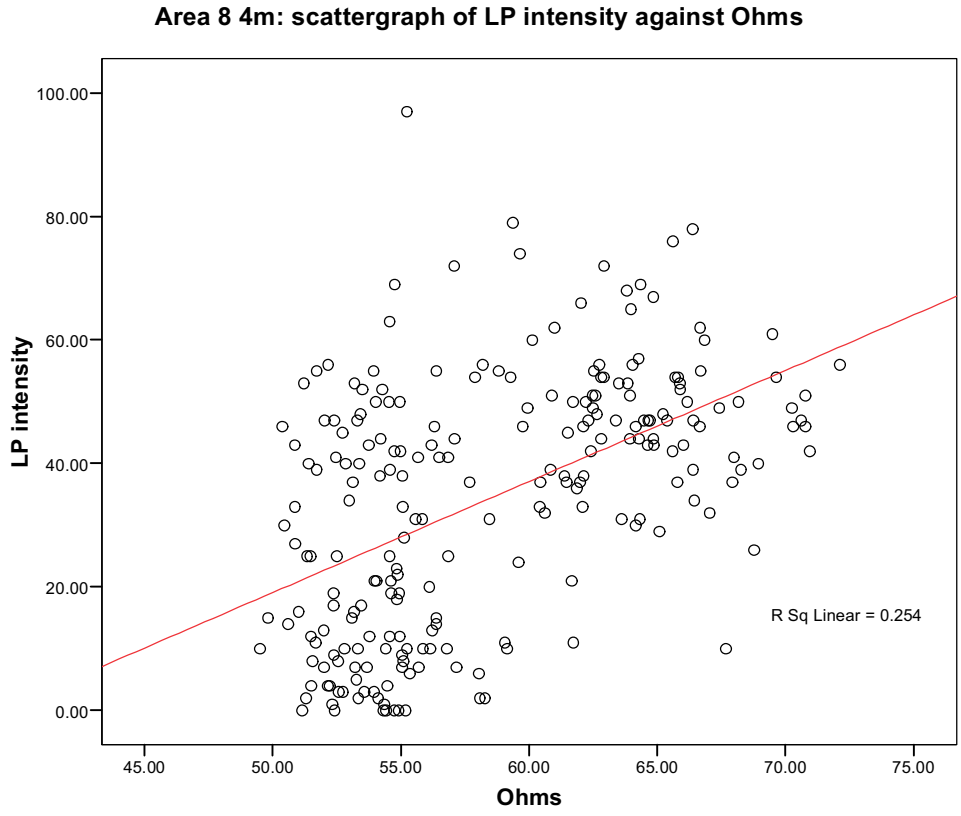

Fig 3.108: Ohms against LP intensity.

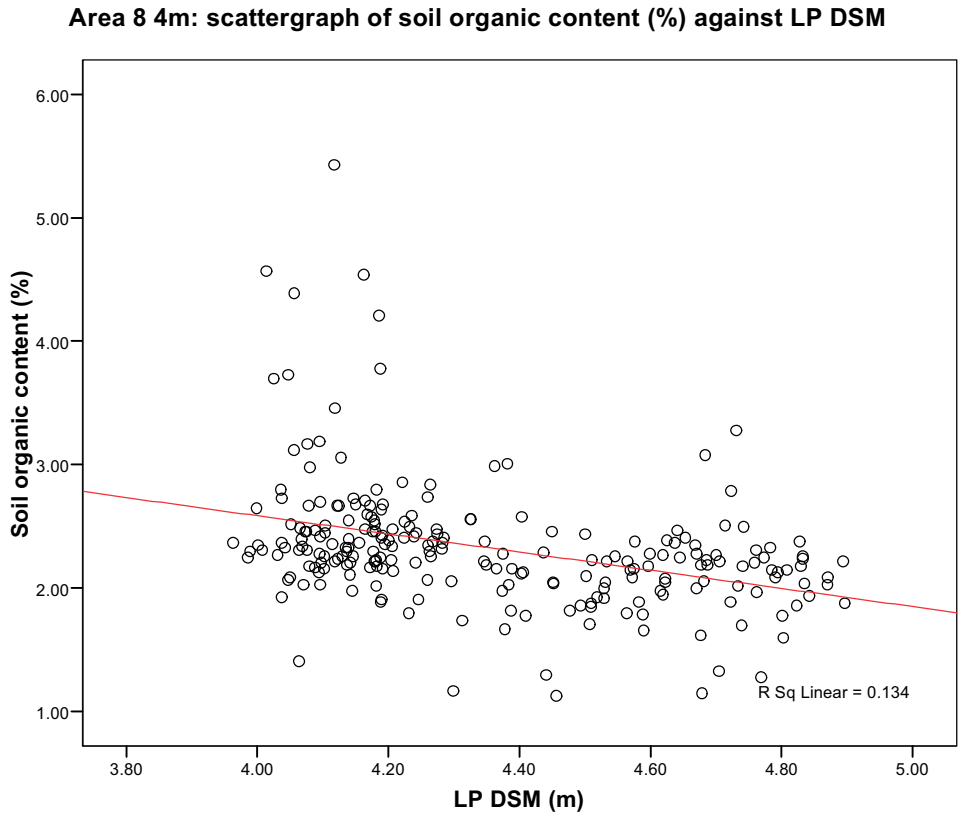

Fig 3.109: Soil organic content against LP DSM.

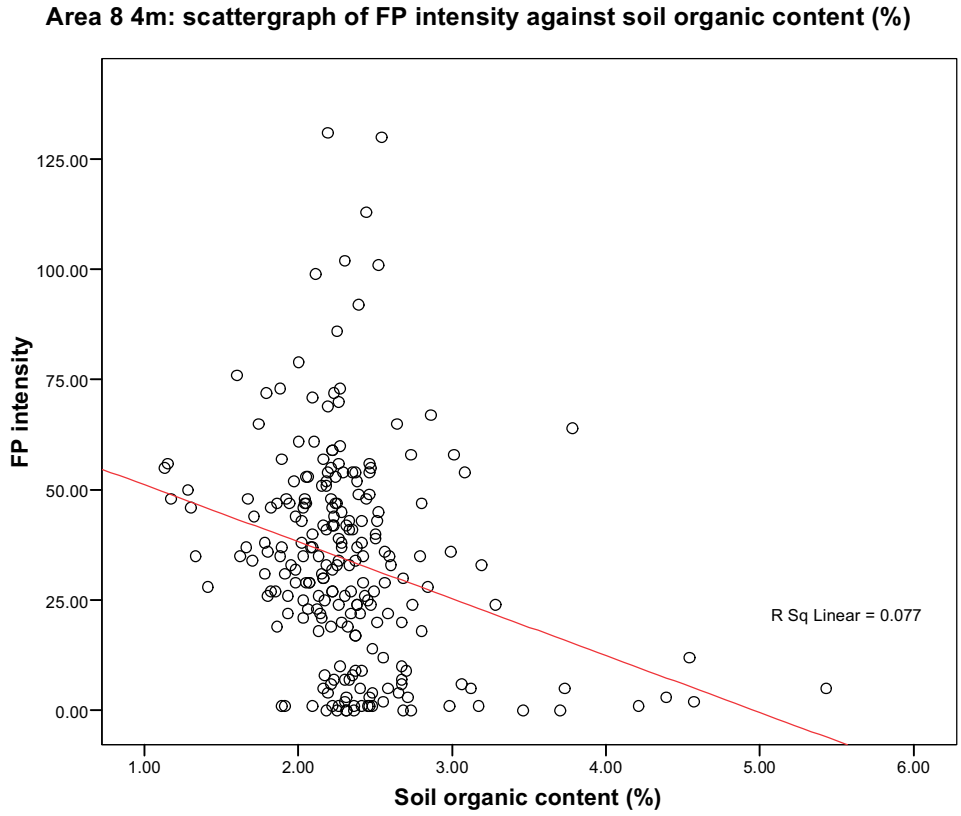

Fig 3.110: FP intensity against soil organic content.

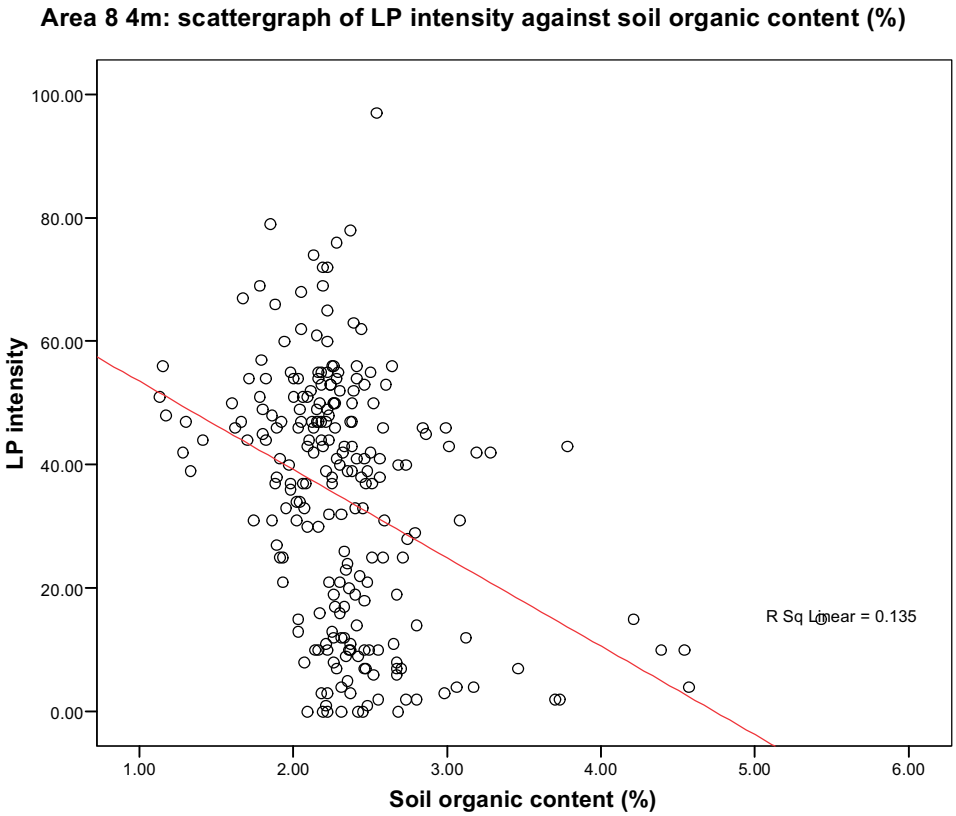

Fig 3.111: LP intensity against soil organic content.

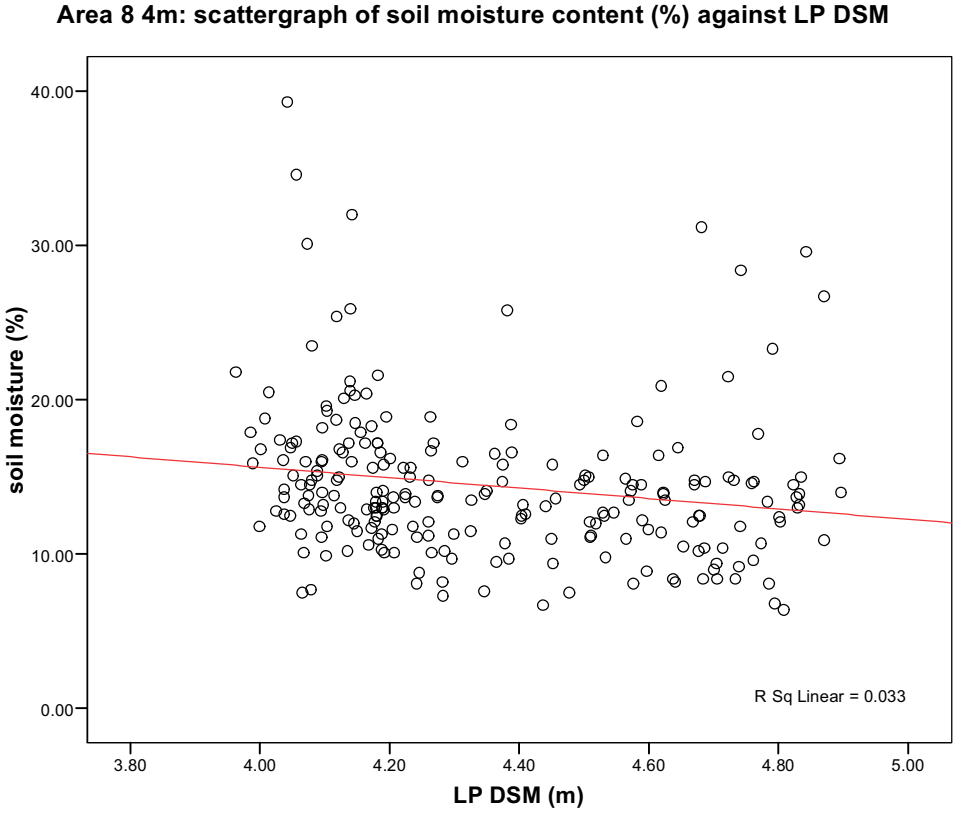

Fig 3.112: Soil moisture against LP DSM.

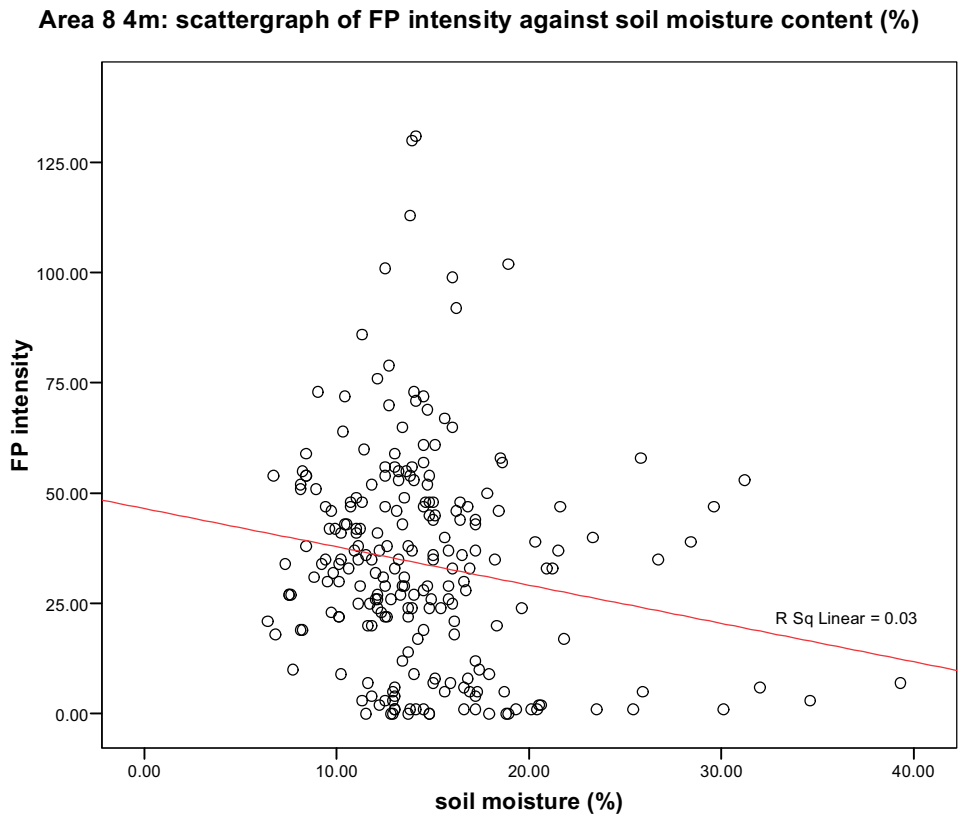

Fig 3.113: FP intensity against soil moisture.

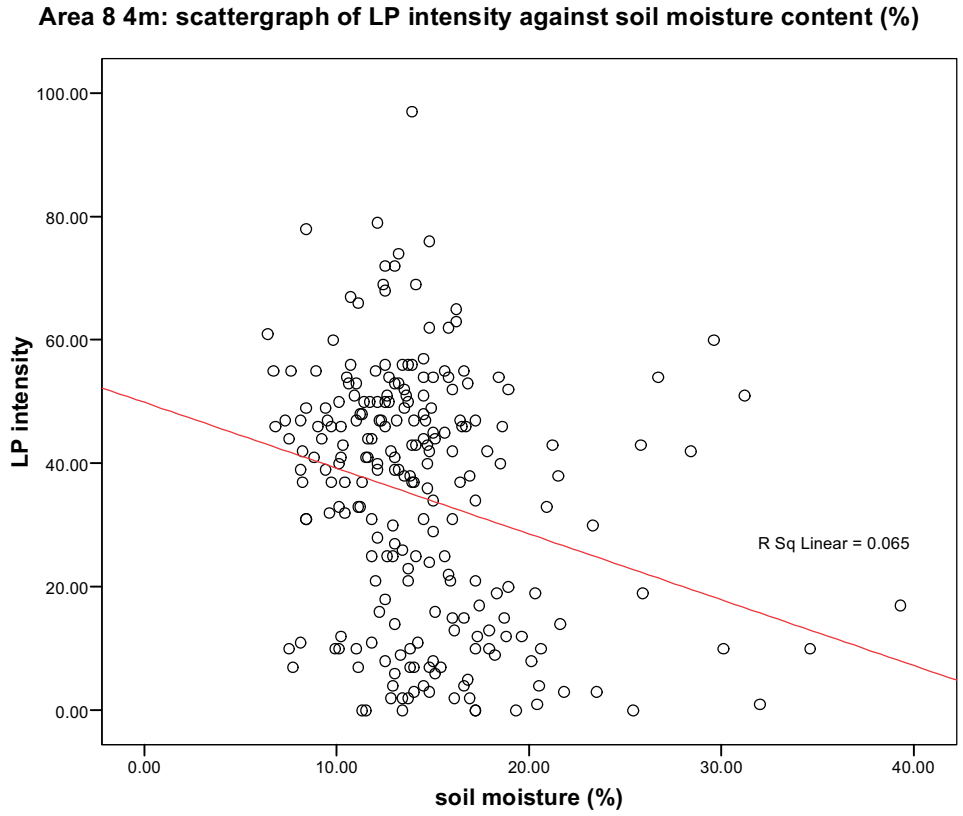

Fig 3.114: LP intensity against soil moisture (%).

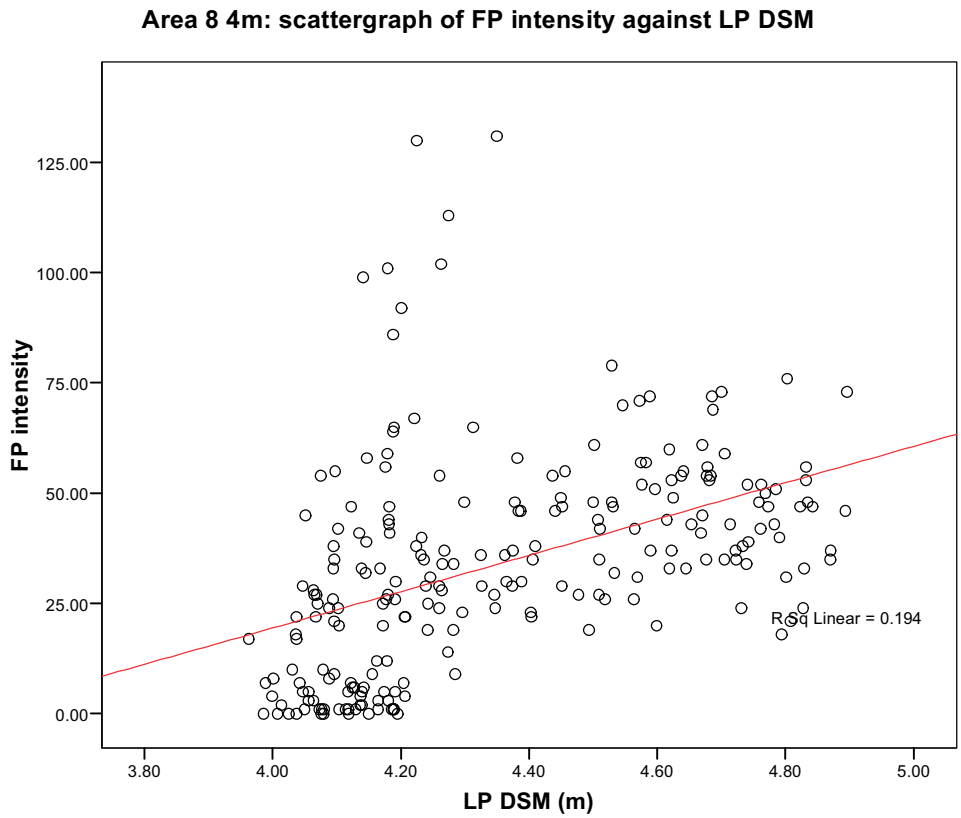

Fig 3.115: FP intensity against LP DSM.

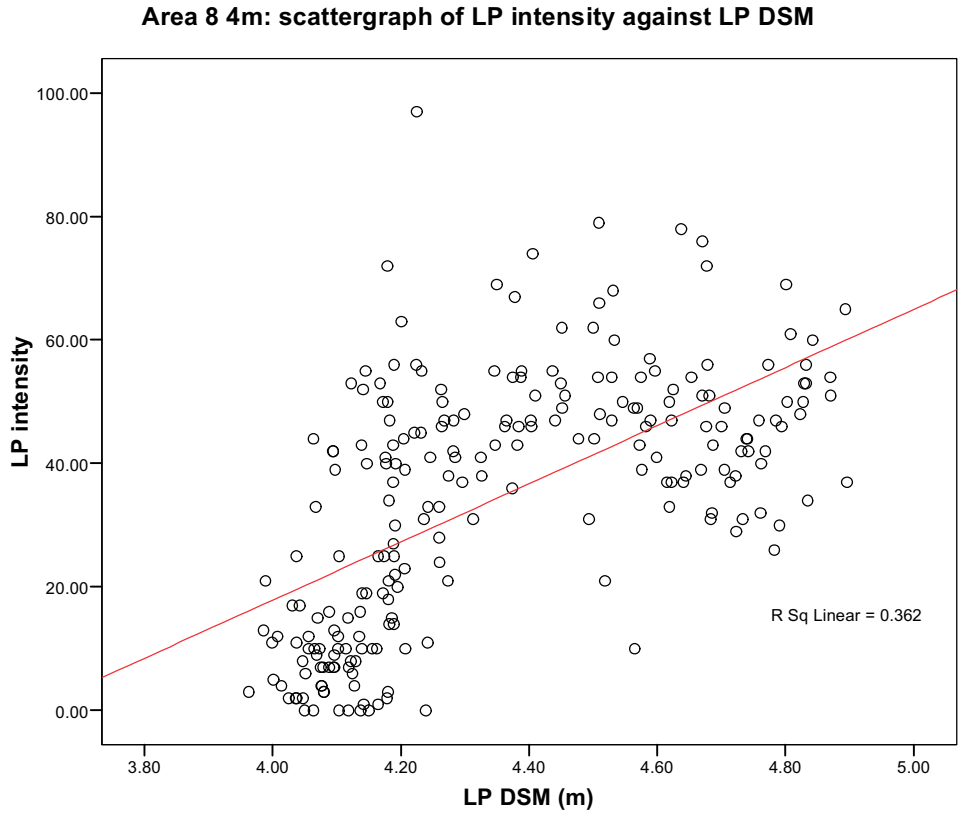

Fig 3.116: LP intensity against LP DSM.

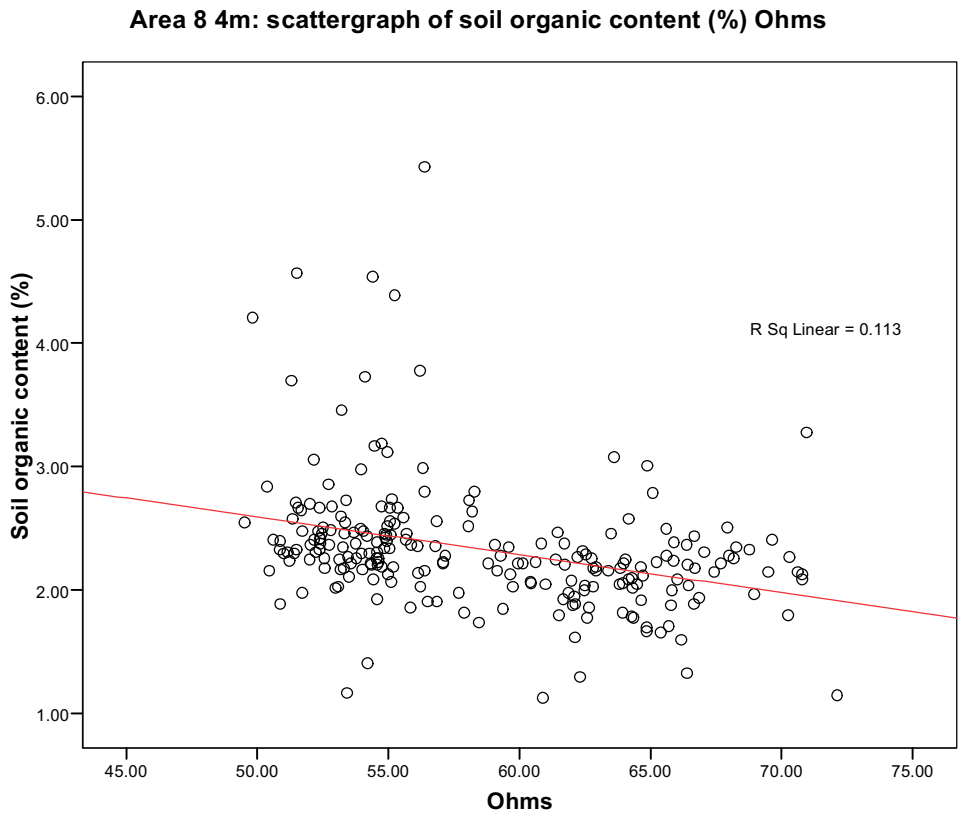

Fig 3.117: Ohms against soil organic content.

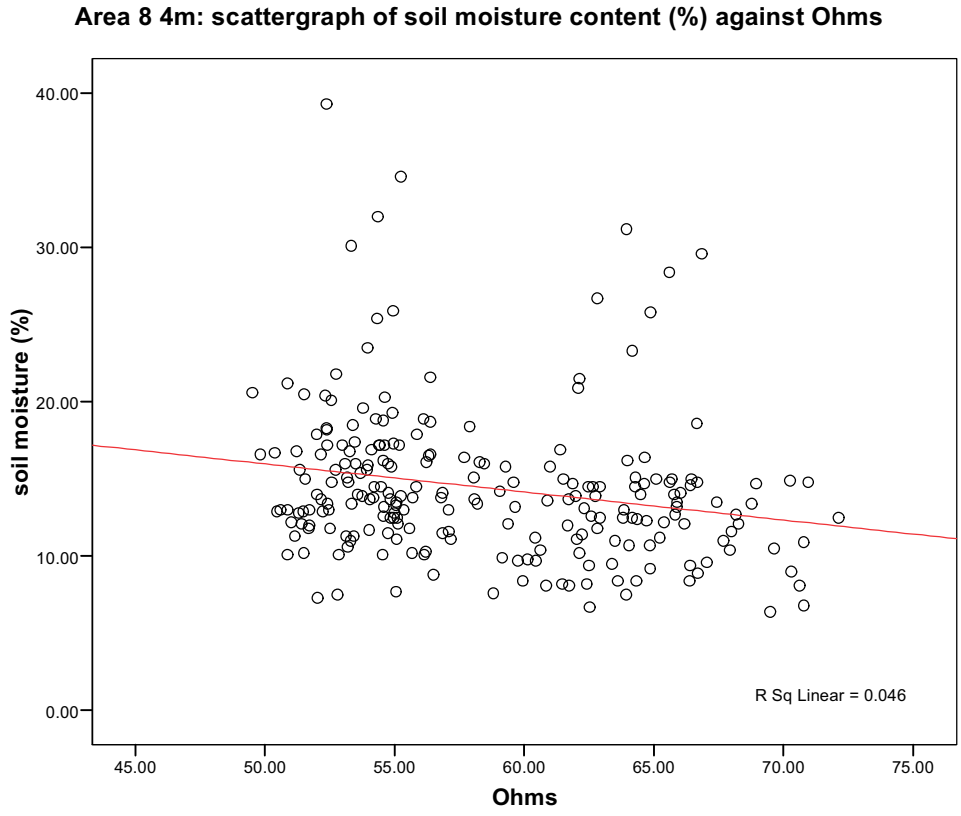

Fig 3.118: Ohms against soil moisture.

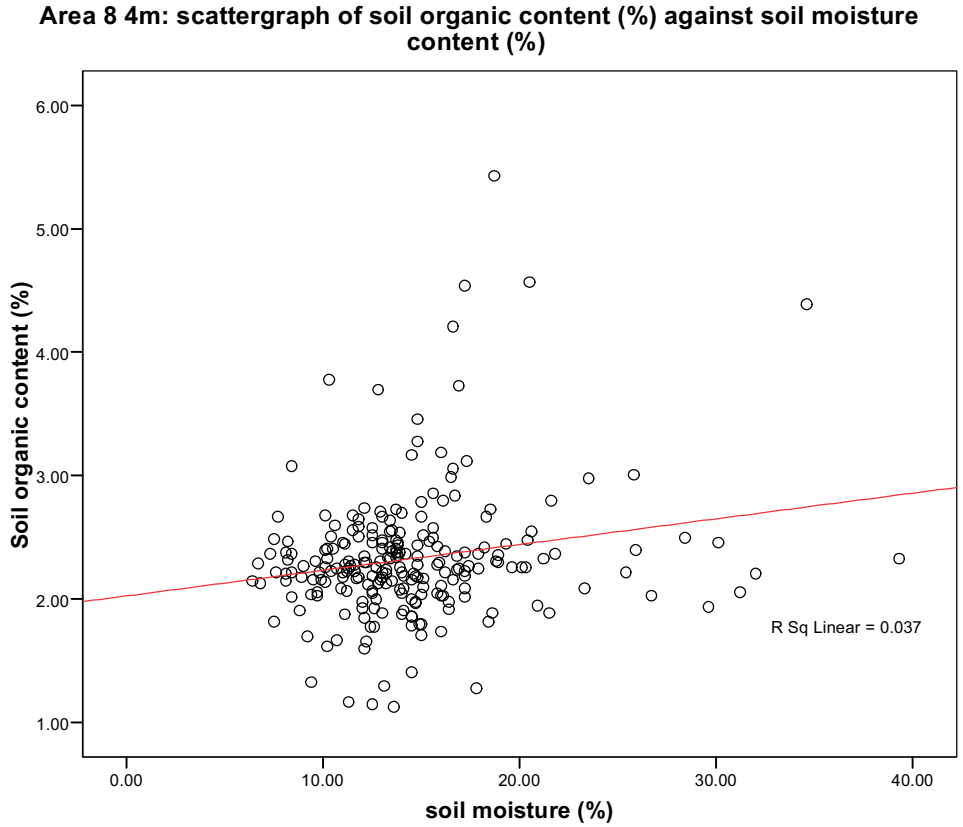

Fig 3.119: Soil organic content against soil moisture content.

Correlations

		soil moisture (%)	Ohms	LP DSM (m)	FP intensity	LP intensity	Soil organic content (%)
soil moisture (%)	Pearson Correlation	1	-.214**	-.180**	-.174**	-.254**	.193**
	Sig. (2-tailed)		.001	.006	.008	.000	.003
	N	230	229	230	230	230	230
Ohms	Pearson Correlation	-.214**	1	.852**	.383**	.504**	-.337**
	Sig. (2-tailed)	.001		.000	.000	.000	.000
	N	229	229	229	229	229	229
LP DSM (m)	Pearson Correlation	-.180**	.852**	1	.441**	.601**	-.365**
	Sig. (2-tailed)	.006	.000		.000	.000	.000
	N	230	229	230	230	230	230
FP intensity	Pearson Correlation	-.174**	.383**	.441**	1	.636**	-.278**
	Sig. (2-tailed)	.008	.000	.000		.000	.000
	N	230	229	230	230	230	230
LP intensity	Pearson Correlation	-.254**	.504**	.601**	.636**	1	-.368**
	Sig. (2-tailed)	.000	.000	.000	.000		.000
	N	230	229	230	230	230	230
Soil organic content (%)	Pearson Correlation	.193**	-.337**	-.365**	-.278**	-.368**	1
	Sig. (2-tailed)	.003	.000	.000	.000	.000	
	N	230	229	230	230	230	230

**. Correlation is significant at the 0.01 level (2-tailed).

Tab 3.7: Pearson Correlation Coefficients of the relationships between variables in Area 8 4m data set.

3.4.4 Area 8: 1m data set analysis

The analysis of the Area 8 1m data set showed further evidence of the strong linear positive relationship between Ohms and topography (Fig. 3.120; linear R square 0.705). Again FP intensity shows a weak positive linear relationship to Ohms (Fig. 3.121; linear R square 0.113), as does LP intensity to Ohms (Fig. 3.122; linear R square 0.201). FP intensity displays a weak positive linear relationship to topography (Fig. 3.123; linear R square 0.165), as does LP intensity to topography (Fig. 3.124; linear R square 0.292). Overall it can be seen that within the Area 8 1m data there are no linear relationships between variables, except for the positive linear relationship between Ohms and topography as defined by the LP DSM. The table of computed correlation coefficients shows high significant statistical correlations between all of the variables (Tab. 3.8). However, only the relationship between Ohms and topography is considered suitably linear to be used in a regressive predictive model.

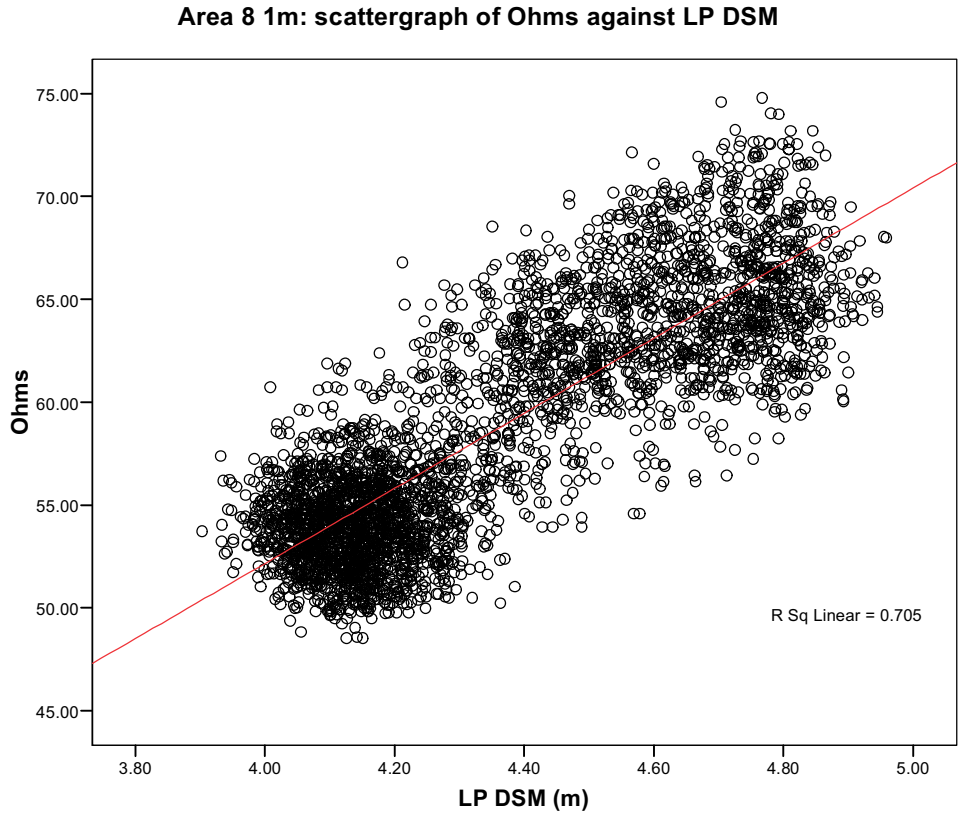

Fig 3.120: Ohms against LP DSM.

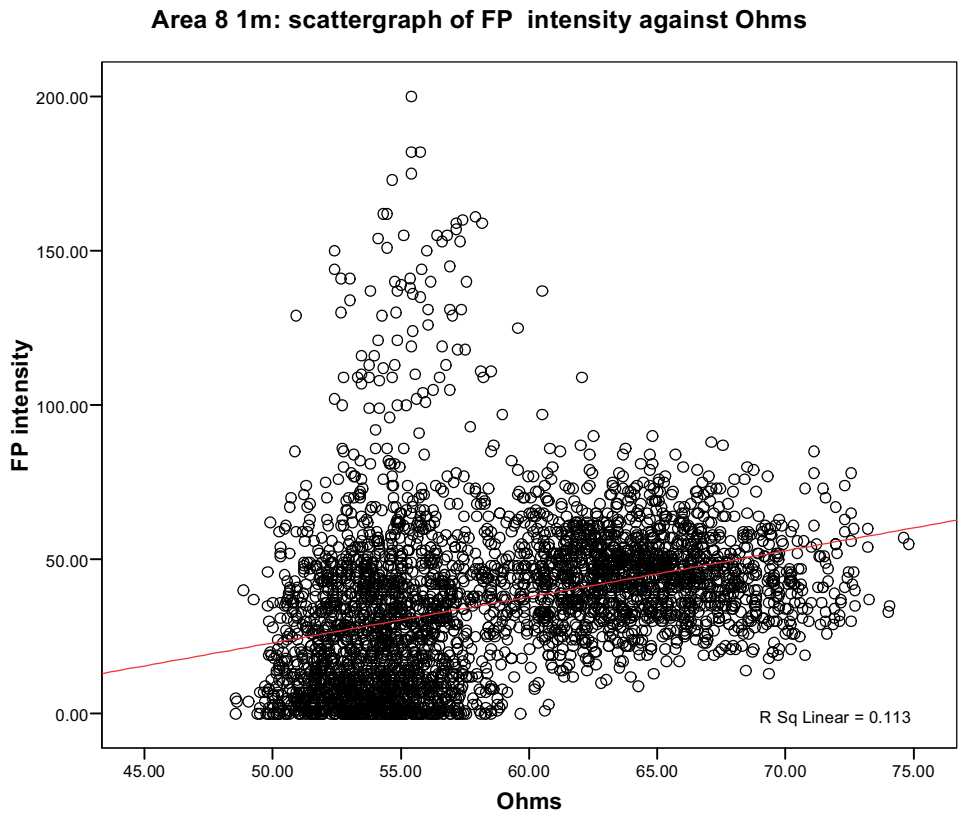

Fig 3.121: FP intensity against Ohms.

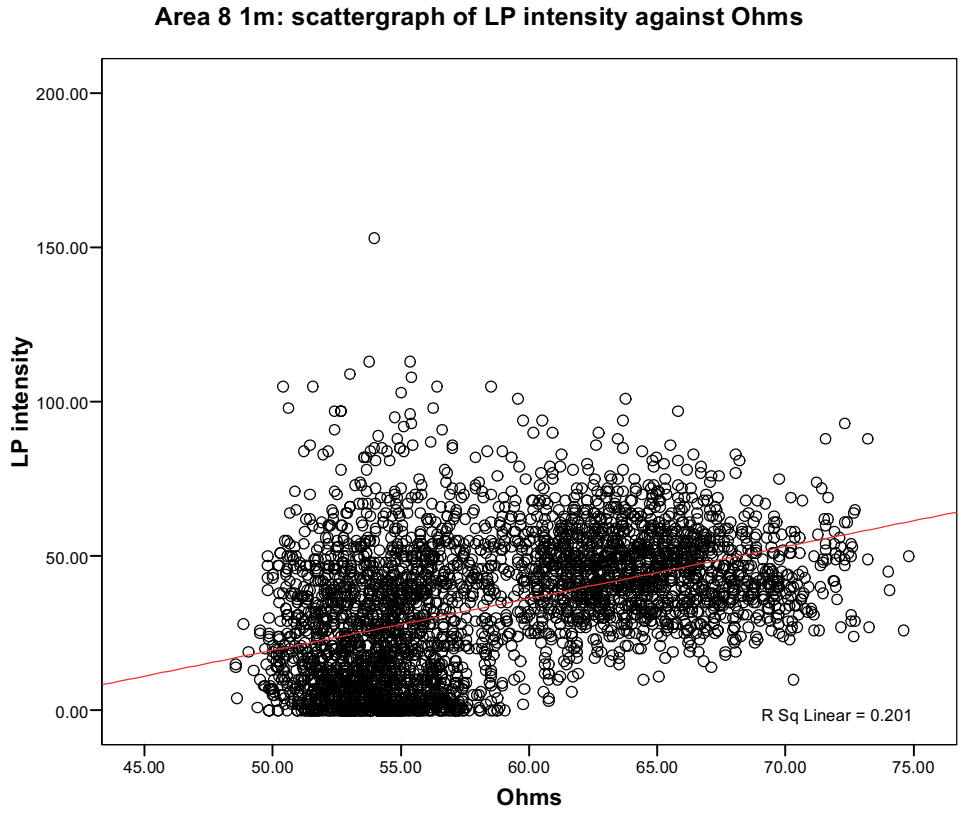

Fig 3.122: LP intensity against Ohms.

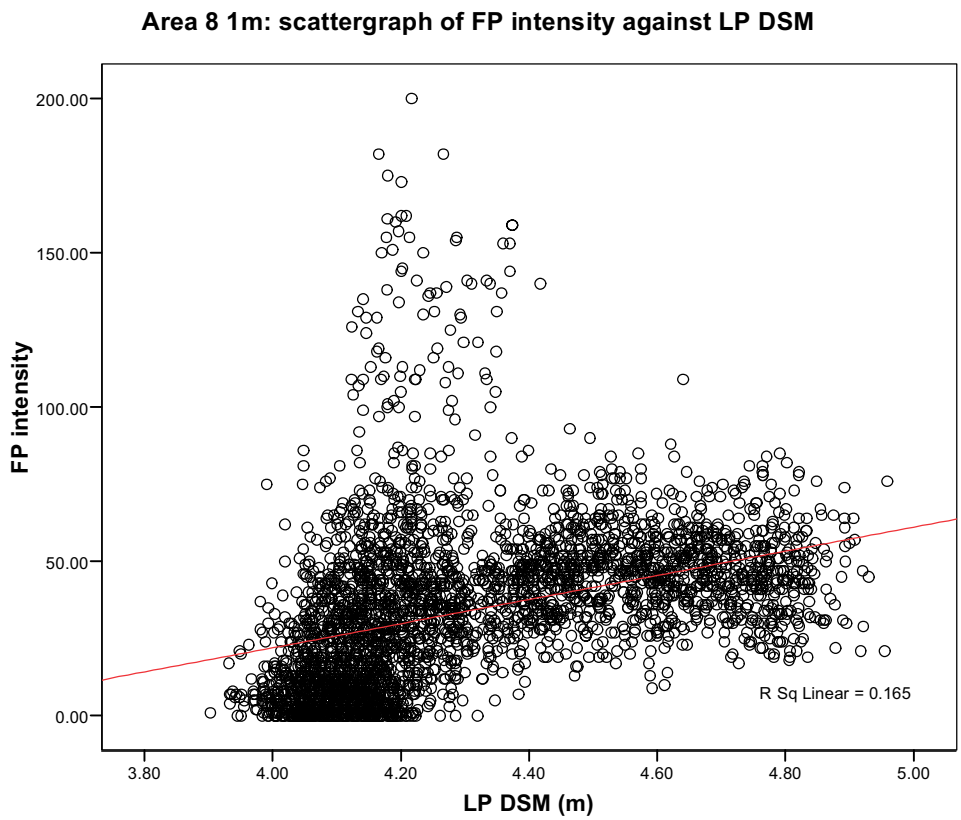

Fig 3.123: FP intensity against LP DSM.

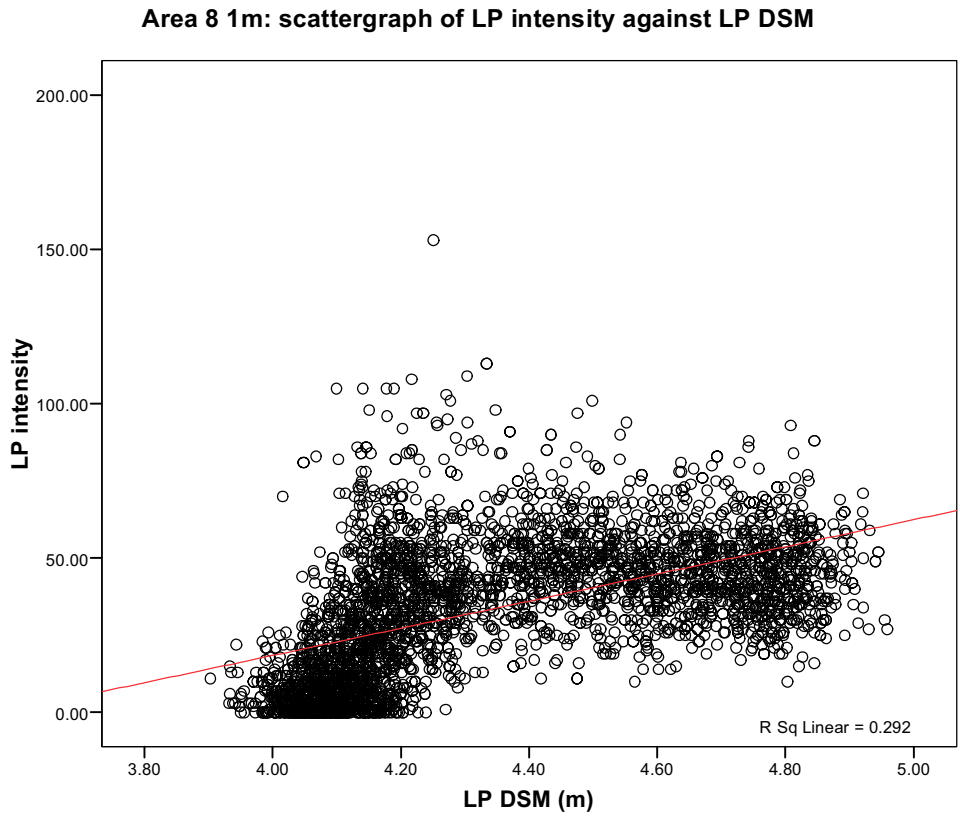

Fig 3.124: LP intensity against LP DSM.

Correlations

		Ohms	LP DSM (m)	FP intensity	LP intensity
Ohms	Pearson Correlation	1	.840**	.337**	.448**
	Sig. (2-tailed)		.000	.000	.000
	N	3673	3673	3673	3673
LP DSM (m)	Pearson Correlation	.840**	1	.406**	.541**
	Sig. (2-tailed)	.000		.000	.000
	N	3673	3680	3680	3680
FP intensity	Pearson Correlation	.337**	.406**	1	.590**
	Sig. (2-tailed)	.000	.000		.000
	N	3673	3680	3680	3680
LP intensity	Pearson Correlation	.448**	.541**	.590**	1
	Sig. (2-tailed)	.000	.000	.000	
	N	3673	3680	3680	3680

**. Correlation is significant at the 0.01 level (2-tailed).

Tab 3.8: Area 8 1m data set correlations.

3.4.5 Area 8 relationship of surface intensity to sub-surface sediment stratigraphy

A gouge core transect in Area 8 was made across the survey grid from north to south (Fig. 3.125). The stratigraphy recorded describes a relatively simple, shallow, sediment sequence (Fig. 3.126). The top of the alluvial stratigraphy is dominated by a brown sandy silt with a trace of clay (unit A), underlain by an orange brown medium sand, at the top of the terrace gravels. This orange brown medium sand was a thick deposit and was not cored through during sampling. This stratigraphy of unit A underlain by unit B was the extent of the above gravel alluvial stratigraphy seen on the Holme Pierrepont Terrace.

The minor palaeochannel is evident in the gouge core transect as sequence of slightly deeper (c. 97cm) alluvial sediments above Unit B, the orange brown medium sand. However, Unit A dominates the upper stratigraphy of the entire gouge core transect and this will undoubtedly influence the results, as the lidar laser pulse is effectively encountering a similar sediment architecture across the transect. This stated, the minor palaeochannel was notably wetter during field survey and lidar data collection, and this maybe expected to affect intensity returns. The fill of the palaeochannel consists of a brown sandy clayey silt (Unit C), underlain by an orange brown silty clay (Unit D), underlain by a grey brown sandy clay with Fe mottling (Unit E), with a basal unit of grey brown clayey sand with Fe mottling. From the gouge core stratigraphy, it is evident that the palaeochannel is a relatively shallow, narrow feature.

Lidar intensity returns when compared to the Area 8 gouge core stratigraphy show an area of slightly higher lidar reflectance on the northern part of the Holme Pierrepont Terrace (Fig. 3.127). When the palaeochannel is initially encountered some relatively strong spikes are observed in both FP and LP returns, but the general trend is for lower intensity values within the palaeochannel. However with movement back onto the terrace the intensity returns for both FP and LP show a variety of high and low values, with final very high values at the end of the transect for both FP and LP returns.

Overall, lidar intensity data does show some general trends, such as general lower values over the palaeochannel and general higher values over the terrace segments. However, this

differentiation of geomorphological units would not be possible solely using the lidar intensity returns. Areas of high intensity return are recorded over the palaeochannel and areas of low intensity return are recorded over the terrace, highlighting the ambiguity inherent in using lidar intensity to map different sediment properties.

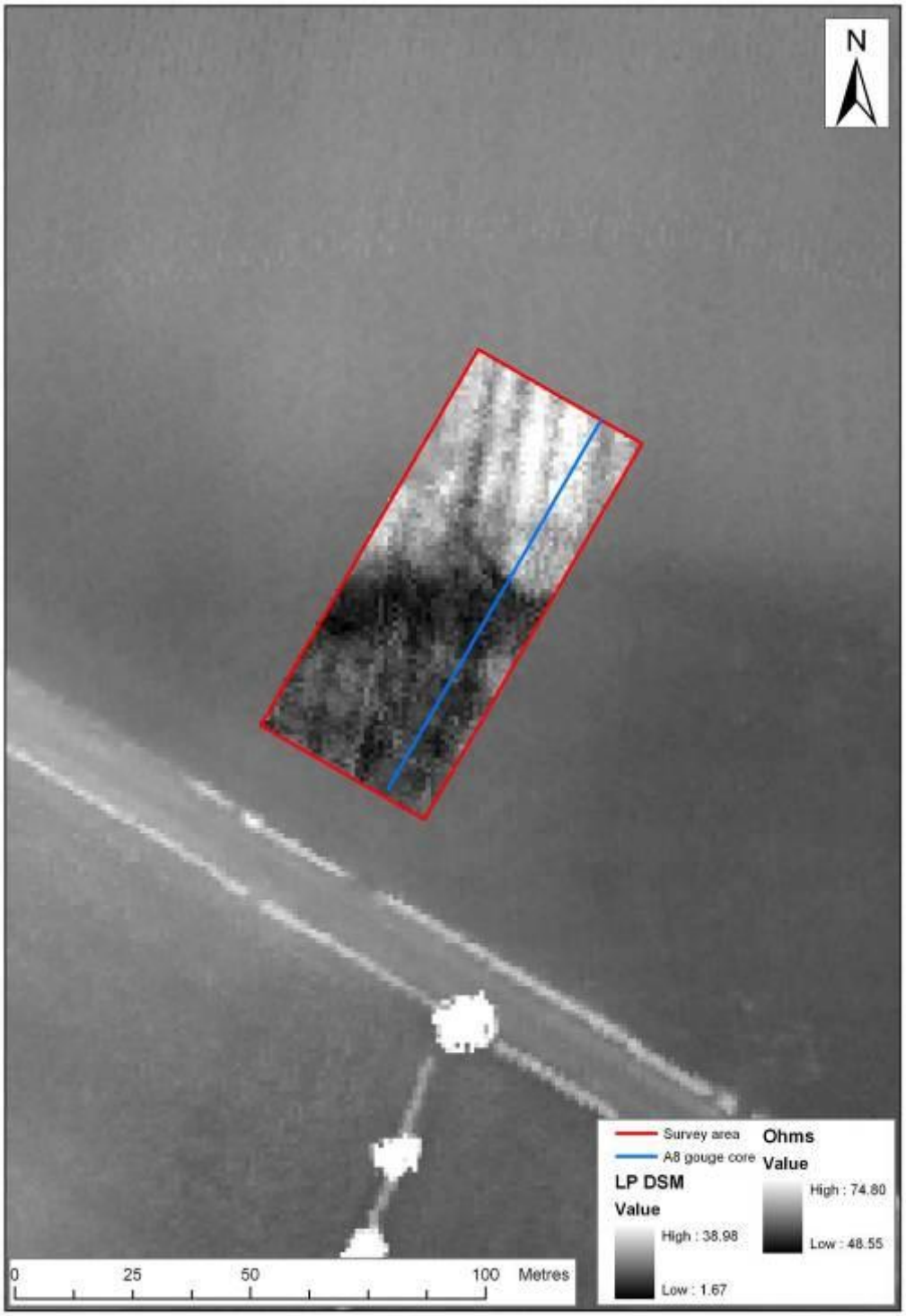

Fig 3.125: Location of the Area 8 gouge core transect.

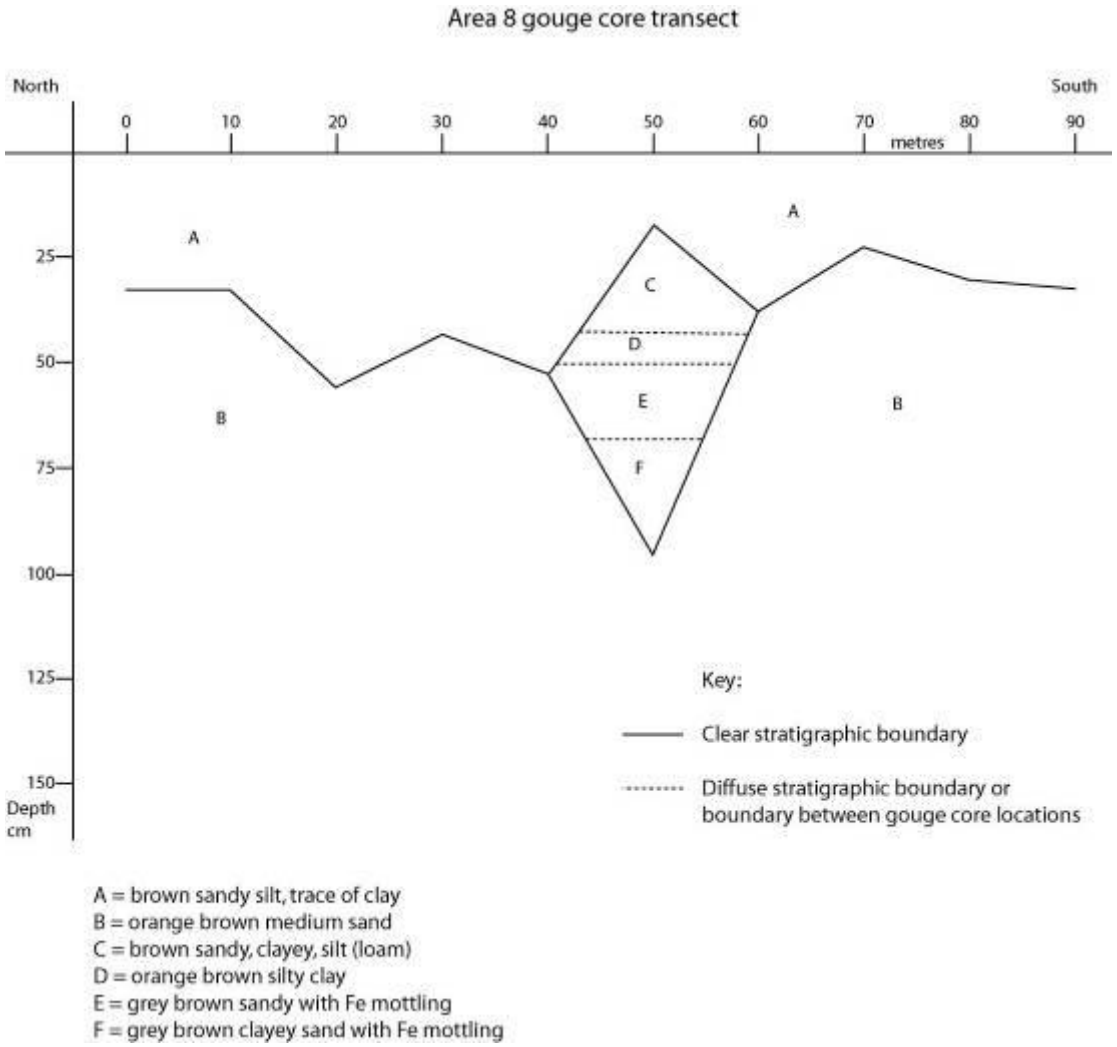

Fig 3.126: The Area 8 gouge core transect showing the sediment stratigraphy.

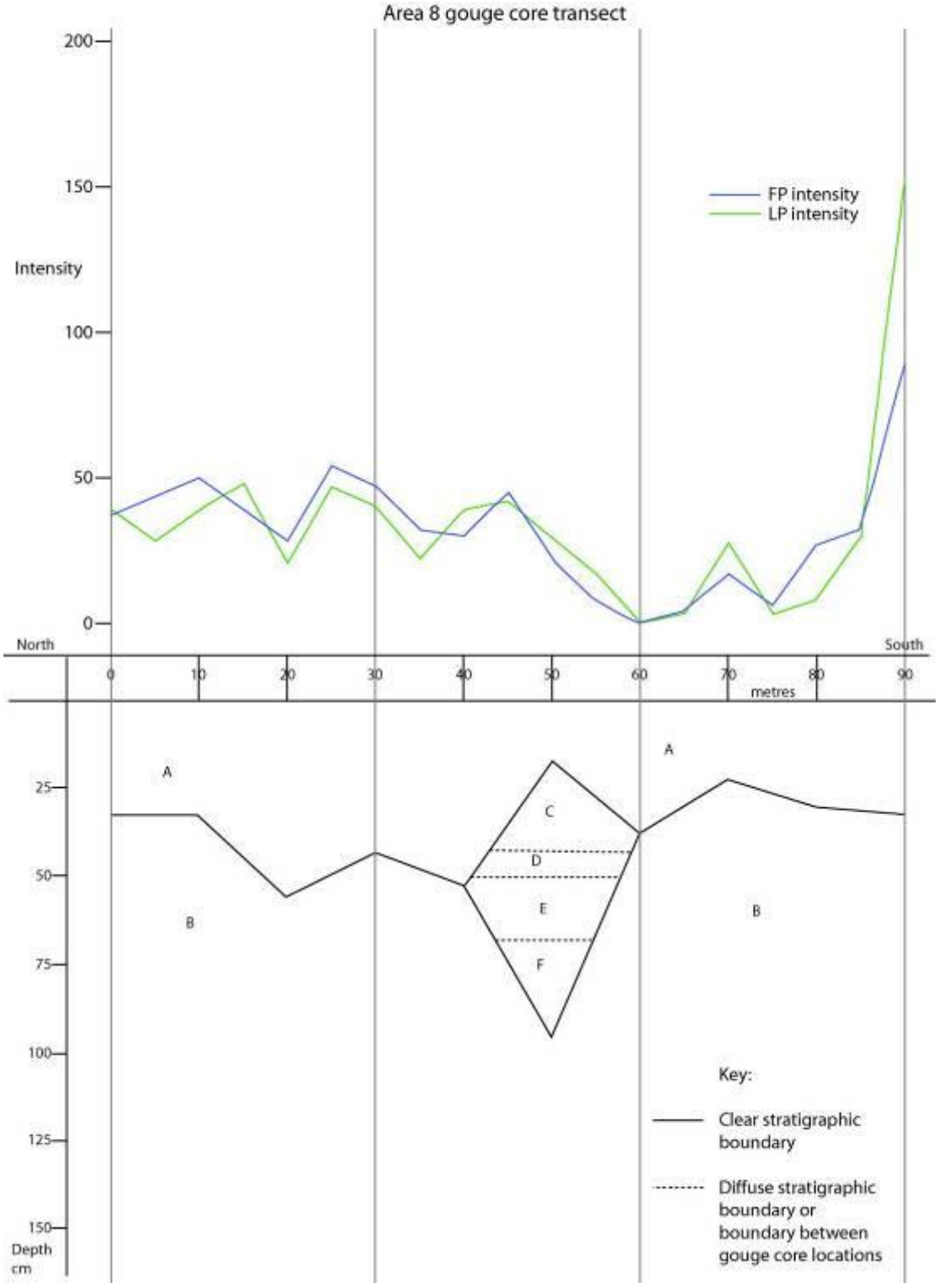

Fig 3.127: Area 8 gouge core transect shown against FP and LP intensity response.

3.4.6 Area 8 summary of main results

The Area 8 data is interesting as it encompasses a bare earth area to investigate both FP and LP returns and relate these to changes in sediment architecture. Since the site was devoid of vegetation this was expected to reduce variance in the data set, through differentiation in vegetation structure affecting returns. Overall, although visual analysis of surface models suggested strong inter-variable relationships, these relationships were shown to be mathematically non-linear and therefore not usable in a robust predictive manner to identify sediments character. Lidar intensity returns showed weak relationships to soil moisture and soil organic contents. Again the lidar LP DSM and earth resistance survey were the most useful data sets for the identification of changes in geomorphology and hence sediment structure.

The results from the visual analysis of the Area 8 data set are summarised as:

- The LP DSM defined the change from terrace to palaeochannel.
- Both FP and LP intensity defined the change from terrace palaeochannel.
- The earth resistance survey showed the form of the minor palaeochannel, the terrace and plough furrows on the terrace with clarity.
- Soil organic contents were relatively low across the whole survey area, but slightly higher values were seen over the minor palaeochannel, although elevated soil organic contents did not define the palaeochannel.
- Soil moisture contents were also slightly elevated across the palaeochannel, but again they did not define the palaeochannel.

The results from the analysis of the Area 8 4m data set are summarised as:

- Ohms produced a strong positive linear relationship with LP DSM.
- Soil moisture content had a weak negative linear relationship with LP DSM.
- Soil organic content had a weak negative linear relationship with LP DSM.
- Soil organic content and Ohms displayed a weak linear negative relationship.
- Soil moisture content and Ohms displayed a weak linear negative relationship.
- Ohms defined the changes in geomorphology better than either soil organic content or soil moisture content.
- Both FP and LP intensity had weak linear positive relationships with Ohms.
- Both FP and LP intensity had weak linear negative relationships with soil moisture content.
- Both FP and LP intensity had weak linear negative relationships with soil organic content.
- The table of correlations showed significant inter-variable correlation. However, except for the relationship of Ohms to LP DSM, these relationships are non linear and cannot be used for predictive modelling of sediment character.

The results from the Area 8 1m data set analysis are summarised as:

- The strong positive linear relationship of Ohms and LP DSM was again emphasised, showing how changes in topography within the survey grid relate to changes in sediment architecture.
- Both FP and LP intensity returns showed weak positive relationships to Ohms.
- Both FP and LP intensity returns showed weak positive relationships to LP DSM.

- The table of correlations showed significant inter-variable correlation. However, except for the relationship of Ohms to LP DSM, these relationships are non linear and cannot be used for predictive modelling of sediment chracter.

The results from the Area 8 gouge core transect are summarised as:

- The gouge core stratigraphy across the survey area was relatively shallow and simple.
- A difference in stratigraphy was evident between the terrace deposit and the minor palaeochannel.
- Both FP and LP intensity recorded slightly elevated values over the terrace and slightly lower values over the palaeochannel. However, the data was still noisy, with some high values over the palaeochannel and some low values over the terrace.
- Both the FP and LP intensity returns were ambiguous in their definition of the terrace and minor palaeochannel.

4 QUALITATIVE ANALYSIS OF ARCHIVE LIDAR DATA

4 QUALITATIVE ANALYSIS OF ARCHIVE LIDAR DATA

4.1 INTRODUCTION

As originally conceived the project aimed to investigate archive lidar data for selected river corridors in England held by the Environment Agency (EA). In the event, there proved to be no intensity data within the EA archive for areas of interest to the project team. In fact, discussion with EA suggests that intensity data is not held in archive with the uniformity that was originally anticipated.

One anticipated project outcome, that archive intensity data *thought* to be available for much if not all of the EA lidar dataset (now standing at approximately 16 million hectares, or 66% of the land surface of England and Wales) might be tested as an off-the-shelf source of data for assessment of the preservation environment, was thus thwarted.

Instead, work has been redirected to the examination of archive intensity data from Infoterra for the Lockington study area (Figure 4.1) and for Sturton-le-Steeple in Nottinghamshire (Figure 4.2) where data collected for the ALSF project number 5366 FASTRAC) was available to the project team.

4.2 OBJECTIVES

The revised aim of this section of the project is to assess the potential of existing lidar intensity data to provide qualitative information that might assist in assessment of the character of the burial environment, for example through identifying areas potentially of enhanced preservation of palaeoenvironmental and cultural archaeological deposits.

4.3 METHODS

Last pulse ground lidar elevation and intensity data for ten sample areas from Lockington and Sturton were examined visually within the project GIS.

This process was undertaken in a ‘blind’ manner, not allowing existing data from the site to hamper interpretation of the lidar intensity.

Data was examined in order to make a series of empirically based statements about the character of floodplain and terrace topography and sediments and their archaeological potential such as might provide a framework for the rapid assessment of large areas using a similar method.

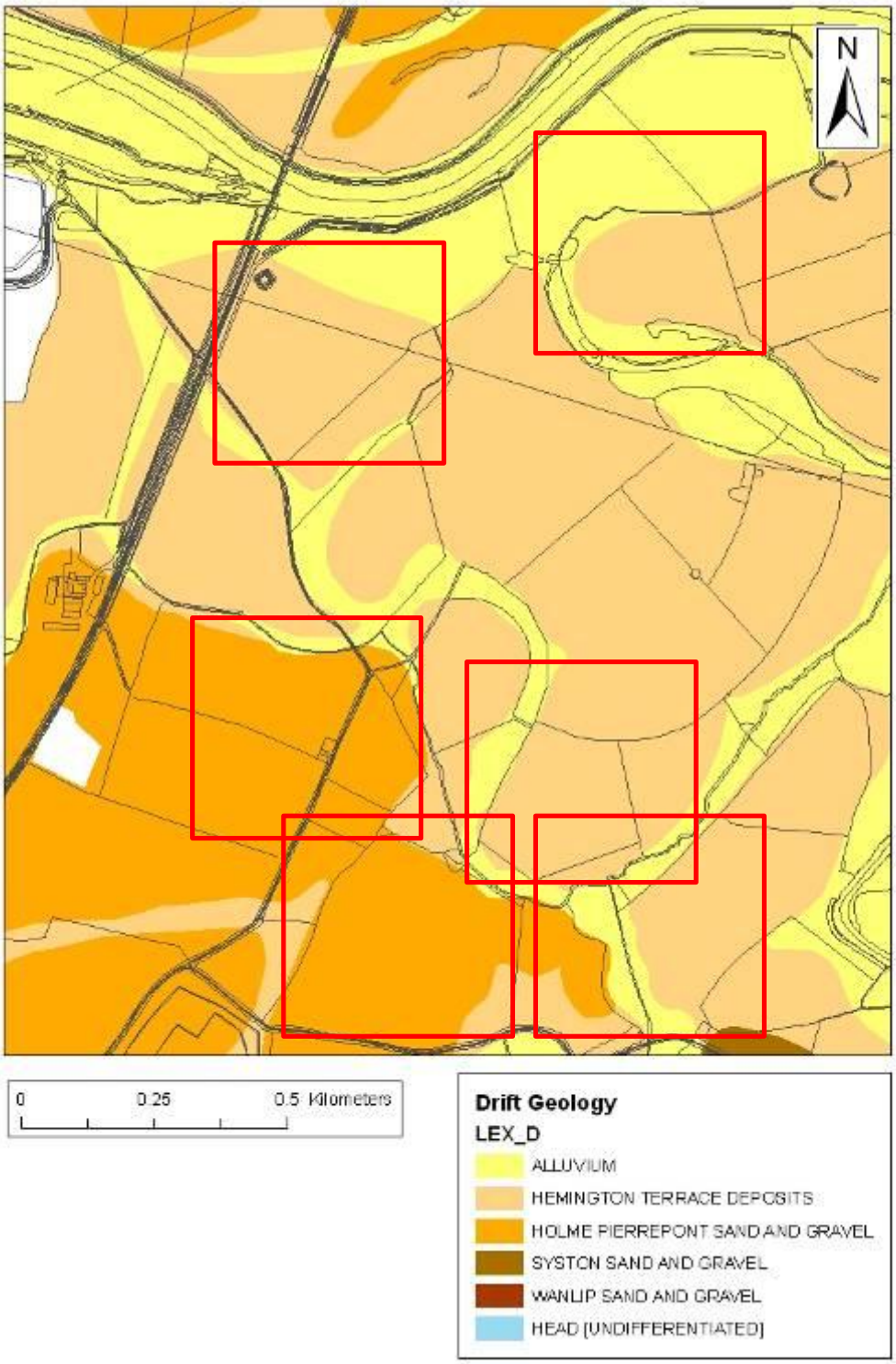

Fig 4.1 Lockington study area, map shows drift geology and the locations of the lidar intensity study windows

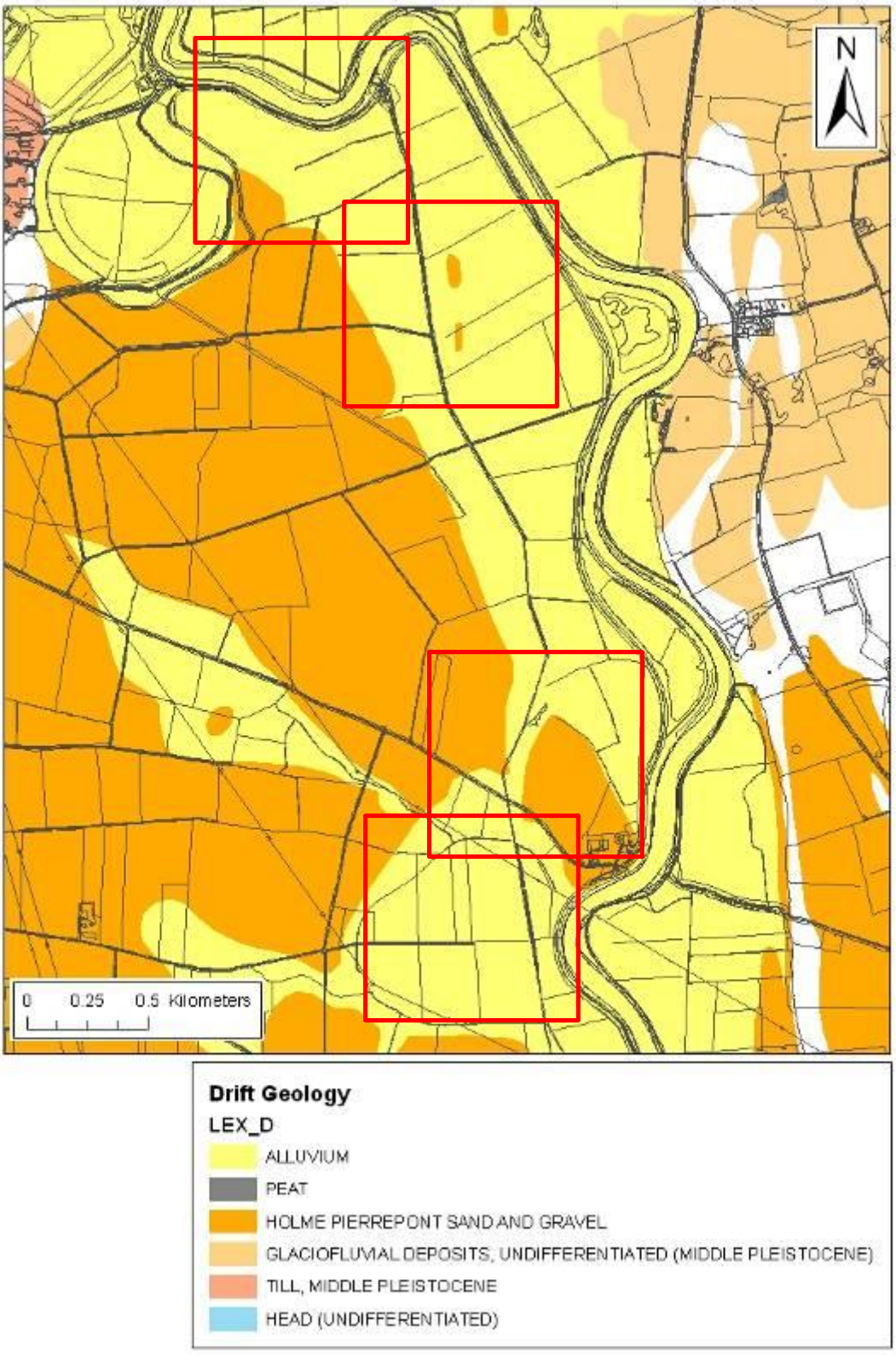

Fig 4.2 Sturton study area, map shows drift geology and the locations of the lidar intensity study windows

4.4 ANALYSIS AND DISCUSSION

4.4.1 Area 1

This study window comprises an elevated lobe of sand and gravel terrace (the Holme Pierrepont Terrace deposit). Examination of lidar elevation data (Fig 4.3a) indicates that the terrace edge at the northern end of the area is flanked by a substantial sinuous depression, probably a palaeochannel of the River Soar. To the north-west and south-east wide, shallow depressions in the terrace, followed by the line of substantial, field drains) may indicate further palaeochannels, perhaps in this instance indicating former braid channels of late Pleistocene origin. A similar very shallow depression crossing the terrace from south to north may be of the same origin.

Lidar intensity data for the same area (Fig 4.3b) mainly reflects variation in land use and cropping. The majority of the study window is seen to reflect in the mid intensity range and can be interpreted (based on the observed cultivation tram-lines) as growing crop – perhaps a winter sown cereal. Areas to the north and south have higher intensity values, and are probably pasture, which might be expected to exhibit greater NIR reflectance. There is a little variation within these broad largely homogenous areas, for example the channels within the main body of the terrace are mirrored by slightly lower intensity values. To the north of the terrace there is a clear correlation between "island" features within the palaeochannels, probable mid channel gravel bars, and lower intensity values.

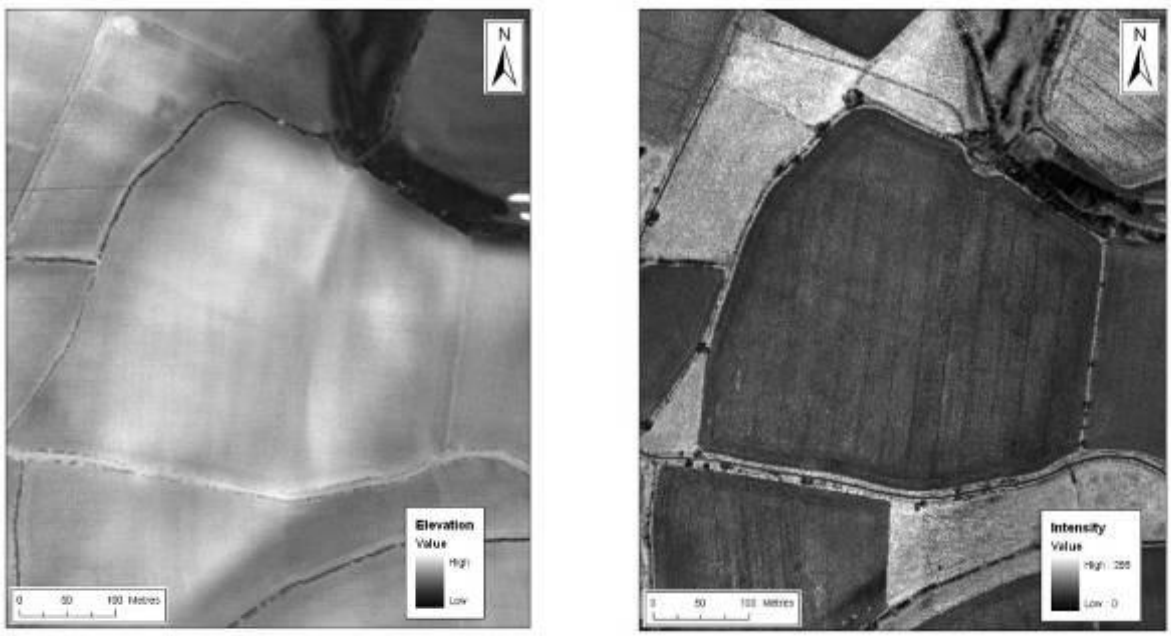

Fig 4.3 Area 1, left lidar LPG elevation data, right lidar LPG intensity

In this instance examination of lidar intensity data adds little to the overall empirical model of the study area, which is based largely on interpretation of the elevation data. It might be

reasonable to assume that both palaeochannels and terrace surface depressions might represent an enhanced burial environment (deeper sediments; finer gain size, wetter) and intensity data, though largely varying due to land use, does reflect these broad geomorphological variations.

Interestingly, the terrace area at the centre of this study window contains extensive anthropogenic archaeological remains associated with a Romano-British villa (Cooper 2006). These remains, although often evident as cropmarks, are not at all apparent in the lidar intensity or elevation data.

4.4.2 Area 2

Study window 2 comprises a further substantial area of sand and gravel terrace with the terrace edge to the north flanked by a substantial depression indicating a palaeochannels (Fig 4.4a). Variation within the microtopography of the terrace surface is evident, with lower lying areas to the east and south (that to the south followed by a field drain) probably once again reflecting braid plain topography. Broad rectilinear ridges to the western side of the terrace are probably the ploughed-out remnants of medieval or later agricultural features.

Here again lidar intensity varies largely as a result of land use (Fig 4.4b). Some variation within the large, mid intensity range area that occupies most of the terrace is evident, with diffuse areas of slightly lower intensity to the north of the terrace mirroring the topographic depression. Once again it is evident that the majority of the useful information for empirical analysis of the study window is derived from the topographic portion of the lidar data, with intensity adding little to our understanding of this area.

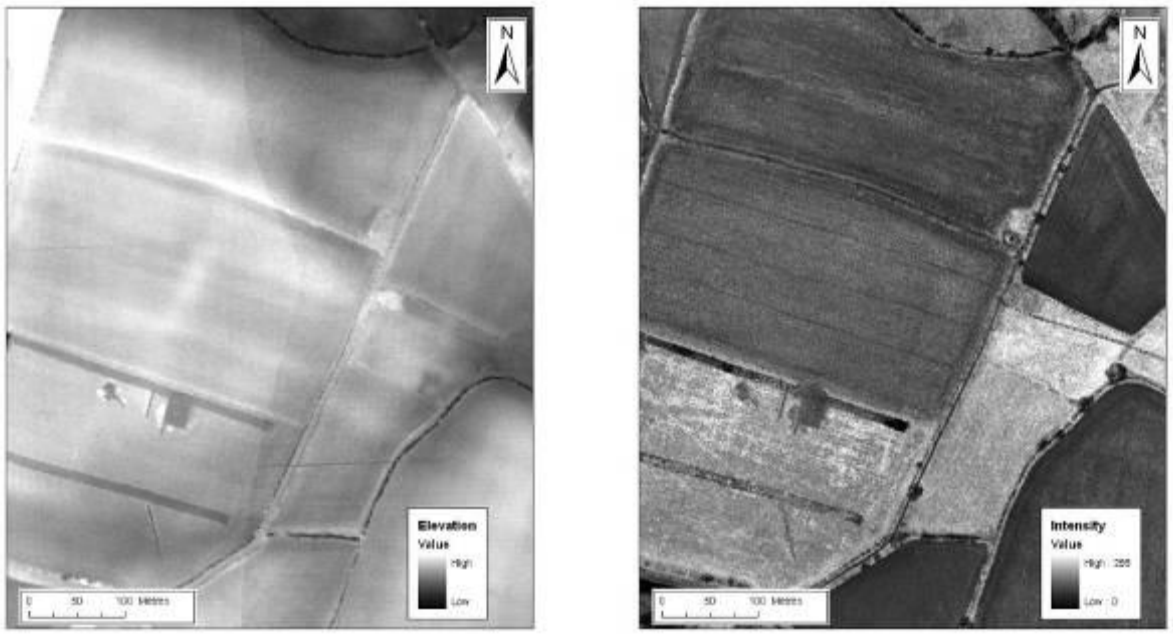

Fig 4.4 Area 2, left lidar LPG elevation data, right lidar LPG intensity

4.4.3 Area 3

Study window 3 (Fig 4.5) comprises and area of more complex geology and geomorphology comprising Holme Pierrepiont terrace to the west, Hemington Terrace to the East and lower lying terrace/floodplain deposits to the north (undifferentiated by the geological survey and recorded as Hemington Terrace). A wide, sinuous, flat bottomed channel marks the north-south boundary between the two major terrace units and drains the higher Wanlip Sands and Gravels to the south; while a broad sinuous palaeochannels of the Soar (the eastward continuation of that seen in window 1) marks the northern limit of the Hemington Terrace deposits. Some variation in microtopography is evident in both the terrace and floodplain deposits (Fig 4.5a). In particular the Hemington Terrace on the eastern side of the study window is both lower lying and clearly covered with extensive well-preserved earthwork ridge and furrow. Curvilinear ridge and swale is evident in the low lying terrace/floodplain deposits at the northern edge of the study window.

Examination of intensity data for this study window (Fig 4.5b) again reveals gross variations that are the result of land use. However, some useful variation in intensity is apparent within individual land use area, particularly the eastern portion of Hemington Terrace, where darker bands of lower intensity indicate drainage features crossing the terrace, and in the floodplain where darker, lower intensity bands are formed at the base of the swale depressions in the ridge and swale topography. In both instances it seems likely that the lower intensity reflect changes in vegetation properties due to increased soil wetness.

In this study window examination of lidar intensity data does appear to add useful information to an empirically based examination of landscape and burial environment using lidar data.

4.4.4 Area 4

Study window 4 (Fig 4.6) comprises an area mapped as Hemington Terrace deposits, bounded to the south by the substantial palaeochannels of the River Soar also seen in windows 1-3. Considerable variation in topography, attributable to both geoarchaeological and anthropogenic features, is evident in the lidar terrain data (Fig 4.6a). The parallel sinuous corrugations of ridge and swale topography are evident in the meander core to the south of the study window, while a roughly east-west channel crosses the neck of the meander. Within the body of the terrace itself there is some variation in relief, with land to the north and east of lower elevation. An inverted T-shaped earthwork bank is evident at the centre of the terrace fragment and probably indicates former plough headlands.

Lidar intensity data for this study window (Fig 4.6b) also shows considerable variation. Land use across the majority of the study window is homogenous, providing background mid-level intensity values. Within this a number of darker, low intensity bands may be seen corresponding to the depressions within the ridge and swale and the channel crossing the meander neck. No trace of the archaeological earthworks evident in the elevation data is apparent in the corresponding intensity image. Intensity values within the meander forming the southern edge of the window are uniformly high. In this instance low intensity values in some negative relief features reflect soils and vegetation variations of uncertain origin. It seems unlikely that sediments in the slight topographic features within the terrace are significantly wetter than those in the substantial palaeochannels, and so variations might be more readily attributable to other soil and vegetation properties.

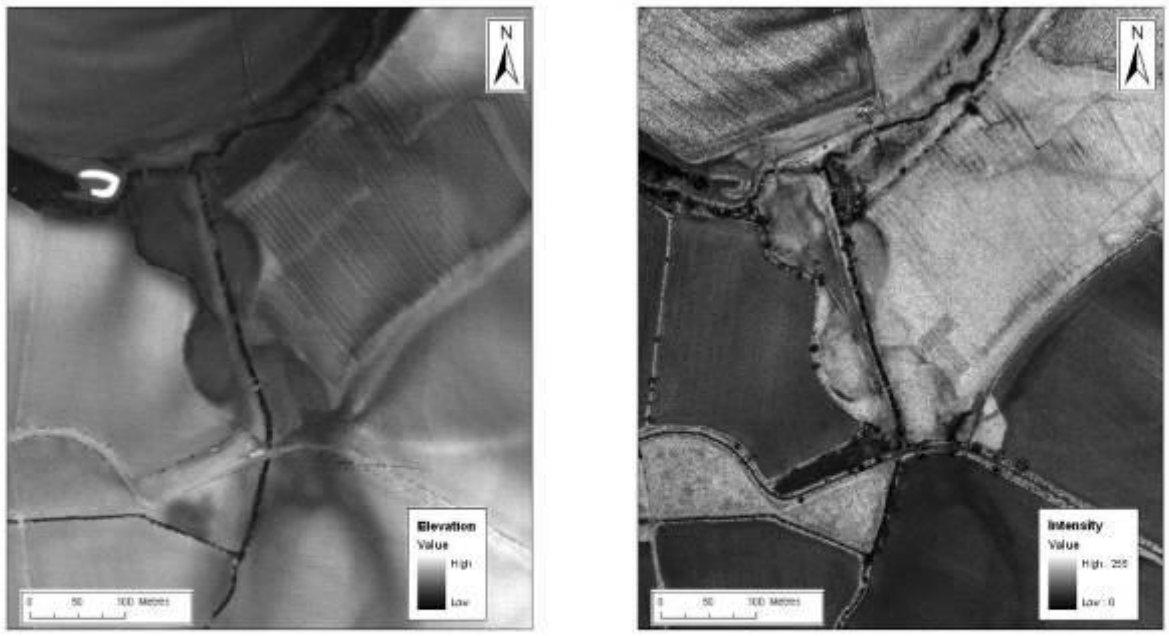

Fig 4.5 Area 3, left lidar LPG elevation data, right lidar LPG intensity

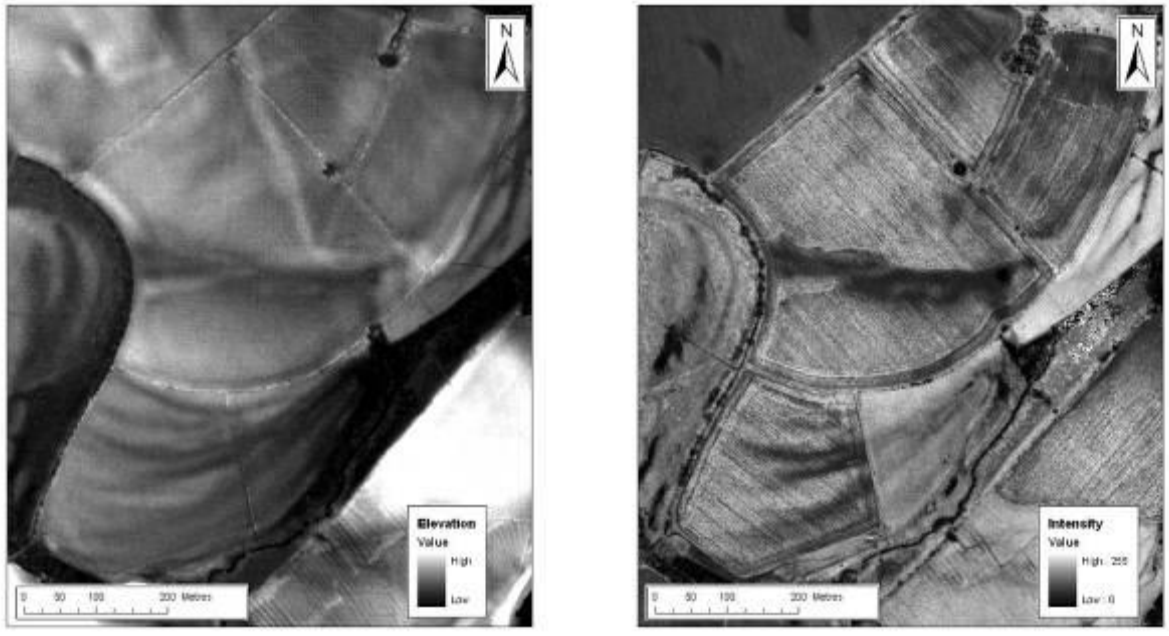

Fig 4.6 Area 4, left lidar LPG elevation data, right lidar LPG intensity

4.4.5 Area 5

Study window 5 comprises an area mapped as Hemington Terrace with alluvium at its northern edge. Lidar elevation data (Fig 4.7a) shows considerable topographic complexity, probably results of both geomorphological and anthropogenic features. A broad, sinuous depression that follows the mapped terrace edge may be a palaeochannel, with a central ridge perhaps a mid-channel bar. The land to the north of this channel is of similar elevation to the terrace to the south and probably represents a continuation of this deposit. A faint rectilinear platform with possible surrou8nding ditch may be anthropogenic. Linear depressions to the south probably represent channels draining the terrace, while several roughly north-south linear ridges may be plough headlands. To the north-west, adjacent to a railway embankment, the earthworks of a small well-defined rectilinear embanked platform are evident.

Land use across the study window is almost entirely pasture, within which some subtle variation in intensity values reflect several of the topographic depressions as areas of slightly lower intensity. Here variation in intensity seems most likely to be linked to vegetation variations caused by underlying geomorphological features.

4.4.6 Area 6

Study window 6 comprises an area of modern floodplain alluvium adjacent to the present channel of the Trent bounded to the south by a substantial relict meander of the Soar, probably marking a former confluence point with that river.

Examination of lidar elevation data (Fig 4.8a) clearly indicates the substantial curving depression of the former Soar channel as well as several other channel like depressions in the floodplain. It seems likely that the varied topography of this area accurately reflects the complex geomorphology of this former confluence zone, with isolated islands of terrace material and gravel bars flanking the Soar channel. It is probably that only the area to the extreme north-east is recent alluvium of the River Trent. In addition linear ridge and swale depressions are evident in the meander core to the south.

The lidar intensity data for this area, land use largely homogenous pasture, reflects much of the topographic detail, albeit with only very slight variations in intensity for the less pronounced topographic features. However, the former Soar channel and the more topographically pronounced features of the modern floodplain are clearly evident as very low intensity features. It seems likely that in this instance the low intensity areas reflect very heavily waterlogged sediments (parts of the meander to the south may in fact be water filled), locally affecting vegetation character and reflected as lidar intensity variations.

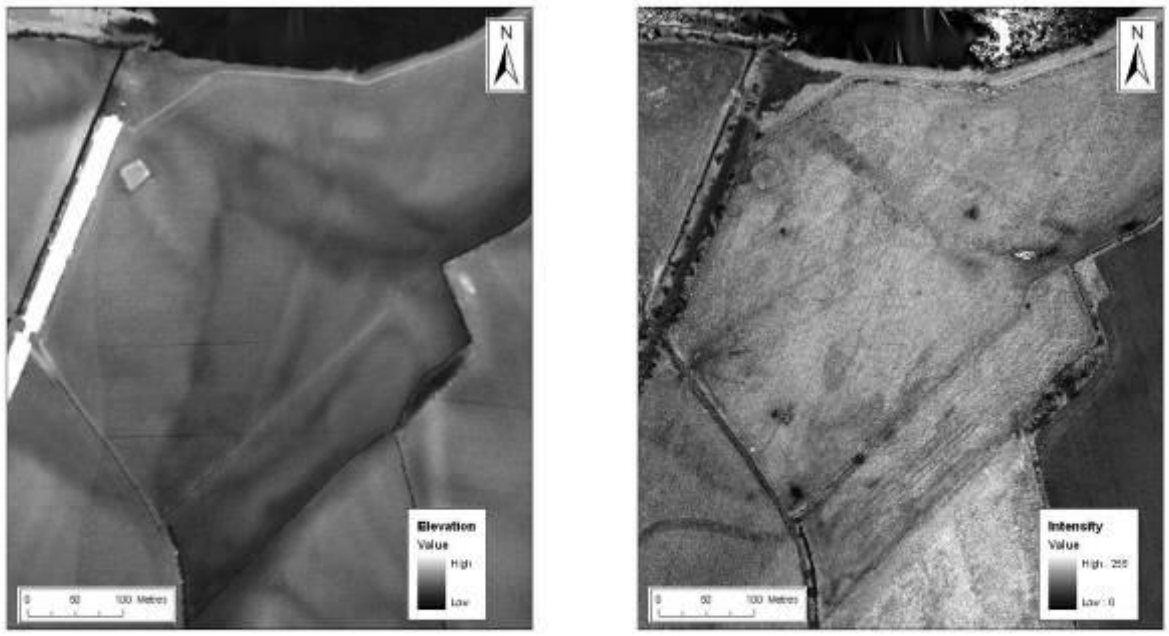

Fig 4.7 Area 5, left lidar LPG elevation data, right lidar LPG intensity

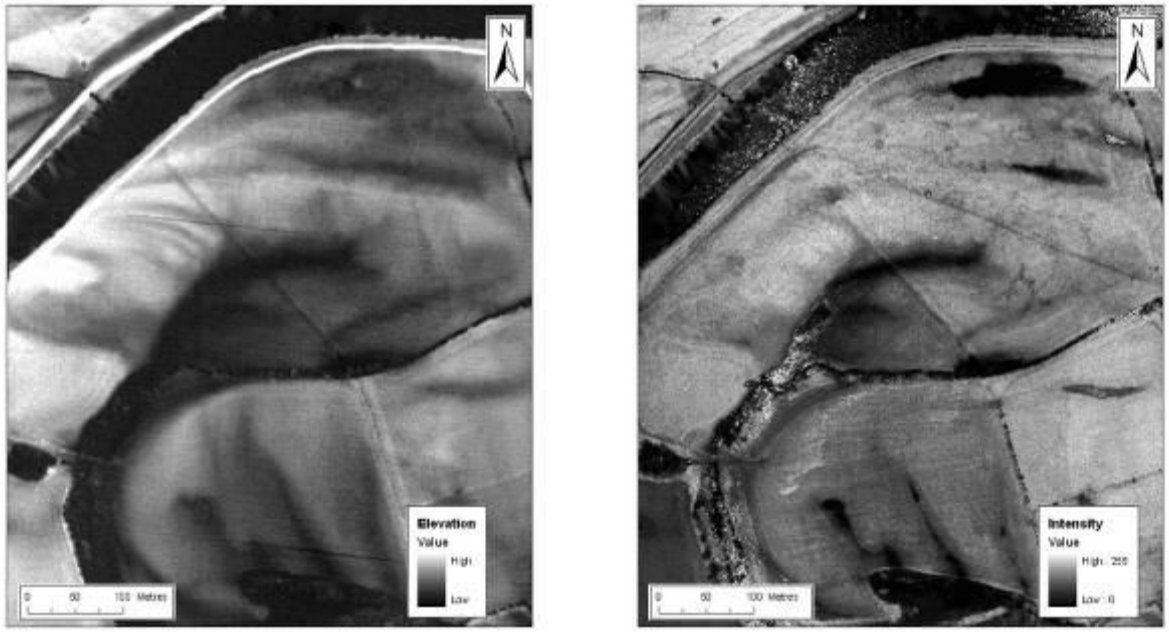

Fig 4.8 Area 6, left lidar LPG elevation data, right lidar LPG intensity

Study windows 7 - 10 comprise four sections of the lower Trent Valley at Sturton-le-Steeple. The character of the valley here differs from that at Lockington in that vertical accretion of sediments dominates. The lower terrace (Hemington) is absent, and earlier terrace deposits represented by the Holme Pierrepont Sand and Gravel flanks the floodplain of the Trent.

4.4.7 Area 7

Study window 7 comprises a lobe of Holme Pierpont sand and gravel bisected by a deeply incised channel, probably a former course of the Trent. Although the terrace boundary is clearly evident as a topographic feature, there is little pronounced topographic variation present within either terrace or floodplain in this area (Fig 4.9a). Faint rectilinear earthwork banks within the isolated lobe of terrace material to the south-east may be associated with the Roman town of Littleborough *(Segelocum)*.

Lidar intensity data for this area (Figure 4.9b) is dominated by variations due to land use. Some faint areas of low intensity are evident within the medium intensity pasture field through which the land drain marking the relict Trent channel bisecting then terrace flows. These might reflect local variations in vegetation associated with coincidental linear sinuous depressions; probably former meandering stream channels.

4.4.8 Area 8

Study window 8 comprises a substantial relict meander of the Trent, one of several in this reach isolated in the medieval and post-medieval period and clearly evident in field boundaries.

Lidar elevation data (Fig 4.10a) clearly shows the relict meander as a marked topographic feature as well as smaller channels draining the terrace to the south and west. The meander core is slightly elevated above the level of the palaeochannels, which might suggest some survival of undisturbed terrace deposits, significant given the proximity of the meander to Roman *Segelocum.*

Lidar intensity data for this area is again dominated by variations in land use. However, careful examination does reveal some lower intensity areas associated with topographic depressions (in the meander core and to the north-west) suggesting that variations in soil and vegetation caused by geomorphological features can be detected in intensity data

4.4.9 Area 9

Window 9 comprises an area of terrace and floodplain. Considerable subtle topographic variation is evident in the lidar elevation data (Fig 4.11a) showing both the clearly defined terrace edge, islands of terrace material within the floodplain and the subtly varying topography of the floodplain itself. The floodplain to the north of the study area display faint, dendritic channels of indicated by positive relief, suggesting roddon-like features and perhaps indicating the presence of extensive peat deposits within the floodplain (peat is mapped to the east on the Lincoln side of the Trent).

Few of these topographic variations are reflected in the intensity data (Fig 4.11b). However, the roddon-like features are clearly evident as intensity variations in probably due to varying crop character, the topographic depressions having formed dark, positive cropmarks.

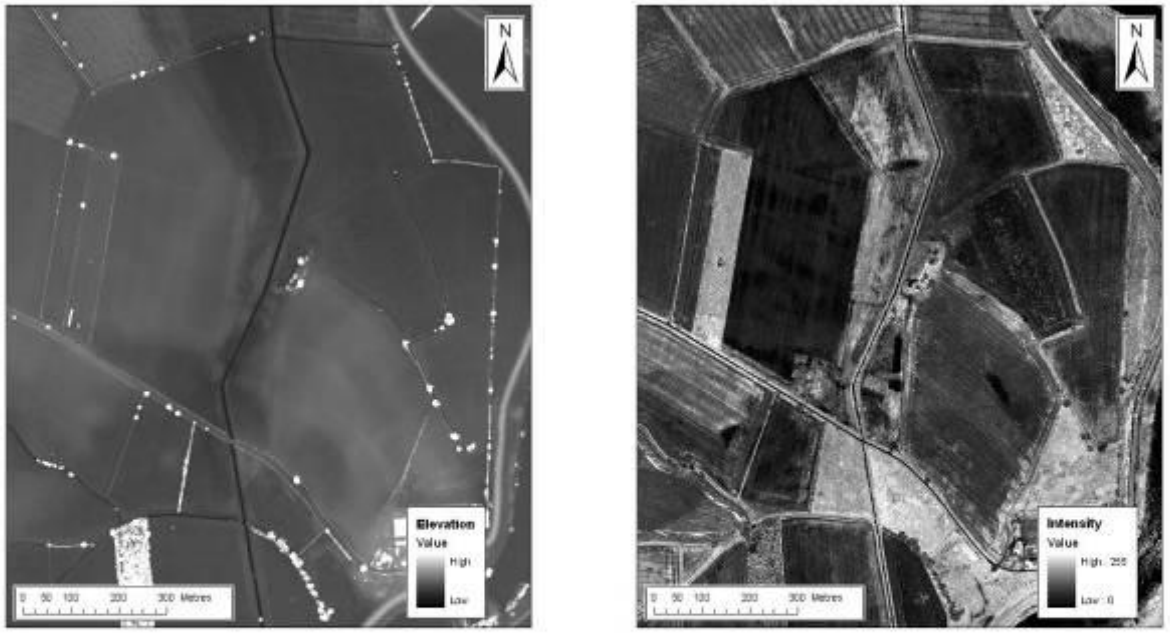

Fig 4.9 Area 7, left lidar LPG elevation data, right lidar LPG intensity

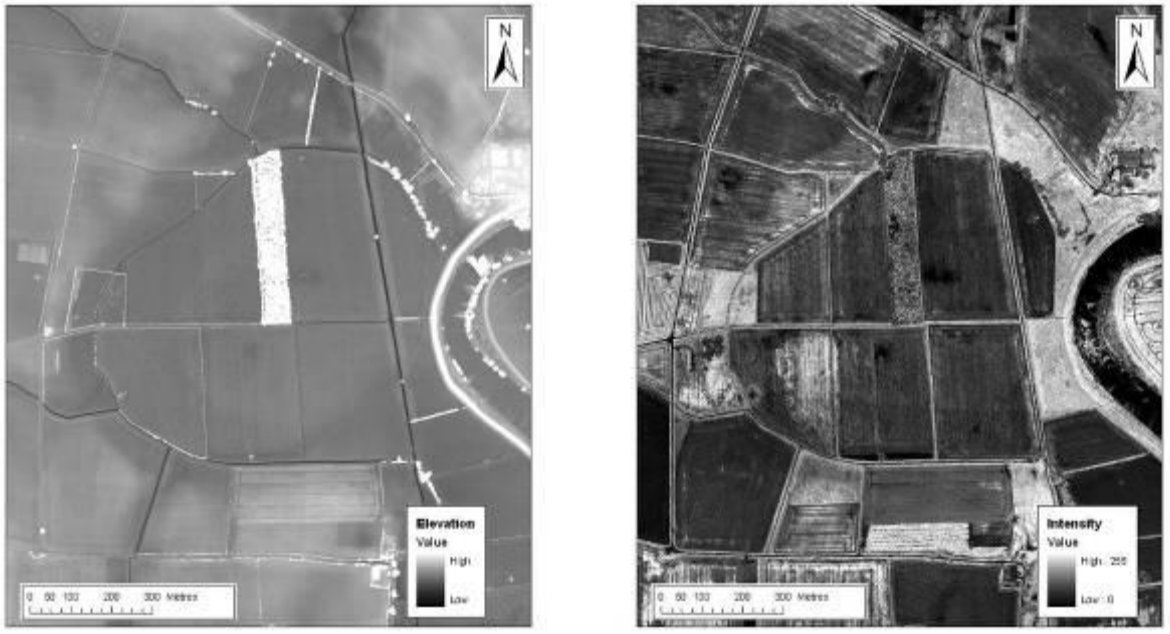

Fig 4.10 Area 8, left lidar LPG elevation data, right lidar LPG intensity

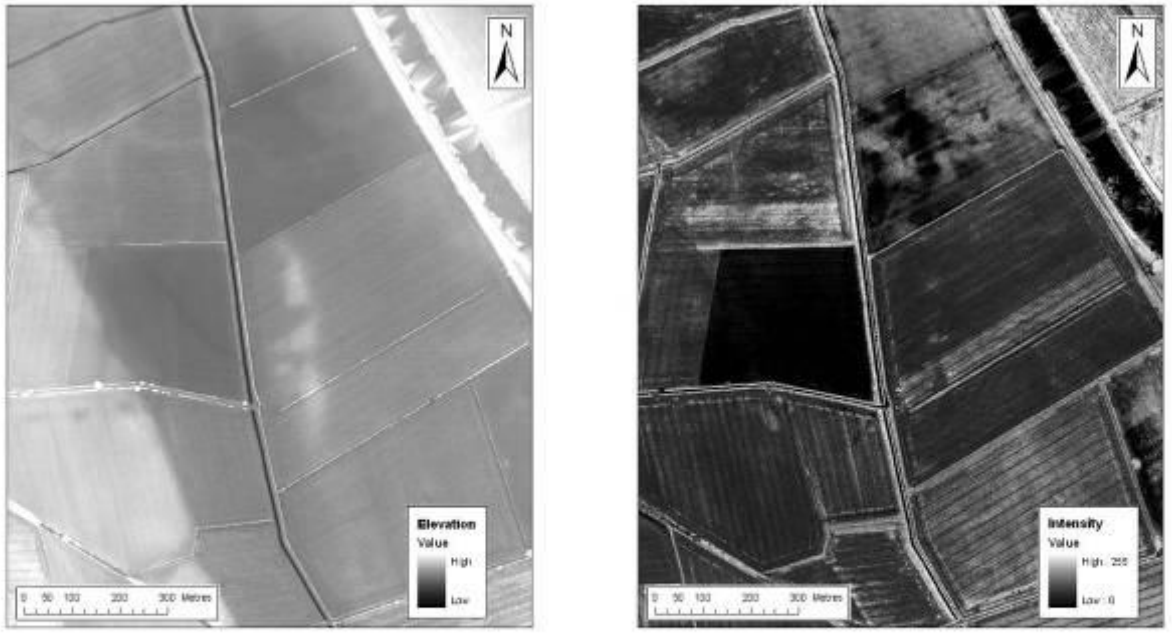

Fig 4.11 Area 9, left lidar LPG elevation data, right lidar LPG intensity

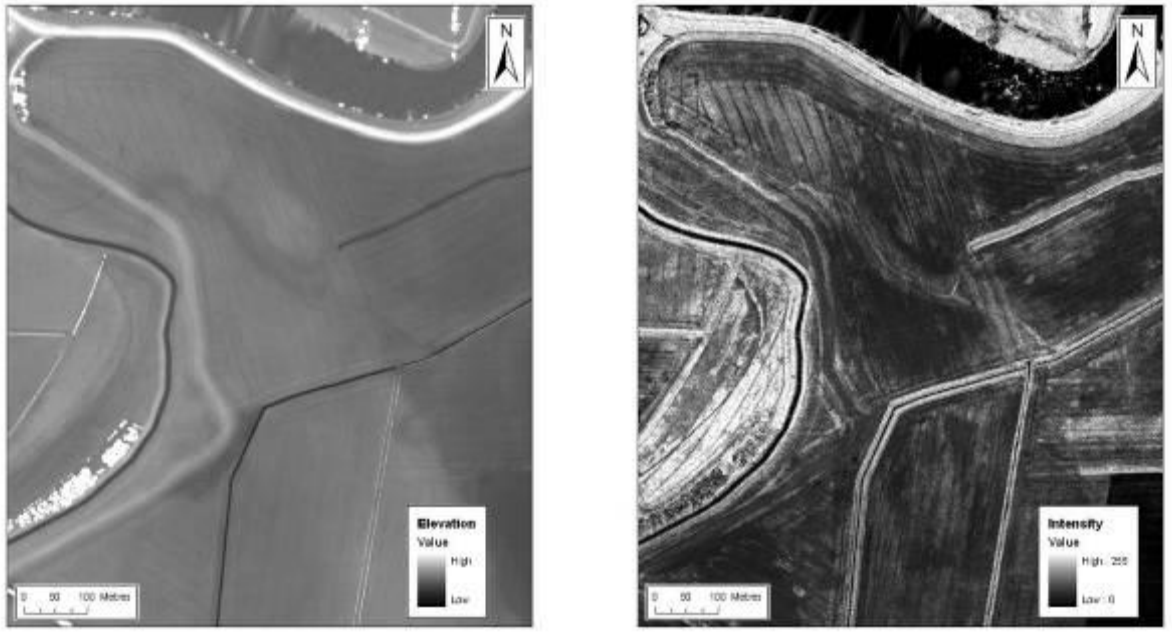

Fig 4.12 Area 10, left lidar LPG elevation data, right lidar LPG intensity

4.4.10 Area 10

The final study window comprises an area of terrace and floodplain immediately north of window 9. Once again the terrace edge is readily apparent as a topographic feature (Fig 4.12a). A sinuous depression in the terrace surface indicates a channel draining the terrace, an area of higher elevation within the floodplain at the where this channel meets is probably due to the deposition of alluvial fan deposits. Intensity data for this area (Fig 4.12b) clearly shows the channel and fan as area of higher intensity, probably reflecting the presence of sandy sediments within these units.

4.5 CONCLUSIONS

Examination of lidar intensity imagery from a variety of geomorphological settings indicates that these data do contain information not present in the corresponding elevation data. Empirical interpretation, based on a common understanding of the character of soils, sediments and vegetation in the area under examination, allows the use of intensity images to add qualitative information to the interpretation of a landscape area, even in the absence of the ability to generate robust predictive models of soils and sediment properties. In effect the intensity image is subject to the same knowledge-based interpretation as might be used to extract information from a conventional aerial photograph.

Since intensity data is (or can be) routinely collected during a lidar flight aimed primarily at gathering topographic data, it is suggested that the examination of these data are routinely incorporated in the archaeological interpretation of existing lidar data, and that their collection always form part of the parameters of a an airborne lidar survey commissioned for archaeological purposes.

5 USING LIDAR TO INVESTIGATE CULTURAL ARCHAEOLOGY

5 USING LIDAR TO INVESTIGATE CULTURAL ARCHAEOLOGY

5.1 INTRODUCTION

The application of lidar to map cultural archaeological features with a topographic expression across large landscapes is becoming increasingly common within archaeological research, (Challis *et al* forthcoming; Crutchley 2007). However, lidar intensity has been less frequently applied to investigate cultural archaeological features with a topographic expression or to investigate spectral reflectance of cropmark features with little or no topographic element. This section explores aspects of using lidar intensity to map cultural archaeological features, both upstanding earthworks and cropmarks. Data are subject to visual analysis to compare the effectiveness of lidar intensity and topography to identify and visualise cultural archaeological features.

5.2 FACTORS AFFECTING CROP AND SOIL MARK FORMATION

In general the amount of illumination reflected by different earth surface materials varies greatly in both intensity and wavelength across different materials (Fig. 5.1). Such differences may be a result of their different:

1. bio-physical properties,
2. chemical composition and
3. surface geometry (roughness).

Archaeological cropmarks are produced when buried archaeology affects the growth of overlying crops (Fig. 5.2). This may be as a result of soil moisture stress in summer and/or because of the variations in availability and supply of nutrients, in particular nitrogen and calcium. Generally crops grow taller, more vigorously and mature later over buried negative features, which provide a greater depth of sediment containing moisture and nutrients. Conversely, over buried positive features such as walls that restrict the supply of nutrients and moisture, crops grow with less vigour and mature quicker. In general these phenomena are most evident freely draining soils and substrates, subject to summer moisture stress. Soils that tend to retain water are less prone to cropmark formation.

The essential element of the cropmark is the variation in crop colour and vigour. Spectral response in the visible and NIR parts of spectrum reflects changes in vegetation type, leaf moisture content and the presence of key nutrients. In the visible part of the spectrum (400 – 700nm) the amount of solar radiation reflected is determined by composition and concentration of chlorophylls a and b, caretenoids and xanthophylls which vary due to vegetation type and nutrients status. In the Near Infrared (NIR) part of the spectrum (700-1300nm) the principle variations in spectral reflectance are caused by the number and configuration of internal air spaces within leaf and moisture content of plant. In the Short Wave Infrared (SWIR) part of the spectrum, between 1350 and 2500nm, reflection is most affected by water concentration in plant tissue.

Archaeological soilmarks are largely the results of plough disturbance truncating archaeological features and deposits and by so doing introducing discrete areas of sediment of different character into the ploughsoil. They are most readily seen in areas of shallow soil,

with a subsoil of contrasting colour. Differences in sediment character might relate to a number of characteristic, including organic content, mineralogy and particle size. Soilmarks of palaeochannels are perhaps more likely to be betrayed by variations in soil moisture, sediment character (silt/clay channel fills) and organic content of soil if peat or other organic sediments are disturbed. All of these soil characteristics are likely to cause variations in reflectance in the NIR and SWIR parts of the spectrum These are particularly likely to be evident in the thermal infrared (TIR) part of the spectrum (beyond 8500nm) where variations in soil and sediment moisture and microtopography may affect ground temperature.

Shadow features are caused by variations in illumination of the ground surface due to upstanding earthwork features. Such features differentially affect the amount of solar radiation reaching the ground surface. The shadow effect may also lead to local variations in the thermal properties of the ground.

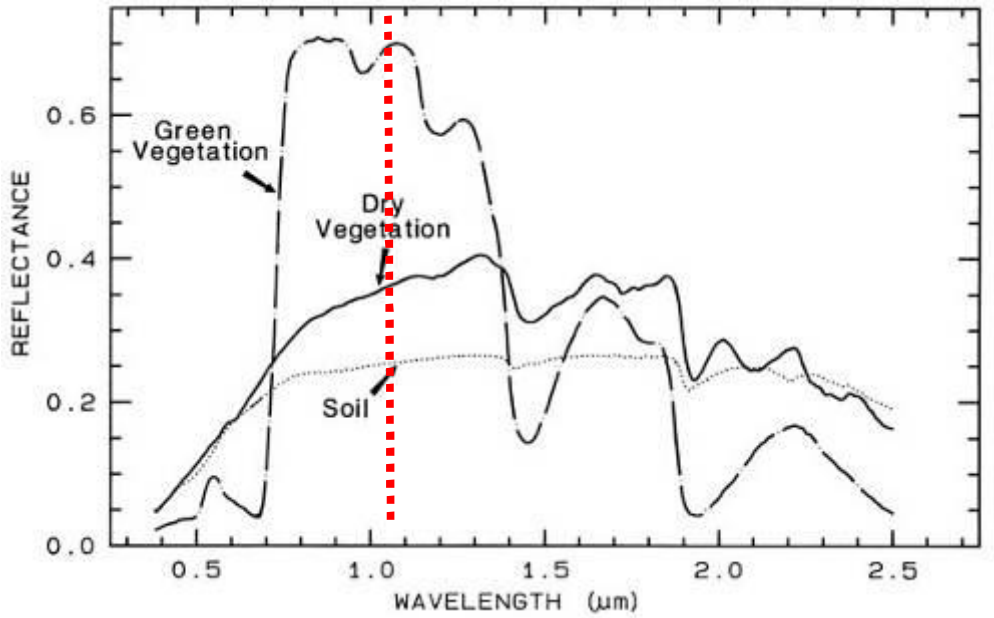

Fig. 5.1. Graph showing theoretical reflectance of vegetation and soil in the visible, NIR and SWIR portions of the spectrum. The Optech lidar laser wavelength is shown in red

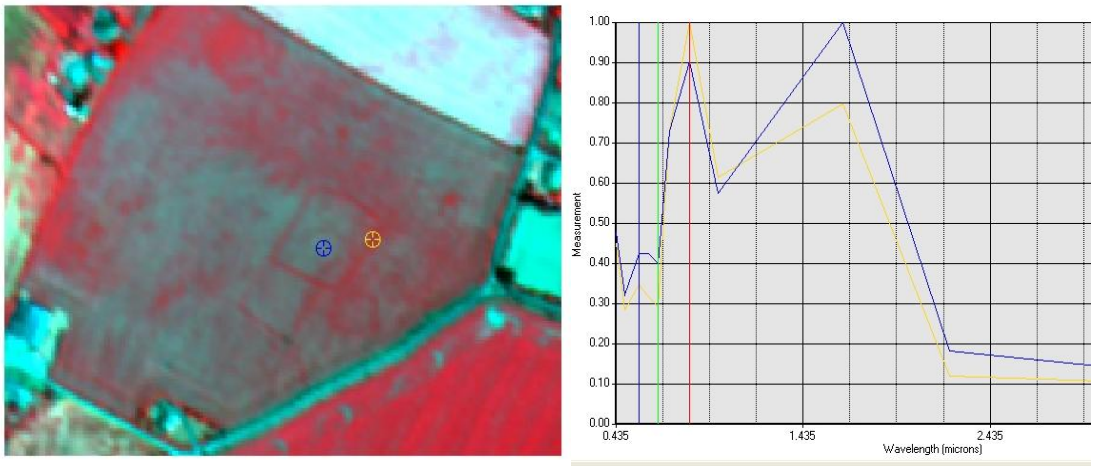

Fig. 5.2. Actual spectral reflectance of a cropmark recorded by Daedalus 1268 ATM imagery. In this instance the cropmark (green symbol and graph) appears as a darker green crop in the visible part of the spectrum (ie low green reflectance, high red reflectance) but is most clearly evident in the SWIR (*c.*1500nm) where the cropmark is less reflective than the parched crop that surrounds it.

5.3 USING LIDAR INTENSITY TO INVESTIGATE UPSTANDING ARCHAEOLOGICAL EARTHWORKS

The application of lidar to map and investigate earthworks is demonstrated through two case studies. The first example is an enclosure close to study Area 6, where an upstanding earthwork is recorded as a Civil War redoubt (Fig. 5.3, NGR: 478690, 354450). OS mapping of the enclosure is shown superimposed on the LP DSM model (Fig. 5.4) which is clearly evident as a topographic feature (Fig. 5.5). From the LP DSM it is possible to define the extent of the enclosure, which largely comprises well-defined earthwork banks. The enclosure is just visible in the FP intensity surface model, but it is vaguely defined (Fig. 5.6) and if its location was not already known it could not be identified from the FP intensity data alone. Similarly, the LP intensity data poorly defines the enclosure, although it is still just discernable (Fig. 5.7).

The second case study investigates a small sub-square enclosure on the Trent Soar floodplain at Lockington (Figs. 5.8 and 5.9; NGR: 447810, 330640). The enclosure is clearly defined by the LP DSM with the external bank and raised interior platform visible (Fig. 5.10). There is alos some indication of an external ditch visible in the LP DSM surface model. The lidar data set from the Trent Soar confluence zone only has LP intensity data. The LP intensity surface model also clearly defines the earthwork (Fig. 5.11). The interior of the enclosure is visible as an area of higher intensity values, whilst the morphology of the exterior ditch is well defined through lower intensity values. In this example the earthworks defined with at least equal clarity in the LP data when compared with the LP DSM.

These examples demonstrate that lidar intensity can be used to identify upstanding cultural archaeological features. However, identification of features with equal topographic expression is unequal in intensity data. The difference in identification of different upstanding cultural features from lidar intensity data is liable to be a product of many variables including for example differences in material/sediment composition between banks, ditches, and other component parts of the earthworks that affect physical parameters at the near surface such as soil moisture and vegetation growth. These variables affect changes in intensity return, causing some earthwork features to be visible in intensity data. In situations where the sediment and vegetation structure is very similar between topographic features it is doubtful that lidar intensity can be used even in a qualitative way to map earthwork features.

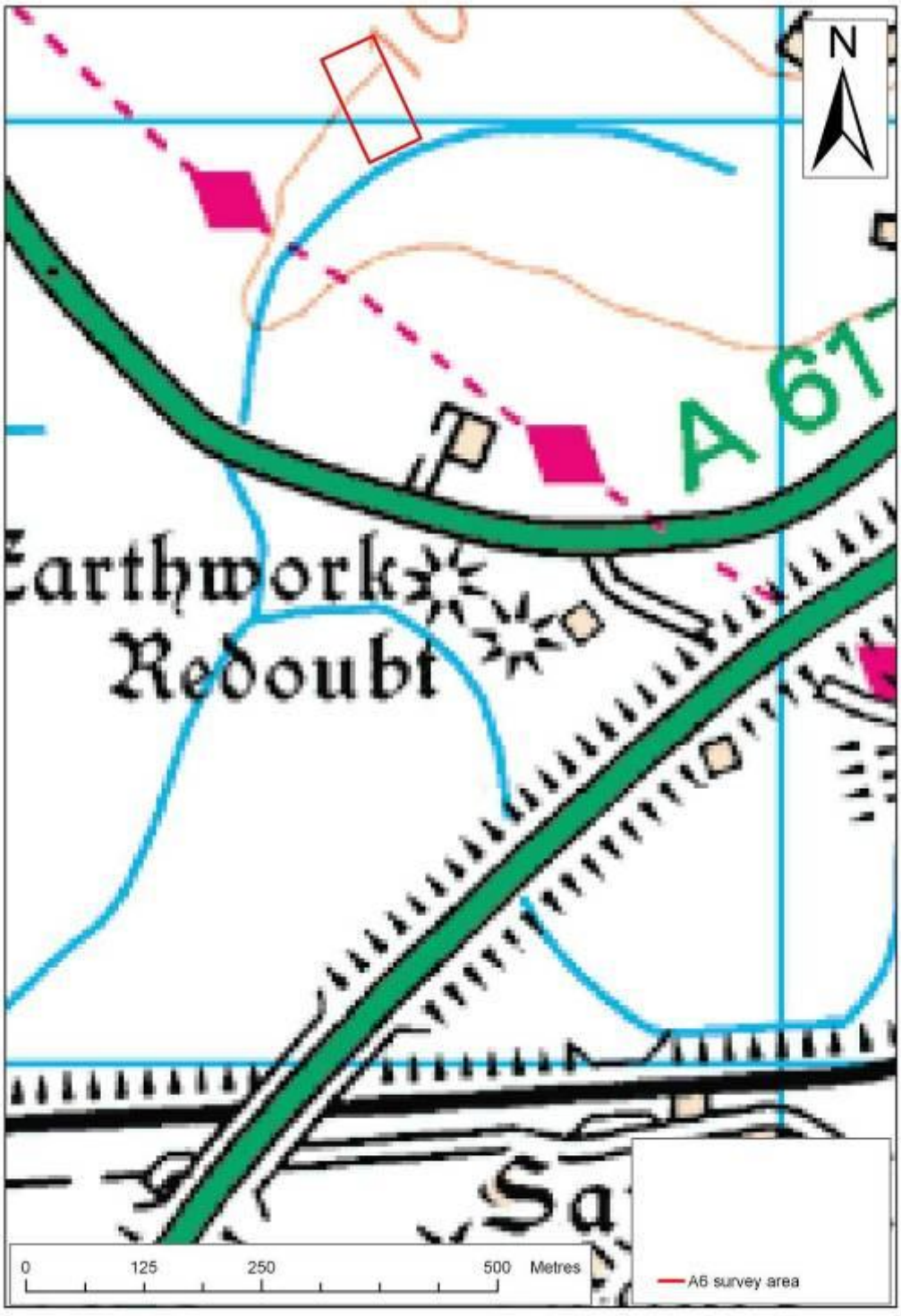

Fig 5.3: The location of the earthworks used for lidar data set comparison, close to Area 6, north of Newark on Trent.

Fig 5.4: The LP DSM with OS 1:10, 000 map, showing the location of a Civil War redoubt, visible as an upstanding earthwork.

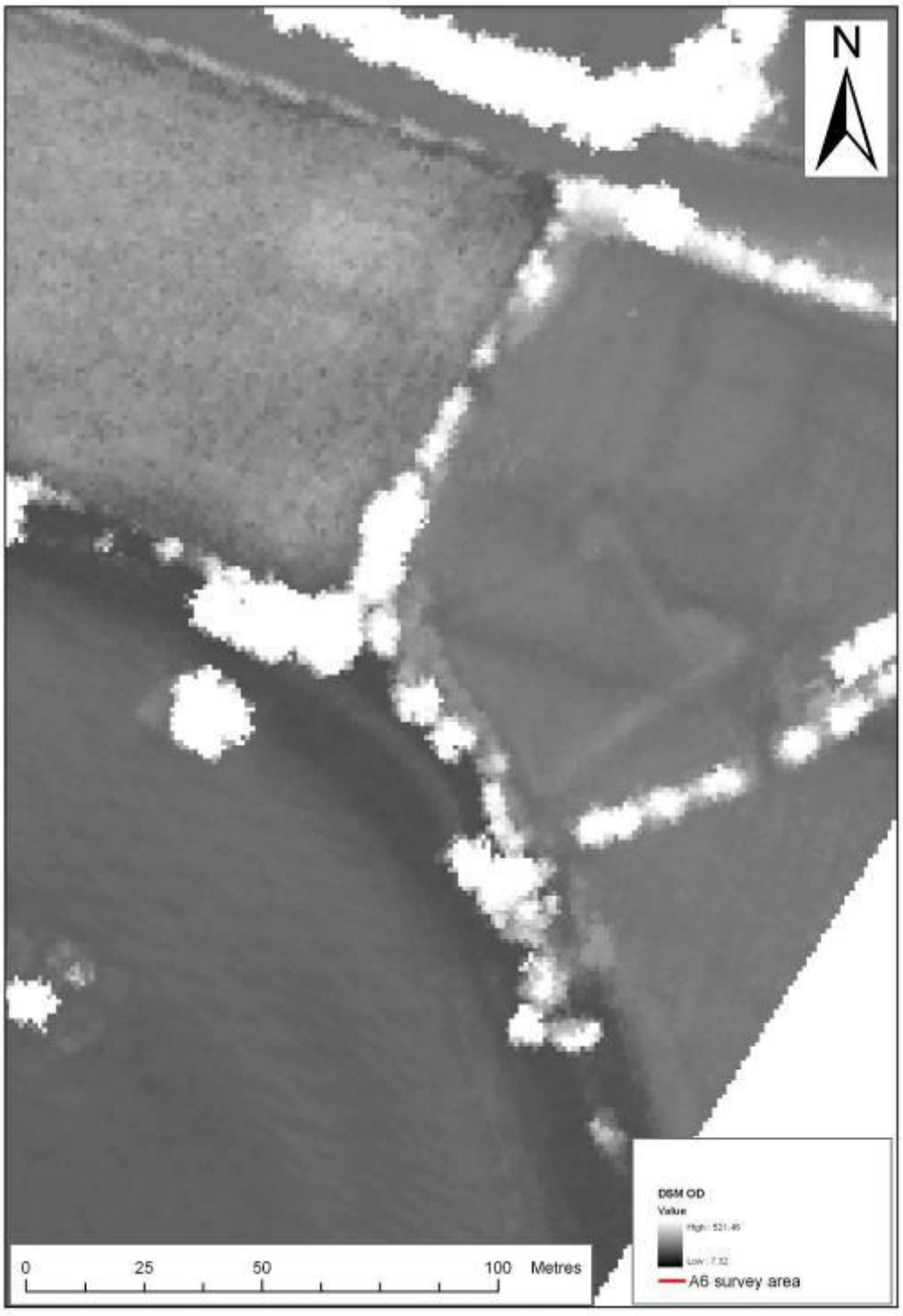

Fig 5.5: The LP DSM of the earthworks near Area 6, showing clear definition of the banks of the enclosure.

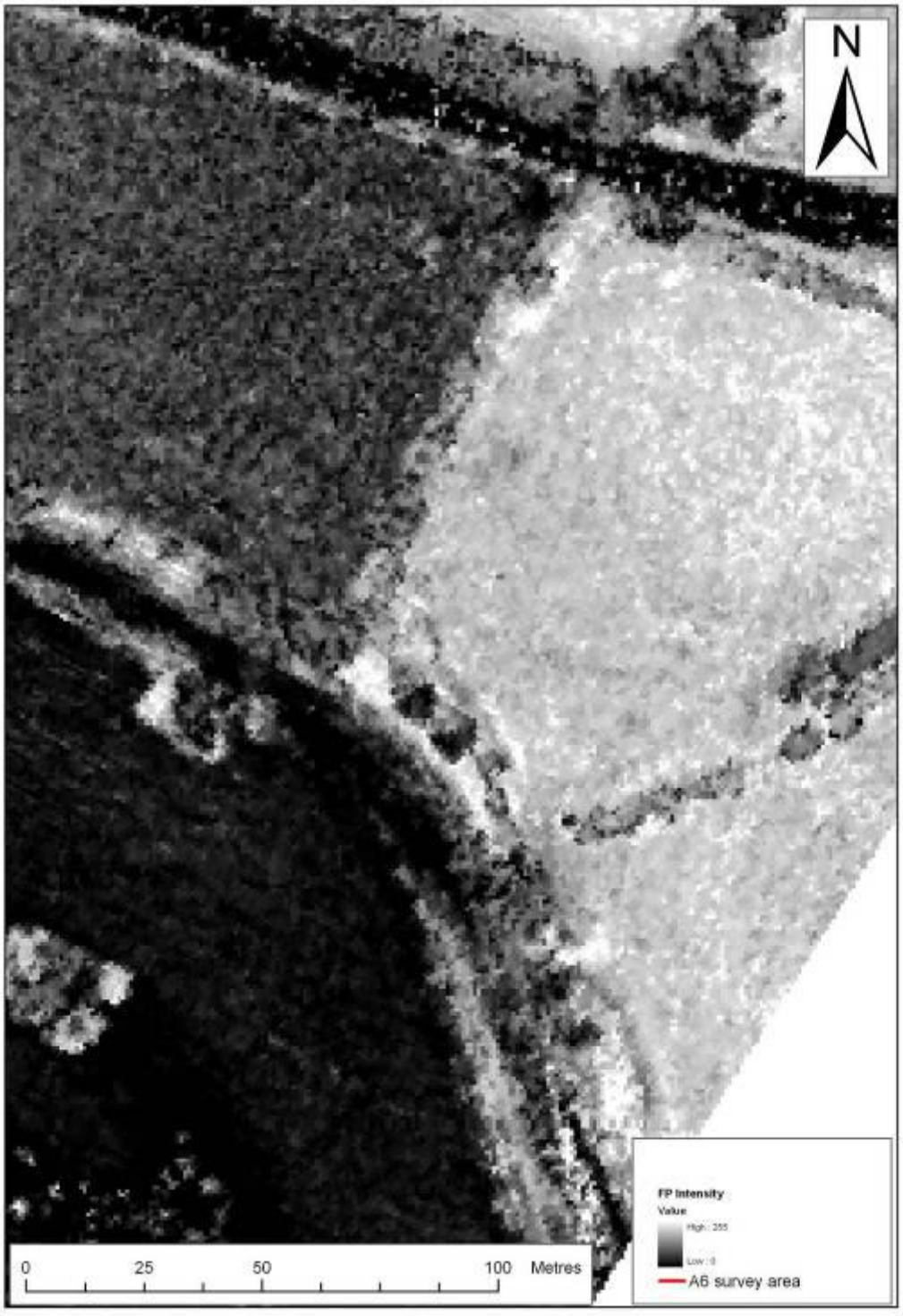

Fig 5.6: The lidar FP intensity surface model of the earthworks near Area 6. There is only a vague definition of the cultural remains on the image.

Fig 5.7: The lidar FP intensity surface model of the earthworks near Area 6. There is only a vague definition of the cultural remains on the image.

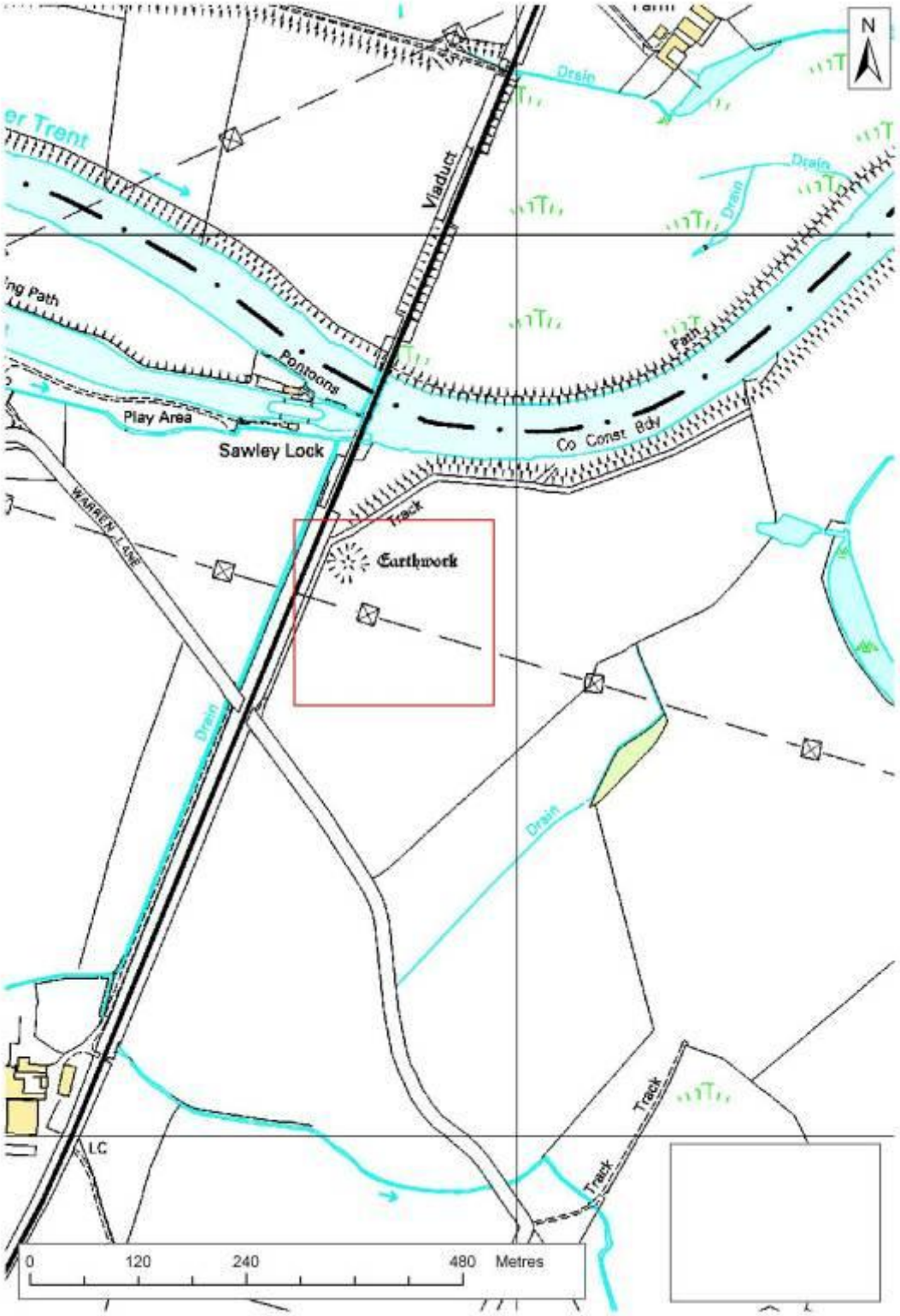

Fig 5.8: The location of the small rectilinear enclosure on the Trent Soar confluence zone.

Fig 5.9: The small rectilinear enclosure as mapped by the OS 1:10,000 map, shown overlying the LP DSM.

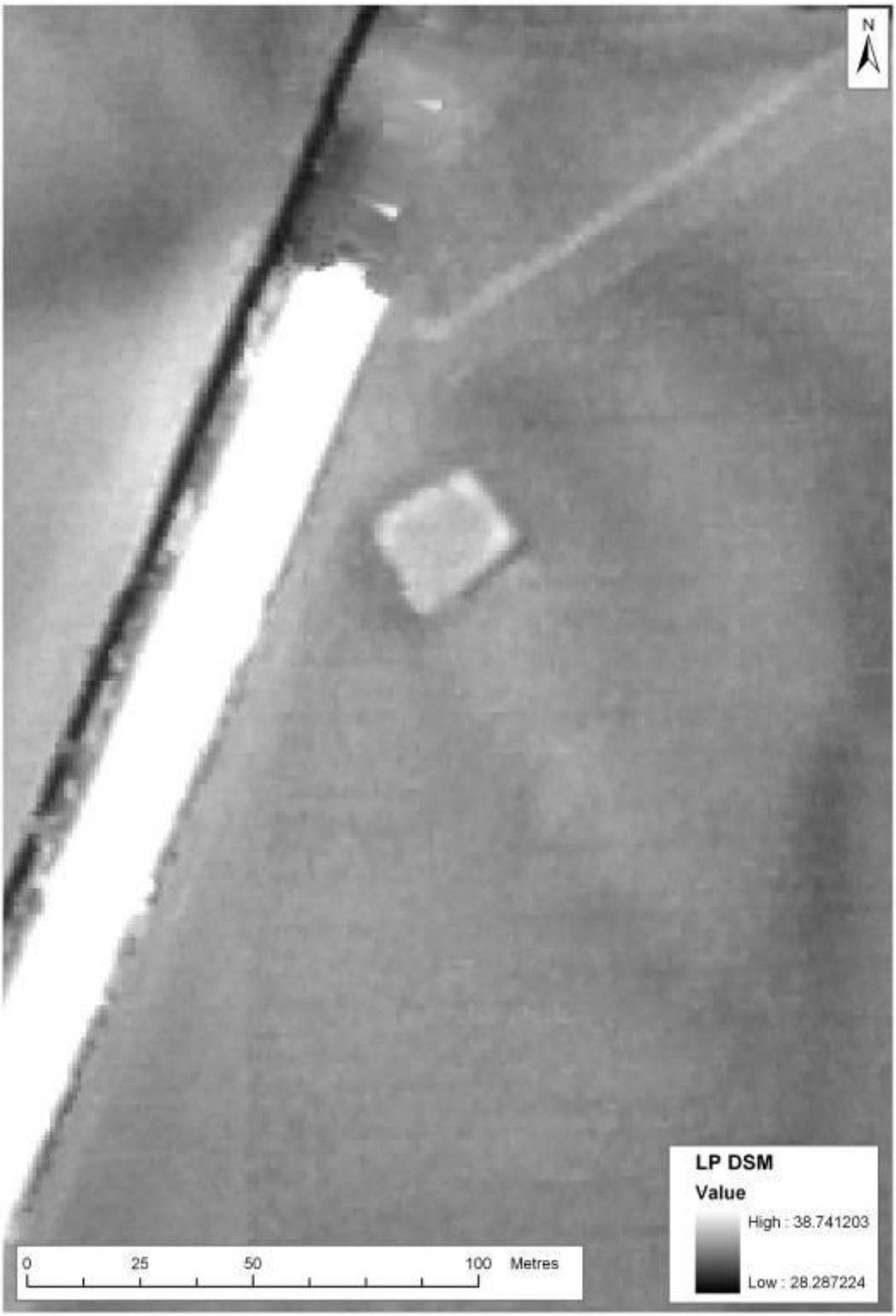

Fig 5.10: The LP DSM clearly defining the enclosure on the Trent Soar confluence zone.

Fig 5.11: The LP intensity model clearly defining the enclosure on the Trent Soar confluence zone.

5.4 USING LIDAR INTENSITY TO INVESTIGATE ARCHAEOLOGICAL CROPMARKS

The application lidar data to investigate cropmark features has been less widely explored than its use to map upstanding earthworks. However, archaeological cropmarks affect spectral reflectance through changes in vegetation growth, character and colour which are evident in the NIR spectral region used by typical airborne lidar. In addition the underlying archaeological features giving rise to cropmarks may affect soil moisture and sediment composition and thus may also be visible at time of low crop growth or in bare soils. As noted in section 3, these variables can affect intensity responses and be used to visually identify gross features of the landscape such as palaeochannels. This examination of the potential of lidar intensity data to identify archaeological cropmarks takes the form of two case study areas, both based around Holme, in the Trent Valley (Fig. 5.12).

The cropmark data used is from previously transcribed aerial photographs, undertaken as part of the National Mapping Programme by English Heritage, prior to the lidar flight. This does put a substantial *caveat* to this analysis. While cropmarks were visible at the time that aerial photographs were taken, it is not necessarily the case that cropmarks were visible at the time of the lidar flight and since there are no comparable air photographs contemporary with the lidar data flight, it is not possible to check for the presence or otherwise of archaeological cropmarks using conventional means.

The first study investigated cropmark group 1 comprising a series of rectilinear ditches defining a number of enclosures and associated field boundaries south of Holme (Fig. 5.13; NGR: 480560, 358210). The features are shown against the LP DSM (Fig. 5.14). examination of which makes it clear that the cropmarks had no topographic expression at the time of the lidar flight (Fig. 5.15). The lidar FP intensity data is also shown with the transcribed cropmarks (Fig. 5.16), since the FP intensity data reflects changes at the top of the vegetation canopy, it potentially has the ability to define cropmarks.

No cler cropmark features are evident in the FP intensity data (Fig. 5.17). However, the FP intensity does show some subtle variation in intensity where some of the cropmarks are recorded. These changes in intensity do not define the features recorded as cropmarks, but the changes may be suggestive of areas where cropmarks are liable to occur. It is not possible to define whether this is coincidental or causal based on this analysis. The LP intensity surface model produces a very similar image to the FP intensity model, and again shows some broader changes in intensity that coincides with the areas of recorded cropmarks (Figs. 5.18 and 5.19).

The second study examines cropmark group 2, a rectilinear enclosure and associated double ditch trackways east of Holme (Fig 5.20; NGR: 480560, 359330). Again the LP DSM does not show any of the recorded cropmarks, suggesting that these features had no definable topographic expression at the time of survey (Figs. 5.21 and 5.22). The FP intensity data does not show any of the cropmarks recorded by the aerial photographic transcription (Figs. 5.23 and 5.24). Likewise, the LP intensity data does not identify any of cropmarks (Fig 5.25 and 5.26). The current planting detail of the crops is evident in both fields in the lidar intensity surface models, but there is no indication of archaeological cropmarks.

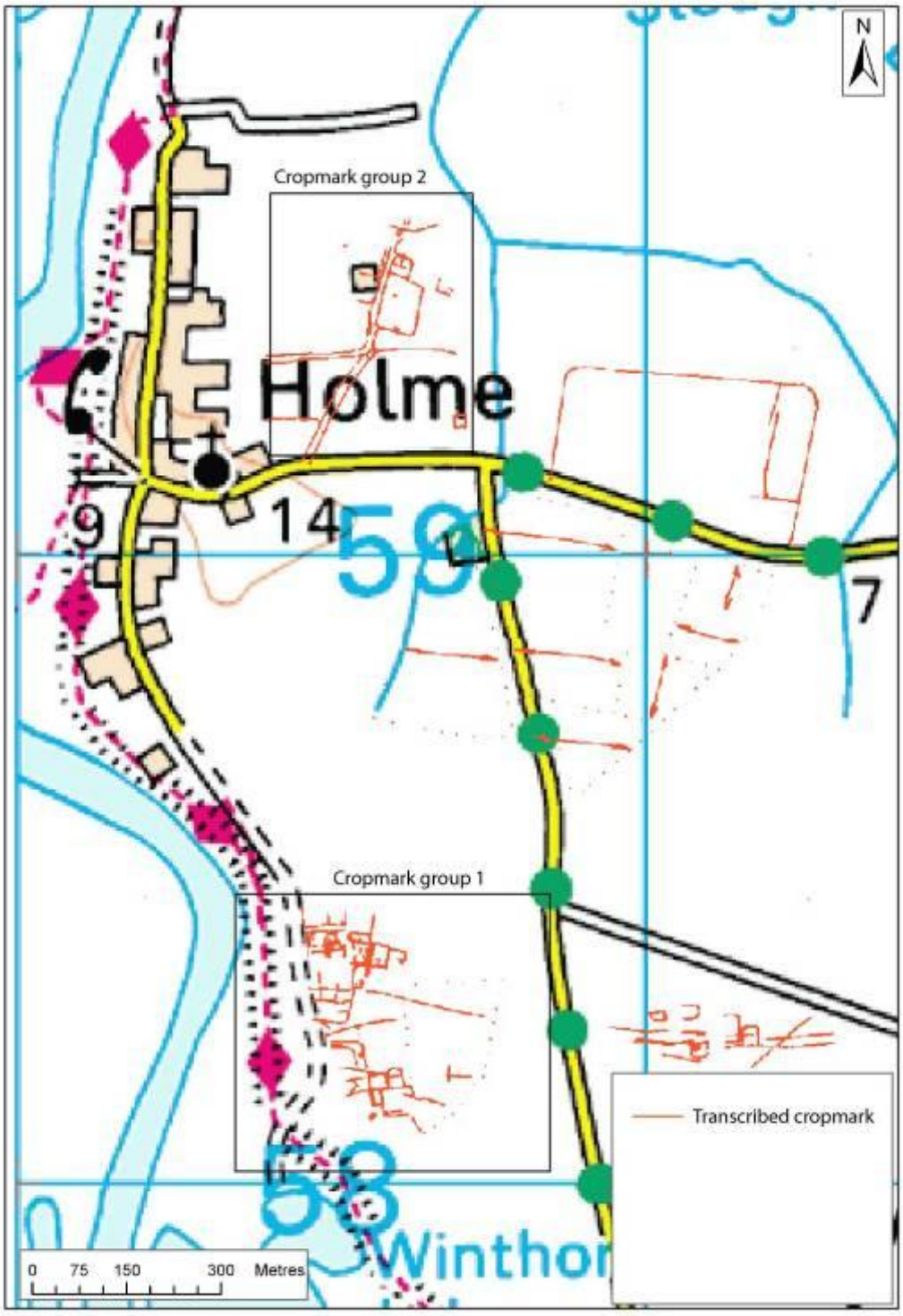

Fig 5.12: The location of Holme with the two groups of transcribed cropmarks investigated during this analysis.

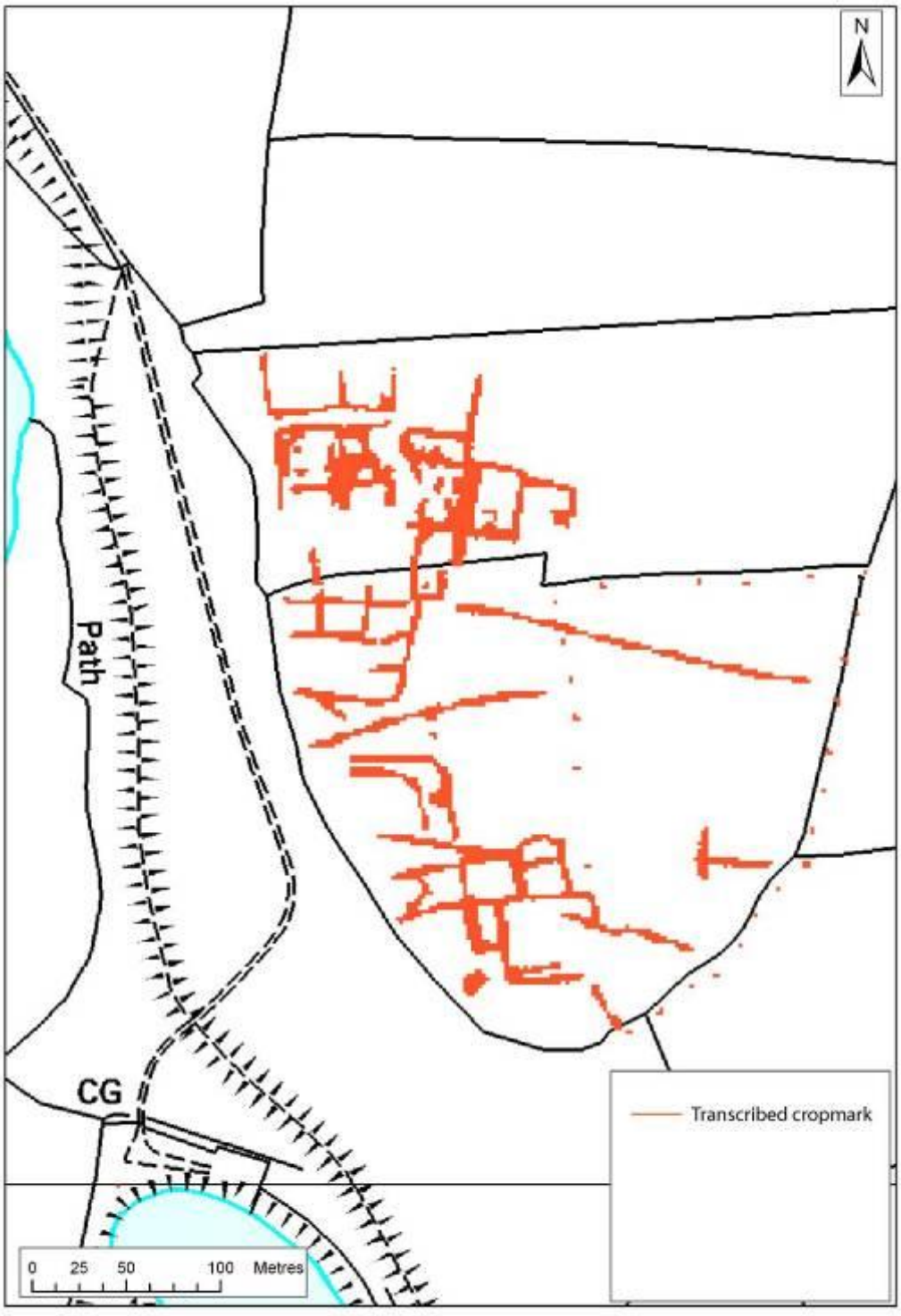

Fig 5.13: The transcribed cropmarks in group 1 shown against the 1:10,000 OS map.

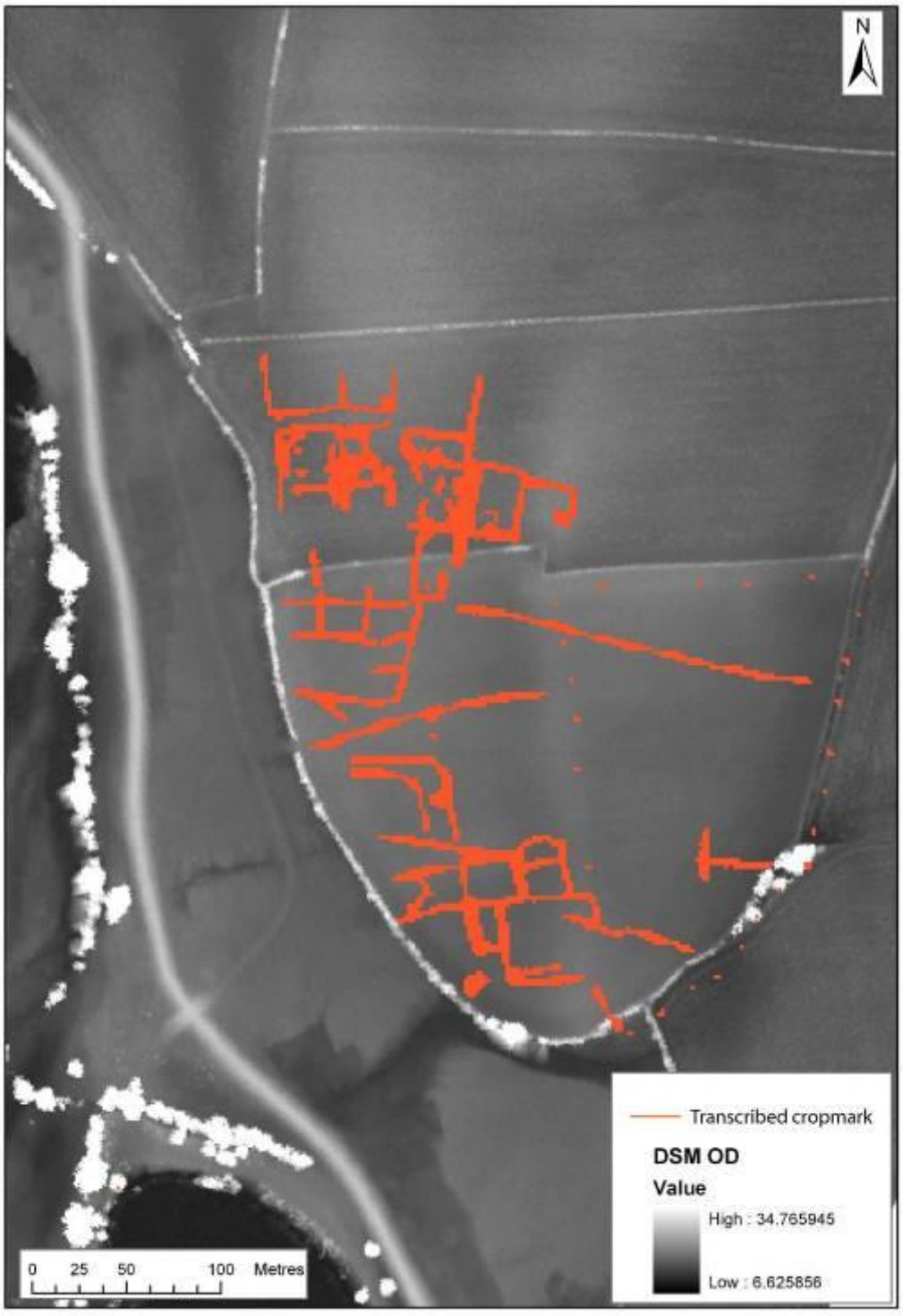

Fig 5.14: Cropmark group 1 shown on the LP DSM topographic model.

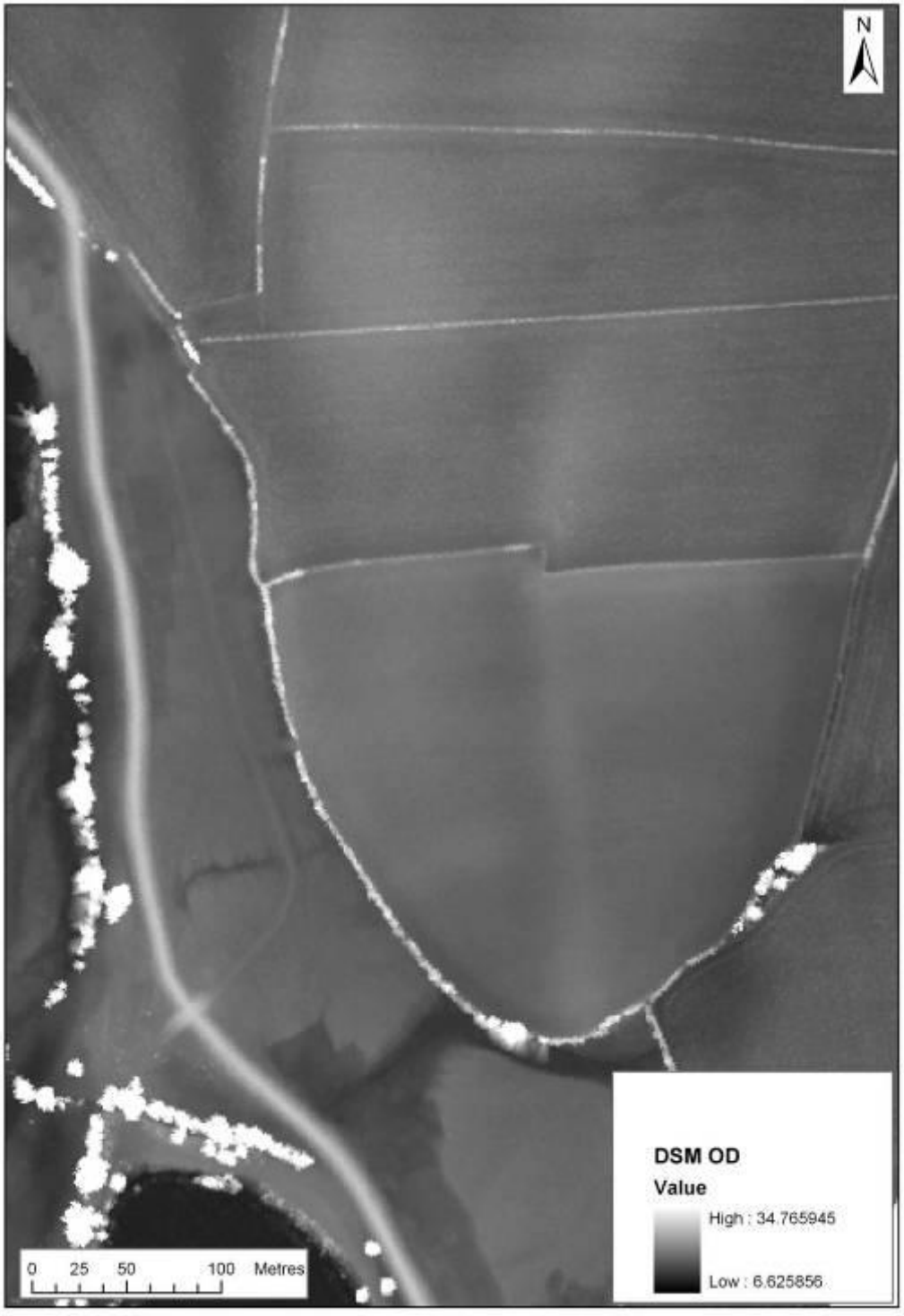

Fig 5.15: The LP DSM topographic model shown in isolation. None of the cropmark features are evident.

Fig 5.16: Cropmark group 1 on the FP intensity surface model.

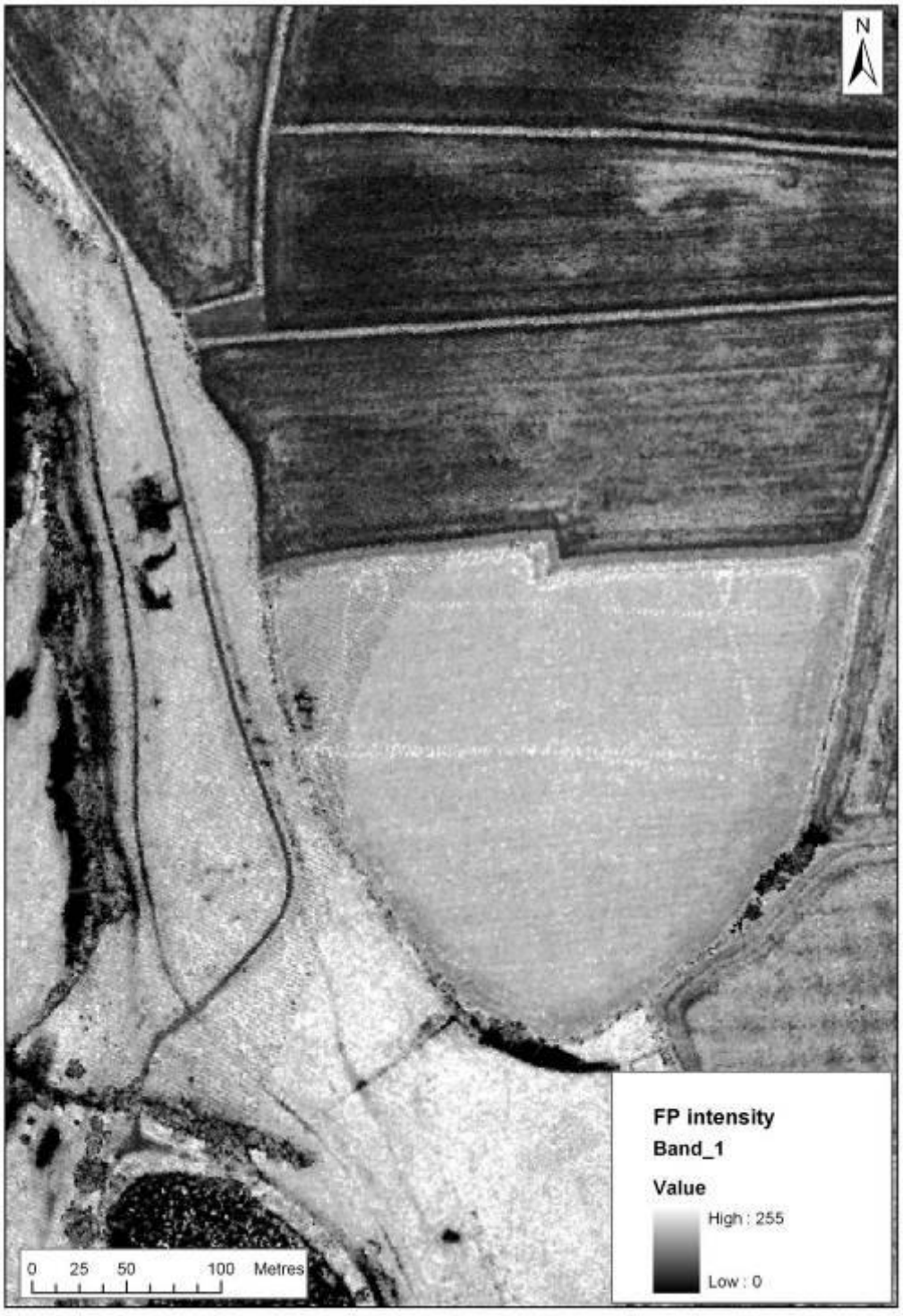

Fig 5.17: The FP intensity surface model shown in isolation. None of the transcribed cropmark features are visible in the FP intensity surface model.

Fig 5.18: Cropmark group 1 on the LP intensity surface model.

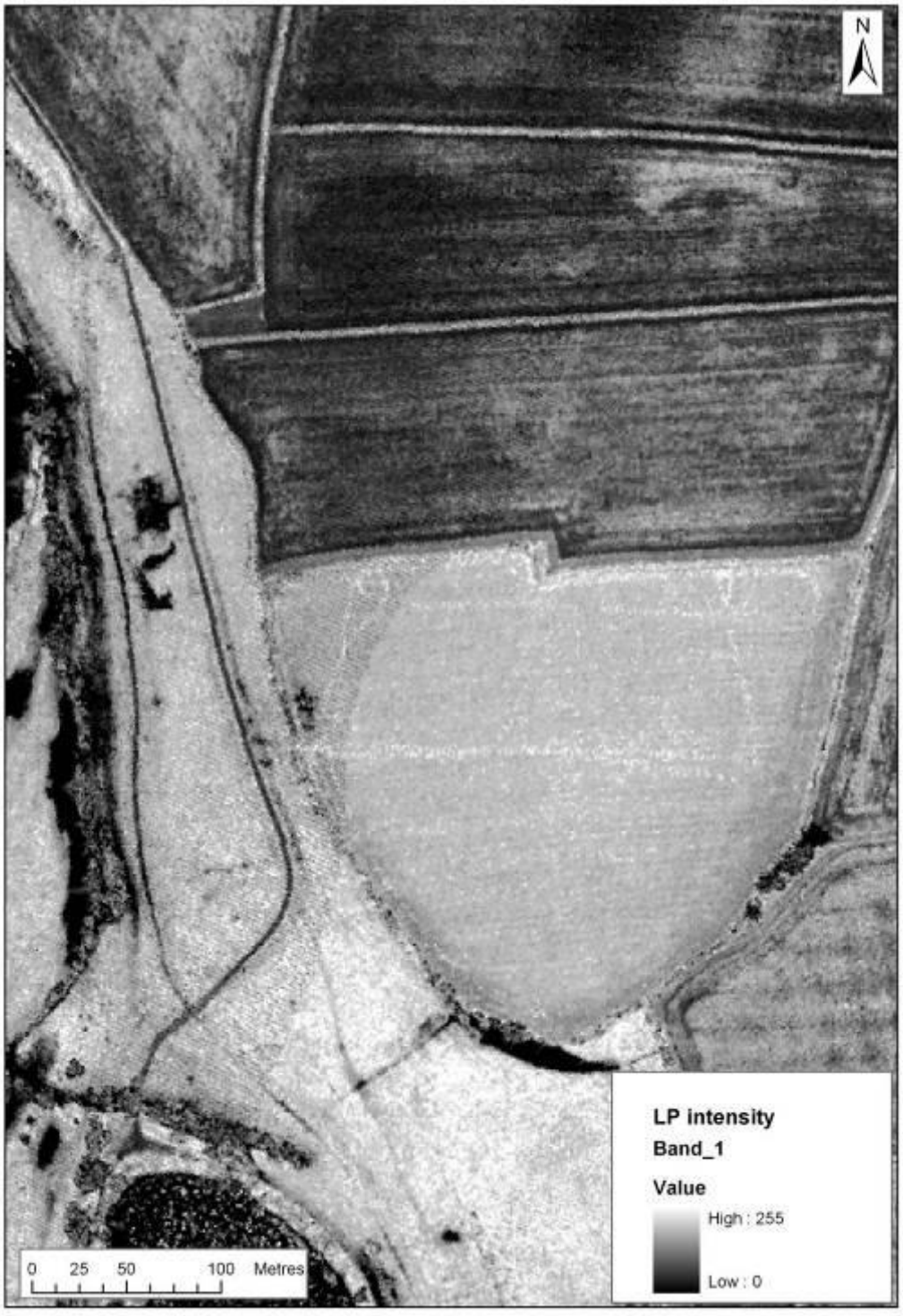

Fig 5.19: The LP intensity surface model shown in isolation. None of the transcribed cropmark features are visible in the LP intensity surface model.

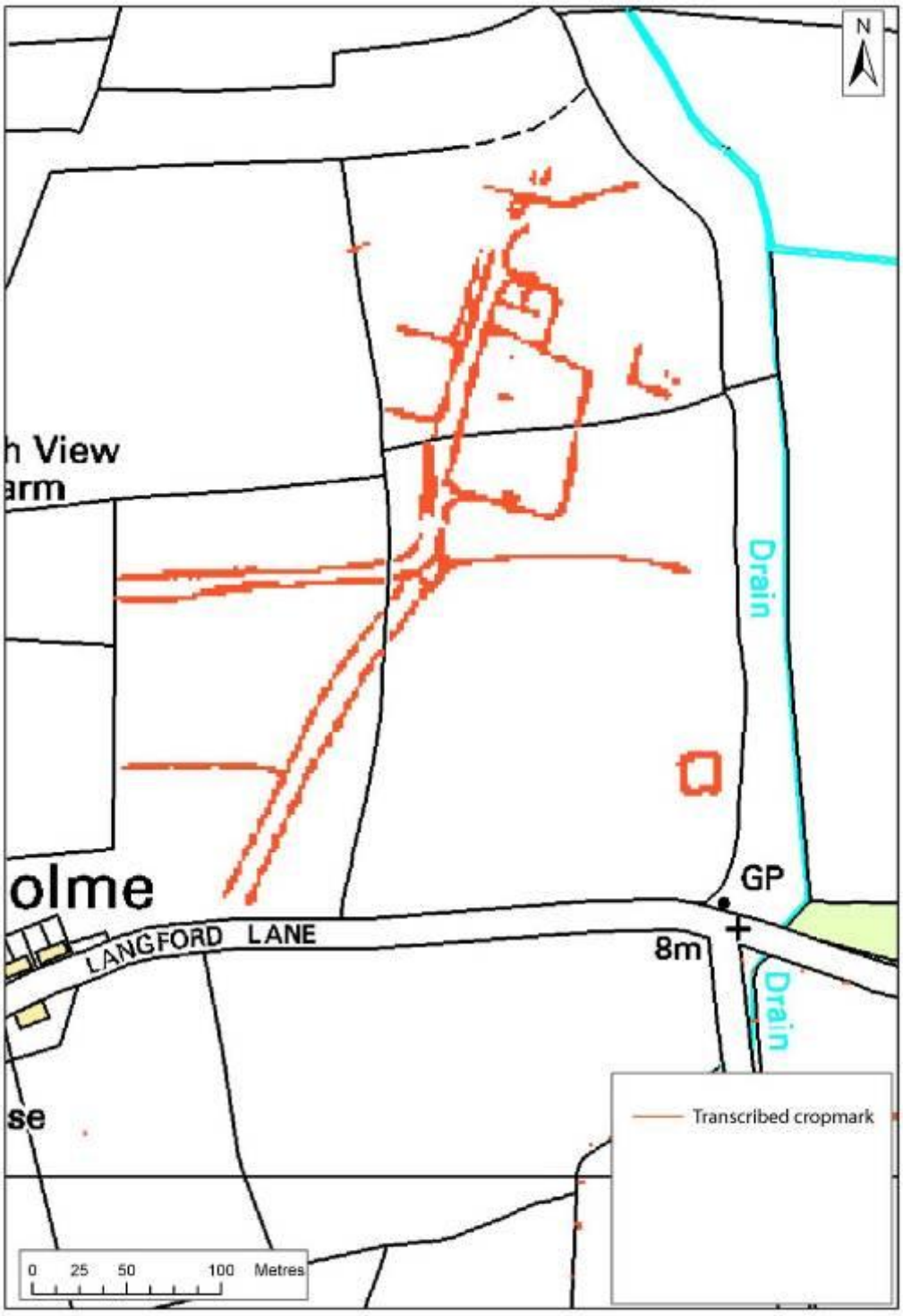

Fig 5.20: The transcribed cropmarks in group 2 shown against the 1:10,000 OS map.

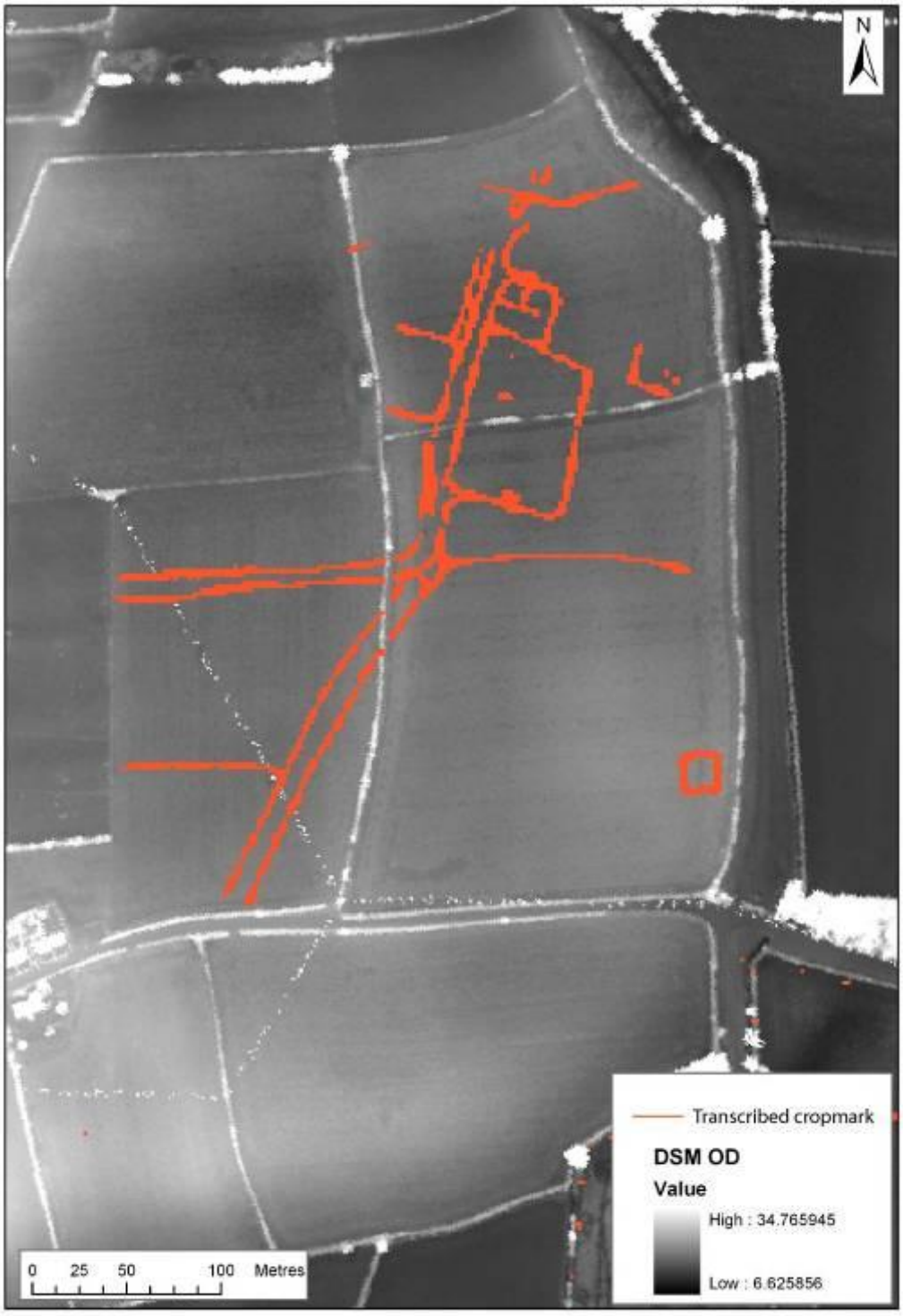

Fig 5.21: Cropmark group 2 shown on the LP DSM topographic model.

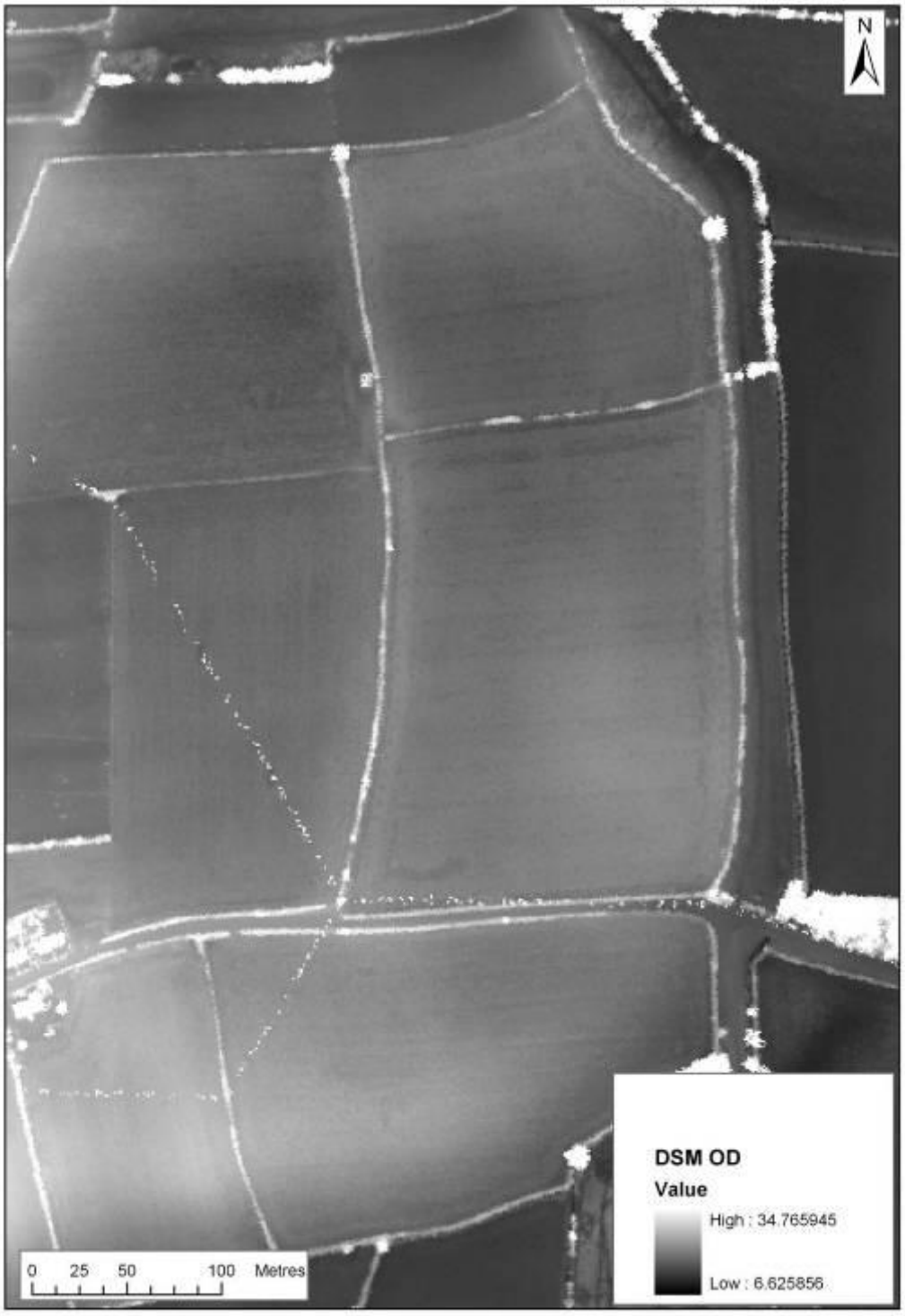

Fig 5.22: The LP DSM topographic model shown in isolation. None of the cropmark features are evident.

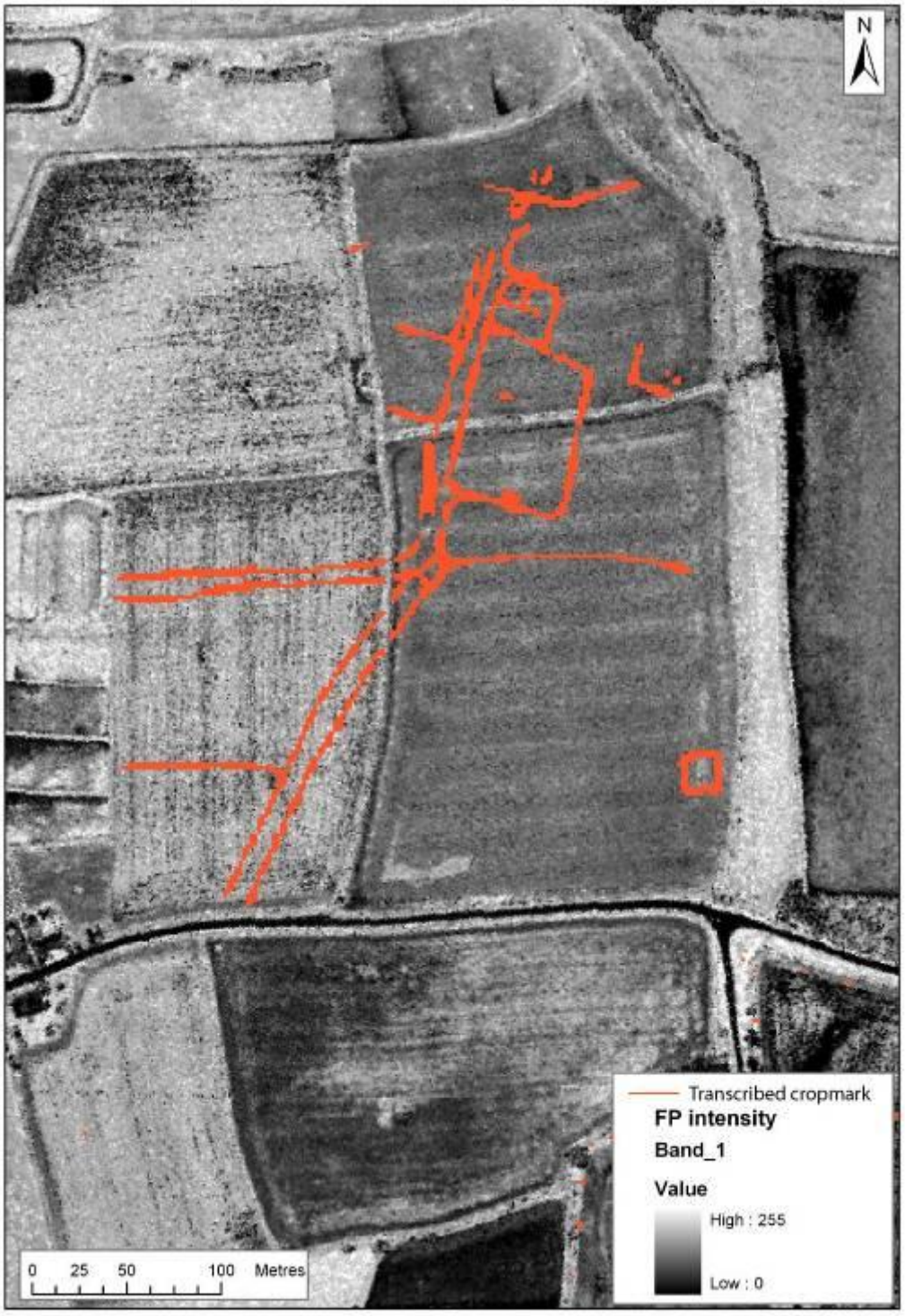

Fig 5.23: Cropmark group 2 shown on the FP intensity surface model.

Fig 5.24: The FP intensity model shown in isolation. Again, none of the transcribed cropmark features from group 2 are evident in the lidar data.

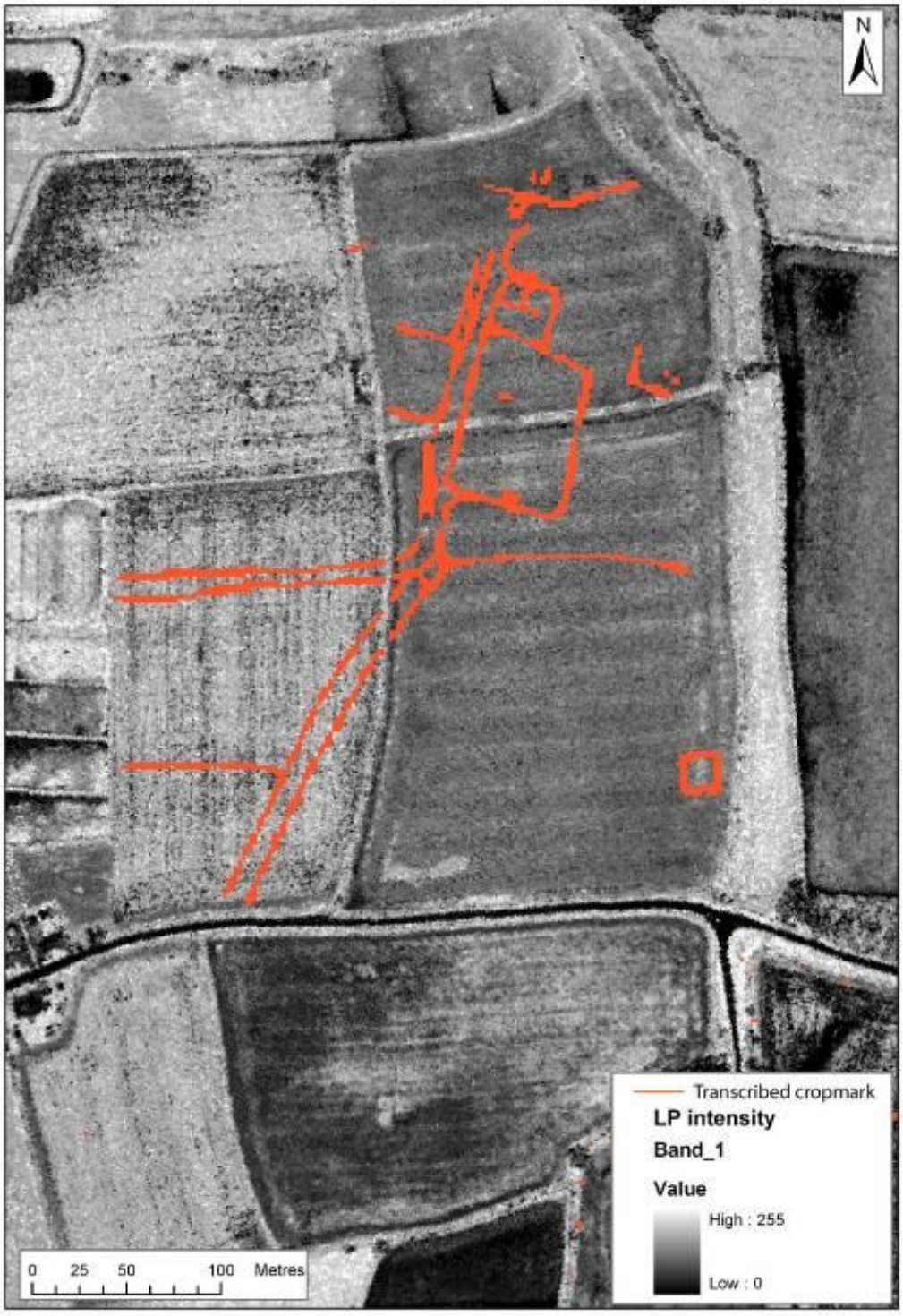

Fig 5.25: Cropmark group2 shown on the FP intensity surface model.

Fig 5.26: The LP intensity model shown in isolation. Again, none of the transcribed cropmark features from group 2 are evident in the lidar data.

5.5 SUMMARY: USING LIDAR TO INVESTIGATE CULTURAL REMAINS

This investigation of the application of lidar data to map cultural archaeology has clearly shown that LP DSM data can be employed to map basic morphology of the upstanding earthworks. The application of FP and LP intensity surface data provided mixed results. The small enclosure on the Trent-Soar floodplain was well defined by the LP intensity data. However, the significant earthworks of the Civil War redoubt close to Area 6 produced very little in the way of intensity response.

It is hypothesised that in order for a cultural feature to be visually definable in lidar intensity data, there must be significant differences material or vegetation cover in the constituent parts of the earthworks and between the earthworks and surrounding land surfaces. Section 3 demonstrated that lidar intensity data can be used to visually identify gross changes in geomorphology, such as the difference between a palaeochannel and terrace deposit. Thus, the ability of intensity to identify upstanding earth works is dependant on differences in sediment composition between features such as banks and surrounding land surfaces, affecting variables such as soil moisture, vegetation growth, etc. This effectively limits the use of lidar intensity data for this purpose, as not all features will exhibit such variation.

The application of lidar intensity to map cropmarks showed that within the present study area lidar intensity was not able to define differences in crop development related to underlying archaeological remains. This result is qualified by the observation that cropmarks may not have been evident at the time of the lidar flight. However, as the flight was undertaken in late July 2007 and it does seem surprising that no differences were defined in lidar intensity in either area of transcribed cropmarks. This may be attributable to the unfavourable weather conditions and consequent high levels of groundwater and soil moisture immediately prior to the survey flight.

The analysis of area 3 (Section 3.1) did show that lidar intensity could partially identify segments of a pasture mark. Therefore, it is possible that lidar intensity data can be used to identify some aspects of vegetation change relating to sub-surface archaeological remains. However, the results presented here do suggest that it would be relatively ineffective compared to the use of standard archaeological aerial photographic techniques or other forms of airborne remote sensing (cf Challis *et al* 2007). In considering the substantial costs of lidar flights and its unproven ability to detect cropmarks features, it must be concluded that lidar intensity as supplied in its current form is not suitable as a prospection technique for the identification of archaeological remains derived from differentiation in crop growth.

6 ANALYSIS OF DIRECTION OF FLIGHT ON LIDAR INTENSITY VALUES

6 ANALYSIS OF DIRECTION OF FLIGHT ON LIDAR INTENSITY VALUES

6.1 INTRODUCTION

Three separate areas were selected for the direction of flight analysis and have been labelled using letters, to avoid confusion with the case study examples labelled with numbers in section 3. The land units were selected by looking for areas of homogenous agricultural land use within a field, i.e. an area planted with the same crop, where an obvious flight swathe boundary occurred.

6.2 AREA A FLIGHT DIRECTION ANALYSIS

Area A comprises an area of homogenous land use with pronounced visual differentiation in intensity values between adjacent flight swathes. Two identically sized polygons were created, each occupying an adjacent swathe (Fig. 6.1). The difference in data collection resolution between the flight swathes is obvious when the individual data collection points of the lidar are viewed (Fig. 6.2). From each polygon sample values at 1m spacing were extracted from the underlying FP intensity surface model (Fig. 6.3). The population size of each grid is 2500 lidar intensity data points.

The boxplot of the two grid populations shows that the southern grid has a higher mean than the northern grid, with a skewed distribution of data points to lower standard deviations (Fig. 6.4). The southern grid has a large number of outlying and extreme data points below 2SD. In comparison the northern grid has a more normalised distribution around the mean and only four outliers in the greater than –2SD range.

The ANOVA test clearly shows there is significantly greater between population variance than within population variance (Tab. 6.1). The southern grid has significantly higher FP intensity values at the 0.01 level. This unequivocally shows that within Area A, large differences in FP intensity are observed due to data collection parameters between flight swathes.

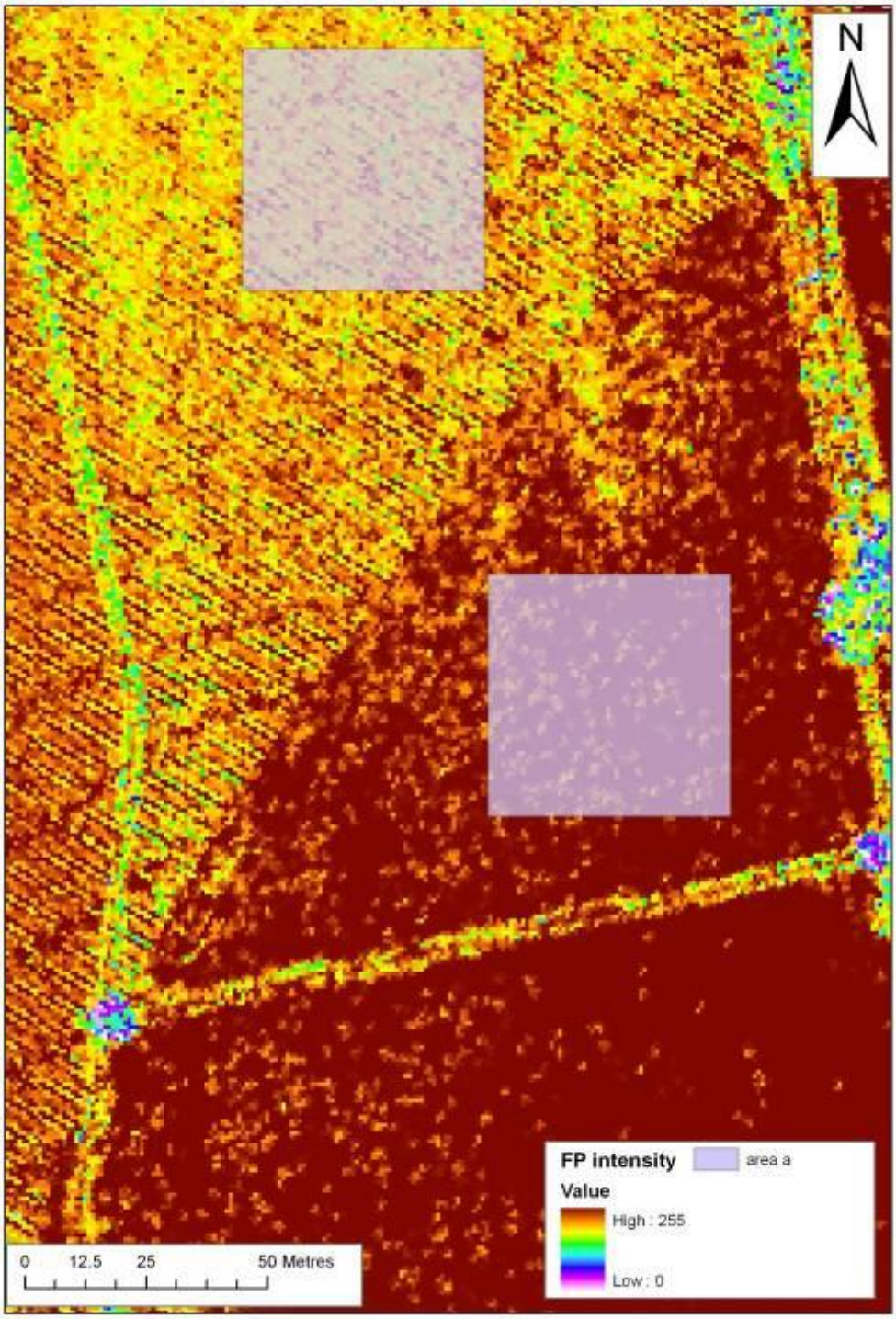

Fig 6.1: The two flight swathes over Area A, showing the polygons for data collection. Clearly there is a marked contrast between flight swathes effecting lidar intensity values.

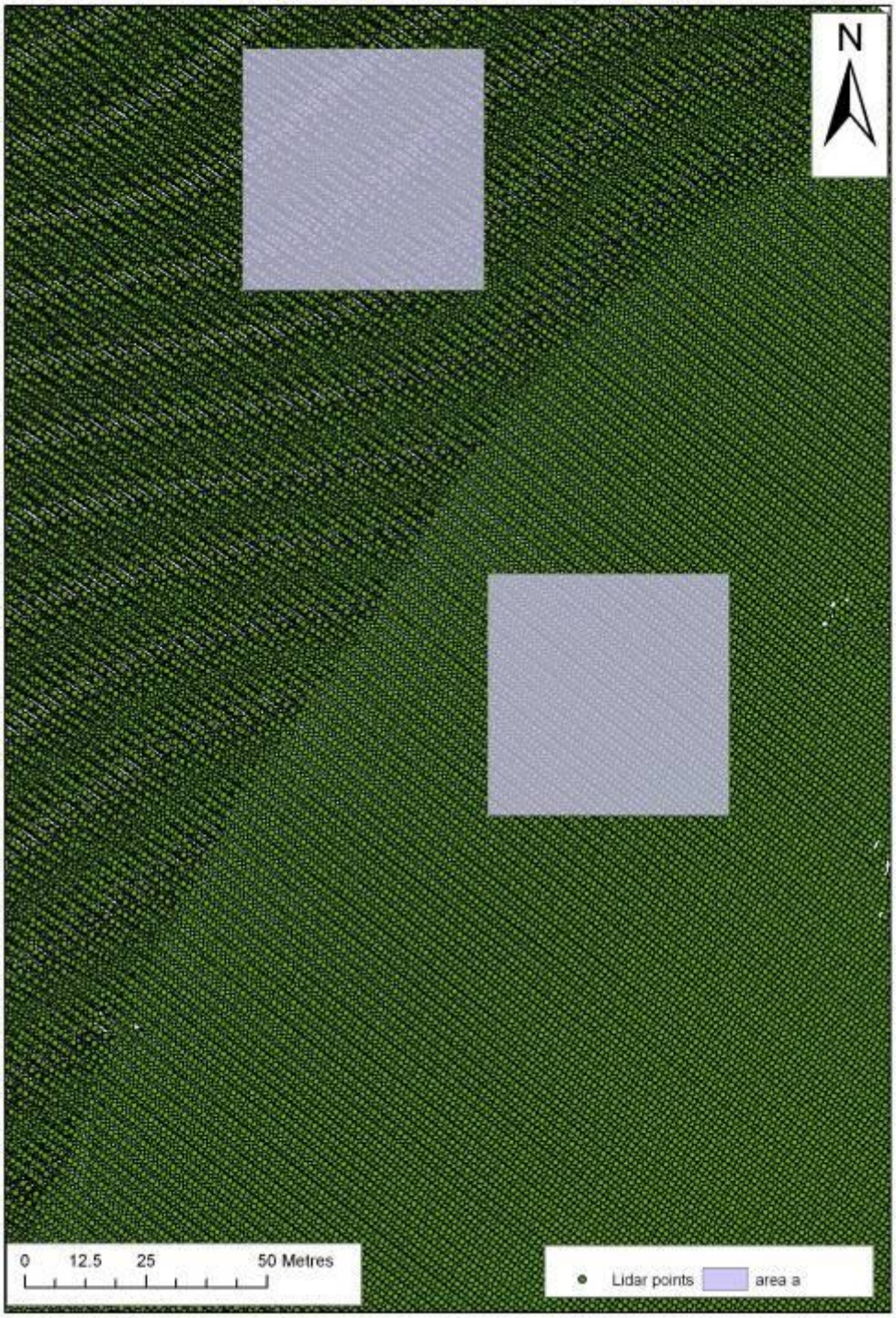

Fig 6.2: The original lidar data collection points, showing the grids for data collection in Area A. There is clearly a difference in the density of data collection between the two grids.

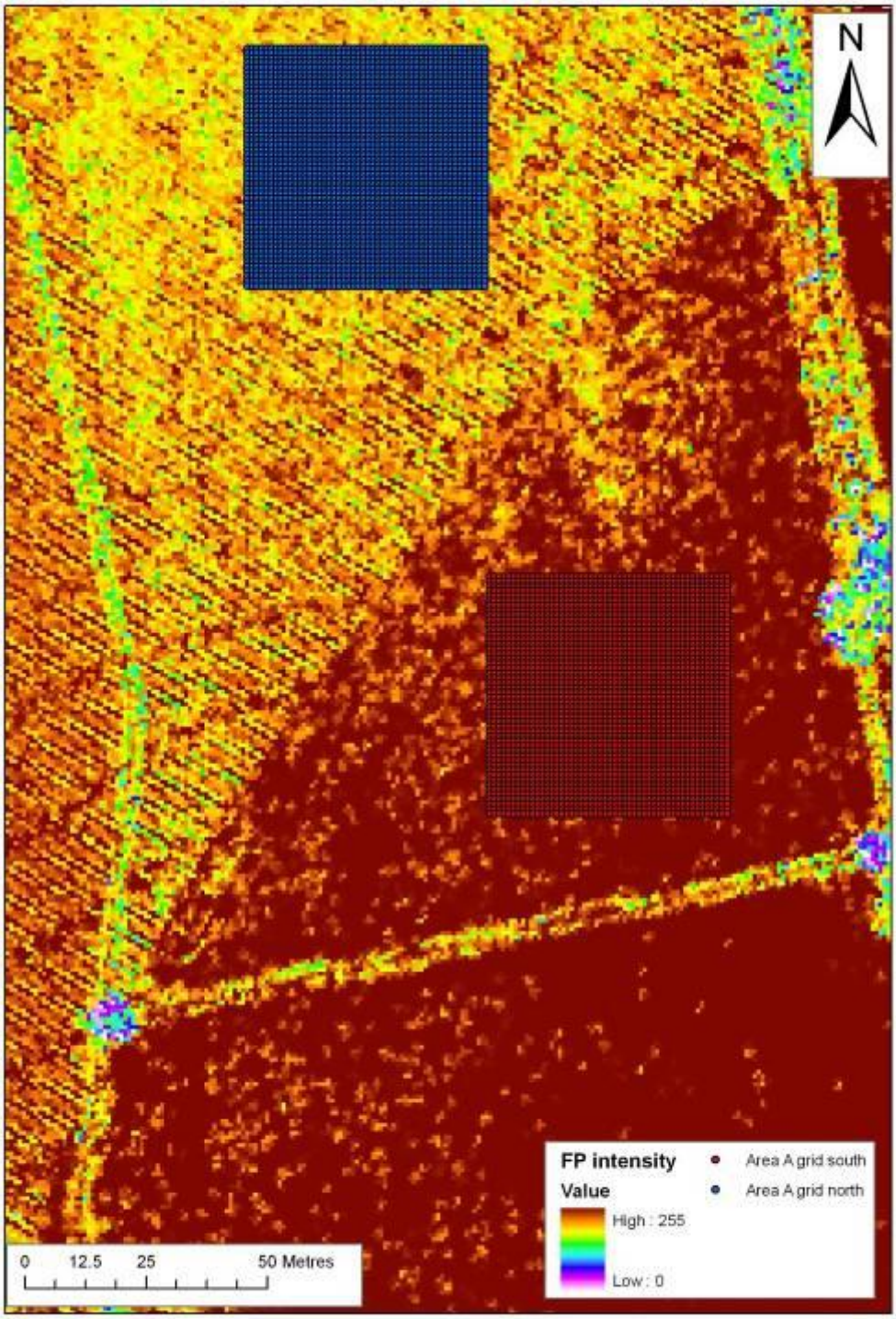

Fig 6.3: The Area A grids, showing the homogenisation of population sizes between north and south grids. All data was extracted from centroids with a 1m data posting.

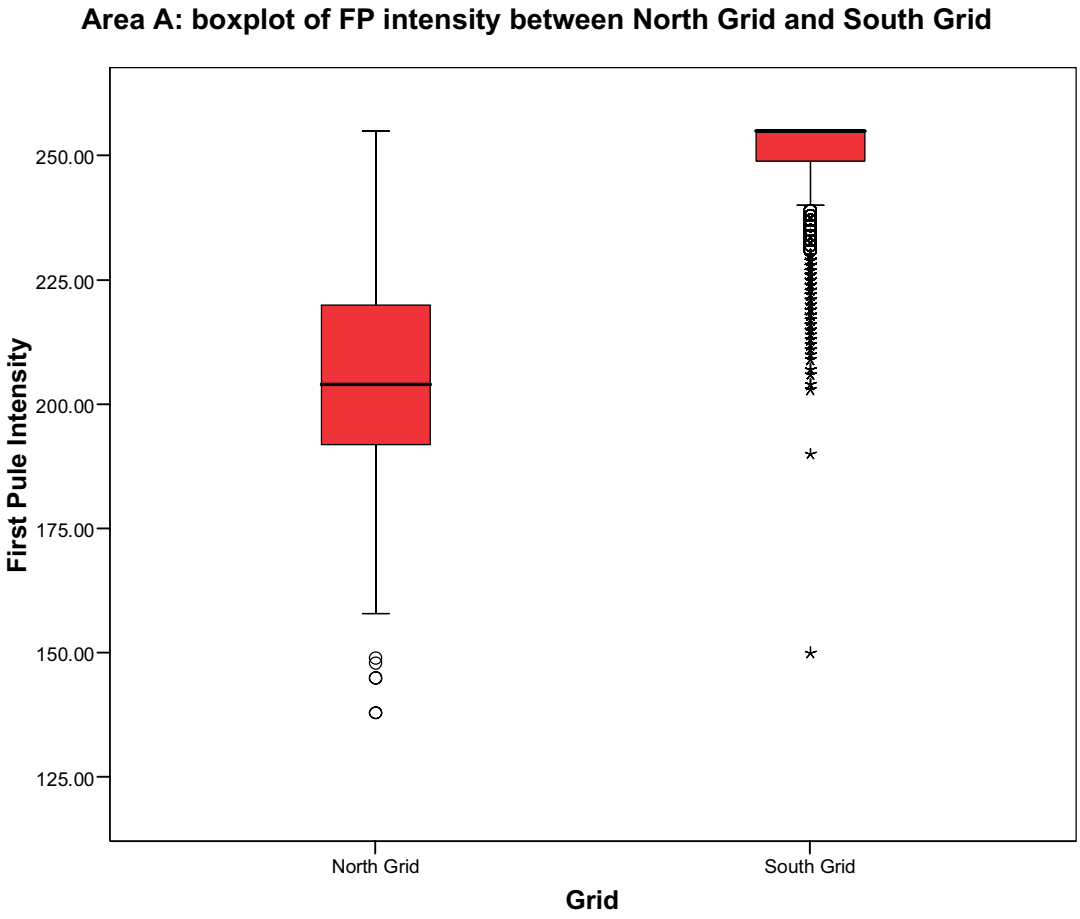

Fig 6.4: Boxplot of the North grid and South grid, Area A. There is a clear visual difference between the two grids, with the south grid having higher FP intensity values.

ANOVA

First Pule Intensity

	Sum of Squares	df	Mean Square	F	Sig.
Between Groups	2282743	1	2282743.445	8279.432	.000
Within Groups	1378011	4998	275.713		
Total	3660755	4999			

Tab 6.1: The ANOVA output for Area A, showing a significant difference between the south grid and the north grid at the 0.01 level.

6.3 AREA B FLIGHT DIRECTION ANALYSIS

Area B also comprised an area of homogenous land use, with clear visual differentiation in intensity values between adjacent flight swathes. Three separate flight swathes are evident within the field (Fig. 6.5). Two identically sized polygons were created, each occupying an adjacent swathe. The difference in data collection resolution between the flight swathes is obvious when the individual data collection points of the lidar are viewed (Fig. 6.6). The two polygons had sample values at 1m spacing extracted from the underlying FP intensity surface model and were split into Area B north grid and Area B south grid (Fig. 6.7). The population size of each grid is 15625 lidar intensity data points.

The boxplot of the separate populations shows there is a visual difference between the two grids, with the southern grid having a higher mean value (Fig. 6.8). Both the southern grid and the northern grid have similar distributions to +/-2SD of the mean. Both grids have a large number of outlying and extreme values below the mean. The ANOVA table clearly shows there is a statistically significant difference between the FP intensity values between the two grids, with the southern grid having higher FP intensity values (Tab. 6.2). From these results it is evident that the between swathe variance is greater than the within swathe variance. Again it can be clearly stated that adjacent swathes introduce a large degree of variance into the FP intensity data set.

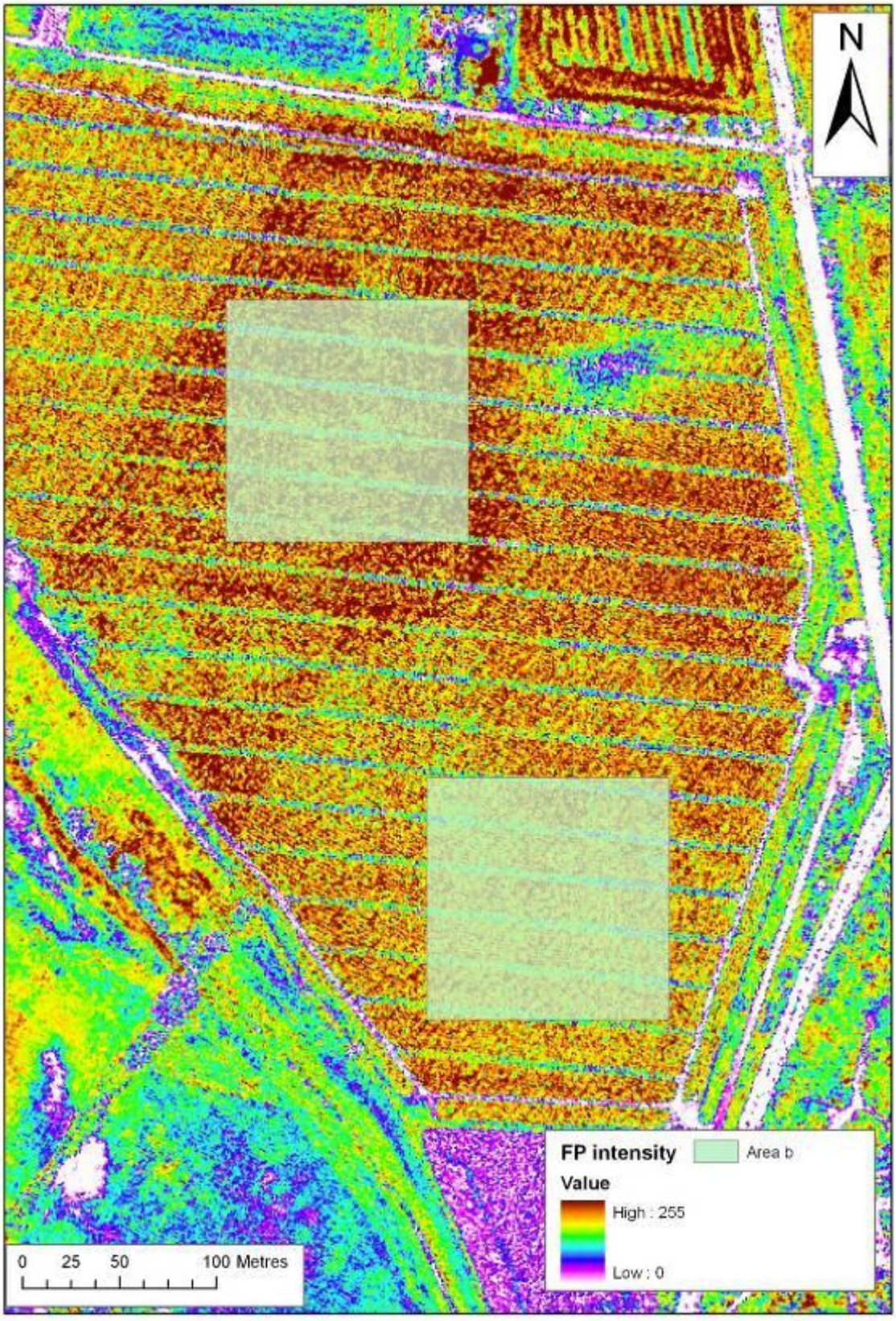

Fig 6.5: The location of the Area B grids on the FP intensity surface model.

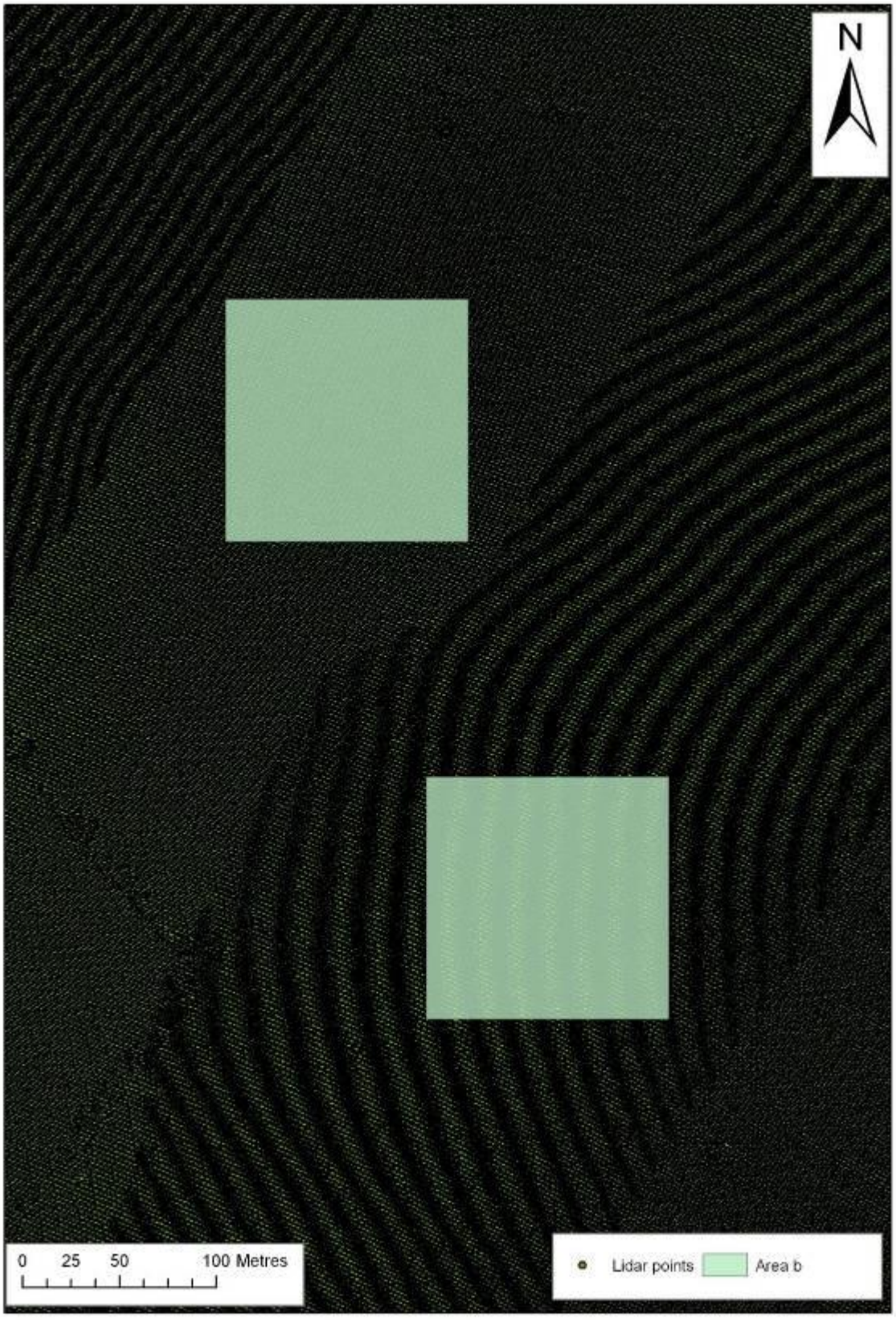

Fig 6.6: The original lidar data collection points, showing the grids for data collection in Area B.

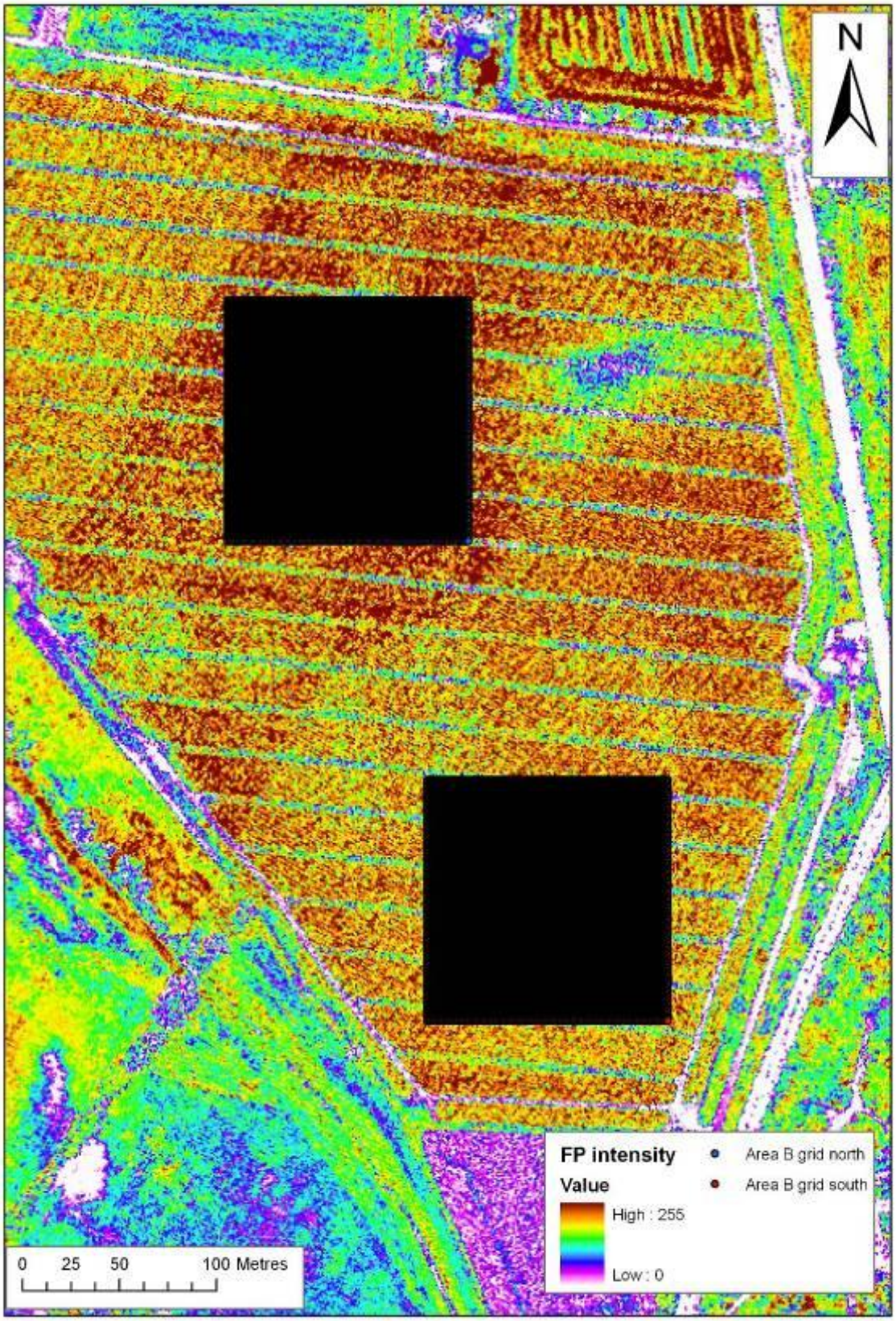

Fig 6.7: The Area B grids, showing the homogenisation of population sizes between north and south grids. All data was extracted from centroids with a 1m data posting.

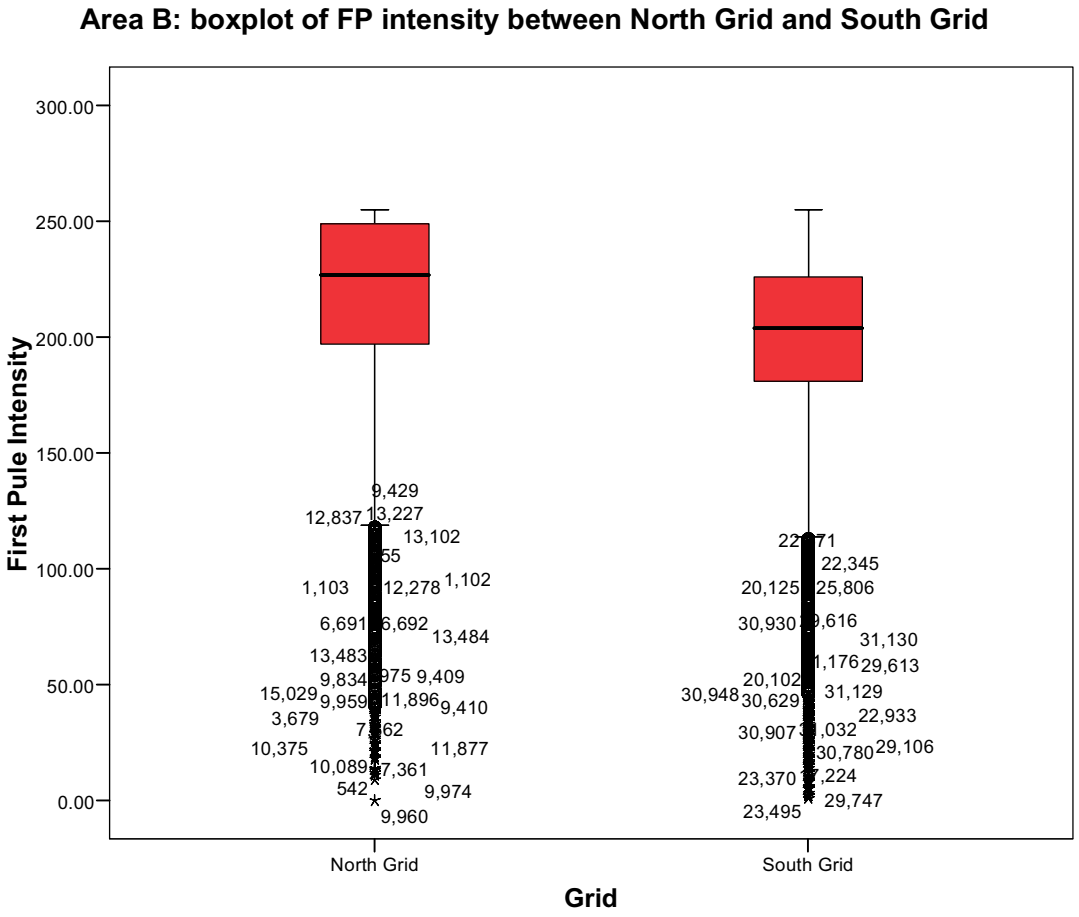

Fig 6.8: The boxplot of the north and south grids from Area B. There is a visual difference between the means in the two grids, although both grids share a similar distribution in data points.

ANOVA

First Pule Intensity

	Sum of Squares	df	Mean Square	F	Sig.
Between Groups	2553167	1	2553167.239	1432.801	.000
Within Groups	55682111	31248	1781.942		
Total	58235279	31249			

Tab 6.2: The ANOVA output comparing the north grid to the south grid Area B. Again there is a significant difference in FP intensity values between the two survey grids at the 0.01 level.

6.4 5.3 AREA C FLIGHT DIRECTION ANALYSIS

Area C comprised an area of homogenous land use, with clear visual differentiation in intensity values between adjacent flight swathes. Two identically sized polygons were created, each occupying an adjacent swathe (Fig. 6.9). The difference in data collection resolution between the flight swathes is obvious when the individual data collection points of the lidar are viewed (Fig. 6.10). Each polygon had 1m-spaced sample values extracted from the underlying FP intensity surface model and were split into Area C northern grid and Area C southern grid (Fig. 6.11). The population size of each grid is 6400 lidar intensity data points.

Again the boxplot clearly shows large differences between the two grid populations, with the northern grid having a visually higher mean than the southern grid (Fig. 6.12). The northern grid has outlying and extreme values only below the mean, whilst the southern grid has outlying and extreme values both below and above the mean. The ANOVA table again shows there is a significant difference between the flight swathes at the 0.01 level between the two area, with the northern grid having higher FP intensity values.

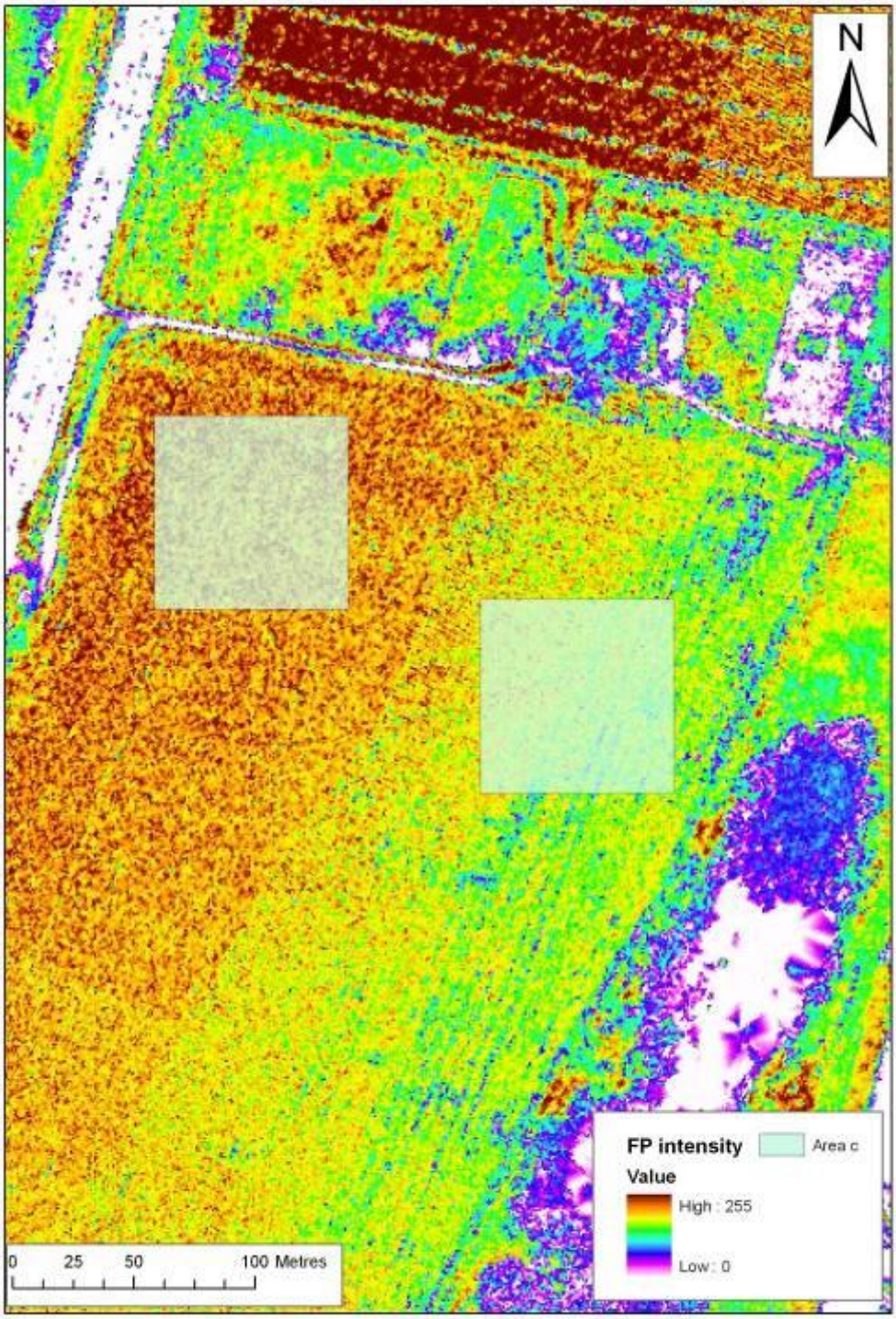

Fig 6.9: The location of the Area C grids on the FP intensity surface model.

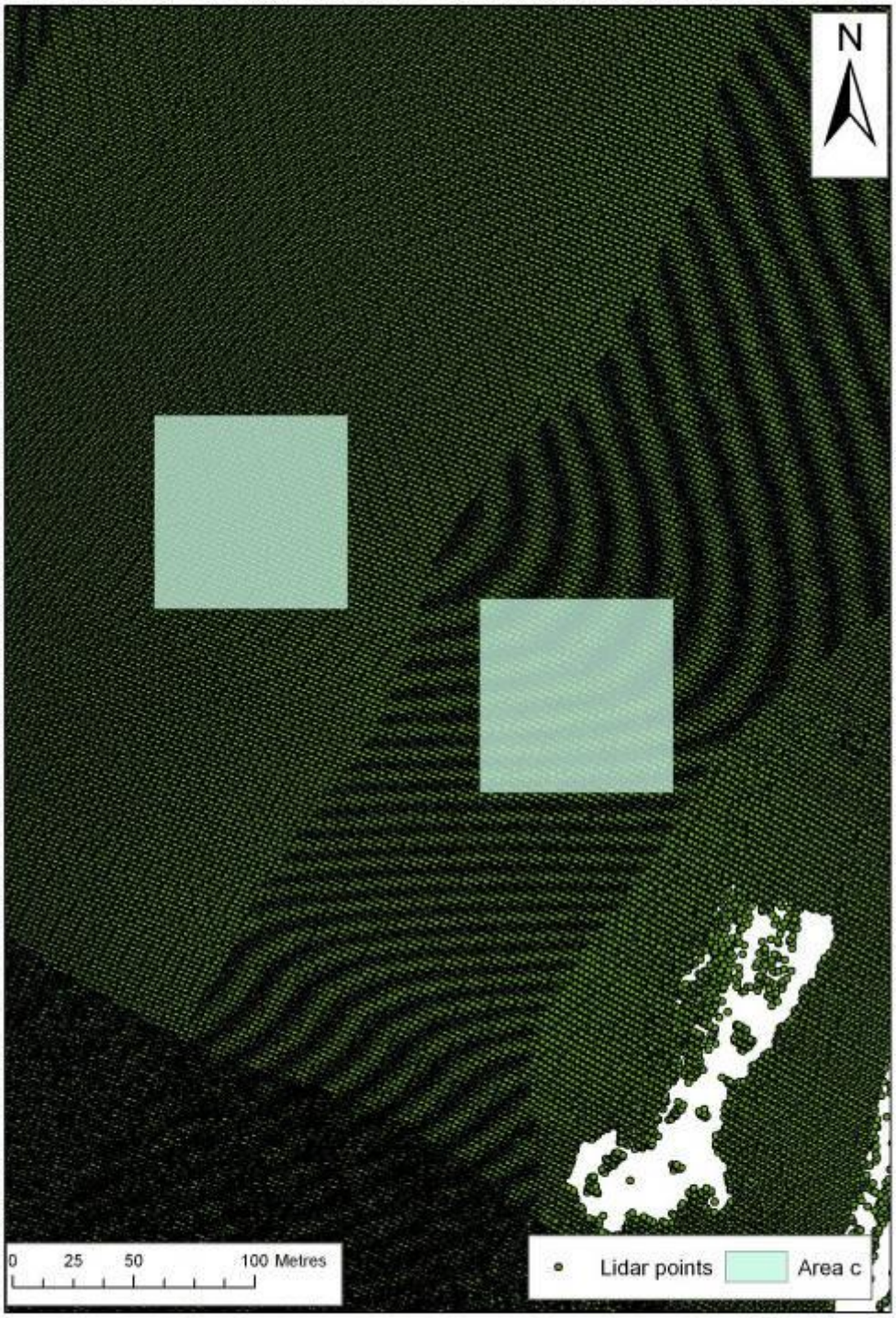

Fig 6.10: The original lidar data collection points, showing the grids for data collection in Area C.

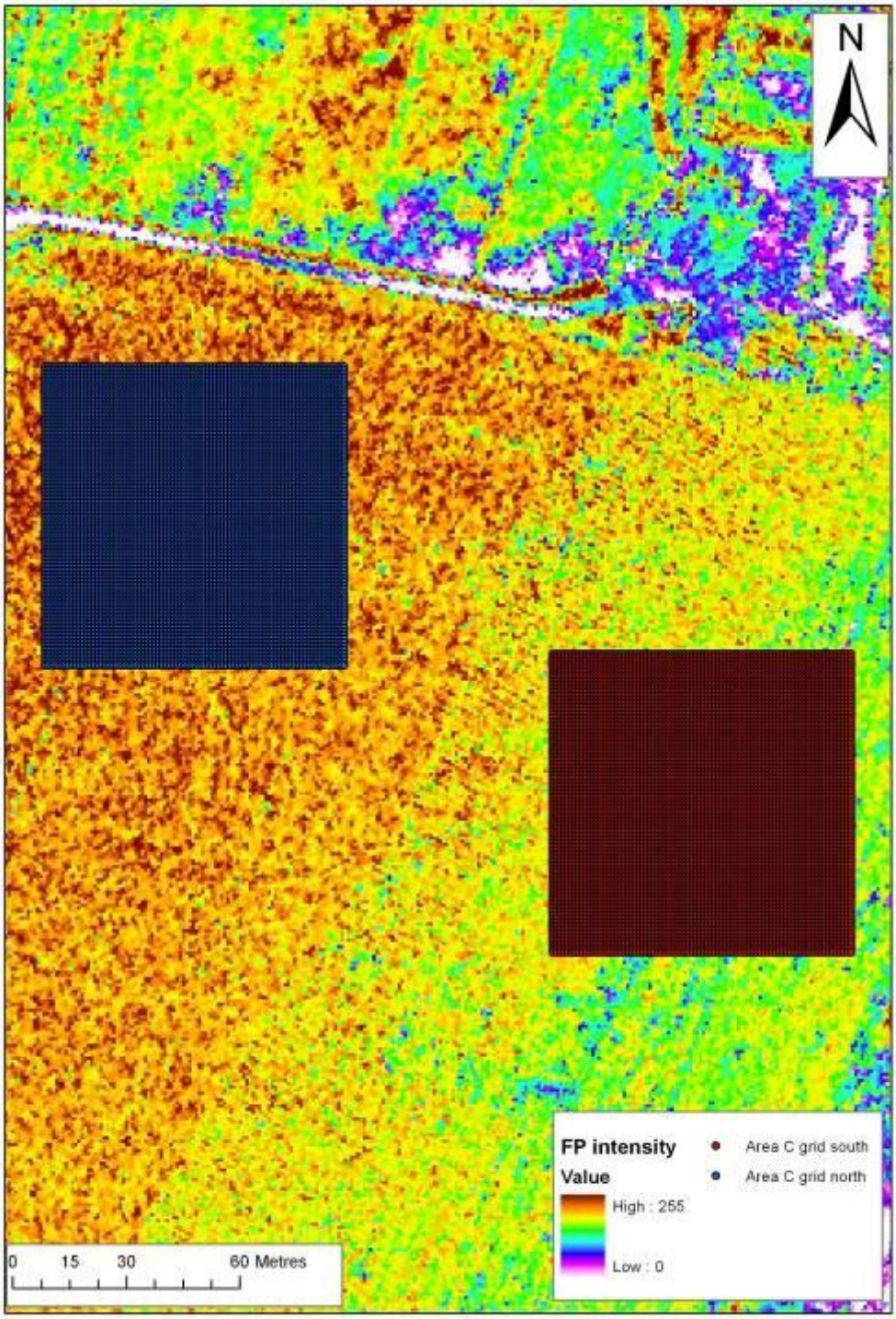

Fig 6.11: The Area C grids, showing the homogenisation of population sizes between north and south grids. All data was extracted from centroids with a 1m data posting.

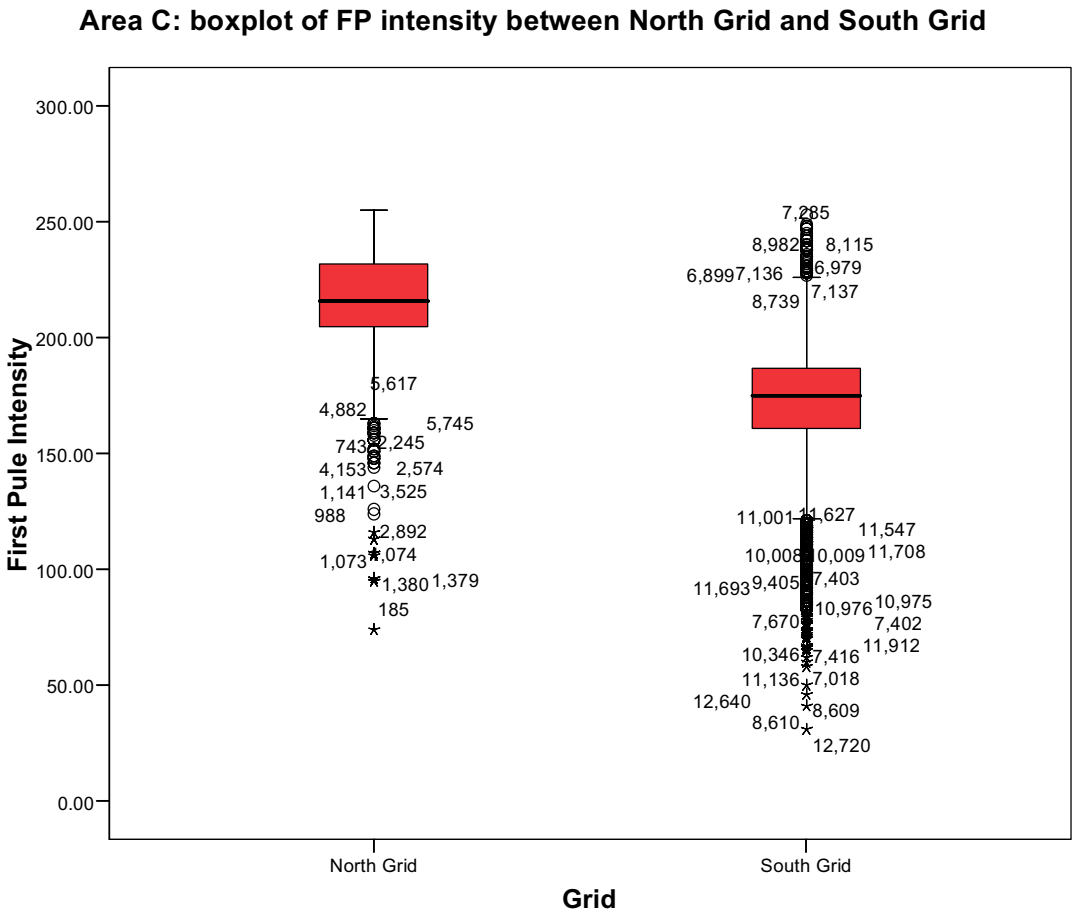

Fig 6.12: The boxplot of the north and south grids from Area C. There is a visual difference between the means in the two grids, although both grids share a similar distribution in data points about the mean.

ANOVA

First Pule Intensity

	Sum of Squares	df	Mean Square	F	Sig.
Between Groups	6846295	1	6846295.061	13519.207	.000
Within Groups	6481067	12798	506.412		
Total	13327362	12799			

Tab 6.3: The ANOVA output comparing the north grid to the south grid Area C. Again there is a significant difference in FP intensity values between the two survey grids at the 0.01 level.

6.5 TRANSECT ANALYSIS BETWEEN ADJACENT FLIGHT SWATHES

To further illustrate the effect that adjacent flight swathes have on recorded lidar intensity values, two transects were investigated across adjacent swathes, plotting FP and LP intensity against distance. Since transect data is continuous this allows graphical representations to be made visualising the join between swathes.

Transect 1 runs from east to west across the same land unit as Area A. The transect is shown on both the FP and LP intensity surface models (Figs. 6.13 and 6.14). The graphical representation of the lidar intensity values shows that FP intensity is generally lower in value in the eastern swathe and higher in value in the western swathe (Fig. 6.15). The LP intensity values show markedly lower intensity values in the eastern swathe and higher intensity values in the western swathe (Fig. 6.16). The approximate join between the swathes is marked on the graphs, although the exact position of the join is difficult to identify due to some overlap between swathes. However, a clear divide is observed in the line graphs at c. 48m, which agrees with measurements made along the transect in ArcGIS.

Transect 2 runs from north to south in the same land unit as Area B. The transect is shown on both the FP and LP intensity surface models (Figs. 6.17 and 56.18). The approximate join between swathes marked on the graphs. The FP intensity again has a marked changed in laser reflectance between the two flight swathes (Fig. 6.19). Even more marked is the change between the LP intensity values (Fig. 6.20). In this case the LP intensity values are markedly lower in the southern half of the transect.

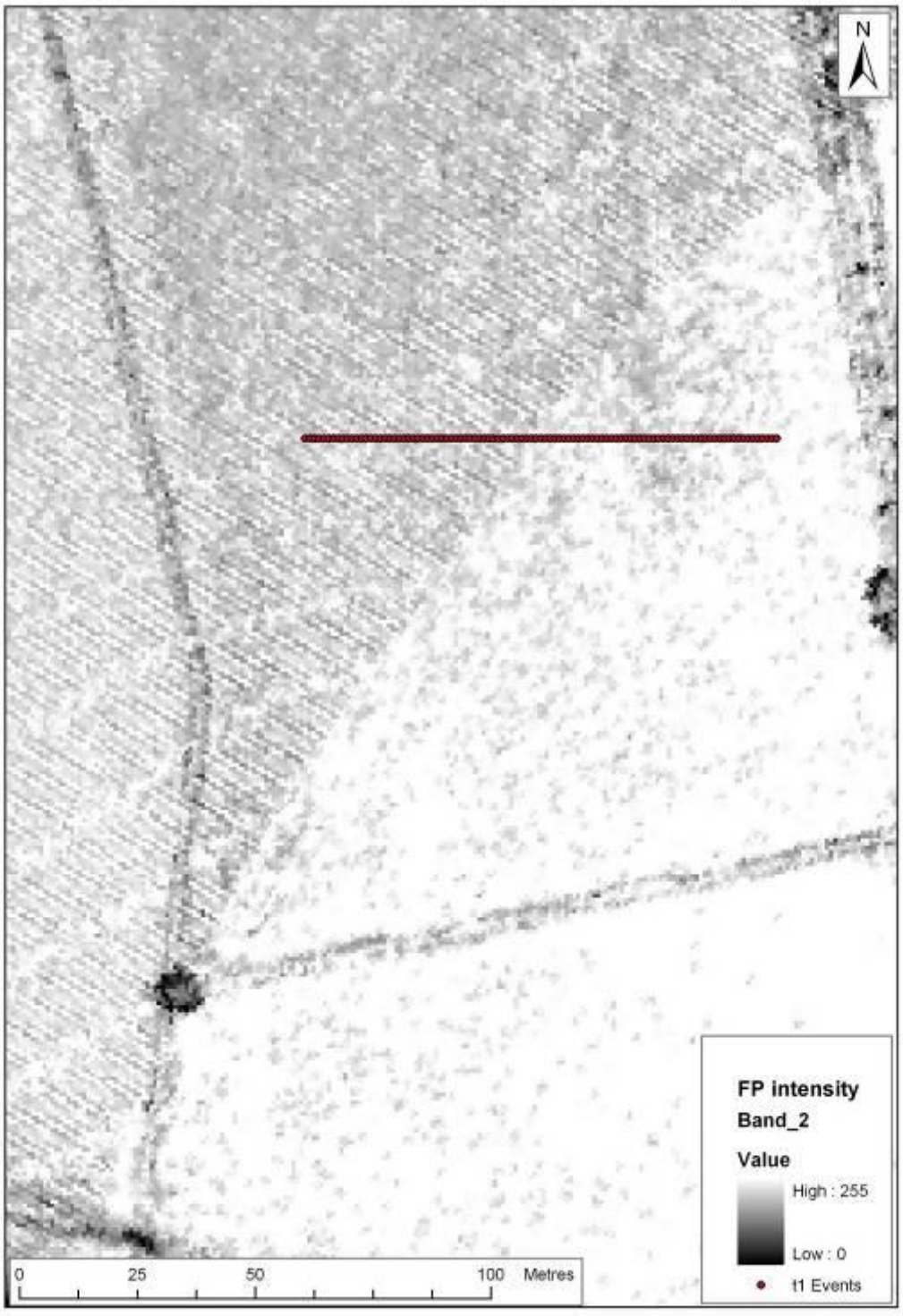

Fig 6.13: Transect 1 shown on the FP intensity.

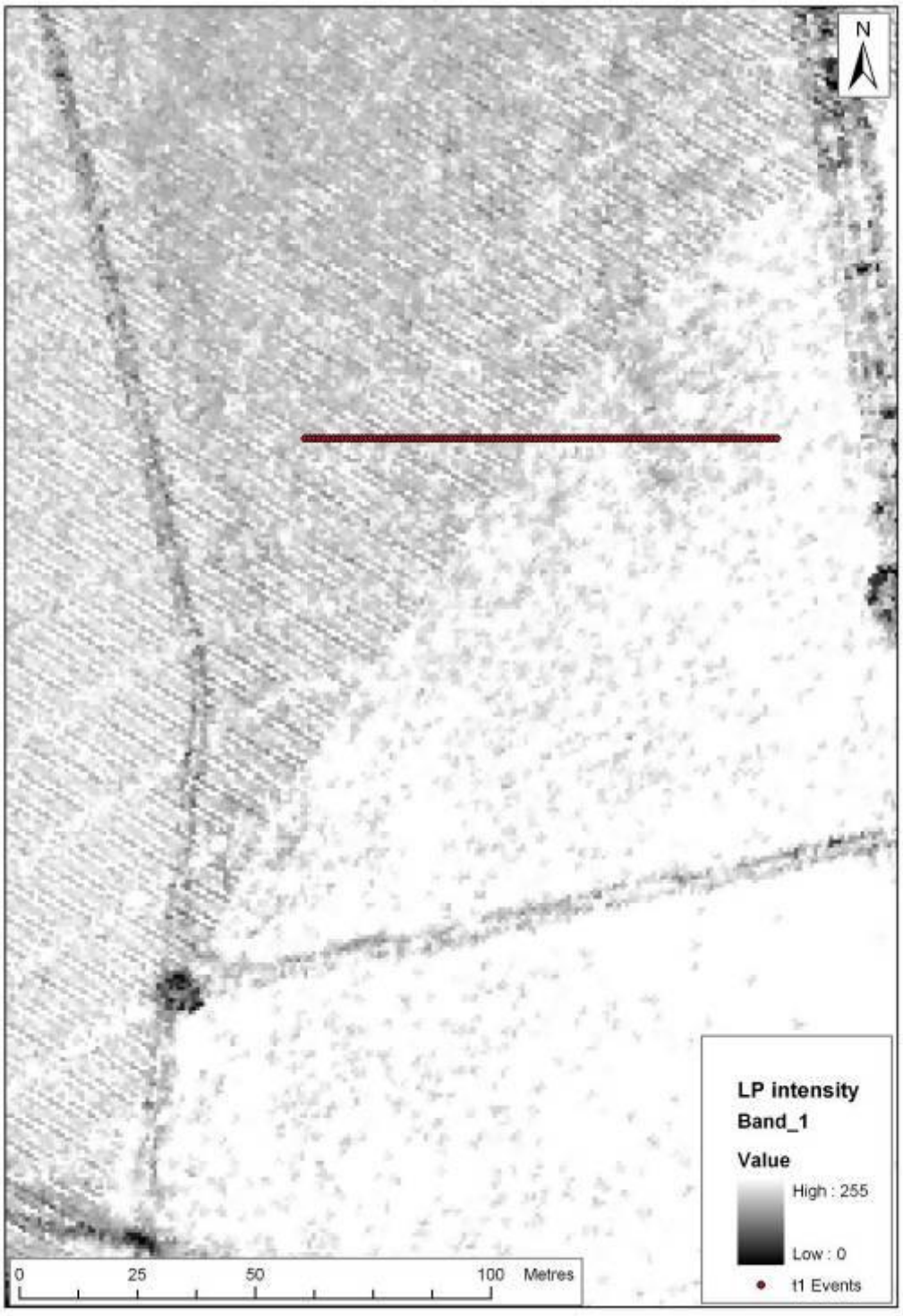

Fig 6.14: Transect 1 shown on the LP intensity.

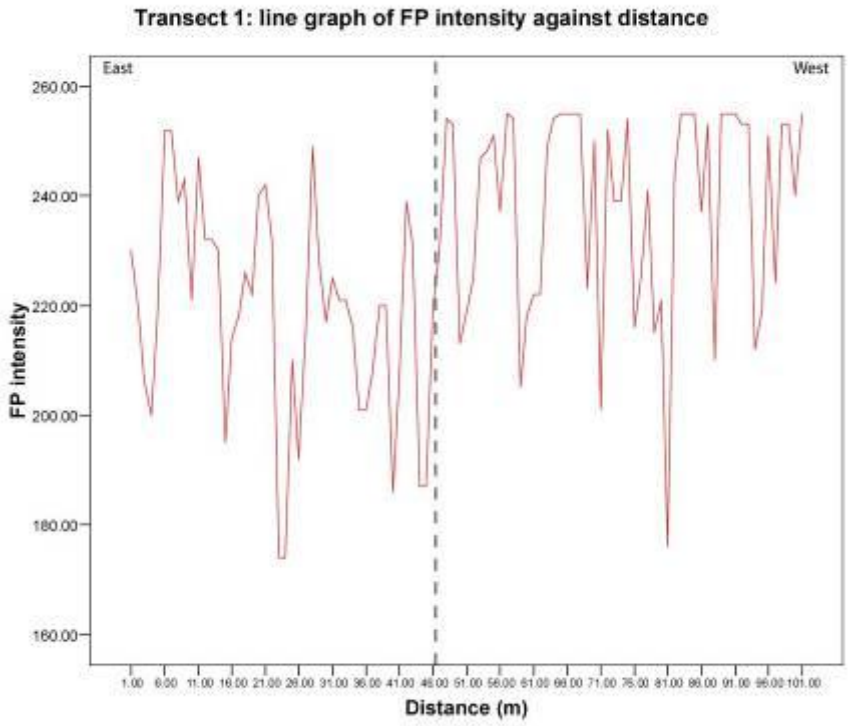

Fig 6.15: Transect 1 line graph of FP intensity against distance.

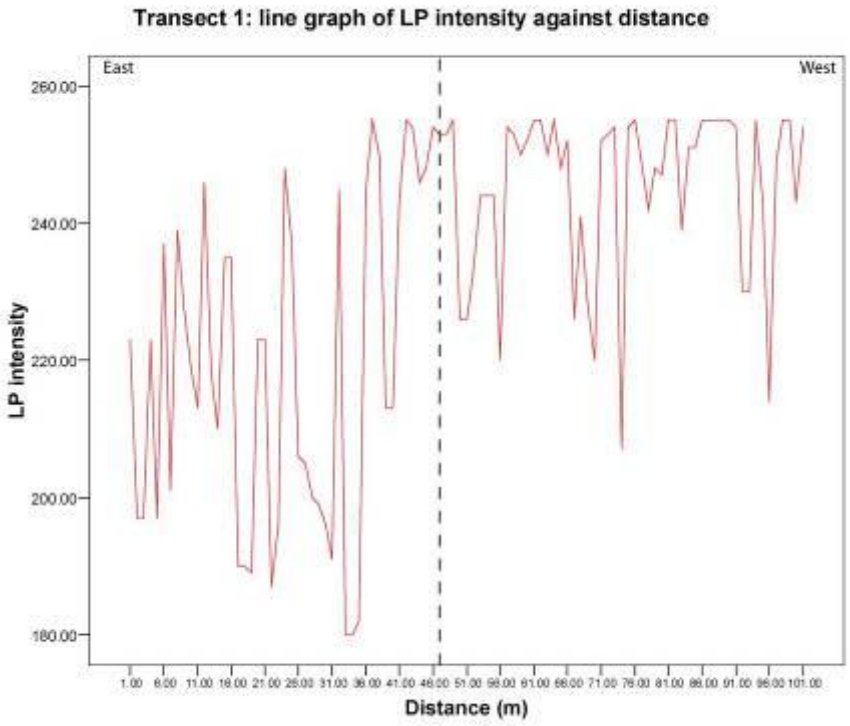

Fig 6.16: Transect 1 line graph of LP intensity against distance.

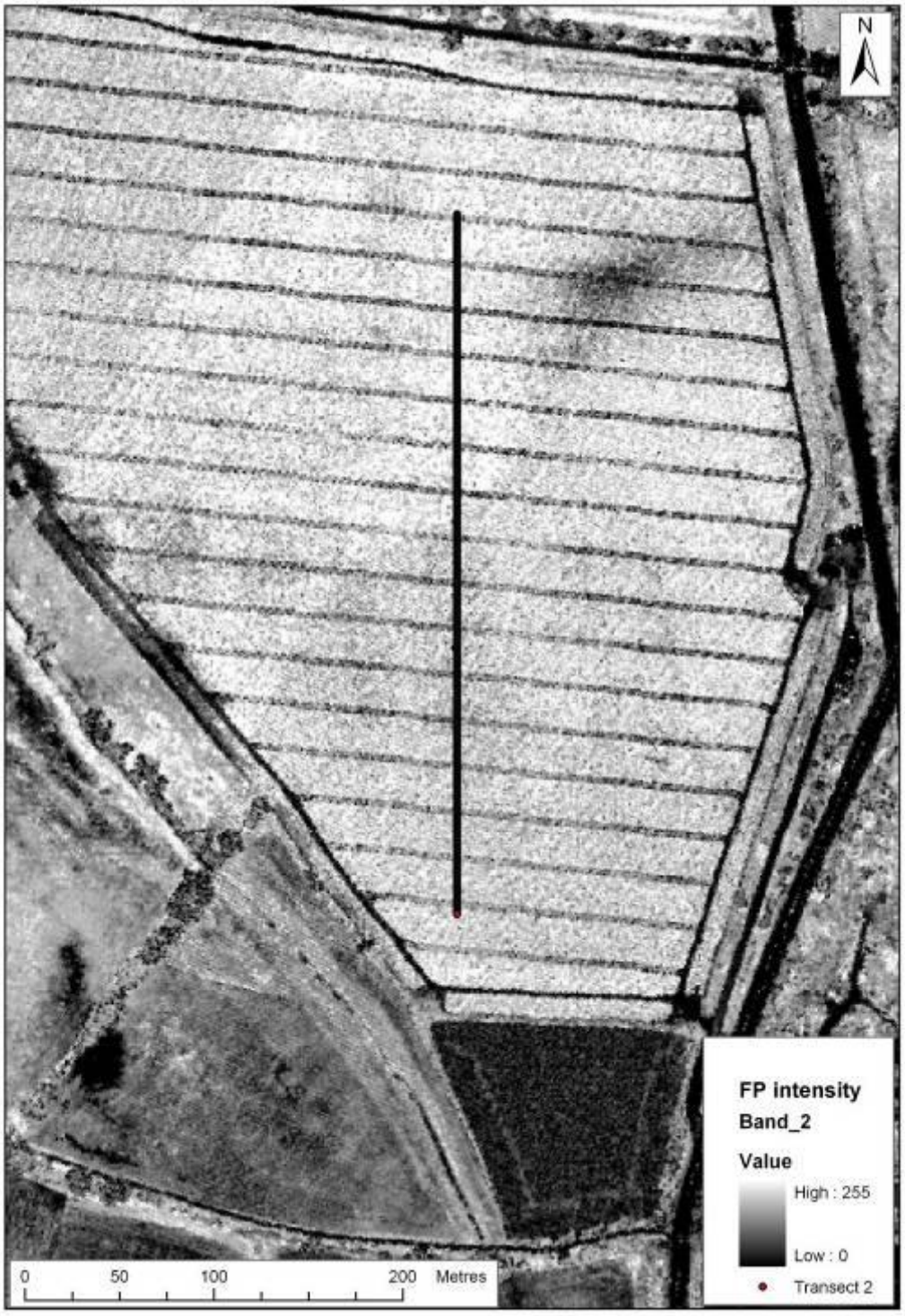

Fig 6.17: Transect 2 shown on the FP intensity.

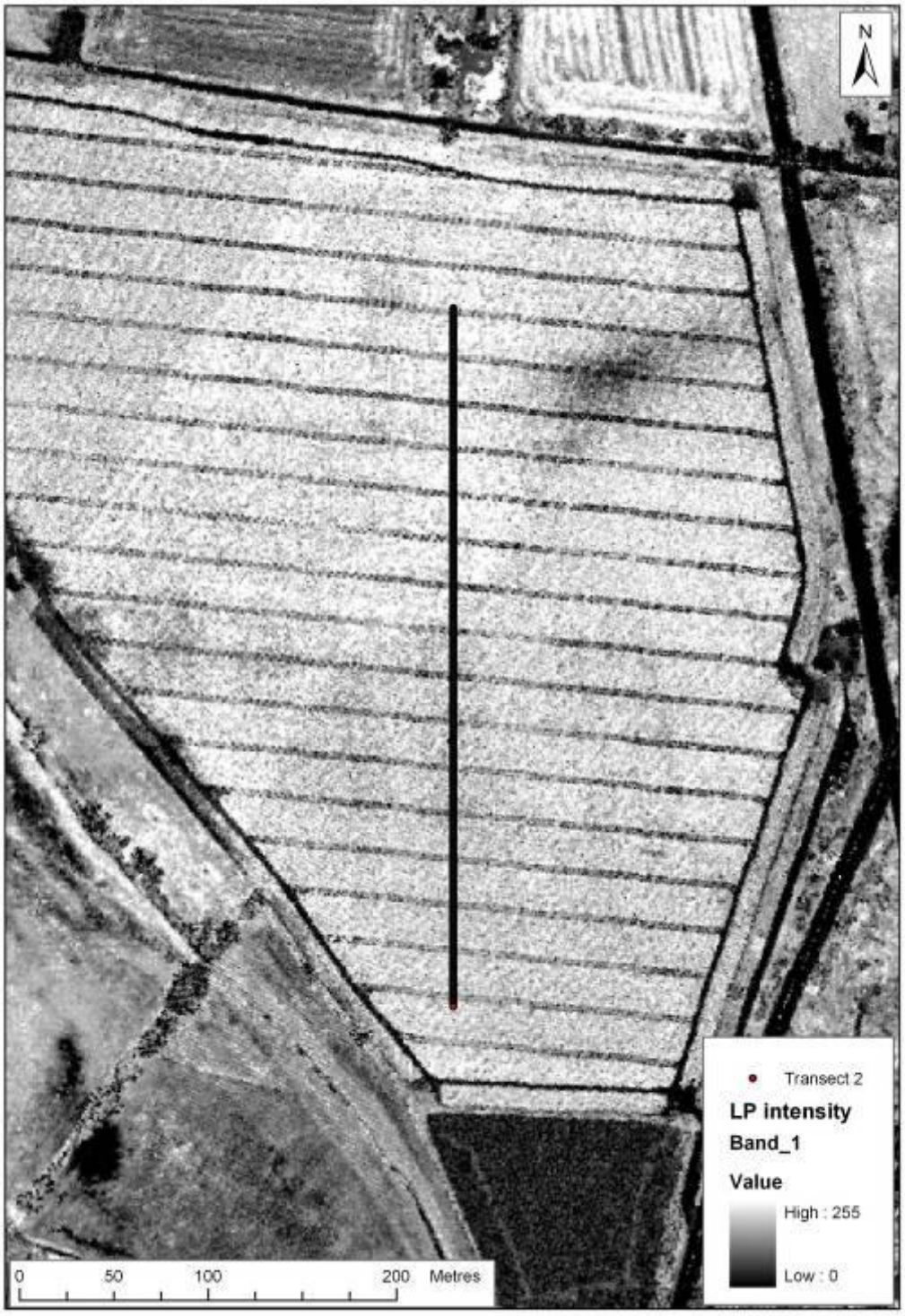

Fig 6.18: Transect 2 shown on the LP intensity.

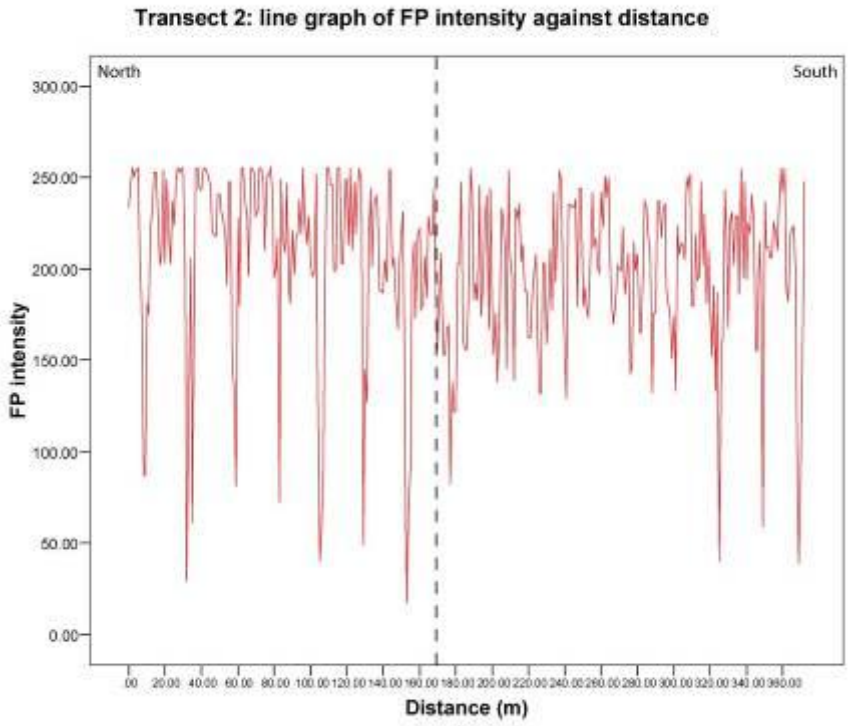

Fig 6.19: Transect 2 line graph of FP intensity against distance.

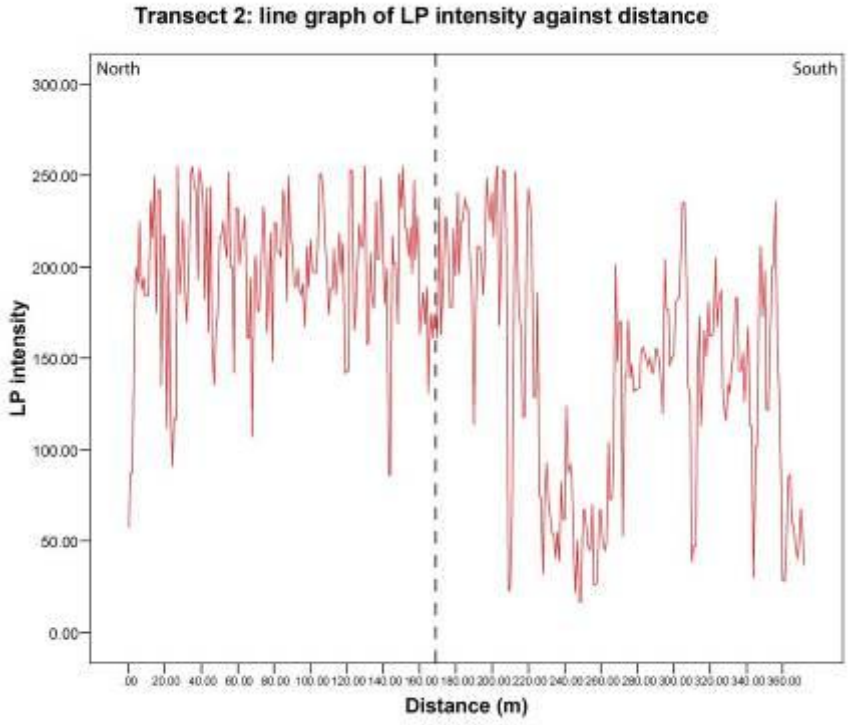

Fig 6.20: Transect 2 line graph of LP intensity against distance.

6.6 SUMMARY: ANALYSIS OF DIRECTION OF FLIGHT ON INTENSITY VALUES

The analysis of recorded intensity data from adjacent flight swathes has demonstrated that intensity values systematically vary between adjacent flight swathes. The population analysis of Areas A, B and C demonstrated that there were significant statistical differences at the 0.01 level between identical sized populations from adjacent flight swathes, on homogeneous land units. The line graph analysis demonstrated that in continuous transect data collection the intensity values were markedly different between adjacent flight swathes.

While clearly a parameter of data collection, the precise mechanism at work in introducing the observed variance is unknown. However, the fact that a large degree of variance is introduced into data in adjacent flight swathes indicates that FP and LP intensity responses between flight swathes are not directly comparable. This problem is compounded over an entire survey flight, where an intensity image is usually a compound of data collected from several flight swathes, where data points from multiple swathes overlap at swathe joins or where the aircraft has turned during data collection. In effect this limits the extent to which intensity data can be used to predictively model sediment character across adjacent flight swathes.

7 DISCUSSION

7 DISCUSSION

7.1 THE INVESTIGATION OF AIRBORNE LIDAR INTENSITY

The analysis of lidar intensity has used a series of survey areas throughout the middle and lower Trent Valley to assess the relationships of Lidar FP and LP intensity, and lidar topography, to a range of cultural and geomorphological features and their associated sediment properties. The earth resistance survey, soil organic and soil moisture data sets added valuable information, through which the lidar data sets could be assessed. A series of questions about how lidar data can be used within geoarchaeological research can now be rigorously addressed through the data collected during this project. Primarily, a detailed assessment can now be made about the use of lidar topography, FP intensity and LP intensity, to identify and investigate a series of different archaeological and geomorphological features. The discussion below considers the relevance of lidar data to each of these different feature types.

7.2 USING LIDAR INTENSITY AND TOPOGRAPHY TO IDENTIFY VEGETATION CHANGES AND SOIL MARKS

Area 3 comprised a clear pasture mark in which botanical species composition did not change over the cropmark, only the height of the vegetation. Investigation of the survey area using earth resistance showed this to be a low resistance linear feature, which turned through 90^{O} within the survey grid. These factors indicate an anthropogenic ditch; although the date of formation and exact dimensions of the feature are not known.

Both the lidar FP and LP data sets showed a change in intensity values over the feature and define the linear form of the ditch in places. Whilst this pasture mark is not overly obvious in the FP and LP intensity data sets, it is visible and therefore should be taken as an indication that intensity can be used to identify pasture marks. Both the FP and LP intensity values are elevated over the ditch. This is probably caused by changes in vegetation growth, rather than reflecting underlying soil properties. The lidar LP DSM failed to identify the feature, although this should not be considered surprising, as no changes in topography were identifiable during field survey.

It should be emphasised that the greatest clarity of the features in Area 3 was provided by the earth resistance survey. This should not surprising, as ground based prospection being routinely used in archaeology research to confirm and add further detail to features identified by aerial photographic survey. It would be extremely useful to compare an aerial photograph taken at the same time as the intensity data collection, to evaluate the effectiveness of aerial photography and intensity to identify the pasture mark.

Area 7 provided a comparison of lidar intensity to changes in vegetation structure. These vegetation changes were linear in form and are interpreted as relating to underlying changes in sediment architecture and geomorphology. The FP and LP intensity data both showed changes in values over these linear changes in vegetation structure and these visually correlate to the changes in soil resistance. Lower intensity values are visible over the palaeochannel, with higher intensity values to the east of the palaeochannel.

Within the Area 7 survey, the greatest clarity was again provided by the earth resistance survey. A linear broad feature with low resistance values is evident to the northwest of the survey grid and is interpreted as a palaeochannel, with higher resistance values to the east of the feature. The lidar LP DSM provides little detail on the form of the features within the survey grid. However, there was little topographic variation within the survey grid identifiable during field survey. From this analysis of the Area 7 data set it is clear that lidar FP and LP intensity can be used to identify changes in vegetation structure. The morphology of the features identified was larger than the cultural artefacts investigated in Area 3 and as a result are more clearly defined by lidar intensity.

Area 8 provided a bare earth site where changes in soil colour were evident associated with increased soil moisture content over a minor palaeochannel. In this example lidar intensity revealed lower values over the palaeochannel, with corresponding lower earth resistance readings. Although the earth resistance survey again provided greater clarity than the lidar intensity for the identification of features within the survey grid, both the lidar intensity data sets identified the palaeochannel. Whether the cause for the change in intensity signal was the soil colour or the soil moisture content, or both, is unclear. However, as changes in soil colour are often accompanied by changes in soil properties, such as soil moisture, it is clear that on bare earth sites lidar can be used to identify soil marks relating to geomorphological and possibly by extrapolation archaeological phenomena. Within Area 8 a topographic change was also evident, that was clearly defined by the LP DSM data.

7.3 USING LIDAR INTENSITY AND TOPOGRAPHY TO IDENTIFY GEOMORPHOLOGY

The identification of geomorphological features has been well documented through the use of lidar LP DSM (Challis 2006; *Carey et al. 2007)*, but not through lidar intensity analysis. The identification of different sediment architectures through using lidar intensity is a key theme of this research. Changes in sediment architecture often correlate with broader geomorphological changes, such as a palaeochannel adjacent to a terrace deposit.

Area 6 provided a large survey area with geomorphological differentiation traversing the survey grid. A large palaeochannel meander was adjacent to an area of Holme Pierrepont Terrace (Devensian). Both the earth resistance survey and the lidar LP DSM clearly defined the two geomorphological units. The lidar intensity data did define a change between the palaeochannel and the terrace, although the change in intensity did not precisely define either geomorphological unit. The visual analysis of this survey area is partly obscured by a flight swathe join to the north of the survey grid, which runs broadly parallel to the palaeochannel and terrace edge. Slightly elevated intensity responses are visible on the terrace, whilst lower intensity responses are evident within the palaeochannel. However, in this survey area the most useful tools for the identification of geomorphological units were the lidar LP DSM and earth resistance survey.

The survey grid for **Area 8** also provided a geomorphological and topographical contrast, with clear definition in the lidar LP DSM and earth resistance data sets. Within the Area 8 survey lidar intensity does define the form of a minor palaeochannel and again can be used to positively identify geomorphological change. However, from Area 8 it is also clear that the lidar topographic model defines the geomorphological change more precisely than either the

lidar FP or LP i. In common with Areas 3 and 6, the geomorphological variation in Area 8 was most clearly defined by the earth resistance survey.

In summary, lidar intensity can be used to visually identify changes in geomorphological units. However, in the case studies undertaken within this research the LP DSM and earth resistance survey provided greater clarification of the changes between geomorphological units. It would be problematic to map changes in geomorphology from lidar intensity data alone. When investigating geomorphology, lidar intensity should be used in conjunction with topographic models, to aid interpretation. Likewise, earth resistance survey is more useful for defining geomorphological variation than lidar intensity, but the intensity surface models can be used to aid interpretation of the earth resistance survey.

7.4 USING LIDAR INTENSITY AND TOPOGRAPHY TO IDENTIFY CHANGES IN SEDIMENT COMPOSITION AND PRESERVATION POTENTIAL

Discussion has so far concerned the visual identification of cultural and geomorphological features from lidar data. Whilst it can be observed that there is a visual correlation between intensity data and cultural and geomorphological features can the lidar intensity data be examined further to reveal evidence of changes in sediment architecture, soil moisture organic content and, by proxy, preservation potential?

Analysis from survey Areas 3, 6, 7 and 8 showed there were statistically significant correlations between FP and LP intensity, soil moisture and soil organic content. The mathematical shape of the correlation between lidar intensity and soil moisture and soil organic content is currently undefined. The graphical analysis showed each of these relationships were non-linear in form and currently cannot be used in a robust, regressive manner to predictively model sedimentary deposits of high preservation potential.

Contrastingly, the lidar LP DSM and earth resistance data sets showed linear relationships in the Area 6 and Area 8 analyses, due to marked topographic changes defining geomorphological units. This is clear evidence that in these survey areas the DSM models of topography are most useful for identifying changes in sediment composition and related changes in sediment architecture. However, when survey is undertaken on relatively flat areas, lidar topographic models are of limited use in defining changes in sediment architecture. In Areas 3 and 7 there was limited topographic variation, but the earth resistance survey showed there to be variation in sub-surface sediment architecture. In Areas 3 and 7 the relationship between earth resistance survey and LP DSM was not linear.

Therefore, in areas of marked topographic change, lidar topographic models are extremely useful for the identification of geomorphological units. When surveys are conducted in areas of little topographic variation, such as across relatively flat terrace surfaces, lidar topography is of more limited use. Of all the techniques compared in this study, earth resistance survey was the most consistent in defining both broad geomorphological trends and cultural features. Whilst earth resistance survey is time consuming and does not offer the landscape perspective afforded by lidar, it can be used in conjunction with lidar for the detailed investigation of specific survey areas first identified from analysis of lidar topographic data.

Of further general interest in assessing sediments of high geoarchaeological potential from remote sensed data are the relationships of soil organic content and soil moisture content to

the lidar and earth resistance data. In all the study areas these relationships were generally non-linear and this maybe considered surprising. However, it does serve to emphasise that remote sensed data, such as lidar topography, are most productively used for initial assessment of geoarchaeological potential, such as identifying targets for further ground based assessment.

The analysis of the surface to sub-surface relationships through the gouge core transects did provide some indication that lidar intensity responses reflect broader changes in sub-surface alluvial stratigraphy. In general, some lower responses were observed over cut features such as palaeochannels, with higher responses recorded over features such as terraces. However, although general trends did emerge from the lidar intensity, it was also clear that the lidar intensity data was noisy and results far from consistent; some palaeochannels provided high intensity data values, whilst some areas of terrace low intensity data values.

The application of surface intensity to model sub-surface sediment architecture is problematic. Most of the areas investigated displayed broadly similar sediment architecture at the top of the soil profile, with variation and stratigraphic complexity only observed at depths. Therefore, in some of the surveys conducted, such as Areas 7 and 8, lidar FP and LP intensity were detecting changes in soil moisture within a homogeneous top sediment unit, caused by changes in sediment architecture at greater depths. Thus lidar intensity did not demonstrate a robust relationship with sub-surface sediment architecture that could be used in a predictive manner to identify sediments of high preservation potential. Whilst there was some qualitative visual comparison between alluvial stratigraphy and surface intensity, this cannot be used with confidence to identify waterlogged deposits of high organic content.

7.5 USING LIDAR INTENSITY AND TOPOGRAPHY TO IDENTIFY UPSTANDING ARCHAEOLOGICAL EARTHWORKS

The application of lidar intensity to evaluate upstanding earthworks provided mixed results. The small enclosure on the Trent-Soar floodplain was clearly defined by the LP intensity data, whilst the Civil War redoubt near Area 6, north of Newark on Trent, proved to be almost undetectable on the lidar FP and LP intensity data. The relationship of lidar intensity to upstanding cultural earthworks is unclear. In both studies the lidar topographic models clearly defined the upstanding earthworks. From the results presented in this study, the application of lidar intensity to identify earthworks would seem limited. Some earthworks are clearly not evident in the lidar intensity surface models. Therefore, it is suggested that lidar topographic models are the most effective of the lidar data sets for mapping earthwork features.

From the visual comparison undertaken it is not clear which variables determine the visibility of upstanding earthworks to lidar intensity. The visual analysis of the lidar surface models in Areas 3, 6, 7 and 8 showed there were some visual relationships between lidar intensity and gross changes in geomorphology, such as palaeochannels and terraces. However, linear, robust relationships between lidar intensity and variables such as soil moisture and soil organic content were not present. Thus it is hypothesised that a large number of variables are causing changes in the reflectance of lidar laser pulses. For earthwork features to be identifiable it is suggested that there needs to be significant gross changes in a number of variables such as vegetation cover, soil moisture and colour, between the earthworks and surrounding landform surfaces. Since lidar intensity has proved to be unreliable for the

mapping of earthwork features, lidar topographic models should be used in the first instance; additional information may be derived from lidar intensity data, if the earthwork is visible in that data.

7.6 USING LIDAR INTENSITY AND TOPOGRAPHY TO IDENTIFY CROPMARKS DERIVED FROM ARCHAEOLOGICAL REMAINS

The visual analysis of lidar surface models to investigate cropmarks relied on using transcriptions of cropmarks from previous campaigns of flying and superimposed on to the lidar data. This does have inherent problems, due to comparing data sets that are not contemporary. However, the lidar flight was indertaken in late July, and although meteorological records show, May, June and July were wetter in 2007 than in previous years, it would be very surprising if no cropmarks were extant in either of the two survey areas. Clearly, no cropmarks were identifiable in either the FP or LP intensity surface models within the study area. There are three possible non exclusive explanations for this result:

A) Lidar data posting: The data posting of the lidar intensity may have been too coarse at a 1m interval to detect any cropmarks that were apparent at the time of survey. The application of lidar data posted on a 0.5m sample interval may help remedy this issue and future work might usefully investigate the relationship of lidar intensity to cropmarks using a smaller data posting such as 0.5m.

B) No cropmarks were visible at the time of the lidar flight: the aerial photographs transcriptions were made from flights that predated the lidar flight for this project. Therefore, the two data sets are not directly comparable. It is possible that no cropmarks were visible at the time of the lidar flight.

C) Difference in the reflective properties of vegetation to NIR laser light were not sufficient to be detected. It is also possible that cropmarks were visible at the time of flight, but not within the NIR part of the spectrum used by lidar pulse.

Additional information about the application of lidar intensity to identify cropmarks comes from the survey in Area 3, where the presence of a ditch and associated pasture mark was visually apparent on the FP and LP intensity data. Whilst the feature was not overly clear in the data, parts of the parch mark were identifiable. This suggests that lidar intensity may have a limited application in the detection of vegetation changes relating to cultural features. Further research is needed to fully address how useful lidar intensity data are for the identification of cultural remains from vegetation differentiation.

7.7 SUMMARY: THE USE OF LIDAR INTENSITY AND TOPOGRAPHY TO IDENTIFY SEDIMENT ARCHITECTURES OF HIGH PRESERVATION POTENTIAL AND CULTURAL SIGNIFICANCE

The results from lidar intensity analysis clearly show that lidar intensity cannot be used in a robust way to predictively model sediment architectures of high preservation potential. The reasons for this are multifaceted. It appears that many factors cause variance in intensity data, limiting their use for the identification of cultural and geomorphological features.

Throughout the analysis of the lidar data, the strongest linear relationships were observed between LP DSM topography and soil moisture and soil organic contents, routinely stronger than the linear weak relationships visualised between lidar intensity and soil moisture and soil organic contents. However, it should be emphasised that linear relationships between LP DSM topography and soil moisture and soil organic contents were still relatively weak.

The results from this analysis do provide some firm conclusions on the use of remote sensed and geoprospection data to predictively model waterlogged and organic rich deposits. To identify large-scale geomorphological trends, topographic models produced from lidar data are invaluable. Lidar intensity data can be used to compliment interpretation of the lidar topography, but it cannot be used in place of lidar topography. Once potential targets have been identified from the analysis of topographic data, ground based geoprospection should proceed. Techniques such as earth resistance survey (used in this project) and also electrical resistivity profiling can be used to identify both shallow and deep subsurface features, and provide an indication of preservation potential based on resistance or resistivity values. For the identification of cultural remains, conventional aerial photography remains a far more effective tool than lidar. Whilst lidar intensity showed a limited capacity to identify vegetation changes relating to archaeological and geomorphological phenomena, it is suggested that aerial photography is a much more powerful tool for the visual identification of cultural features.

7.8 ARCHIVE INTENSITY ANALYSIS

Examination of lidar intensity imagery from a variety of geomorphological settings indicates that these data do contain information not present in the corresponding elevation data. Empirical interpretation, based on a common understanding of the character of soils, sediments and vegetation in the area under examination, allows the use of intensity images to add qualitative information to the interpretation of a landscape area, even in the absence of the ability to generate robust predictive models of soils and sediment properties. Since intensity data is (or can be) routinely collected during a lidar flight aimed primarily at gathering topographic data, it is suggested that the examination of these data are routinely incorporated in the archaeological interpretation of existing lidar data, and that their collection always form part of the parameters of a an airborne lidar survey commissioned for archaeological purposes.

7.9 ANALYSIS OF THE DIRECTION OF FLIGHT ON LIDAR INTENSITY VALUES

Analysis of variation in intensity values due to the direction of flight of the aircraft produced significant results. Primarily, lidar intensity data collected from adjacent flight swathes has markedly different intensity values. The reason for this difference in intensity values between flight swathes is a function of data collection, although the precise mechanism at work is not understood.

The level of variance introduced into the data is high and statistically significant at the 0.01 level. This high level of variance will undoubtedly disguise subtle trends in intensity data, which have the potential to be usefully employed as an indicator of organic rich, waterlogged

sediments. The results categorically show that intensity values from different flight swathes are not directly comparable. As much of the data set is made up from data of multiple swathes this effectively limits the use of lidar intensity to identify sediments of high preservation potential. This renders the use of lidar intensity to productively model organic rich, waterlogged deposits is limited.

8 CONCLUSIONS

8 CONCLUSION

8.1 GENERAL CONCLUSIONS

A number of key themes have emerged from the present research; for clarity these are summarised as bullet points:

Using lidar to visually identify geomorphological features:

- Lidar LP DSM topographic models proved of greatest use for the identification of major geomorphological units, such the difference *between* palaeochannels and terraces.
- Lidar LP DSM was less effective at identifying variation *within* geomorphological units.
- Lidar intensity data can be used to identify some major geomorphological units, but there is less clarity and definition than in LP DSM data.
- When small surveys are conducted on single geomorphological units with little topographic variation, lidar intensity proved capable of visually defining features such as palaeochannels and other smaller geomorphological and sometimes cultural features.
- The ability of lidar intensity to define changes in geomorphology is considered to be largely a product of the impact of surface vegetation difference on the reflectance of the lidar laser pulse.
- Earth resistance survey proved to be the most reliable tool for the visual identification of larger geomorphological units and smaller variations within geomorphological units.

The mathematical relationships of lidar data to physical soil parameters:

- Neither lidar FP or LP intensity were shown to have a mathematically linear relationship to soil moisture values.
- Neither lidar FP or LP intensity were shown to have a mathematically linear relationship to soil organic values.
- Neither lidar FP or LP intensity were shown to have a mathematically linear relationship to soil Ohms values from the earth resistance survey.
- Lidar intensity cannot currently be used in a mathematical predictive model to identify sediments of high moisture content and high preservation potential.
- In survey areas where there was a marked topographic change between geomorphological units, lidar LP DSM and earth resistance Ohms had a strong linear positive relationship to each other.
- The linear relationship of lidar topography to soil organic content was stronger than that of lidar intensity, but still relatively weak overall.
- The linear relationship of lidar topography to soil moisture content was stronger than that of lidar intensity, but still relatively weak overall.

The impact of the direction of flight on lidar intensity values:

- Lidar FP intensity values were shown to display large differences between adjacent flight swathes.
- Much of the survey area was made up from data from multiple swathes.
- The differences in intensity values between adjacent flight swathes are a product of data collection, although the exact variable introducing this variance is not known.

- The differences in FP intensity values between adjacent swathes means that land units located in different swathes do not have directly comparable lidar intensity values.

Using lidar to visually identify cultural features:

- Lidar intensity proved capable of detecting part of a small parch mark in survey Area 3.
- Lidar intensity did not provide any indication that it could be used to detect archaeological features highlighted by cropmarks.
- Lidar intensity did define several vegetation changes relating to geomorphological change.
- Lidar LP DSM topographic models were effective at defining upstanding archaeological earthworks.
- Lidar intensity surface models proved capable of defining some upstanding earthworks, but did not reveal others.
- It is suggested that lidar intensity has a limited role to play in the identification of cultural features from either earthwork or cropmark survey.
- For earthwork survey lidar topography should be used in the first instance, potentially complemented by lidar intensity.
- For cropmark survey aerial photography should be used in the first instance and complemented by lidar topography and intensity survey.

8.2 THE APPLICATION OF LIDAR DATA SETS WITHIN GEOARCHAEOLOGICAL RESEARCH

From the analyses presented in this report, a clear method statement can be developed for the identification of different sediment units within alluvial environments. The application of lidar intensity to predictively model sediment units of high preservation potential can be deemed at present to be untenable. Robust relationships were not witnessed between lidar intensity data and physical soil variables and sub-surface sediment architecture.

However, lidar intensity did prove to be useful in visual qualitative analyses of specific survey areas. The application of earth resistance survey showed the reliability of this technique to map both geomorphological and cultural features. Lidar topographic models were shown to be robust in their identification of major geomorphological landforms. From these factors the following method statement is presented, incorporating the use of lidar, to identify sediment units of high soil moisture content and high preservation potential.

1. Definition of alluvial area of interest

2. Lidar data capture

3. Visual analysis of lidar topographic models to identify major landform units

4. Visual analysis of lidar intensity data to aid interpretation of lidar topography

5. Visual analysis of aerial photographic data to identify geomorphological and cultural features

6. Addition of known Historic Environment Records (HER) to GIS, to investigate the relationships between geomorphology and archaeological resources

7. Identification of areas for detailed ground survey from factors 1 – 6.

8. Application of ground based survey including earth resistance survey, electrical resistivity imaging and gouge core survey

9. From factor 8, identification of the most suitable samples for palaeoenvironmental analyses

10. From factors 1 – 9, identification of target areas for archaeological investigation.

8.3 FUTURE RESEARCH DIRECTIONS

The research in this project has produced a large database that might be used for further research. The analysis of the results has suggested further research directions for lidar intensity.

- Although the relationship between lidar data and physical soil parameters has been shown to be non-linear, significant correlations still exist between these variables. Further analysis should be undertaken to determine if through advanced mathematical modelling these relationships can be made linear, and therefore useful for predictive modelling.
- The application of using lidar intensity to map cropmarks is an unresolved issue from this project, as no contemporary aerial photographs were available from the time of the lidar flight. It would be worthwhile comparing lidar intensity data with aerial photographs collected at the same point in time, to resolve the issue of the ability of lidar intensity to identify cropmarks caused by archaeological remains.
- Lidar intensity values varied significantly between adjacent flight swathes. It would be worth pursuing further modelling of this data to attempt to correct for this variation, allowing data from adjacent swathes to be directly compared.
- As new lidar equipment becomes available results should be revisited, for example through use of 12-bit intensity data from the new Optech Gemini lidar, and through higher spatial resolution data produced by new sensors with high laser pulse frequencies. The use of full waveform lidar data (*cf* Doneus and Briese 2006) should be investigated when such equipment becomes available in the UK.

9 REFERENCES

Barnes, I. 2003. Aerial remote-sensing techniques used in the management of archaeological monuments on the British army's Salisbury Plain training area, Wiltshire, UK. *Archaeological Prospection* 10: 83-90.

Bewley, R.H. Crutchley, S.P and Shell, C.A. 2005. New light on an ancient landscape: lidar survey in the Stonehenge World Heritage Site. *Antiquity* Volume: 79 Number 305: 636–647

Bewley R and W. Rączkowski 2002. *Aerial Archaeology. Developing Future Practice*. NATO Series 1: vol. 337.

Bewley, R. 2003. Aerial survey for archaeology. *The Photogrammetric Record* 18, 104: 273-292

Bofinger, J., Kurz, S. and Schmidt, S. 2006. Ancient Maps – modern data sets: different investigative techniques in the landscapes of the Early Iron Ahe princely hill fort Heuneburg, Baden-Wurttemberg. in Campana, S. and Forte, M. (eds) *From Space to Place*: Proceedings of the 2nd International Workshop on Remote Sensing in Archaeolo;gy, CNR, Rome, Italy, Dec 4-7, 2006. British Archaeological Reports, International series 1568: 87-92.

Carey, C. Brown, T., Challis, K. Howard, A.J. and Cooper, L. 2006. Predictive modelling of multi-period geoarchaeological resources at a river confluence: a case study from the Trent-Soar, UK. A*rchaeological Prospection.* Vol 13, No4: 241-250.

CEH 2008. *Monthly Hydrological Summery for July 2007*. Centre for Ecology and Hydrology. (http://www.nerc-wallingford.ac.uk/ih/nrfa/monthly_summaries/2007/07/summary.htm)

Challis, K., AJ Howard, M Kincey, D Moscrop, CJ Carey, T Hill, DN Smith, BR Gearey A Thompson. 2007. *Analysis of the Effectiveness of Airborne Lidar Backscattered Laser Intensity for Predicting Organic Preservation Potential of Waterlogged Deposits*. HP Vista Unpublished Report

Challis, K. et al**.** 2006. Using Airborne Lidar Intensity to Predict the Organic Preservation of Waterlogged Deposits. in Campana, S. and Forte, M. (eds) *From Space to Place*: Proceedings of the 2nd International Workshop on Remote Sensing in Archaeolo;gy, CNR, Rome, Italy, Dec 4-7, 2006. British Archaeological Reports, International series 1568: 93-98.

Challis, K. 2005. Airborne LiDAR: A Tool for Geoarchaeological Prospection in Riverine Landscapes. in Stoepker, H. (ed) *Archaeological Heritage Management in Riverine Landscapes.* Rapporten Archeologische Monumentenzorg, 126: 11-24

Challis, K. 2006. Airborne laser altimetry in alluviated landscapes. A*rchaeological Prospection.* Vol 13, No2: 103-127

Challis, K.,. Kokalj, Z., and Moscrop, D. In press. Enhancing historic environment records using airborne lidar.et al. in preparation. *Antiquity*

Challis, K. 2005. *Predictive Modelling Of Multi-Period Geoarchaeological Resources At A River Confluence. Airborne Remote Sensing: Analysis of the Effectiveness of Aerial Photography, LiDAR and IFSAR.* HP Vista Centre, Institute of Archaeology & Antiquity, University of Birmingham.

Challis, K. and Howard, A.J. 2003 "GIS-based modelling of sub-surface deposits for archaeological prospection in alluvial landscapes" in Howard, A.J. and Passmore, D. (eds) *The Alluvial Archaeology of Europe*." Balkema, Rotterdam.

Charlton ME, Large ARG, Fuller IC. 2003. Application of airborne LiDAR in river environments: the River Coquet, Northumberland, UK. *Earth Surface Processes and Landforms* 28: 299-306.

Crutchley, S. 2006. Light detection and ranging (lidar) in the Witham Valley, Lincolnshire: an assessment of new remote sensing techniques. A*rchaeological Prospection.* Vol 13, No4: 251-257

Devereux, B.J. Amable, G.S. Crow, P. and Cliff, A.D. 2005. The potential of airborne lidar for detection of archaeological features under woodland canopies. *Antiquity*, Volume: 79 Number: 305: 648–660

Doneus, M. and Briese, C. 2006. Digital terrain modelling for archaeological interpretation within forested areas using full-waveform laserscanning. Proceedings of the 7th International Symposium on Virtual Reality, Archaeology and Cultural Heritage (VAST 2006): 155-162

Gaffney, C. and Gaiter, J. 2003. *Revealing the buried pas*t. Tempus, Stroud.

Garton, D. 2002. Walking fields in South Muskham and its implications for Romano-British Cropmark-Landscapes in Nottinghamshire. *Trans Thoroton Soc Notts.* 106: 17-39

Harmon, James M., Leone, Mark P., Prince, Stephen D. and Snyder, Marcia. 2006. LiDAR for Archaeological Landscape Analysis: A Case Study of Two Eighteenth-Century Maryland Plantation Sites. *American Antiquity*. Volume 71 Number 4

Jones, R.J.A, and Evans, R. 1975. Soil and crop marks in the recognition of archaeological sites by air photography, in Wilson, D.R. (ed) *Aerial Reconnaissance for Archaeology.* CBA Research report 12.

Powlesland, D., Lyall, J., Hopkinson, G,. Donoghue, D., Beck, M., Harte, A., and Stott, D. 2006. Beneath the sand - remote sensing, archaeology, aggregates and sustainability: a case study from Heslerton, the Vale of Pickering, North Yorkshire, UK**.** A*rchaeological Prospection.* Vol 13, No4: 291-299.

Risbol, O., Kristian Gjertsen, A. and Skare, K. 2006. Airborne laser scanning of cultural remains in forests: some preliminary results from a Norwegian project. in Campana, S. and Forte, M. (eds) *From Space to Place*: Proceedings of the 2nd International Workshop on Remote Sensing in Archaeology, CNR, Rome, Italy, Dec 4-7, 2006. British Archaeological Reports, International series 1568: 107-112.

Shell, C.A. & Roughley, C.F. 2004. Exploring the Loughcrew Landscape: a New Approach with Airborne Lidar, *Archaeology Ireland*, 18, no.2, Issue no. 68, 20-23

Whimster, R. 1986. *The Emerging Past. Air Photography and the Buried Landscape.* RCHME, London.


birmingham
archaeology